Development of aptamer based targeted reversibly attenuated probes

by

Xiangyu Cong

A dissertation submitted to the graduate faculty
in partial fulfillment of the requirements for the degree of
DOCTOR OF PHILOSOPHY

Major: Biochemistry

Program of Study Committee:
Marit Nilsen-Hamilton, major professor
Gloria Culver
Ted Huiatt
Robert Jernigan
W. Allen Miller

Iowa State University
Ames, Iowa
2006

Graduate College
Iowa State University

This is to certify that the doctoral dissertation of

Xiangyu Cong

has met the dissertation requirement of Iowa State University

Signature was redacted for privacy.

Major Professor

Signature was redacted for privacy.

For the Major Program

To my family

TABLE OF CONTENTS

ABSTRACT

The targeted reversely attenuated probe (TRAP) is an aptamer-based biosensor in which the aptamer activity can be regulated by a specific nucleic acid sequence such as an mRNA. The TRAP has the potential of being developed for imaging gene expression *in vivo*. The central portion of the TRAP, between the aptamer and the attenuator, is complementary to a target nucleic acid, such as an mRNA, which is referred to as a regulatory nucleic acid (regDNA) because it regulates activity of the aptamer in the TRAP by hybridization with the central (intervening) sequence.

I developed 8att-cmRas20 and 9att-cmRas15 ATP DNA TRAPs with regDNA-dependent aptamer activity. The results suggested that, as well as inhibiting the aptamer, the attenuator also acted as a structural guide, much like a chaperone, to promote proper folding of the TRAP such that it can be fully activated by the regDNA. We also showed that activation of the aptamer in the TRAP at physiological temperatures by a regDNA complementary to the intervening sequence was sensitive to single base mismatches.

I then utilized a tiled microarray to identify the regions on the mRNA that can be easily targeted by antisense oligonucleotides and the results showed that the microarray approach provided a better match with the *in vivo* antisense than computational analysis.

Selected from a microarray study, the 20nt antisense oligonucleotide that targets positions 741-760 of Lcn2 mRNA was chosen for the malachite green (MG) RNA TRAP. To develop the probe, the structure of the 38nt MG RNA aptamer was first destabilized by introducing truncations and mutations. The K_Ds for MG of several truncated and mutated MG RNA aptamers were estimated and the results showed that the K_Ds of 34nt and 32nt MG RNA aptamers were within a 2-fold range of the 38nt MG K_D. By rational design and after screening different MG RNA TRAPs, the aptamer activity of a TRAP that consists of a 32nt modified MG RNA aptamer and 9nt attenuator sequence was shown to be increased about 20-fold in the presence of a 20nt regDNA.

A yeast selection system has been designed to test the function *in vivo* of the selected TRAP. In this assay, URA3 translation is inhibited by a MG aptamer sequence

inserted in the 5'UTR of the URA3 mRNA, which results in growth arrest in the presence of tetramethylrosamine (TMR) that can be detected by the yeast spot assay. A hammerhead (HH) ribozyme - aptamer/TRAP - hepatitis Delta Virus (HDV) ribozyme cassette was constructed to produce aptamers or TRAPs with defined and homogeneous 5' and 3' ends. An *in vitro* cleavage assay showed that the HH-MG aptamer-HDV expression cassette produced MG aptamers with homogeneous ends.

CHAPTER 1. GENERAL INTRODUCTION

DISSERTATION ORGANIZATION

Chapter 1 of this dissertation starts with a brief summary of the organization. In the following background section, the research fields closely related to the development of an aptamer based nucleic acid probes for imaging specific RNA molecules are reviewed briefly. In the research aims and significance section, the Targeted Reversibly Attenuated Prob (TRAP) is introduced for developing an aptamer based probe for non-invasive *in vivo* imaging of specific RNA molecules. Questions regarding the theoretical basis and practical design of TRAPs are briefly discussed. Chapter 2 contains a literature review covering topics related to the TRAP. The TRAP design utilizes aptamers that have been selected by SELEX. A brief review of SELEX and aptamers are given in chapter 2. Chapter 2 also discusses some fundamental issues related to the TRAP. Functioning as an allosteic aptamer, the TRAP is indeed a targeted nucleic acid molecule-dependent aptamer. A brief review of artificial and natural allosteric nucleotide acid molecules is included. After a review of selected *in vivo* and applications of aptamer, the development of methods for detection and imaging of RNA molecules *in vitro* and in living cells is briefly discussed. At the end of chapter 2, a brief review of RNA secondary structure prediction is given. In chapter 3, the results of the ATP DNA TRAPs with their aptamer activities regulated by a regulatory nucleic acid molecule (regDNA) are presented. The design and function of the TRAPs and oligonucleotides in the study are shown in figure 1. The activation of the TRAP by sequence specific regDNA is presented in figure 2. In figure 3, the dose-dependent activation of the TRAP by regDNA and the reversibility of activation are shown. The impact of attenuator and intervening sequences on TRAP function is presented in figures 4 and 5. In figures 6 and 7, the results from isothermal titration calorimetry (ITC) and polyacrylamide gel electrophoresis (PAGE) are used to illustrate the role of the attenuator as a structural guide for regDNA hybridization with the TRAP. The TRAP's ability to distinguish a single base mismatch is shown in figure 8. In chapter 4, the results of using of microarray to identify the region(s) on the mRNA that

can be easily targeted by antisense oligonucleotides are presented. In chapter 5, results from the development of a malachite green (MG) RNA TRAP targeting uterocalin/Lcn2 mRNA are reported. The sequence information can be found in tables 1 through 7. In figure 1 is the X-ray crystal structure of MG RNA aptamer with tetramethylrosamine (TMR), a structure analog of MG, solved by Baugh et al.(*1*). In figure 2 are the predicted folding and K_D estimation of selected truncated and mutated MG aptamers. In figure 3 are the results of using short oligo to find out the region on the MG RNA aptamer that can be used as the target of the attenuator. In figure 4, the rational design and screening results of 15 different MG TRAPs are presented. Figures 5 and 6 show the design of yeast *in vivo* selection system and spot assay results to test the practicability of yeast *in vivo* selection system. Figures 7 and 8 show the design of hammerhead (HH) ribozyme-aptamer/TRAP-hepatitis delta virus (HDV) ribozyme expression cassette and the results of *in vitro* cleavage reaction. In figure 9 are the structural information, chemical reaction scheme and thin layer chromatography (TLC) results related to the synthesis of biotinylated MG. Figure 10 contains a summary of the results of fluorescence measurements from TRAP SELEX. In figure 11 some of my thoughts about the thermodynamics related in TRAP design is presented. In chapter 6, general conclusions are drawn based on the data presented above. Chapter 7 is a list of references cited in chapters 1,2 and 6. Those cited in chapters 3, 4 and 5 are listed at the end of the respective chapter. The people who have contributed to my studies are thanked in the acknowledgments.

BACKGROUND

Compared to proteins, which are made of 20 different amino acid residues, RNAs contain only four kinds of nucleosides: adenosine (A), guanosine (G), cytidine (C) and uridine (U). But this simple composition does not limit the biological activities of RNAs which include the messenger RNAs that convey and the ribosome RNAs and tRNAs that interpret the genetic information stored in DNA. Many RNAs provide essential catalytic activity as well as structural support for molecular machinery complex. More recently, small RNAs have been found to be very active and critical in the regulation of

gene expression and gene silencing. The expression levels and stabilities as well as the temporal and spatially distributions of specific RNAs in the cell are directly related to their functions. Knowing the dynamics and localization of RNA molecules is critical for fully understanding the biological mechanisms of RNA molecules in fulfilling their functions in the living cell.

Although fluorescent labeled linear antisense oligonucleotides have been used to imaging mRNA in living cells (*2-4*), they suffer from drawbacks such as high background and low specificity and the inability to distinguish single nucleotide mutations (*5*). The molecular beacon is a nucleic acid probe with a stem-loop structure (*6, 7*). The fluorescent labeled molecular beacon enables the development of homogeneous hybridization assays. The advantages of a homogenous hybridization assay are its speed and simplicity. In these assays the unbound probes do not need to be removed and they provide real-time detection and visualization of target nucleic acid molecules. Molecular beacons and other nano-structured probes have been used to detect RNA in living cells (*5*). The molecular beacon contains one terminal quencher molecule and one terminal fluorophore molecule or one terminal donor fluorescent molecule with an acceptor fluorophore at the other terminus to give target-dependent fluorescence when the two termini separate upon target recognition. Because of the low energy level of fluorescence, it can not penetrate tissue and the whole body. This limits the use of molecule beacons to cultured cells.

Integrating the aptamer/ribozyme into the design of molecular beacon produces the aptamer/ribozyme TRAP (*8, 9*). The aptamer is a single nucleic acid molecule that can bind its ligand with high specificity and affinity (*10, 11*). Aptamers are selected *in vitro* using a procedure named systematic evolution of ligands by exponential enrichment (SELEX) (*10*). Aptamers have been used for a broad range of *in vitro* as well as *in vivo* applications (*12-22*). For imaging RNA molecules in living cells, the aptamer ligand can be labeled with fluorescence, quantum dots (*23*) or radioactive isotopes (*19*) to provide the signal output needed for detection and visualization. It is possible to apply aptamer-

based probes for imaging RNA molecules in tissues or whole organisms by labeling the aptamer ligand using quantum dots or radioactive isotopes.

RESEARCH AIMS AND SIGNIFICANCE

Verification of the Practicality of the Aptamer-Based TRAP Design

After the TRAP idea was formed in the year 2000, the proof of principle was first performed by the work done on the ribozyme-based TRAP (*9*). Selecting the ATP DNA aptamer as a starting point, I designed and tested a series ATP DNA TRAPs *in vitro*. Two functional ATP DNA TRAPs were developed. The 8att-cmRas20-TRAP was shown to be activated by a sequence-specific regDNA in a dose-dependent manner. The 9att-cmRAs15-TRAP was able to distinguish single nucleotide mismatches (*8*). I then chosen the malachite green (MG) RNA aptamer to develop an RNA TRAP targeting uterocalin/Lcn2 mRNA. By rational design and screening a series of MG TRAPs, aptamer activity of the 32MG1-9 RNA TRAP was shown to increase 20-fold upon interacting with a sequence specific regDNA complementary to the intervening sequence of the TRAP.

The Influence of Structure and Stability of the Aptamer to TRAP Design

Because the ATP DNA aptamer undergoes a global ligand-induced conformational change (*24*), I was able to use full length of ATP DNA aptamer to develop functional ATP DNA TRAPs. By contrast, the MG RNA aptamer has a stable structure as shown in the folding of aptamer itself predicted by Mfold (*25*) and by the X-ray crystal structure with ligand-tetramethylrosamine (TMR) (*1*). The binding pocket is located in a central bulge loop flanked by two stems. Because of the stability and lack of a global ligand-induced conformational change of 38nt MG aptamer when it binds MG, the MG aptamer structure was destabilized by truncation and by introducing mutations to get a functional MG RNA TRAP. These two examples indicate that the choice of aptamer had big impact on the subsequent design and optimization of a TRAP. The overall stability of the aptamer itself and the conformational changes upon the ligand binding are important factors to be considered for effective TRAP design.

The Need and Function of Attenuator

The attenuator was designed to interact with the aptamer and inhibit the aptamer activity in the absence of target RNA. Obviously, the length and composition of the attenuator is critical for a successful TRAP design. In the ATP DNA TRAPs and MG RNA TRAPs, I tested different attenuator lengths. The attenuator was not able to inhibit the aptamer activity if it was too short. On the other hand, the TRAP had low regDNA-dependent aptamer activity if the attenuator was too long. The effective targets of the attenuator were the residues of the aptamer that were involved directly in the interactions with the ligand and were crucial for the aptamer binding activity. By analyzing the 0att-cmRas ATP DNA TRAP, I showed that besides inhibiting the aptamer, the attenuator was also needed for guiding the TRAP to fold into the desired conformation. Without the attenuator, the intervening sequence can interact with the aptamer and inhibit its activity. But by doing so, the heavily base paired intervening sequence may not be able to interact with target nucleic acid molecules efficiently. Thus the absence of an attenuator resulted a TRAP with low regDNA-dependent aptamer activity.

The Choice of Intervening Sequence

The function of the intervening sequence is to interact with the target nucleic acid molecule and this interaction helps to overcome the inhibition by the attenuator of the aptamer in TRAP. To choose an intervening sequence for a target mRNA, the first consideration was whether the region it targeted was available in the folded mRNA. mRNA has a secondary structure and it folds into one or more tertiary conformations. If the target region of intervening sequence is heavily involved in base pairing in the folded mRNA, most likely it would have low availability for interacting with the complementary intervening sequence in the TRAP. There were several computational tools available to predict the antisense availability of certain regions on mRNA molecules (*26, 27*). Experimentally, I used a tiled microarray to identify regions on the mRNA that were easily targeted by 20nt antisense oligonucleotides. The results

showed that the microarray results provided a better match with the *in vivo* antisense experiments than the computer analysis.

The Involvement of Intervening Sequence in TRAP Folding

As the part of TRAP molecule, the intervening sequence is involved in intramolecular interactions. In the TRAP design a strong interaction was needed between attenuator and aptamer so that binding activity of aptamer was inhibited by the attenuator in the absence of target nucleic acid molecules. To achieve the effective inhibition, the attenuator was designed to be fully complementary to the residues of aptamer. As shown in 8att-cmRas20, 9att- cmRas15 ATP DNA TRAP and 32MG1-9 RNA TRAP, the attenuator was fully involved in the interaction with aptamer. There was no interaction between the intervening sequence and attenuator. But, by interacting with the aptamer or base pairing within itself, the intervening sequence could have big impact on TRAP folding and therefore function. In the 8att- cmRas20, 9att-cmRas15 ATP DNA TRAP and 32MG1-9 MG RNA TRAP, the intervening sequences were found to interact with aptamer and to provided extra force to inhibit the aptamer activity in the absence of target nucleic acid molecules. Without this interaction provided by the intervening sequence, the length of attenuator needed to inhibit the aptamer needs to be longer and consequently, the TRAP will be less responsive. The structure of the target nucleic acid also needs to be considered. Interaction of the TRAP with the 20nt linear regDNA as the target molecule may be energetically more favorable than its interaction with a folded mRNA as the target.

Rational Design and *In vitro* SELEX for TRAP

Through rational design, the ATP DNA TRAPs and MG RNA TRAPs with regDNA-dependent aptamer activity were successful developed. Compared to the rational design, the SELEX procedure can be used to examine a much bigger sequence pool. If the randomized region on the TRAP was less than 20nt, theoretically, all the possible combination of TRAP sequences can be screened in SELEX. I tested several parameters for rational design such as the choice of aptamer, intervening sequence

and attenuator sequence. The insights gained could be useful for further TRAP developed. I also tested using SELEX for selecting an effective MG RNA TRAP. The experience so far indicates that the most critical parameter for successful selection of a TRAP by SELEX might be establishing a means of efficient negative selection to eliminate TRAPs with weak attenuators.

In vivo Selection of TRAPs Developed *In vitro*

The TRAP was developed *in vitro* and it was not guaranteed to be functional *in vivo*. I designed a yeast selection system for testing and selecting a TRAP that functions inside cells. The preliminary data suggested that the design was practical and that, following the further testing, it could be used to test the MG RNA TRAP in the yeast cells.

Expression of TRAP Inside the Cells

Expression of a TRAP inside the cells using an expression vector is one way to test and select for a TRAP with the desired properties. I designed an HH-aptamer/TRAP- HDV expression cassette for producing the RNA sequences inside the yeast cell with the desired 5' and 3' ends. The *in vitro* cleavage assay indicated the successful release of RNA sequences with homogenous ends under defined conditions.

Sequence and Thermodynamics Parameters for Systematic Developing of TRAP by Computational Design

Through computational design and experimental validation, oligonucleotide-sensing allosteric ribozymes have been developed (*28*). A similar strategy is needed to identify the sequence and thermodynamics parameters for effective TRAPs. In the process of developing the ATP DNA TRAPs and MG RNA TRAPs, we have begun to understand the parameters that are important for designing TRAPs in general.

CHAPTER 2. LITERATURE REVIEW

SELEX

SELEX, the abbreviation for "Systematic evolution of ligands by exponential enrichment", was first introduced around the 1990s. In 1990, Larry Gold's lab used a procedure they named SELEX to select the RNA that interacts with T4 DNA polymerase (*10*). Around the same time, Jack W. Szostak's lab developed a similar *in vitro* selection procedure to select RNA molecules that bind a specific ligand from a variety of organic dyes (*11*). The selection procedure developed in these two labs followed the same principle although they were independently created for different purposes. The name SELEX was chosen and from then on, this *in vitro* selection procedure has been widely used to select ssDNA and RNA molecules called aptamers that can bind desired target with high specificity and affinity.

The SELEX procedure begins with a synthesized random DNA sequence library. If we want to synthesize a random pool that has one copy of each possible 40 nucleotide (nt) random ssDNA (single strand DNA), in theory, we will have 4^{40} (1.2×10^{24}) different sequences in that pool. For 1.2×10^{24} 40 nt ssDNA molecules, the mass is about 23,920 g ($300\ g/mol \times 40 \times 1.2 \times 10^{24}$) / ($6.02 \times 10^{23}$). It is about 24 kg of ssDNA. In practice, a typical combinatorial oligonucleotide library obtained from a 1μmol scale solid phase DNA synthesis is limited to 10^{14} - 10^{15} unique sequences. This is about 1-20 ug of ssDNA. Even so, the diversity of the library presented by different ssDNAs is much higher than in other combinational libraries, such as peptide libraries used for phage display and libraries made up of small molecules (*29*).

The SELEX procedure places a high evolutionary pressure on the nucleic acid library and an aptamer is selected that binds specifically to a given ligand. The resulting aptamer has high affinity and specificity for the given ligand. Examples include the two tobramycin RNA aptamers have dissociation constants (K_D) about 9 nM and 12 nM (*30*). The DNA ATP aptamer has K_D about 6 μM (*31*). The two RNA

aptamers for the HIV Rev peptide have 4 nM K_D (*32*). The DNA aptamer for thrombin, a protease functioning in coagulation, has a 25nM K_D (*33*).

The general procedure for SELEX is shown in Fig.1 (*34*). The random ssDNA pool is synthesized such that every sequence has a contiguous random sequence in the middle and a fixed sequence region in each end (■). To obtain a DNA aptamer, the ssDNA library is placed directly into the selection cycle. For an RNA aptamer, a promoter for an RNA polymerase (such as the T7 RNA polymerase) is attached immediately after one of the two fixed sequence regions of the library sequence in order to synthesize the RNA sequence by *in vitro* transcription (▨). Under defined conditions (including buffer, temperature etc.), the ssDNA or RNA library is incubated with the target molecule of interest. Sequences that bind to the target are separated from unbound sequences by the chosen partitioning method. If the target is immobilized on an affinity matrix such as a column or membrane, the column or membrane is eluted with the chosen buffer after washing to remove unbound sequences. The sequences obtained after eluting are a mixture of sequences with high and low affinities for the target molecules. To obtain high-affinity binding molecules, the low-affinity binding molecules need to be eliminated by sequential rounds of selection. The selected sequences are amplified for the next round. If it is a ssDNA library, the mixture is amplified directly by PCR using the two fixed sequences at the ends of all sequences in the library. After PCR, a standard method is used to separate the two strands of the PCR products (such as one primer being labeled with biotin and then the PCR product run through a streptavidin affinity column). The amplified ssDNA is then prepared to be taken through the next selection. For RNA aptamer selection, RNA sequences are first converted to DNA by reverse transcription. The corresponding DNA sequences are amplified by PCR. The amplified RNA library is obtained by *in vitro* transcription. After amplification, the ssDNA library or the RNA library will be mixed with fresh target molecules to go through the second round of selection. With increasingly stringent conditions, the selection will be continued until affinity saturation is observed, which means that the affinity of the library could not be improved any more by selection. The percent of oligonucleotides left on the column after washing can be

used to indicate the number of molecules in the population with a relatively high affinity for the target. The PCR product after the final selection round is cloned and a number of clones are sequenced. In Fig.1, the black arrows show steps in a DNA-based aptamer selection; gray arrows show the steps in a RNA-based selection (*34*). Usually, it is necessary to go through 8-15 cycles in the SELEX procedure to select a group of aptamers with high affinities for the target molecule.

Since SELEX was introduced, many modifications have been made to improve this technique to meet the need for broader applications of aptamers. The purpose of SELEX is to get an aptamer that binds a target molecule with high specificity and affinity. The high specificity can be achieved by including a negative selection during the SELEX procedure. Usually, the negative selection is done by applying the ssDNA or RNA pool to the support used in the SELEX procedure for partitioning the target-nucleic acid complexes from the remaining nucleic acid pool. For example, in the selection of an RNA aptamer that targets a protein, filters are often used as the support to separate RNA molecules that bind to target from RNA molecules do not bind. A negative selection against the support can successfully eliminate sequences that bind to the support instead of the target molecule. Negative selections are routine procedures in SELEX to give the selected aptamer high specificity for the target molecule.

Another way to improve the specificity of selected aptamers is to do the selection against a structural analog of the target molecule in order to eliminate nucleic acid sequences that do not recognize the target molecule with high specificity. The theophylline RNA aptamer has 10,000-fold greater binding affinity to theophylline than for caffeine (*35*). Caffeine differs from theophylline by a single methyl group at nitrogen atom N–7. Negative selection against caffeine was used to achieve high specificity. After eight rounds of selection using a theophylline affinity column, caffeine was applied to the bound RNAs to elute any RNA sequence that could bind caffeine. This approach was named "counter-SELEX" by the authors (*35*).

Specificity seems to be easy to achieve using SELEX. Then what about affinity? Typically, aptamers have dissociation constants in the μM range when directed against small molecules such as ATP and in the low nM to pM range when directed against proteins. To achieve a dissociation constant in the low nM range, the target concentration used in the SELEX rounds should be limited and gradually decreased with subsequent rounds. Also, the non-specific binding should be minimized. New developments of SELEX procedure, such as PhotoSELEX, could be used to lower the non-specific binding during the SELEX because extensive washing can be applied after the cross-linking. In PhotoSELEX, a modified nucleotide that can be activated by light replaces a native base in either ssDNA or RNA randomized oligonucleotide libraries (*36*). The crucial part of PhotoSELEX is the choice of modified nucleotide to be one that is activated by light, reacts with the target molecule and remains non-reactive and stable without light activation. Also, the modified nucleotide needs to be recognized by the polymerases in order to allow the PCR and *in vitro* transcription reactions to work. In photoactivatable nucleotides 5-bromo-2'deoxyuridine usually replaces thymidine. 5-bromouracil is also used but it is less reactive than 5-bromo-2'deoxyuridine. Both modified nucleotides will react with aromatic groups or thiols when exposed to the appropriate wavelength of light (~310nm). A nucleic acid:protein adduct is formed through cross-linking. Using polyacrylamide gel electrophoresis (PAGE), aptamers that cross-link to the target are partitioned from those that did not. The protein component is digested to generate sequences that could be amplified by PCR. Even with efficient digestion, not all of the protein is removed. This limits the number of usable templates in the PCR reaction. A mixture of *Taq* and *Pwo* polymerase enzymes was shown to amplify the low copy number templates more efficiently and accurately than *Taq* polymerase alone (*37*). Reasonable amplification of sequences in photoSELEX was achieved by a combination of *Taq* and *Pwo* polymerase enzymes. Both *Pwo* and *Taq* DNA polymerase can incorporate 5-bromouracil. The *Pwo* polymerase possesses proofreading activity and its efficiency is lower compared to the *Taq* DNA polymerase, which does not have proofreading activity. To achieve efficient amplification and keep

the low level of errors, *Taq* and *Pwo* polymerase were used together as a 1:1 mixture (*38*).

In the process of PhotoSELEX, the oligonucleotide library and protein target mixture are exposed to a laser of a certain wavelength to activate the modified nucleotide. The activated nucleotide will react with an aromatic group or thiol in the protein target molecule to form a permanent covalent bond. The protein target molecule with covalently bound oligonucleotide is separated from other molecules (proteins and unbound oligonucleotides) by PAGE. After extraction from the gel, a protease is used to digest the protein. After digestion, PCR is used to amplify the sequences that were covalently bound with the protein. Further rounds of selection can then be carried on.

After 6 rounds of PhotoSELEX selection, an aptamer binding to human basic fibroblast growth factor (bFGF) with a low pM dissociation constant was selected using a ssDNA oligonucleotide library (*38*). There are two reasons why PhotoSELEX is very effective in selecting high affinity aptamers. First, in order to efficiently form the covalent bond between the modified nucleotide and target protein molecule, the modified nucleotide must be within a certain distance of the amino acid side chain and the angle between modified nucleotide and aromatic or thiol group must be in a certain range. These requirements of the coupling reaction exclude the capture of oligonucleotides and proteins that are transiently or nonspecifically interacting. Second, because of the permanent covalent bond formed between oligonucleotide and bound protein target, more stringent washing conditions can be used during the selection. This will further eliminate non-specific binding.

Another similar approach to selecting aptamers with high affinity and specificity is a SELEX procedure called blended SELEX (*39*). Human neutrophil elastase (hNe) is a target for an aptamer that could be used to inhibit acute respiratory distress syndrome (ARDS). Prior to the aptamer, various inhibitors of hNE had been developed but many of them suffered problems such as low specificity and low affinity. An RNA-based inhibitor for hNe was developed through blended SELEX (*39*). A diphenyl phosphonate

derivative of valine (valP) that irreversibly inhibits hNe by reacting with the serine in the active site of hNe to form a covalent bond with the 5' end of a ssDNA. The sequence at the 3'end of the ssDNA was complementary to the 5' end of an RNA pool with a 40 nucleotide random sequence in the middle. Annealing the ssDNA and RNA brought the RNA random sequence close to the valP-hNe complex. During SELEX, a low concentration of target, in this case, hNe was used. The use of ssDNA-valP into SELEX allowed the selection of an RNA sequence-valP complex that gives an additional approximately 20-fold increase in inhibitory activity compared to the valP alone. Also, there was more than a 100-fold reduction in the relative rate of cross-reaction of this inhibitor with another serine protease, cathepsin G (*39*).

Natural ssDNAs and RNAs are easily degraded by endonucleases and exonucleases present in the blood and inside the cell. For example, in the bloodstream, nucleic acids are degraded with half lives from seconds to minutes (*40*). The major mechanism by which RNA is degraded is an attack of 2' hydroxyl of pyrimidine by pyrimidine-specific endonucleases, which appear to be the most abundant nucleases in the blood and inside the cell (*41, 42*). For *in vivo* applications, the half-lives of aptamers made of natural nucleotides are too short. However,, there are many ways to make modified RNA molecules that are resistant to nucleases. Modification of the 2' position of the sugar of the RNA is an efficient way to achieve nuclease-resistance (*42*). RNAs with 2'-NH2 and 2'-F functional groups have enhanced life times in biological fluids (*43, 44*). The enzymes used in PCR and *in vitro* transcription can use as their substrates pyrimidine nucleotides substituted with amino (NH2) and fluoro (F) functional groups at the 2' position of the sugar and modified nucleotide bases have been used in SELEX to improve RNA stability. For example, 2' -amino and 2'-fluoro-2'-deoxypyrimidine RNAs have significantly increased stability compared with unmodified RNAs. These modified RNAs are resistant to nucleases and are well suited for both diagnostic and therapeutic applications.

A 2'-amino-2'deoxypyrimidine RNA aptamer was selected to bind basic fibroblast growth factor (bFGF). The dissociation constant for the aptamer is about 0.5 nM and

the stability is at least 1,000 fold higher than the natural RNA in human serum (*45*). The affinity of this 2'amino-2'-deoxypyrimidine RNA aptamer for bFGF is similar to a natural RNA aptamer selected for bFGF (*46*). So far, 2'-amino and 2'-fluoro -2'-deoxypyrimidines are the modified nucleotide bases most widely used in SELEX. Nucleoside 5'-(α-P-borano) triphosphates (*47*) and nucleoside 5'-(α-thio) triphosphates (*48*) also have been used as the basis of modified triphosphates for SELEX. Although they confer nuclease resistance, 2'-amino and 2'-fluoro-2'-deoxyribopyrimide have some disadvantages compared to the natural nucleotide bases. These disadvantages include that the 2'-amino-2'-deoxyribopyrimidine does not have 2' hydroxyl group. The 2' -hydroxyl group on the natural nucleosides can participate in hydrogen bonding and provide support for nucleic acid structural stability. The amino group is much bigger than the hydroxyl group, and 2' amino-2'-deoxyribopyrimidine RNA suffers from a low melting temperature in the duplex structure because the large amino group destabilizes the duplex structure. On the other hand, 2'-fluoro-2'-deoxyribopyrimidine RNA has comparable duplex stability with natural RNA because the fluorine is not as big as the amino group. But both 2'-amino and 2'-fluoro-deoxyribopyrimidine RNA are less efficient substrates for T7 RNA polymerase compared to the natural pyrimidine nucleotides. Additionally, people suspect that the modified nucleotide bases interfere with Watson-Crick interactions, which makes the secondary structure less stable. Recently, 4'-thioUTP and 4'-thioCTP were synthesized and successfully used in SELEX (*49*). These two new NTP analogues are better substrates for T7 RNA polymerase compared to 2'-amino and 2'-fluoro-2'deoxypyrimidine. RNAs with incorporated 4'-thioUTP and 4'-thioCTP are 50 times more stable than the natural RNA (*49*).

There is another expensive but clever method that improves the RNA aptamers' stability. Spiegelmers are specialized aptamers made of L-nucleic acid instead the natural D-nucleic acid (*50-53*). L-nucleic acids can not be recognized by endonucleases, so they are more stable in plasma compared to their mirror images, the natural D-nucleic acids. To select a spiegelmer, the aptamer for the mirror image of the true target is first selected by conventional SELEX procedure. For example, if the target is a protein, a mirror image of the natural protein will be chemically

synthesized first. The natural amino acids are all L -isomers. So, instead of using L-amino acids as the building block, D-amino acids are used to synthesize a target for SELEX. After an aptamer made of natural D-nucleic acid is selected for the target made of D-amino acids, the mirror image of the aptamer is chemically synthesized. The interfaces between the D-nucleic acid/D-amino acid complex interaction are maintained in the L-nucleic acid/L-amino acid complex. The synthesized L-nucleic acid aptamers are named spiegelmers, as spiegel means mirror in German. Spiegelmers can be made for any target that is a chiral molecule for which its chiral isomer (mirror image) could be chemically synthesized. These requirements limit the number of available spiegelmers. Natural nucleic acids have half-lives from seconds to minutes in plasma (*54*). The biggest gain of the spiegelmer is its half-life in plasma which reportedly is 60h (*50*).

Besides improving the selected aptamers' affinity and stability, another important aspect of SELEX is how fast it can be done. In the laboratory, special care is need to be taken to avoid degradation and loss of RNA during each round of SELEX. This might increase the time consumed in each round of SELEX. The transcription reaction, PCR and isolating the binding sequences in each round may take several days. Usually, 8-14 rounds of SELEX are needed for a significant binding increase. It usually takes weeks and months to complete a SELEX experiment and the successful isolation of an aptamer is not guaranteed. These drawbacks prevent more wide use of this procedure. Consequently, there have been considerable efforts made to improve the throughput of the SELEX procedure.

Ellington and colleagues brought a robot into the picture and successfully automated the SELEX procedure (*55, 56*). In the automated SELEX, a mechanical system handles all the operation including the PCR, *in vitro*-transcription, partition of binding species and RT-PCR. In the demonstration of automated SELEX, an RNA aptamer targeting lysozyme was selected using automated SELEX. Lysozyme was biotinylated and the RNA binding to the lysozyme was captured by streptavidin-magnetic beads. After 12 rounds of selection, the aptamer with the highest affinity had

a dissociation constant of 65nM for biotinylated lysozyme, and 31nM for the unbiotinylated lysozyme (*55*). In a further development of automated SELEX, the biotinylated protein from *in vitro* transcription and *in vitro* translation was used in the automated selection (*57*). This optimization relieves the SELEX process from requiring a purified biotinylated protein . The cDNA sequence encoding the target protein was used to synthesize biotinylated protein for use in the automated SELEX. In this procedure, biotinylation is catalyzed by biotin protein ligase and the biotinylation site is at the N-terminus of the target protein which has a 24 amino acid biotin acceptor peptide sequence. The biotin protein ligase is produced as a fusion protein with the target protein for aptamer selection. This allows for uniform and targeted biotinylation of the aptamer target compared to the nonuniform and random biotinylation of purified protein achieved through a chemical reaction.

In SELEX protocols that use affinity chromatography and filter capture to separate the binding from the non-binding species, there is always potential that the nucleic acid sequence could interact with the linker or the supporting material. Browser and colleagues used capillary electrophoresis (CE) to perform SELEX and named the process CE-SELEX (*58, 59*). In CE-SELEX, the target is mixed directly with a nucleic acid pool without any modification and there is no support material as in affinity chromatography and filter capture. The separation is based on the different migration rates of the unbound nucleic acid and the nucleic acid target molecule complex. Without a support material, there are no non-specifically bound sequences and the resolving power is great increased. As few as two rounds of SELEX resulted in an aptamer with high affinity. This technique greatly increases the throughput of the SELEX procedure. If automated SELEX could be combined with CE-SELEX, it may provide further boost for the more broad use of SELEX technique.

Clearly, SELEX is a procedure with great potential. Many problems existing in the procedure have been resolved. Further optimization of this fast-spreading technique will provide a solid foundation for the development and application of its product aptamers.

Usually, the nucleic acid used in the SELEX is a random pool that has been chemically synthesized *in vitro*. There is another SELEX procedure developed to use fragments of genomic DNAs as the beginning materials for SELEX. Genomic SELEX is a SELEX procedure developed to find the binding sites of a certain protein on the genomic DNAs or the transcripts (mRNA) (*60*).

Fragments of genomic DNA or RNA transcripts from the constructed genomic DNA library can be used in genomic SELEX to identify the interaction network between a particular protein and nucleic acids in a pool of molecules (genomic DNAs or transcripts). In this process, there is no random sequence pool. The complexity of the pool comes from the genome. The potential binding sites in genomic DNA of a nucleic acid binding protein could be acquired through genomic SELEX. Thus, through genomic SELEX, we can get more insights into the regulation of the transcription and translation by the nucleotide acid binding proteins.

APTAMERS

The most important biological role of nucleic acids (DNA and RNA) in the living organism is as the genetic "hard disk", which is the genetic material that transfers the genetic information from generation to generation. Transfer RNAs, messenger RNAs and ribosomal RNAs are the functional nucleic acids to "output" genetic information in the form of proteins. Recently, small RNAs were recognized as the regulatory components hiding behind the central dogma. It took a long time and luck to discover that short RNA sequences are very powerful in gene regulation. At the same time, many non-natural short nucleic acid molecules have been developed to fulfill the needs of biological and biomedical research and applications. Aptamers were one of many types of such non-natural short nucleic acid molecules.

The specificity and affinity of aptamers makes them very attractive biological tools. The term aptamer, is derived from the Latin word "aptus", means "to fit" (*11*). As the name implies, aptamers are RNAs and DNAs derived by an *in vitro* procedure (SELEX) that, starting from random sequence libraries, optimizes the nucleic acid for high affinity binding to a given ligand (*61*). The SELEX procedure is now generally recognized as a powerful tool for obtaining a nucleic acid for almost any target molecule that binds to that target with high specificity and affinity. Target molecules that have been used to select aptamers include aminoglycosides and antibiotics (*30, 62-64*), theophylline (*35*), citrulline (*65*), ATP (*31, 66*), amino acids (*67-70*), peptides (*71-73*), FMN and FAD (*74, 75*), vitamins (*76*) and carbohydrates (*77*). Because SELEX is an *in vitro* selection procedure, there is almost no limit to the target molecule and the conditions of selection. More and more aptamers are reported for various target molecules. The fastest growing group of aptamers is for protein molecules. All kinds of proteins have been selected as the target molecules: viral proteins (*78-83*), enzymes (*76, 84*), proteases (*81, 85-93*), growth factors (*94-96*), cytokines ((*97*), transcription factors (*73, 98, 99*) and cell adhesion proteins (*77, 100-102*).

Some of the aptamers selected to various targets are listed above. Since the SELEX procedure was introduced in 1990, there have been hundreds of aptamers

selected through SELEX. Most of them are RNA aptamers. Along with the growing number of aptamers, at least two databases were created to keep track of functional nucleic acids as well as natural aptamers, named riboswitches (*103, 104*). One database, SELEX_DB, can be found at http://wwwmgs.bionet.nsc.ru/mgs/systems/SELEX/ (*104*). The other database, the Aptamer Database, can be found at http://aptamer.icmb.utexas.edu/ (*103*). The SELEX_DB focuses on how *in vitro* selection could help to define the natural DNA and RNA sequences that are recognized by proteins. Although there is some overlap, the Aptamer Database is a more complete database for aptamers produced through SELEX compared to the SELEX_DB database. The Aptamer Database is updated monthly and by August, 2005 it contained 3,498 sequences from 306 articles in the Aptamer Database.

Three-dimensional structural analyses (NMR and X-ray crystallography) have been used to establish the characteristics of ligand-binding pockets in aptamers and the molecular interactions that occur between aptamer and target. In aptamers binding to aminoglycoside ligands, electrostatic interactions, shape complementarity and hydrogen binding provide the strength for the highly specific ligand discrimination (*105-107*). For the flat targets, such as molecules with aromatic rings, the specificities and binding affinities are achieved by a combination of stacking and hydrogen-bonding (*61*). A comparison of DNA and RNA ATP aptamers shows how two independently selected aptamers can vary in structure yet bind the same target molecule. The base sequence and secondary structures of these aptamers are different. Each DNA aptamer binds to two ATP molecules (*24*) while each RNA aptamer binds only one ATP molecule (*108, 109*). But the binding pockets of the DNA and RNA aptamers and the interactions between ATP and nucleic acid are almost the same (*44*). There is a reverse Hoogsteen G-G pair as a stacking platform in both the aptamers, the ATP pseudo-base pairs with one guanine located in a pocket between a G-G pair and the adenosine. There is also extensive stacking interaction among ATP • G, and the G-G pair and adenosine. Similar to the interaction between aptamer and ATP, specific and high affinity binding of aptamers to peptides or proteins is also based on multiple interactions. When RNA aptamers bind to the HIV-1 Rev peptide, an arginine-rich

peptide from the human immunodeficiency virus (HIV-1) Rev protein, non-specific interactions between the arginine guanidinium groups of the peptide and the phosphate groups of the RNAs provide strength to stabilize the complex. Then specific hydrogen bonds between RNAs and arginine pairs of the peptide make specific recognition possible (*110*).

In summary, aptamers can be generated for a broad range of targets. By investigating the interactions of aptamers with their target molecules, the general structural elements critical for these types of interaction can be derived. Knowledge about the interaction between aptamer and its target can help to explain how natural nucleic acids, consisting of four kinds of nucleotide bases, can participate and play important roles in so many biological precesses inside cells. In the end, it might be possible to design nucleic acid molecules with desired functions and required properties to be used in the biological and biomedical research and applications.

PRINCIPLES OF THE TRAP DESIGN

Targeted Reversibly Attenuated Probe (TRAP)

The TRAP is a single stranded DNA or RNA sequence (Fig. 2). Every TRAP has three modules. At one end of the TRAP there is a ligand-binding aptamer sequence. At the other end of the TRAP is the attenuator sequence that is the reverse complement of the aptamer sequence. In the middle of the TRAP, there is an antisense sequence, which is complementary to the target mRNA sequence.

Aptamers are between10-100nt in length. One DNA aptamer for thrombin is 15nt (*111*). The ATP DNA aptamer is 25nt (*31*). The ATP RNA aptamer is 40nt (*66*). Two tobramycin RNA aptamers are 26nt and 27nt (*112*) and the neomycin B RNA aptamer is 23nt (*113*). There are two considerations for choosing an aptamer for a TRAP. One consideration is affinity; the higher affinity, the more sensitive the TRAP. The other consideration is specificity; the aptamer should bind very specifically to the ligand.

The attenuator sequence of the TRAP is 5-10 nt. Because the TRAP has 5' end and 3' ends that are reverse complementary sequences like molecular beacons (*6*), that adopt a stem loop structure.

In the middle of the TRAP sequence is a 15-30 nt antisense sequence. The function of this intervening antisense sequence is to anneal with the complementary sequence on the target mRNA and to provide the energy to separate the stem of the TRAP.

The Theoretical Basis of the TRAP

The rigidity of short double strand DNA (dsDNA)

Molecular beacons have a stem-loop structure (*6*). The loop is about 15-30nt. It has been shown *in vitro* and *in vivo* that after the loop has annealed with its complementary sequence, the stem is opened (*6, 114*). The idea is that a single

stranded DNA can easily bend and has no rigidity. So the two ends of an oligonucleotide can come together to create a stem.

Knowledge of the inflexibility of dsDNA is very important for understanding the activation of transcription, chromosome structure and the recognition of DNA-binding proteins (*115*). In the elastic model, DNA is regarded as a stiff elastic rod (*116*). The bending free energy (ΔG_{bend}) represents the DNA flexibility and describes the bending motion of the helix (*115*). The free energy for DNA bending can be expressed as follows: $\Delta G_{bend} = \frac{R \cdot T \cdot P}{2L} \cdot (\Delta\theta^2)$. Where R is the gas constant, T is the absolute temperature, L is the length of the DNA under strain, $\Delta\theta$ is the bending angle in radians, and the P is an experimental estimated constant called the persistence length of the DNA duplex (*115*). The experimental estimation of the persistence length, P, of bulk DNA was about 150 base pairs (bp) or 500 Å (*117*). Early studies provided the data to calculate the ΔG_{bend} for a certain length of DNA. Energy is needed to bend short dsDNAs. In the stem-loop structure, if the loop is annealed with its complementary sequence and becomes dsDNA, the tendency of this dsDNA to be straight will compete with the stability of the stem. If the ΔG_{bend} is high enough, then the stem will come apart. For the TRAP, the situation is more complicated than it is for the molecular beacons. The aptamer itself has the potential to fold into a certain structure. The attenuator must destroy the aptamer's natural folding. On the other hand, the interaction between aptamer and attenuator should not be too strong. Otherwise, ΔG_{bend} may not be large enough to open the TRAP.

Intermolecular and intramolecular interactions in the TRAP

For a single stranded DNA or RNA with a stem loop structure, one question is about the intermolecular interaction. Because the 5' and 3' ends are complementary, it is possible that two molecules could anneal with each other through their terminal sequences. A recent study showed that both DNA and RNA complementary strands preferentially form intramolecular hairpin structures (*118*). In the 3' noncoding regions of the chicken glutamine synthetase gene, there is an A-T rich DNA sequence region.

Within this region there are several sequences that could conceivably form intramolecular hairpin structures. Riccelli *et al.* (*118*) used optical and calorimetric melting and gel electrophoresis to investigate the intermolecular and intramolecular interactions of the hairpin-forming sequences. The DNA and RNA oligomer sequences synthesized were: DNA, 5'd-T-T-T-T-T-T-A-A-T-A-A-T-T-A-A-A-A-A-A-3'; and RNA, 5'r-U-U-U-U-U-U-A-A-U-A-A-U-U-A-A-A-A-A-A-3'. The DNA and RNA oligomers alone and in various mixtures with their DNA and RNA complementary strands were analyzed using gel electrophoresis. The experiments revealed that both strands alone preferentially form intramolecular hairpin structures (*118*). In mixtures in which their complementary strands were in vast molar excess (stoichiometric ratios > 10:1), the intramolecular structures were converted to intermolecular duplexes. For the DNA and RNA strands examined, the conversion was not complete until over a 1,000-fold excess of the complementary strand was added (*118*).

It is important for proper function of the TRAP that it forms an intramolecular structure that includes the attenuator hybridized with the aptamer. The evidence provided by the experiments consistently indicate that TRAP will strongly preferentially form intramolecular hairpin structures.

The enhanced specificity of a stem-and-loop structure

Antisense probes can identify their complementary sequences in the presence of unrelated nucleic acid sequences. But they cannot discriminate targets that differ from one another by only a single nucleic acid. However, probes with a stem-and-loop structure have the ability to recognize targets with an accuracy of a single difference in a nucleic acid sequence (*6, 7*). The thermodynamic basis of the enhanced specificity of stem-and-loop DNA probes was investigated in a molecular beacon with a fluorophore attached to one end and a fluorescence quencher attached to the other end, in which the fluorescence of the fluorophore is quenched when the quencher becomes located a close within 100Å of the fluorophore (*119*). The stem-and-loop structure, such as in molecular beacons, can exist in three different states: bound to its target; free in the form of the hairpin structure; free in the form of random coils (*119*).

The results showed that the structural constraints on the molecular beacon's conformational change resulted in enhanced specificity. The unstructured probe does not experience conformational changes when it binds to its targets. At 37°C or lower temperatures, the unstructured probe can not differentiate the perfect target from the single mismatch target. On the other hand, when the molecular beacons binds to its target, it undergoes a conformational change from a hairpin structure to an open structure. In this transition, hybridization of the target to the molecular beacon needs to be strong enough to open the stem structure of the probe. So even though the difference in the binding energy between the perfectly matched target and one single mismatch target is small, it can be differentiated by stem-and-loop structure probes, such as molecular beacons, in a much low temperature range compared to that required for the unstructured probe. The experiment evidence obtained from thermodynamic analysis showed that the nucleic acid probes with stem-loop structures had enhanced specificity compared to the non-structured linear nucleic acid probes (*119*).

The sequence and length of attenuator

The function of the attenuator in the TRAP is to prevent the natural folding of aptamer and to hold the aptamer in an inactive state until the TRAP is annealed with its target mRNA. The attenuator should interact with key residues of the aptamer. The attenuator should be adjusted to a length that will shield the aptamer binding activity totally in the absence of target mRNA and release the aptamer after the binding of the target mRNA. Too long or too short an attenuator will not function properly.

ALLOSTERIC NUCLEIC ACID MOLECULES

Artificial Allosteric Nucleotide Acid Molecules

Allosteric regulation was first recognized in enzymes involved in metabolism (*120*). Under allosteric regulation, the catalytic activity of an enzyme can be regulated by a small molecule called an effector. The binding site of the effector on the enzyme is different from the substrate's binding site. Binding to the effector induces a

conformational change of the enzyme that regulates the enzyme's activity by altering the structure or availability of the enzyme's active site.

The TRAP functions by allosteric regulation. The regulatory nucleotide sequence interacts with the antisense segment on the TRAP and this interaction regulates the aptamer's binding activity to its target through allosteric regulation. Allosteric regulation is also observed in other small non-coding nucleic acid sequences.

The broad and important functions of small non-coding RNA molecules in the cell have just begun to be fully appreciated in recent years. Because of the limited knowledge and awareness of the capabilities of natural small RNAs, allosteric nucleic acid molecules were first developed through rational design. Only more recently have many natural RNA sequences under allosteric regulation been discovered. There are three kinds of artificial allosteric nucleotide acids: allosteric ribozymes (aptazymes, maxizymes), allosteric deoxyribozymes and allosteric aptamers.

To this day, the hammerhead ribozyme is the most widely used for developing allosteric ribozymes. In 1995, an allosteric ribozyme activated by a single strand DNA (ssDNA) effector was created through rational design (*121*). In the inactive state, the RNA molecule containing ribozyme could not cleave its substrate. After the ssDNA effector hybridized withthe complementary RNA sequence on the ribozyme, the ribozyme was activated and the substrate was cleaved. In this case, strictly speaking, it was not a true allosteric ribozyme. The reason was that the sequence on the ribozyme with which the effector ssDNA interacted prevented the substrate from binding by base pairing with the substrate binding site. The effector ssDNA released the inhibition of ribozyme by forming a long stable helix with the sequence that occupied the substrate binding site. A later developed ribozyme-based TRAP is an actual allosteric ribozyme (*9*). In a hammerhead (HH) ribozyme TRAP, a 20nt polyAC sequence was used as the intervening sequence in the TRAP design to link the attenuator and HH ribozyme. By annealing to conserved bases in the catalytic core of HH ribozyme, the attenuator keeps the ribozyme inactive. Binding of RNA or DNA to the intervening sequence that links the ribozyme and attenuator frees the ribozyme

core to fold into an active conformation, even though the intervening sequence itself does not interfere with the ribozyme. HH ribozyme TRAPs were shown to be activated more than 250-fold upon addition of the regulatory RNA oligonucleotide (*9*).

In another approach to developing an allosteric ribozyme, an aptamer is linked to the ribozyme to provide allosteric regulation by the ligand of the aptamer. This kind of aptamer-ribozyme hybrid is named as "aptazyme" or "maxizyme". An allosteric aptamer-hammerhead ribozyme was developed in 1997 by Jin Tang and Ronald Breaker using ATP as the effector molecule (*122*). They linked an ATP RNA aptamer to a hammerhead ribozyme through a designed linker. Through rational design, different linker sequences were found that resulted in ribozymes with catalytic activity inhibited or activated by ATP. In the allosteric ribozyme with cleavage activity inhibited by ATP, the cleavage rate of ribozyme was reduced by 180 fold in the presence of ATP. Allosteric regulation is realized in the aptazyme by interaction between the aptamer domain and stem I of the hammerhead ribozyme (*123*). The secondary structure of the hammerhead ribozyme forms three stems. Stem I and III are formed by annealing with the substrate. The ATP RNA aptamer was linked with the ribozyme to form an aptamer-ribozyme hybrid through stem II. In the active form of the ribozyme, stem II and stem I form a certain angle. After the aptamer domain was linked to the ribozyme through stem II, stem I and stem II could still form the required angle for the ribozyme to be active. The reason is that in the absence of its ATP ligand, the RNA ATP aptamer does not form a rigid and homogenous secondary structure (*124*). The lack of a defined structure in the ATP RNA aptamer without its ligand leaves the ribozyme active. Upon the binding of ATP to the aptamer, the aptamer and ATP now have a more rigid and uniform structure (*125*). This structure prevents the stem II and stem I from reaching the relative spatial position required for activity of ribozyme. By altering the spatial position of the target RNA relative to the active site of the ribozyme, ATP complexed with the aptamer portion of the aptazyme is able to inhibit the activity of the ribozyme.

The stability of stem II of the hammerhead ribozyme is important for ribozyme catalytic activity. By increasing the length of stem II, the ATP-aptamer domain and stem I will be far enough apart that the ATP-aptamer domain does not prevent stem II and stem I from forming the angle needed for ribozyme activity. If non-Watson-Crick base pairs are introduced into stem II then, in the absence of ligand, the loop structure of the aptamer will destabilize stem II. After ATP is bound by the aptamer, the ATP-aptamer domain has a uniform and stable structure and stabilizes stem II to support the ribozyme's activity. In this way, the aptamer-ribozyme hybrid that is catalytically activated by ATP was developed (*122*).

Through rational design, many other allosteric ribozymes have been developed. An FMN (flavin mononucleotide) RNA aptamer was attached to a hammerhead ribozyme through stem II (*126*). As described previously, when stem II is short (4bp), the ATP aptamer binds ATP and inhibits the ribozyme activity by spatial interference. But if the ATP aptamer is replaced by the FMN RNA aptamer, the situation is changed. When the FMN aptamer binds to its ligand-FMN there is no spatial interference that requires a longer stem II as for the ATP aptazyme. The reason is that the tertiary structure of FMN aptamer with its ligand is different from the ATP aptamer with its ligand. With only 3 bp in stem II, the FMN aptamer-ribozyme hybrid is positively regulated by FMN. Without FMN, the short stem II cannot form the stable structure that is necessary for activity of the hammerhead ribozyme. The structure of the FMN aptamer without its ligand is also heterogenous, which is similar to the ATP RNA aptamer (*75, 126*). Upon the binding of FMN by the FMN aptamer, the structure becomes more rigid and homogeneous. This conformational change in the FMN aptamer due to FMN binding makes stem II much more stable. The increase in the stability of stem II results in an increase in the catalytic activity of the hammerhead ribozyme.

The combination of rational design and combinational selection has resulted in the development of many allosteric ribozymes. In combinatorial selection, a region in an RNA molecule containing the ribozyme is randomized. Usually an allosteric selection

is performed by applying negative selection first, followed by positive selection. For example, in the allosteric selection of an effector-activated allosteric ribozyme, the RNA molecule that is active in the absence of the effector molecule will be eliminated by negative selection. After negative selection, the effector molecule is added to the RNA pool and the RNA effector molecules are added to activate the ribozyme. The active molecules are separated from others by a partition method such as denaturing polyacrylamide gel and then amplified by RT-PCR. Breaker and colleagues applied allosteric selection to the hammerhead ribozyme and generated a ribozyme with catalytic activity that is regulated by the second messengers cGMP and cAMP (*127*). In this selection, the linker region was not randomized. Instead, a 25nt randomized region replaced the FMN aptamer sequence in the allosteric FMN-hammerhead aptazyme. The linker region was unchanged from that in the FMN-hammerhead aptazyme. The RNA pool was put through allosteric selection and RNAs isolated from this pool exhibited a 5,000 fold increase in ribozyme activity upon addition of cGMP or cAMP.

Other ribozymes than the hammerhead ribozyme, like the ribozyme ligase, were also used to develop three different allosteric ribozymes activated by the small effector molecules: ATP, theophylline and FMN, respectively (*128*). DNA enzymes activated by ATP have also been created by fusing the ATP DNA aptamer with deoxyribozyme ligase (*129*). In table 1, the allosteric ribozymes thus far developed *in vitro* are summarized.

Most allosteric ribozymes developed so far are activated by a small effector molecule. Although the detailed mechanism of allosteric regulation is different for each allosteric ribozyme, in general the attachment of the effector binding module (the aptamer) inhibits the catalytic activity of ribozyme through direct base pairing or indirect destabilization of the structure needed for activity. After the aptamer binds to its effector molecule, the inhibition is released and the ribozyme is activated.

Fewer allosteric aptamers have been created through rational design and *in vitro* selection than allosteric ribozymes. In table 2, the artificial allosteric aptamers so far

developed are summarized. The development of allosteric aptamers has usually been done by rational design combined with allosteric selection. Even though allosteric selection has greater potential to produce a molecule with the required properties, rational design is still very efficient.

An example of an allosteric selection procedure was carried out to select an allosteric RNA aptamer that binds to the DNA repair enzyme, formamidopyrimidine glycosylase (Fpg) in the absence of neomycin but dissociates from Fpg upon the addition of neomycin (*130*). In the first six rounds of selection, urea was used in the elution buffer to elute any RNA that bound to the Fpg, which was captured on filter paper. Starting with the seventh round, neomycin was used to elute the RNA from the filter paper. This produced an aptamer that binds to Fpg but dissociates from Fpg upon the presence of neomycin. Structural probing of this aptamer indicated that the binding site for neomycin on the RNA aptamer and the binding site for Fpg on the selected RNA aptamer overlapped. This overlap makes neomycin a competitor for the binding of Fpg. Strictly speaking, this regulation is not allosteric regulation because neomycin acts as a competitive inhibitor of Fpg binding to the aptamer. The aptamer has a higher affinity for neomycin compared to Fpg, which explains why neomycin could make the aptamer dissociate from Fpg. Even though this regulation is not allosteric, the aptamer's activity is still regulated by a small effector molecule, in this case neomycin. The success of this regulation indicates that it is possible to design and select an aptamer that is under allosteric regulation.

Malachite green (MG) undergoes a fluorescence change upon binding to its RNA aptamer. Free MG has a maximum absorbance at 617nm but does not fluoresce because the absorbed energy can be relieved through vibrations. After MG is bound by its RNA aptamer, the absorbing maximum moves to 630nm and the quantum yield of MG increases up to ~2,000 fold (*131*). The secondary structure of the malachite green aptamer (MGA) includes a 6bp stem I that is formed by the 5' and 3' end, followed by a bulge loop closed by a 4 bp stem (stem II) with a hairpin loop. The binding site for MG lies in the bulge loop. The 6bp stem I and 4bp stem II at the two

ends of bulge loop provide the stability needed for binding MG. By varying the length and composition of stem I and II, the overall stability of the MGA can be increased or decreased. Furthermore, if the hairpin loop is removed and another aptamer is adjoined through stem II, the stability of MGA module in the aptamer-aptamer hybrid can be regulated by the attached aptamer. Taking this strategy of rational design, Stojanovic *et al* (*132*) developed a modular aptameric sensor by joining the truncated MGA module with ATP DNA , FMN RNA or theophylline RNA aptamer (ATPA, FMNA or THA). In the absence of their small aptamer ligand, the ATPA, FMNA and THA do not have homogenous and rigid structures, especially at the region connecting with the MGA module through short stem II. When it binds its ligand molecule, the aptamer ligand-induced conformation change provides a stem structure in the connecting region. With this structural help from the aptamer, the stem II now becomes stable enough to support binding of MG by the MGA module with the result that a fluorescence increase will be observed. The best sensor of the three constructs prepared by this group is the MGA-FMNA which has about 30-50 fold increase in the fluorescence upon the addition of MG.

Recently, allosteric ribozymes regulated by binding to oligonucleotides were successfully developed by computational design and validated by experiments (*28*). Folding of nucleic acids is mainly guided by Watson-Crick base pairing for which thermal dynamic parameters for base pairing are well determined from experimentation. This makes a solid base for computational prediction of the secondary structure of RNA and ssDNA. Using the RNA secondary structure prediction method developed based on equilibrium partition function as described by McCaskill (*133*), Breaker and Penchovsky designed four different kinds of allosteric ribozymes with AND, YES, OR and NOT boolean logical functions (*28*). The computational design process began with inserting a short (16-22nt) random segment into the hammerhead ribozyme. The position of insertion of random segment was carefully chosen based on the previously developed allosteric ribozymes through rational design and allosteric selection (*122, 123, 127, 134-136*). The computer generated all possible sequence combinations. For example, a 22nt random region on the ribozyme will represent 10^{13} different sequences.

Each sequence was folded by software and the base pairing probability of each nucleotide on the sequence was calculated. By applying the criterion that a certain number of bases within the random region must pair with bases in the ribozyme catalytic core, sequences not matching this criterion were discarded. In the first selection process the random region on each sequence was allowed to freely pair with other bases in the sequence. After the first selection process the random region was not allowed to base pair with any other nucleotide in the sequence by including an effector ssDNA complementary to the random region which would form a stable duplex. Under this restricted condition, each sequence from the first selection was folded again and the sequences matching the applied criterion were kept.

The two stage selection process generated sequences that folded into different secondary structures with *vs.* without effector ssDNA. If one structure was set to deactivate the ribozyme and the other was fully active, the effector ssDNA regulated the ribozyme activity.

The next selection criterion was that the free energy gap between the structures with and without effector ssDNA must be larger than -6 and less than -10 $kcal.mol^{-1}$. This gap allowed the structure without effector ssDNA to be stable enough and at the same time, it was not too stable that it could not be overcome *via* the energy of the effector ssDNA binding. The final selected sequences were verified through experiments to behave as allosteric ribozymes with activity regulated by effector ssDNA. All four kinds of selected allosteric ribozyme showed >1000 fold difference in activity upon the addition of the effector ssDNA.

Combining computational design with modular rational design opens up an exciting new approach for the development of allosteric nucleotide acid molecules. We can anticipate more advances in the field of developing of artificial allosteric nucleic acid molecules in the future.

Riboswitches; Natural Allosteric Nucleic Acid Molecules

The word aptamer appeared as a description of an artificial nucleic acid molecule selected through the process of SELEX. More than ten years after SELEX was first introduced in 1990, the first example of an mRNA element that controls genetic expression by metabolic binding was discovered in bacteria (*137*). It turns out that Nature utilizes the binding capacity of nucleic acids to regulate transcription and translation. The natural allosteric nucleic acids that exist as mRNA elements and regulate transcription or translation were called 'riboswitches'. A riboswitch usually contains two parts: one is the binding module, which is a natural aptamer module that binds small molecules, the other is an expression platform that transmits the effect of the binding event to transcription or translation. To date, the majority of riboswitches have been found in bacterial RNAs. There are very few riboswitches yet found in the eukaryote. These are the mRNA elements in fungi and in plants that match the consensus sequence and structure of thiamine pyrophosphate-binding domains of prokaryotes (*138, 139*). In table 3, the riboswitches and their roles in regulation of bacterial metabolism are summarized.

Regulation by a riboswitch of transcription and translation is unique in the sense that the process does not need any protein factors or tRNA. The riboswitch can utilize the structural change that occurs upon the binding of its ligand, usually a small metabolic molecule, to influence the interaction between mRNA and the transcriptional termination and/or translation complex. The riboswitch acts as a natural allosteric nucleic acid module of the mRNA that responds to the concentration of a small metabolite in the cell. Through these natural allosteric nucleic acid modules, the cell adjusts the metabolic pathway involving the riboswitch ligand.

In the thiamine pyrophosphate(TPP)-sensing riboswitch in Gram positive bacteria, the thiamine genes are negatively controlled by thiamine and TPP. In the absence of TPP, the *thi*-box in the 5'UTR of *thi* operon participates in the structure of an anti-terminator. Transcription continues in the absence of TPP. After TPP is bound by the *thi*-box, the anti-antiterminator and terminator both form and transcription is shut down.

This terminator—antiterminator—anti-antiterminator system is widely used in riboswitches that control transcriptional termination in both Gram positive and Gram negative bacteria. Flavin mononucleotide(FMN)-sensing, adenosylcobalamin-sensing and hypoxanthine, guanine-sensing riboswitches in Gram positive bacteria, S-adenosyl-methionine-sensing and lysine-sensing riboswitches in Gram positive and Gram negative bacteria all utilize the terminator—antiterminator—anti-antiterminator configuration in the 5'UTR of mRNAs to regulate transcriptional termination of specific genes.

Besides transcriptional termination, riboswitches can also control translational initiation. In most cases, riboswitches inhibit translational initiation upon binding to their metabolic ligands. For example, in *E.coli*, the flavin mononuleotide-sensing riboswitch (*rfn*-box) participates in a stem loop structure in the absence of FMN that excludes the Shine-Dalgarno (SD) sequence. Thus, the ribosome is able to recognize the SD sequence and begin translation. Upon binding to FMN, the FMN-sensing riboswitch changes its secondary structure and a new stem-loop structure is formed in which bases in the SD sequence base pair and participate in a double stranded stem structure. Because the SD sequence is part of the double stranded stem after FMN has bound, the ribosome can no longer recognize it and translational initiation is inhibited. The TPP-sensing riboswitch in Gram negative bacteria employs a similar strategy to the FMN riboswitch to inhibit translational initiation.

Riboswitches can be not only allosteric aptamers but also allosteric ribozymes. In Gram positive bacteria, one riboswitch with a self-cleaving ribozyme activity has been discovered (*140*). Located in the 5'UTR of *glmS* (glutamine-fructose-6-phosphate amidotransferase) mRNA, the metabolite-responsive ribozyme element binds glucosamine-6-phosphate (GlcN6P) and self-cleaves. The gene *glmS* encodes an enzyme participating in GlcN6P synthesis. The ribozyme activity of this riboswitch requires the present of GlcN6P. Without binding to GlcN6P, the ribozyme self-cleavage activity is inhibited though folding into an inactive conformation. Upon binding to GlcN6P, a ligand-induced conformational change releases the inhibition and the

ribozyme becomes active. It is not clear how cleavage of *glmS* mRNA leads to the reduction of gene expression. It was speculated that the truncated mRNA was targeted for degradation by RNases or the translation of truncated mRNA was inhibited.

So far, all but two of the known riboswitches inhibit translation upon binding the metabolite of the regulated metabolic pathway. One of the two known riboswitches that activate gene expression is the adenine riboswitch found in *Bacillus subtilis*. Upon binding to adenine, the adenine riboswitch prevents the formation of a premature transcriptional terminator in the *ydhL* (also know as *pbuE*) mRNA (*141*). In this case, the adenine riboswitch acts as an activator to suppress premature transcriptional termination. The second example of a ribozyme that is an ON switch is the glycine-dependent riboswitch discussed next.

Recently, a riboswitch has been found that binds to its ligand cooperatively (*142*). The glycine-dependent riboswitch found in *gcvT* operon in *Bacillus subtilis* consists of two similar glycine aptamers structurally linked by a short linker. The striking features of this glycine-sensing riboswitch are the short aptamer sequence and the cooperative binding to glycine. The length of aptamer structure is only 10nt, which is not common in aptamers produced through SELEX even after they have been reduced to their minimum effective length. After binding to the first glycine by one aptamer, the affinity of the other aptamer to the glycine increases about 1,000 fold. This is the first known natural nucleic acid molecule that binds to its ligand cooperatively. It was shown both *in vitro* and *in vivo* that upon binding to glycine, the glycine-dependent riboswitch activates transcription of the gcvT operon in *Bacillus subtilis* (*142*). So, this makes the glycine-dependent riboswitch also an 'ON' switch.

Riboswitches are also found in fungi and plants where they appear to regulate splicing (*138, 143*). Through genomic and bioinformatics methods, we can anticipate that more and more natural allosteric nucleic acid elements will be discovered in a wide range of organisms.

SELECTION *IN VIVO*

The power of SELEX procedure lies in its simultaneous access to a huge number of different sequences through random sequence pools combined with exponential amplification of the desired sequences by PCR. These two steps limit the use of SELEX procedure *in vivo*. To express the random pool *in vivo*, cloning and expression vectors need to be used. This reduces the possible complexity of the pool significantly because of the practical considerations of the mass of the pool and the number of individual cells that can be used in the selection. Also it limits the choice of the nucleic acid to RNA. To do SELEX *in vivo*, the broad range of target choice is lost compared to SELEX *in vitro*. Molecules that are toxic to the cell or molecules that can not easily enter the cells are not good targets for SELEX *in vivo*. So far, most *in vivo* related combinatorial selection has been done to target proteins.

The yeast two-hybrid system is a combinatorial method for probing protein-protein interactions (*144*). Using the yeast two-hybrid system as a starting point, the yeast three-hybrid system was created to select aptamer and allosteric nucleic acid molecules (*145-147*)}. SenGupta et al. (*148*) created the yeast three-hybrid system to detect RNA-protein interactions *in vivo*. The yeast two-hybrid system has two fusion proteins: one has a DNA binding domain (BD) to provide the ability to bind the enhancer element of the reporter gene, the other has activation domain (AD) to activate the transcription of reporter gene. Each protein or protein pool for which interaction will be tested is fused with BD and AD, respectively. Interaction between the proteins of interest is verified by expression of the reporter gene. In the three-hybrid system, the protein fused with BD is the MS2 coat protein. The MS2 coat protein binds to MS2 RNA elements with very high affinity. The protein of interest is fused with AD. The RNA molecule of interest is fused with the MS2 RNA elements. The RNA of interest could be a single sequence or a random sequence pool. Interaction between the RNA and protein of interest is verified by expression of the reporter gene. So, the yeast three-hybrid system is a modified version of the yeast two-hybrid system and was specifically designed to detect RNA-protein interactions.

An RNA decoy that binds NF-κB and inhibits its transcriptional activation activity was selected using the yeast three-hybrid system. An early-round *in vitro* NF-κB aptamer SELEX pool was cloned into a yeast vector and the RNA pool was expressed in yeast. After optimization and selection through the three-hybrid system, an RNA molecule that interacts with NF-κB *in vivo* was obtained.

Recognition by the NF-κB aptamer of its target- NF-κB was verified through the yeast three-hybrid system *in vivo* (*145*). The yeast system was also used to select an RNA element with a transcriptional activation function (*146*). The random RNA library was cloned into a yeast expression vector in which the expressed RNA was fused with MS2 RNA element. The RNA element that could activate transcription of the reporter gene was selected through the yeast selection system. The RNA-based transcriptional activator selected through this *in vivo* evolution could activate expression without the protein factor. The fold increase upon the activation by this RNA transcription activator was comparable with the most powerful protein transcription activator (*146*). The detailed mechanism of the transcription activation by this RNA transcription activator is still unknown. However, by linking the RNA-based transcription activator to the malachite green aptamer through a randomized linker region, an allosteric RNA transcription activator was then selected using the yeast *in vivo* selection system (*147*). Transcriptional activation by the selected allosteric RNA molecule was regulated by tetramethylrosamine (TMR), a ligand of the malachite green aptamer. TMR stabilizes the helical region of the aptamer that is required for transcription activation and a 10-fold increase in transcription activation was obtained.

An *in vivo* SELEX procedure was also developed to reveal the critical elements on exons that define alternative splicing (*149*). In higher eukaryotes, alternative splicing of pre-mRNA has an important role in gene regulation. During alternative splicing, the pre-mRNA with multiple exons goes through different splicing processes. One or more exons are skipped for certain transcripts. In order to identify the cis-element in the particular exon that determines whether it will be kept or skipped, the exon of interest was partially or totally randomized. The random pool was cloned into an expression

vector and *in vivo* transcription of pre-mRNA was achieved after transfection. After splicing in the cell, the remaining exon sequence was amplified by RT-PCR. Then it was cloned into the same expression vector to go through *in vivo* SELEX again (*150*). This *in vivo* selection process is much more like the *in vitro* SELEX process than the yeast three-hybrid system. The surviving sequences after each round are preserved and amplified through RT-PCR. The only difference from the *in vitro* sequence was that selection was carried in the cell. This allowed the selection pressure to include the preservation of *in vivo* function as a requirement for the surviving sequences.

APTAMER APPLICATIONS

As a molecule selected to bind its target with high affinity and specificity, the aptamer has been used for a broad range of applications. People naturally compare the aptamer with an antibody because the antibody has dominated the field of detection, imaging and inhibition of target protein molecules. Is it really necessary to develop aptamer-based application techniques? Especially to the protein targets, what is the advantages of an aptamer over an antibody? In table 4, the properties of aptamers and antibodies are compared. From this table, we can see that the aptamers are small and they can be made against a broader range of targets than can antibodies. The aptamer is much more easily modified compared to the antibody and its function is preserved after many different modifications. Once the sequence of an aptamer is determined, chemical synthesis can guarantee a consistent quality of the aptamer. It is not like an antibody, that will change from batch to batch unless it is monoclonal. The target of an aptamer could be any molecule or complex, such as a whole cell or even a tissue. Because the aptamer has great potential to outrun the antibody in many applications, the development of aptamer-based techniques have been growing rapidly.

Bio-sensors and Imaging Applications

An RNA aptamer that targets the Tat protein of HIV was selected and shown to inhibit Tat-dependent trans-activation of transcription, both *in vitro* and *in vivo* (*80*). Utilizing this Tat RNA aptamer, a molecular beacon aptamer that fluoresces in the present of the HIV Tat was created (*151*). The Tat RNA aptamer has a stem loop structure but the loop region is not essential for binding. After removing the loop region, two single stranded RNAs (A and B), each one of the two halves of the remaining aptamer, were synthesized, annealed and binding of the annealed RNAs to the Tat was confirmed by a gel shift assay. Furthermore, one RNA (A) was labeled with a fluorophore dye at the 5' end and a quencher dye at the 3' end and the RNA was designed to be able to form an internal stem loop structure in the absence of Tat. Therefore, in the absence of Tat, the fluorescence was quenched even though both

RNA (A and B) were present. In the presence of Tat, the A RNA undergoes a conformational change to form a duplex with RNA B. The fluorophore dye at the 5' end and the quencher dye at the 3' end of RNA A is separated and the fluorescence output is increased.

Signaling aptamers were also engineered by replacing the bases on an aptamer by fluorescent reporters (*152*). Many aptamers, such as the ATP aptamer, are believed to go though an 'induced fit' conformational change after binding to the target molecule (*124*). In the presence of adenosine, the engineered DNA and RNA ATP fluorescent reporter aptamers show increases in fluorescence that are presumably due to conformational changes induced by the interaction of aptamer and adenosine.

Blank *et al* used a FITC-^{18}C -conjugated DNA aptamer to visualize a rat brain tumor using fluorescence microscopy (*153*). The FITC-^{18}C -conjugated DNA aptamer could selectively bind to tumor micro vessels but not normal blood vessels. The theophylline-dependent allosteric ribozyme was also used to give fluorescence in the presence of theophylline (*154*). Here, the substrate of the ribozyme was modified to have a fluorophore in the 5' end and a quenching dye in the 3' end. Upon substrate cleavage in the presence of theophylline, the quencher dye was separated from the fluorophore and a 4-fold fluorescence increase was observed.

To develop a sensor for cocaine, thirty five dyes were screened for changes in spectrum upon adding cocaine to a mixture of the cocaine aptamer and a given dye. Thereby an aptamer-based colorimetric probe for cocaine was developed using the dye, diethylthiotricarbocyanine iodide, with the cocaine aptamer (*155*). In the presence of cocaine, an immediate attenuation in the absorbance of dye was observed.

The thrombin aptamer forms a loose random coil in the absence of thrombin. Upon binding to thrombin, the aptamer forms a compact unimolecular quadruplex. Labeling the aptamer with a fluorophore dye in the 5' end and a quencher dye in the 3' end creates a molecular aptamer beacon (*156*). Without thrombin, the two dyes were not close in space and the fluorescence was not quenched. In the presence of thrombin,

the two dyes were brought close together and the quencher dye quenched the fluorescence. Replacing the two dyes with a pair of dyes that participate in fluorescence resonance energy transfer gives a molecular aptamer beacon that increases in fluorescence in the presence of thrombin.

An RNA aptamer that targets the variant surface glycoprotein of African trypanosomes was selected using SELEX (*157*). Biotin-labeled RNA aptamer was used to image the live trypanosomes, which were visualized by Alexa Flour 488-conjugated streptavidin.

Modular aptameric sensors were developed utilizing the fluorescence increase that occurs after malachite green is bound by its RNA aptamer (*132*). Using rational design, the ATP RNA aptamer, theophylline RNA aptamer or flavine mononucleotide RNA aptamer, respectively were fused with the truncated malachite green RNA aptamer. The presence of adenosine, theophylline or flavine mononucleotide could be detected by an increase in the fluorescence of malachite green.

A signaling aptamer was designed to fluoresce in the presence of adenosine (*158*). Two short single stranded DNA (ssDNA) oligonucleotides were designed to interact with a ssDNA that includes the sequence of a DNA adenosine aptamer. One ssDNA oligo (FDNA) had a fluorophore at the 5' end and included the sequence of the DNA adenosine aptamer, the other ssDNA oligo (QDNA) had a quencher dye at the 3' end. QDNA is complementary to part of the FDNA and anneals with part of the DNA adenosine aptamer in FDNA. When they are annealed, the fluorophore on FDNA is adjacent to the quencher in QDNA so the fluorescence is quenched in the absence of adenosine. In the presence of adenosine, the DNA adenosine aptamer sequence undergoes a conformational change that separates the QDNA from the FDNA. Thus, the fluorescence increases upon adding adenosine. This signaling aptamer can also be used to detect ADP and AMP because the DNA adenosine aptamer also binds ADP and AMP.

Gold nanoparticals have distance-dependent optical properties that can be used to detect polynucleotides (*159*). A colorimetric sensor was created by combining the adenosine-dependent DNAzyme and gold nanoparticles (*160*). The adenosine-dependent DNAzyme cleaves its substrate in the presence of adenosine. Gold particles were cross-linked at a close distance by the substrate of the adenosine-dependent DNAzyme to form aggregates. The separated gold particles have a blue color that changes to red when they aggregate. In the presence of adenosine, the substrate of the DNAzyme is cleaved, the gold particles dispersed and the color of gold particles changes to reveal the presence of adenosine.

When the single stranded DNA thrombin aptamer binds to thrombin its conformation changes from a loose random coil to the compact G-quartet (*161*). Mario Leclerc and colleagues developed a water-soluble, positively charged polymer named "polymeric stain" that can transduce the binding of the DNA thrombin aptamer to thrombin into an optical signal (*162*). In the absence of thrombin, the polymer forms a duplex with the negative charged ssDNA thrombin aptamer. Upon addition of thrombin, the aptamer forms a compact structure. The polymer still interacts with the aptamer, but due to the conformational change of the aptamer upon binding thrombin, the optical signal of the polymer changes and it reflects the presence of thrombin.

Recently, a novel strategy was used to develop a small-molecule-based sensor (*163*). N-(p-methoxyphenyl) piperazine (MPP) was chemically synthesized to link with dichloro-fluorescein and form a new chemical with one dichloro-fluorescein and two MPP in one molecule. MPP quenches the fluorescence of dichloro-fluorescein. An RNA aptamer targeting MPP was selected through SELEX. Upon adding the MPP RNA aptamer, the fluorescence increased. The reason for the increased fluorescence is thought to be that quenching by MPP of the fluorophore is greatly reduced after the MPP is bound by the RNA aptamer . Thus binding by the aptamer results in a strong fluorescent signal from the MPP-linked dichloro-fluorescein.

DNA and RNA aptamers have also been successfully used to develop microarray assays to detect proteins (*38, 164-170*). Compared to the microarrays using antibodies

to detect proteins, aptamer arrays have been verified to have a similar level of specificity and sensitivity (*164*). An aptamer array can usually tolerate repeated washing and harsh denaturing conditions, which cannot be applied to an antibody array. This feature allows a nucleic acid array to be used many more times than an antibody array. Also, in the photoSELEX-based array, the washing conditions can be very stringent, which lowers the non-specific binding (*38*).

Analytical Applications

Aptamers hold great potential as analytical tools in molecular recognition and separation technologies (*13, 34, 171*).

Immobilized aptamers can be used to separate enantiomers (*172*). For example, a D-peptide was separated from an L-peptide by HPLC or through small columns containing an immobilized DNA aptamer selected specifically for binding to the D-peptide. In another study, an adenosine DNA aptamer was biotinylated and linked to streptavidin-glass beads. The resulting beads were used as the stationary phase in a packed capillary tube for liquid chromatography to monitor the adenosine levels in samples collected from the somatosensory cortex of chloral hydrate anesthetized rats (*173*). The results showed that the adenosine was strongly retained in the column and that it could be detected by UV absorbance. Moreover, the aptamer-based column showed good scalability after more than 200 injections.

Aptamers that recognize proteins have also been developed as probes to detect their target proteins. Murphy *et al.* (*174*) used the thyroid transcription factor 1 (TTF1) aptamer to purify TTF1. The TTF1 aptamer was biotinylated and attached to streptavidin magnetic beads. The affinity chromatography purification assay on protein mixtures from bacteria lysates showed good specificity for TTF1. A fluorescence-labeled aptamer targeting HIV type 1 reverse transcriptase was used in affinity capillary electrophoresis (*175*). HIV type I reverse transcriptase (HIV-1 RT) could be specifically detected in the affinity complex formed by aptamer and HIV-1 RT. Non-equilibrium capillary electrophoresis of equilibrium mixtures (NEC-EEM) was developed to detect

a protein using an aptamer that does not form a stable complex with its target protein (*176*). Aptamers also have been shown to work in affinity mass spectrometry (*171*). With the thrombin aptamer immobilized to the matrix surface thrombin was specifically detected through MALDI-TOF-MS.

Utilizing aptamers, an impressive method was developed to detect zeptomole (40 x 10^{-21} mol) amounts of platelet-derived growth factor (PDGF) without washes or separations (*177*). The method employed proximity-dependent DNA ligation to transduce the present of PDGF into a ligated a long single stranded DNA. DNA aptamers were designed to form the affinity probes. Because PDGF forms a homodimer one aptamer affinity probe will bind to each monomeric unit in the dimer, which brings the ends of the two probes close enough so that the T4 DNA ligase can ligate the two ends together in the present of a common connector. The resulting long ssDNA can be detected by real time PCR.

In vivo Applications of Aptamers

Aptamers are developed *in vitro* through SELEX. To apply ssDNA and RNA aptamers for *in vivo* application, the first challenge is the short half-life of natural nucleic acid in biological fluids. Tested *in vitro* in plasma, the half-life of a typical RNA molecule is about few seconds and a typical DNA molecule is about 30 to 60 minutes (*178*). During SELEX, 2'-fluoro, 2'-amino or 2'-O-alkyl nucleotides can be used to increase the stability of the resultant aptamer (*45*). Recently, 4'-thioUTP and 4'-thioCTP were synthesized and successfully used in SELEX (*49*). The half-lives of RNA oligonucelotides that are synthesized from these modified nucleotides are dramatically longer compared to the half-lives of the natural RNAs. In plasma, the *in vitro* half-life of modified RNA oligonucleotides was in the 5 to 15 hour range (*179*).

Many aptamers have been selected without using non-natural nucleotide triphosphates as substrates. Post-SELEX modification of aptamers has been widely used to improve not only the stability, but also the pharmacokinetics of these aptamers (*12, 180*). Some modifications are also needed for immobilization and signaling

purposes (*12, 180*). In table 5, the most often used post-SELEX modifications of aptamer for *in vivo* application are summarized.

In most cases, aptamers have been used as antagonists to their target molecules. For this kind of application, aptamers can be separated into two categories based on the target type. One is for extracellular targets and the other is for intracellular targets. Until today, most *in vivo* applications of aptamers have been done by targeting extracellular molecules, membrane marker molecules and whole organisms. All these targets could be considered as extracellular. For intracellular targets, the aptamer needs to be delivered across the cell membrane, which is still a difficult task today. This makes the extracelluar application of aptamers easier compared to intracellular application. In table 6, *in vivo* applications of the selected aptamers, which were used against extracellular targets, are listed. As shown table 6, in most cases, the purpose of *in vivo* applications of aptamers targeting the extracellular molecules was to inhibit the target protein by the aptamer. In several cases, the aptamer was used as an imaging tool.

An aptamer can function inside a cell whereas an antibody cannot. As it was in the extracellular application, an aptamer can act as an antagonist of its target protein. By inhibiting the target protein's function, the aptamer could be used to determinethe biological function of natural cellular proteins. Inside the cell, many RNA-protein complexes, such as ribosomes and spliceosomes, fulfill important biological functions (*181*). Intracellular aptamers can be used as a decoy to interact with the RNA-binding proteins to reveal the important structural elements on natural RNA transcripts as well as on RNA-binding proteins. A riboswitch is a natural aptamer sequence located in the 5' or 3' UTR of mRNA transcripts to regulate transcription or translation processes. By mimicking the functions of riboswitches, aptamers can be inserted into the 5' or 3' UTR of the expressed genes' transcripts to regulate transcription or translation. For biomedical applications, aptamers can be used to inhibit the disease-related targets as well as to image cells. Aptamers binding intracellular targets were used to inhibit human immunodeficiency virus (HIV) type I (HIV-1) infection (*182, 183*) . An

oligonucleotide encoding a 33nt pseudoknot RNA aptamer selected *in vitro* for targeting an HIV-1 reverse transcriptase (RT) was cloned into a retroviral vector between mutant tRNA gene and a polymerase III termination signal (TER) (*182*). The tRNA-aptamer transcripts generated by the polymerase III were found in the cytoplasm after being transiently expressed in various human cell lines. In the human 293T cell that wereco-transfected with a tRNA aptamer expression vector and a proviral HIV-1 DNA, HIV particle release was inhibited by more than 75%. The viral particles derived from the transfected 293T cells were used to infect human T-lymphoid C8166 cells that also expressed chimeric tRNA-aptamer RNA. The subsequent viral production was inhibited by more than 75% compared to the controls (*182*).

In another study done by Joshi *et al.* (*183*), aptamers and small hairpin RNAs (sh RNAs) directed against HIV-1 RT was compared for blocking HIV-1 replication in the cell. Oligonucleotides encoding the aptamer and the shRNA were cloned downstream of an RNA pol III driven U6 promoter in the MMP-eGFP retroviral vector, respectively. To produce the desired aptamer sequence after transcription, the aptamer was cloned along with a flanking, self cleaving ribozyme at both 5' and 3' end. GFP on the retroviral vector was used to selected cells that had been transduced by the retroviral vector. The transduced CEMX 174 cells was challenged by the HIV virus. The results showed that the aptamer decreased the levels of the early RT products by about 86-96% as early as 2 h after infection, whereas the shRNAs had about 42-62% inhibition of the same early RT products. The aptamer efficiently inhibited HIV replication at the higher multiplicities of infection. By contrast, although the shRNAs could inhibit HIV-1 replication as efficiently as the aptamers at low viral input, they did not block HIV at the high viral input as the aptamers did. Due to the encapsidation of aptamers into the virion particles, aptamers were able to inhibit two consecutive rounds of reverse transcription of HIV-1virus. Using an RNase protection assay (PRA), about 52% to 85% of aptamer RNAs and shRNAs were found present in the cytoplasm (*183*).

Recently, a study of RNA aptamers targeting an intracellular protein and inducing cell killing was demonstrated in *C.elegans* (*184*). Through *in vitro* SELEX five RNA

aptamers targeting the *C. elegans* Bcl-2 homolog CED-9 with high affinity and specificity were selected. Two of the five selected aptamers were shown to bind CED-9 inside the cell. Over-expression of either of the two aptamers in six touch receptor neurons in *C.elegans* induced efficient killing of these neurons. Several examples listed above are examples of the most recent developments of *in vivo* applications of aptamers targeting intracellular proteins and inhibiting the targets as an antagonists. In the study done by Hu et al. (*185*), *in vitro* SELEX-derived aptamers were used to distinguish critical and non-critical residues for the initiation of reverse transcription in the duck hepatitis B virus (DHBV). A plasmid encoding the complete genome of DHBV was used to test the interaction between DHBV reverse transcriptase and the selected aptamers recognized by DHBV reverse transcriptase. Different aptamer sequences were cloned into the DHBV genome reverse transcriptional initiation site. Plasmids with different aptamer sequences in the genome were transfected into LMH cells, respectively. The cells were harvested 4 days later and the successful replication of virus was verified from cell lysates. The critical consensus sequence for binding reverse transcriptase and supporting viral replication was identified from comparison of the ability of each aptamer to promote replication. This showed the diversity of intracellular applications of aptamers and that they are not necessarily only useful as antagonists.

Another way for an aptamer to function inside the cell is for it to behave as a regulatory element to control the expression of genes. For example, the RNA aptamer that targets the HIV RT was cloned into a position adjacent to the Shine-Dalgarno (SD) sequence of the lacZ gene in *E. coli*. In the presence of the HIV RT protein, the aptamer bound to the expressed HIV RT and blocked access of the 30S ribosomal subunit to the SD sequence of LacZ gene. In the absence of the HIV RT the expression of lacZ was normal (*186*). The translational initiation of bacteria requires base pairing interaction between the SD sequence and 16S RNA in the 30S ribosome subunit. After the aptamer bound to its ligand, RT, the access to the SD sequence was blocked by steric hindrance and expression of lacZ was inhibited (*187*). Following a similar strategy, ligand-regulated translation was also realized in eukaryotes (*188*). In

the Cap-dependent translation of eukaryotic mRNAs, after 40S ribosomal subunit binds to the cap structure, it begins to scan along the 5' UTR sequence and the translation is initiated at the AUG start codon. By inserting three copies of a tobramycin aptamer or kanamycin A aptamer into the 5' UTR of reporter gene, the expression of a reporter gene was regulated by the aptamer's target. In the presence of 60 μM target molecule, more than 90% expression of reporter genes were inhibited compared to the controls (*188*). In the following studies, three copies of an antibiotic aptamer in the 5' UTR of reporter gene was replaced by three copies of an aptamer selected to bind two related Hoechst dyes, H33258 and H333342. The two Hoechst dyes were used because they were permeable to the cells and were not toxic. Ligand dependent translational regulation was observed in wheat germ extracts and in Chinese hamster ovary (CHO) cells that were transfected with DNA encoding the lacZ gene bearing 3 copies of the aptamer to Hoechst dyes in the 5' UTR (*188*).

The malachite green (MG) RNA aptamer was selected by SELEX for use in RNA-chromophore-assisted laser inactivation (*189*). By inserting the MG RNA aptamer before the AUG of a cyclin transcript in *S. cerevisiae*, translation of a modified cyclin transcript was regulated by tetramethylrosamine (TMR, *190*). TMR is a structural analog of MG with an oxygen to bridge two of the benzyl rings. Studies showed that the affinity of the MG RNA aptamer for TMR is more than ten times higher than its affinity for MG (~ 40nM to 800nM, *191*). In the absence of TMR, translation of the modified cyclin transcript was not inhibited. In the presence of TMR, the MG RNA aptamer-ligand complex in the 5'UTR of cyclin transcripts was stable enough to inhibit translation of cyclin by more than 90%. Another example of how a MG RNA aptamer and TMR can work *in vivo* was by engineering a TMR-dependent transcription activator through *in vivo* selection in *S. cerevisiae* (*147*). The transcriptional activation activity of the engineered RNA molecule increased 10-fold in the presence of TMR.

A more detailed description and summary of the extracellular as well as intracellular applications of aptamers can be found in several reviews (*12, 14, 178, 192*). There are still many obstacles on the way to successful application of aptamers in the challenging

biological environment, both extracellular and intracellular. For example, to this day, delivery is still a bottle neck for the successful application of aptamers in the intracellular environment. There are two ways to deliver aptamers into cells. One way is by an expression vector. The second delivery route is microinjection, electroporation or transfection reagents such as liposomes. Both of them are applied in cell culture and do not have guaranteed high efficiency *in vivo*. There is still a long way to go for systematic delivery of aptamers to the living organism and specific targeting to desired organs or tissues. At the same time, there are safety and ethical challenges for further applications in drug development and therapeutic application. We can expect further developments in this field and more aptamers for *in vivo* applications.

Therapeutics

At the end of 2004, the Food and Drug Administration approved the first aptamer drug 'Macugen" (pegaptanib sodium injection, by Pfizer and Eyetech). (http://www.fda.gov/bbs/topics/news/2004/new01146.html). This is a breakthrough in the application of aptamers in therapeutics. The drug Macugen, developed to recognize the $VEGF_{165}$ aptamer, is also called NX1838 or pegaptanib sodium. The $VEGF_{165}$ aptamer is a potent angiogenesis inhibitor and is used to treat age-related macular degeneration (AMD, *96, 193*). During its development, the aptamer underwent several modifications to improve its stability. The aptamer is 27nt and includes 2'fluoro pyrimidine and 2' O-methyl purine modifications to protect it against endonucleases. Also, the 5' end was modified with polyethyleneglycol and a 3' dT was attached through a 3'-3' linkage. All these modifications makes the final drug more stable *in vivo* and to also have better pharmacological kinetic properties in treating AMD in humans (*194*).

Aptamers are being developed as therapeutics in the areas of anti-microbials, anticoagulation, anti-inflammation, antiangiogenesis, antiproliferation, and immune therapy (reviewed in *14, 15, 16*). For example, the aptamer that inhibits HIV replication has entered clinical trials (*195*). Another anti-thrombin aptamer is being developed as

an anticoagulant for use in the coronary artery bypass surgery (http://www.archemix.com/press/pr_jun04.html).

DETECTION AND IMAGING OF RNA IN LIVING CELLS

In 1982, Cech *et al.* (*196, 197*) reported the first catalytic RNA or ribozyme: the self-splicing intron of the *Tetrahymena* pre-rRNA. Over the past twenty years more and more research discoveries that describe the functions of RNAs in biological processes have begun to reveal more fully the kingdom of RNAs hiding from the central land. Now we know RNAs not only play the role of messengers (mRNAs, tRNA) to convey and interpret genetic information stored in DNA, but also have an essential catalytic activity as well as providing a structural basis for the molecular complexes that regulate gene expression (ribosome, spliceosome). Recently, small non-coding RNAs were found to participate in the regulation of gene silencing (siRNAs, microRNAs). The expression levels and stabilities as well as the temporal and spatial distributions of specific RNAs in a cell are directly related to their functions. In order to fully interpret the biological mechanisms of RNA molecules in fulfilling their functions, the dynamics and localization of RNA molecules in the living cell must be understood.

Using purified DNA or RNA samples obtained from cell lysates, gene expression levels can be measured by many *in vitro* methods. An early method used to detect the level of gene expression was Northern blotting (*198*) where RNA is first separated by electrophoresis and then transferred onto a membrane. Labeled nucleic acid probes are applied to the membrane and hybridized with the membrane containing the RNA. Besides Northern blotting, labeled oligonucleotide probes are also used to in *in situ* hybridization to detect intracellular mRNA (*199*). In the process of *in situ* hybridization, the cell are fixed and detergent is used to permeabilize the cells. Fluorescent- or radio-labeled probes are applied to the permeabilized cells and unbound probes are removed by washing. The sites of hybridization between labeled probes and target RNA molecules can be visualized by microscopy.

Without any amplification of target RNA molecules, labeled probes have limited sensitivity. Polymerase chain reaction (PCR) is most widely used to amplify the targets (*200, 201*). In the case of target RNA molecules, reverse transcription is first used to generate a ssDNA from the RNA target. The ssDNA can be amplified in a PCR

reaction (RT-PCR). Guatelli *et al.* (*202*) introduced the method named nucleic acid sequence based application (NASBA) to amplify rare RNA target molecules. During NASBA, the T7 promoter sequence is attached to the cDNA by reverse transcription (RT). The T7 RNA polymerase is then used to generate RNA target molecules. Because the newly synthesized RNAs serve as the templates for a subsequent RT and newly synthesized ssDNA serves as a template for PCR after RT, this method can amplify low copy rare target molecules. It was reported that one copy of RNA molecule can be amplified to 10^9 copies in a NASBA reaction in 90 mins (*203*). After RNA target molecules are amplified, they can be detected as dsDNA by gel electrophoresis or by hybridization with labeled nucleic acid probes.

There are several other *in vitro* methods for identifying RNA target molecules. Expressed sequence tags (ESTs) is a method for the rapid characterization of expressed genes by partial DNA sequencing. An EST is produced by one-shot sequencing of a cloned mRNA, and the resulting sequence is a relatively low quality sequence of a fragment whose length is approximately 500 to 800 nucleotides. ESTs are useful tools in gene discovery and sequence determination. Some recently developed *in vitro* methods for identifying RNA target molecules include serial analysis of gene expression (SAGE) (*204*), differential display (*205*), and DNA microarrays (*206*). Along with the rapidly increasing knowledge of genomic sequences for many organisms, the *in vitro* methods mentioned above enable fast, accurate and systematic detection and quantification of RNA targets in the cell. But these *in vitro* methods can not provide temporal and spatial information about the RNA target in the cell, especially in the living cell.

Methods for imaging the nascent transcripts in the living cells by incorporating Br-UTP (*207*) or FITC-CTP (*208*) into RNA transcripts by RNA polymerases I , II and III label all mRNAs in general and can not be applied to specific RNA species. To image a specific RNA inside living cells, fluorescence-labeled RNA molecules synthesized by *in vitro* transcription reactions can be microinjected into the cells (*209-211*). But this method can not be applied to the endogenous RNA molecules.

Using GFP as a reporter, an indirect method for imaging a specific RNA in living cells was created. Bertrand *et al.* (*212*) made a construct from Ash1 mRNA was expressed that included an insertion of six tandem copies of the stem-loop binding site for the bacteriophage MS2 coat protein. A second construct encoded the MS2-GFP fusion protein containing a nuclear-localization signal. When the two constructs were co-expressed in cells, the MS2-GFP fusion protein bound to the MS2 binding sites on the chimeric Ash1 mRNA. After chimeric Ash1 mRNA was synthesized in the nucleus, it was found to co-localize with the particles that had fluorescence emitted by GFP. By tracking the fluorescence of GFP, the movement and localization of particles in which chimeric Ash1 mRNA molecules were associated with other proteins related to the transportation and localization of Ash1 mRNA could be traced and observed in the living cells. This strategy has been used in several other studies in which the selected RNA targets were imaged through GFP in living cells (*213, 214*). In another study done in *Drosophila* in which GFP was also used as a reporter to trace specific mRNA, GFP and Exu were expressed together as a fusion protein. Exu binds specifically to *Drosophila* bicoid mRNA. When the GFP-Exu fusion protein was expressed inside living cells, the endogenous bicoid mRNA was visualized by the localization of GFP fluorescence. A drawback of this method was that Exu can only used for bicoid mRNA to which it binds specifically. The method using MS2 can be used for any RNA of interest. A general drawback of this latter method is that can it only be used to image the redistribution of GFP in the cell and cannot be used to image the level of RNA expression. The same amount of GFP remains in the cells whether or not the RNA exists.

Besides GFP, fluorescent nucleic acid probes have also been used to image specific RNA in the living cells. Fluorescence *in vivo* hybridization (FIVH) is a method using fluorescent labeled unstructured linear nucleic acid probes to detect and image specific RNAs in the living cells (*2-4*). Unlike the *in vitro in situ* hybridization experiments, the washing step to remove excessive probes can not be done in FIVH experiments. It is also difficult to differentiate the true signal from background caused by unbound probes in the cell. To solve this problem, dual probes for a specific RNAs

were designed (*4*). In the dual probe design for FIVH, one probe has a fluorescence molecule attached to the 3' end to act as a donor in the fluorescence resonance energy transfer (FRET) pair, The second probe has a different fluorescence molecule attached to the 5' end to act as an acceptor. The two probes were designed to target adjacent regions on the selected RNA molecule. The FRET signal was only produced when both probes interacted with the RNA target. Although the dual probe FIVH suffers from the problem of background due to the direct excitation of the acceptor and emission of donor, it was considered an improvement in reducing the high background in FIVH. Besides the high background, another drawback of the linear probe is that it is unstructured and therefore, unlike the stem-loop structured probe, it does not go through a conformational change upon binding to the target. It is difficult to use the FIVH method to detect single base differences. Also, micro-injection of the probe is necessary in order to have a high enough concentration of the chemically modified probes in the cells because the probe can not be produced by the cells. This limits the use of FIVH method to cell culture and to relatively small numbers of cells due to the intense labor requirement.

Because of the advantages of stem-loop structured probes over linear unstructured probes, it is reasonable to use stem-loop structured probes in the detection and imaging of specific RNA in living cells. One widely used stem-loop structure probe that has also been used in real-time RNA imaging is the molecule beacon (*6*). Molecular beacons are single stranded oligonucleotides containing a 15-30 nt loop region closed by a stem that is usually 5 to 6 base pairs long. A quencher is attached to one end and a fluorophore is attached to the other end. In the absence of target RNA, molecular beacons form stem-loop structures so that the fluorophore is quenched. Hybridization with the target nucleic acid opens the stem and the fluorescent signal from the fluorophore is emitted upon excitation. For detecting the mRNA, which is located in the cytoplasm, the location of nucleic acid probe is important. It was found that microinjected oligonucleotides were rapidly transported into the nucleus from the cytoplasm (*215, 216*). Conjugating molecular beacons to a peptide that crosses membranes provided efficient delivery and prevented the molecular beacons from

accumulating in the nucleus. Nitin *et al.* (*217*) conjugated the Tat peptide to molecular beacons to detect human GAPDH and survivin mRNA in living cells using fluorescence. Nuclease-resistant molecular beacons were conjugated with streptavidin and used to target native β-actin mRNA in living and motile chicken embryonic fibroblasts. The native β-actin mRNA was visualized by fluorescence microscopy (*218*). In a recent study, a molecular beacon with 2'- O - methyl - ribonucleotide backbone was linked to tRNA and injected into the nuclei of Hela cells. The chimeric tRNA-molecular beacon RNA was exported from the nucleus into the cytoplasm (*219*). When it was first injected into cytoplasm this chimeric tRNA-molecular beacon RNA remained in the cytoplasm. This new strategy can help to keep molecular beacons in the cytoplasm if needed.

Despite the advances made in using nucleic acid probes it remains a big challenge to develop effective probes for real-time detection and imaging of native RNA targets in living cells. For the system using the MS2-GFP fusion protein, even though the mRNA detected being produced inside the cell, it is still different from native mRNA. Even more importantly, this procedure is a means of imaging the location of a specific mRNA in a cell by way of the redistribution of the GFP, but it is not a method for imaging cells that express the mRNA. The molecular beacon is considered as the front runner in the field of living cell imaging. However, because they are chemically modified, the molecular beacons must be microinjected.

There are a number of challenges for detecting and quantifying RNA targets in living cells. For example, whether the probes introduced into the cells can interfere with normal cell functions is not known. The hybridization between probe and RNA target could have some impact on the translation and stability of RNA target. In living cells, without any amplification, the real-time measurement and imaging of some low copy RNA targets will be difficult. Most nucleic acid probes are fluorescently labeled. Therefore, it is necessary to distinguish the true signal from background, such as the auto-fluorescence of the cell. Although very challenging, the successful detection and

imaging of RNA molecular in living cells will prove to be a significant technical advance for biological and biomedical research.

BRIEF REVIEW OF RNA SECONDARY STRUCTURE PREDICTION

RNA secondary structural models have existed since 1960 (*220*). The major breakthrough in computational predictions of RNA secondary structure came from work done by Nussinoc et al. (*221*) in which the maximum base pairing was calculated through dynamic programing. The brief introduction of the dynamic programming used in base pair folding is presented here (*222*). For a given RNA sequence r with length N, let r_a represents the a^{th} residue in r and let r_b represents the b^{th} residue in r. The maximum number of base pairing of sequence that begins with r_a and end with r_b is represented by r(a, b). A general recursive definition of maximum number of base pairing, r (a, b), can be written as formula below:

$$r(a,b) = \max \begin{cases} r(a+1,b-1) + \delta(a,b) & case\ 1 \\ r(a+1,b) & case\ 2 \\ r(a,b-1) & case\ 3 \\ \max_{a<k<b}\left[\ r(a,k) + r(k+1,b)\ \right] & case\ 4 \end{cases}$$

Simply summarized, there are four possible ways that r (a, b) can be calculated as shown in the formula above. In case 1, r_a base pairs with r_b. So in case 1, r(a, b) equals r (a+1, b-1) plus one more base pair represented by δ (a, b) and here δ (a, b) equals 1 . In case 2, r_a does not participate any base pairing, but r_b forms base pairing . So r(a, b) equals r (a+1, b). In case 3, r_b does not participate any base pairing, but r_a forms base pairing. So r(a, b) equals r (a, b-1). In case 4, r_a and r_b are both base pairing, but not with each other. r_k is any base between r_a and r_b. The r(a, b) can be calculated by taking the maximum value of [r(a,k)+r(k+1,b)].

So, in order to calculate the number of base pairs in four cases, we need to know four numbers : r(a+1,b-1), r(a+1, b), r(a,b-1) and max [r(a,k)+r(k+1,b)]. And to calculate these four numbers, we need the solutions for more smaller problems. We can keep separating each problem into its smaller subproblems and until we reach tiny base pairing subproblems with obvious solutions (the value r(0,0) for base pairing nothing to

nothing is zero). During this dissecting process, the recursive definition of maximum base pairing listed above will provide guidance for every step along the way.

Once we work out the recursive definition of maximum base pairing, we need a dynamic programming matrix for remembering the solutions of subproblems, which are the numbers of maximum base pairing for each subproblem. This is the key difference between dynamic programming and simple recursion: a dynamic programming algorithm remembers the solutions of subproblems in an organized matrix, so each subproblem is solved only once (*223*). In dynamic programming a bottom-up approach is used to fill the matrix by using the recursive definition of r(a,b). In this process, the smallest subproblem will be solved first and eventually the r(1, N) will be calculated. After the matrix is filled, we will know the maximum number of base pairings of RNA sequence r, which is r(1,N), but the folding which has r(1,N) base pairings is not known yet. The folding is recovered by using a recursive traceback of matrix that starts with r(1,N), determines which of four cases was used to reach the r(1,N) and records the choice as part of final folding of RNA sequence r. This step is repeated , until r(0, 0) is reached and finally the folding that has maximum number of base pairing has been constructed. More detailed descriptions of the dynamic programming algorithm used in base pairing folding can be found in publications listed here (*222-225*).

Unfortunately, while the dynamic programming approach maximizes the base pairs, it does not create viable secondary structures because the maximum base pairing was found not to correspond to viable secondary structures (*226*). But the dynamic algorithms presented by Nussinoc et al. opened the door for the further development. People realized that optimization for maximum base pairs is not necessarily valid for correct RNA folding. Another criteria for folding is to use the equilibrium Gibbs free energy where the folded structure with the minimum equilibrium Gibbs free energy is considered to be the optimal secondary structure. Mfold, the RNA folding tool most widely used today, is the incorporation of dynamic programming and experimentally obtained thermodynamic parameters (*25*). In Mfold, thermodynamic parameters are used to calculate each subsequent equilibrium Gibbs free energy. The optimal

secondary structure is chosen based on the minimum equilibrium Gibbs free energy instead of the maximum calculated base pairings (*226-228*). The free energy minimization method can be as much as 73% accurate in predicting the secondary structure of a single sequence without the use of any homologous sequences (*27*).

Different from the free energy minimization method, new methods for RNA secondary structure prediction have been developed based on computing the partition function of an RNA's secondary structure. The partition function is a measure of the number of states accessible to the system at a given temperature. For an RNA secondary structure, the partition function is defined by

$$Q = \sum_{S} e^{-[F(S)/kT]}$$

where Q is the measure of the number of structures accessible to an RNA sequence at temperature T. F(S) is the equilibrium Gibbs free energy of a give folding S. K is Boltzmann's constant. For a particular structure S, the probability of S, P(S) is given by

$$P(S) = \frac{1}{Q} e^{-[F(S)/kT]}$$

The partition function was calculated using dynamic programming algorithms as first shown by McCaskill et al. (*133*). The Vienna RNA package (http://www.tbi.univie.ac.at/~ivo/RNA/) implements the partition function algorithms (*229, 230*). The Vienna RNA package includes RNALfold, RNAfold, RNAinverse, RNAalifold and several other programs. A detailed description can found at the package's website mentioned above. The Vienna RNA package uses the classic algorithms of Zuker and Stiegler (*226*) to calculate the minimum free energy (MFE) for each single sequence and gives the corresponding predicted secondary structure based on the MFE. In addition, the server also calculates the equilibrium base pairing probability using the partition function algorithms developed by John McCaskill in 1990 (*133*). In this package, the structure is still predicted by using MFE algorithms. The equilibrium partition function only provides the base pairing probability and it can not

yet accurately produce valid secondary structures. Also, it cannot be used to predict the single-stranded probability profile of an RNA sequence.

Ding et al. (*231*) further exploited the partition function algorithms for the RNA secondary structure prediction using statistical sampling algorithms. Utilizing some experimentally obtained thermodynamic parameters also used in Mfold algorithms, the forward step of the algorithm used dynamic programming to calculate the equilibrium partition function of the RNA secondary structure. Then the partition function was used to calculate the conditional probability of each probable structure. Using these calculated probabilities, the backward step is a recursive sampling process according to the Boltzmann equilibrium distribution (*231*). The important improvement in using the equilibrium partition function for RNA secondary structure prediction is the development of the statistical sampling algorithm. The statistical sampling algorithm samples exactly and strictly from the Boltzmann ensemble of secondary structures. This sampling method enables the estimation of any structural motif. For example, the algorithms provide the probability profiling of single-stranded regions in RNA secondary structures. This is one of the areas that the MFE algorithms alone could not handle very well. Based on the statistical sampling algorithm, the web server (http://sfold.wadsworth.org/index.pl) was set up to perform several tasks. A detailed description of each program and the Sfold manual are both available from the Sfold website.

The dynamic programming algorithms set the stage for the development of other methods for predicting RNA secondary structure. However, the most used algorithm, the classic MFE algorithm that was developed mainly by Zuker, is still the most widely used RNA folding algorithm. Other methods based on the calculation of equilibrium partition functions of RNA secondary structures provide statistical representations of RNA secondary structure. But, so far there is not enough evidence to show that one method is superior than the other. Further development and experimental validation may result in more accurate folding algorithms.

TABLES AND FIGURES

Table 1. Summary of artificial allosteric ribozymes

Allosteric	Effector Specificity	Ribozyme motif	Fold	Reference
Activation	*Oligonucleotide*	*Hammerhead*	10	(*121*)
	ATP	Hammerhead	8	(*122*)
	FMN	Hammerhead	6	(*126*)
	FMN	Hammerhead	100	(*232*)
	Theophylline	Hammerhead	40	(*232*)
	Oligonucleotide	Hammerhead	-	(*233*)
	Oligonucleotide	L1 ligase	10,000	(*234*)
	Oligonucleotide and	L1 ligase	800	(*234*)
	FMN	Hammerhead	270	(*232*)
	Theophylline	Hammerhead	110	(*232*)
	ATP	Hammerhead	40	(*232*)
	cGMP	Hammerhead	5000	(*127*)
	cCMP	Hammerhead	500	(*127*)
	cAMP	Hammerhead	300	(*127*)
	Theophylline	Hammerhead	2300	(*235*)
	FMN	Hammerhead	-	(*235*)
	3-Methylxanthine	Hammerhead	-	(*235*)
	ATP	L1 Ligase	800	(*128*)
	FMN	L1 ligase	1600	(*128*)
	Throphylline	L1 ligase	260	(*128*)
	Various metal ions	Hammerhead	50,000	(*236*)
	Theophylline	HDV ribozyme	-	(*237*)
	Theophylline	Tetrahymena group I	-	(*237*)
	Theophylline	X-motif ribozyme	-	(*237*)
	FMN	Hammerhead	29	(*238*),
	ERk2 protein	Hammerhead	50	(*239*)
	ppERK2 protein	Hammerhead	230	(*239*)
	Oligonucleotide	Hammerhead	1760	(*9*)
	Oligonucleotide	Hammerhead	1000	(*28*)
Inhibition	ATP	Hammerhead	180	(*122*)
	FMN	Hammerhead	250	(*232*)

Doxycycline	Hammerhead	50	(*240*)
HIV-RT	Hammerhead	-	(*241*)

* fold modulation gives the ratio of the catalytic rate constant determined in the presence (k^+) and absence (k^-) of effector. For allosteric activation and inhibition, fold modulation is k^+/k^- and k^-/k^+, respectively. Dashed indicate values not determined (expanded from table originally published by *134*).

Table 2. Summary of artificial allosteric aptamers

Allosteric Part	Effector	Allosteric Effect	Reference
Cibacron Blue/Cholic Acid Aptamer	Cholic Acid/Cibacron Blue	Binding of either ligand is mutually exclusive	(*242*)
Cytochrome C Aptamer	Hemin	Binding of hemin increases the aptamers affinity for Cytochrome C by 15X	(*243*)
Formamidopyrimidine Glycosylase (Fpg) Aptamer	Neomycin	Binding of neomycin demolishes the binding of Fpg	(*130*)
Activation Domain (AD)	Tetramethylrosamine (TMR)	Binding of TMR releases the inhibition of AD. Results in 10 fold activation of transcription	(*146*)
Malachite Green Aptamer	ATP	Binding of ATP increases the fluorescence by 5 fold	(*132*)
Malachite Green Aptamer	FMN	Binding of FMN increases the fluorescence by 30-50 fold	(*132*)
Malachite Green Aptamer	Theophylline	Binding of ATP increases the fluorescence by 8 fold	(*132*)

Table 3 . Riboswitches and their role in the regulation of bacterial metabolism [a]

Metabolite (ligand)	RNA sensor	Target process	Target genes	Where found	Refs
TPP	*thi*-box	Transcription termination or translation initiation	B1 synthesis and transport	Gram(+) and Gram(-) bacteria, some fungi and plants [b]	(*137-139, 244-247*), (*138, 139*)[b]
FMN	*rfn*-box	Transcription termination or translation initiation	B2 synthesis and transport	Gram(+) and Gram(-) bacteria	(*244, 248, 249*)
Ado-Cbl	B12-box	Transcription termination and/or translation initiation	B12 synthesis and transport	Gram(+) and Gram(-) bacteria	(*250, 251*)
SAM	S-box	Transcription termination	Sulfur metabolism	Gram(+) and Gram(-) bacteria	(*252-254*)
Lysine	L-box	Transcription termination	*lysC*	Gram(+) and Gram(-) bacteria	(*141, 255, 256*)
Guanine, HX	G-box	Transcription termination and antitermination	Purine metabolism and transport	Gram(+) bacteria	(*257*)
Adenine	ydhL A-box	antitermination	*ydhL* gene	Gram(+) bacteria	(*141*)
GlcN6P	*glmS* RNA	*glmS* mRNA self-cleavage	*glmS* gene	Gram(+) bacteria	(*140*)
Glycine	*gcvT* RNA	translation termination	Glycine cleavage gene	Gram(+) bacteria	(*142*)

[a] Abbreviations: Ado-Cbl, adenosylcobalamin; B1, thiamine; B12, riboflavin; B_{12}-box, G-box, glmS RNA, gcvT RNA, L-box, rfn-box, thi-box and ydhL A-box , evolutionarily conserved RNA structures that bind Ado-Cbl, guanine, GlcNP, glycine, lysine, FMN, TPP and Adenine, respectively. FMN, flavin mononucleotide; gcvT, glycine cleavage

system protein T;GlcN6P, glucosamine-6-phosphate; glms, glucosamine-6-phosphate synthase gene; Gram (+), Gram positive; Gram (-), Gram negative; HX, hypoxanthine; Met, methionine; SAM, S-adenosyl-L-methionine; TPP, thiamine pyrophosphate.

[b] The *thi*-box were also found in eukaryotes (information compiled from *258, 259*).

Table 4. Comparison of aptamer and antibody properties

Features	Aptamer	Antibody
Target Selection	Fewer limitations compared to Antibodies	Non-toxic and immunogenic targets
Specificity and Affinity	High, K_D: pico-low nanomolar	High, K_D: pico-low nanomolar
Molecular Weight	5-25 kDa	150 Kda
Target site of protein	Investigator decides	Immune system determines
Immune Responds and Toxicity	None observed	Immune reaction observed
Chemical Modification	Convenient	Not convenient
Physicochemical Stability	Stable after temperature insult	Temperature sensitive
Reversibility	Aptamer-based antidote	No rational method to reverse
Shelf-life	Longer compared to Antobody	Limited
Quality Control	Uniform activity	Vary from batch to batch
Functional Range	Extra- and intracellular	Extracellular

Table 5. Summary of post-SELEX modifications of aptamers for *in vivo* applications[a]

Modification	position/method	Purpose	Reference
2' OMe	Pyrimidine and purines	Protection against minor endonucleases	(*194, 260, 261*)
dT-CAP	3' end	Improved resistance against exonuleases	(*101, 262, 263*)
Locked Nucleic Acids	defined position	Improved resistance against nucleases	(*264, 265*)
Hexaethylene glycol	loop region	Improved resistance against nucleases	(*260*)
Polyethylenegly col (PEG)	5' end	Improved pharmacokinetics (reduced plasma clearance)	(*194, 260*)
Diacylglycerol	5' end	Improved pharmacokinetics (reduced plasma clearance)	(*266*)
Streptavidin	3' end	extends aptamer lifetime in blood circulation	(*267*)
Biotin	3' end	extends aptamer lifetime within a thrombus	(*267*)
Cholesterol	5' end	Improved pharmacokinetics (reduces plasma clearance)	(*268*)
Poly(lactic-co-glycolic) acid Microspheres	aptamers embedded in microspheres	Local sustained release of aptamer	(*269*)
Drug conjugation	3' end or base pariing	Aptamer targeting the drug to the desire location	(*270, 271*)
[^{123}I or ^{125}I]	5' end	Thrombus imaging	(*267*)
[^{18}F]	2' -Py	*in vivo* imaging	(*272*)
[^{99m}Tc]	5' end	*in vivo* imaging	(*273*)

[a] Abbreviations: 2' OMe, 2' -oxygen-methyl; 2'-Py: 2' -pyrimidine (information compiled from*12, 180*).

Table 6. Summary of *in vivo* applications of aptamers for extracellular targets [a]

Targets	in vivo applications	Chemistry
Thrombin	Anticoagulant	ssDNA(*54, 85, 274, 275*)
	Thrombus imaging agents	+ streptavidin +[^{123}I or ^{125}I] labeling (*267*)
Coagulation factor IXa	Antisense antidote-controlled anticoagulant	2' F- Py RNA (*268, 276*)
Human VEGF 165	Pathological neoangiogenesis	2' NH_2-Py RNA + 2' OMe-Pu (*261*)
		+ liposome anchoring (*266*)
	Age-related macular degeneration	2' F-Py- RNA + 2'-OMe-Pu + 40 kDa PEG (*96, 194, 277-279*)
		+ microspheres (*269*)
PDGF	Progressive rental disease	ssDNA (*280*)
	Intimal hyperplasmia	ssDNA + 2'F-Py +2'-OMe-Pu + PEG (*260, 281-284*)
	Reduction of intratumoral pressure to improve chemotherapeutic drugs uptake	
Angiopoietine 2	Corneal neovascularization, cancer	2'F-Py -RNA (*179*)
GnRH	sex steroid-dependent diseases	Spiegelmer (*285*)
Rat mAb 198	Autoimmune disease: myasthenia gravis	2'F-Py -RNA + 5' PEG (*286*)
Neutrophil elastase	Inhibition of lung injury and neutrophil influx	ssDNA + drug conjugation (*287*)
	Inflammation imaging	+ [^{99m}Tc] labeling (*273*)
Human L-selectin	Anti-inflammatory agent	ssDNA + 3' cap + 5' PEG (*101*)
		2'F-Py -RNA + 3'-3' dT + 5' PEG (*262*)
CTLA-4	Cancer immunotherapy	2'F- Py -RNA + tetrametric construction (*288*)
Hemagglutinin	Viral infection prevention	ssDNA (*289*)
U 251 cells (tenascin C)	Cancer	2'F-Py -RNA (*263*)
		[2'F-Py/2'-OMe-Pu/LNA] + 3'-3' dT (*265*)

[a] Abbreviations: VEGF, vascular endothelial growth factor; PDGF, platelet-derived growth factor; GnRH, gonadotropin-releasing hormone; mAb, monoclonal antibodies; CTLA, cytotoxic T cell antigen-4;PEG, Polyethyleneglycol; 2' OMe, 2' -

oxygen-methyl; Py: pyrimidine ; Pu, purine; LNA, locked nucleic acid (expanded from table originally published by *180*).

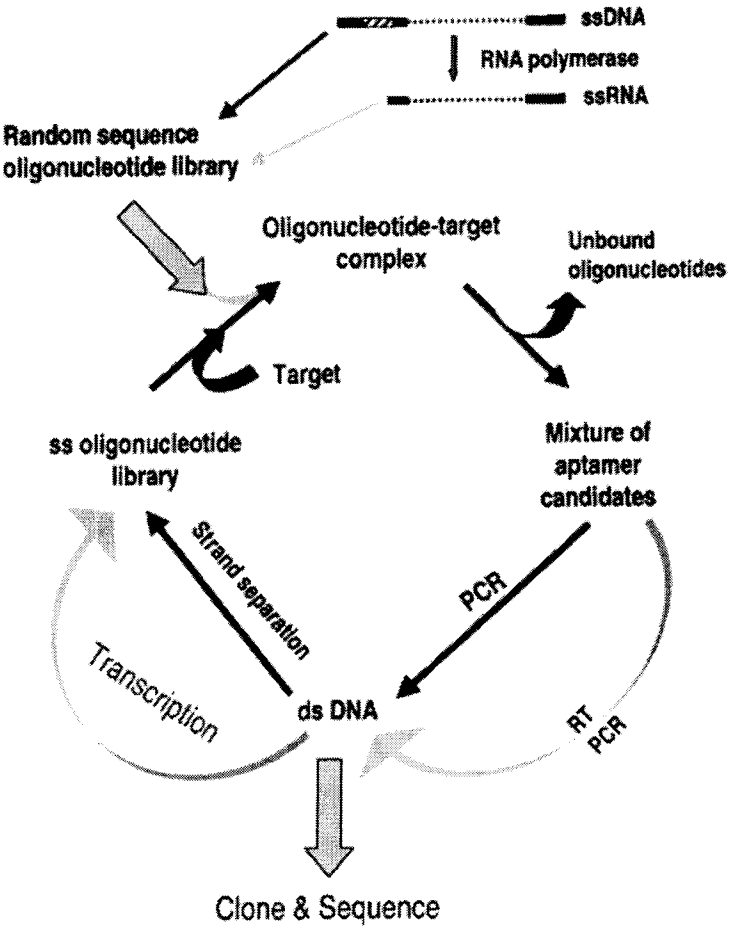

Figure 1. Generalized scheme indicating the key steps in the SELEX process. Reproduced with the permission from *Clin Chem*, 1999; 45; 1628-1650.

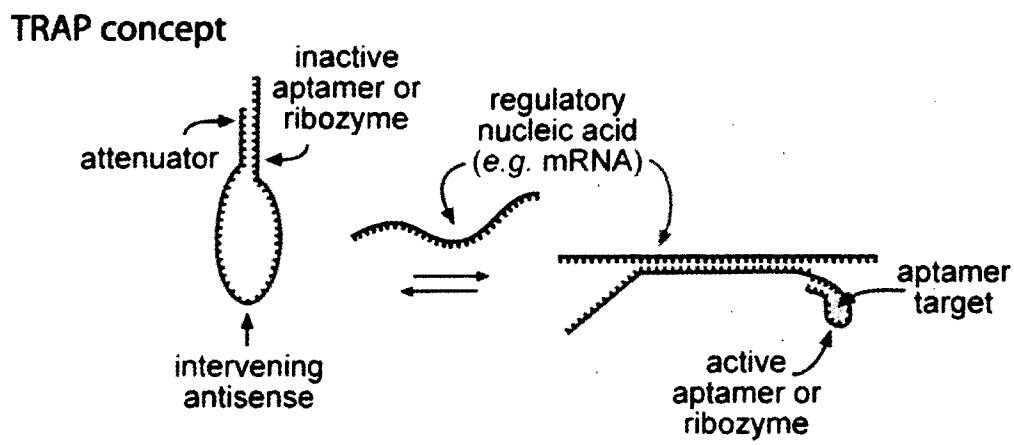

Figure 2. Design of the TRAP. The TRAP consists of three segments: aptamer, intervening antisense, and attenuator. Binding of the complementary sense regulatory nucleic acid to the antisense sequence in the TRAP forces the aptamer and attenuator apart, providing the aptamer sequence with an opportunity to fold and interact with its target molecule.

CHAPTER 3. ALLOSTERIC APTAMERS; TARGETED REVERSIBLY ATTENUATED PROBES (TRAPS)

A paper published in *Biochemistry*, 44(22):7945 - 7954, 2005.

Xiangyu Cong and Marit Nilsen-Hamilton

ABSTRACT

Aptamers are unique nucleic acids with regulatory potentials that differ markedly from those of proteins. A significant feature of aptamers not possessed by proteins is their ability to participate in at least two different types of three-dimensional structure; a folded structure that makes multiple contacts with the aptamer target and a double-helical structure with a complementary nucleic acid sequence. We have made use of this structural flexibility to develop an aptamer-based biosensor (a Targeted Reversibly Attenuated Probe, TRAP) in which hybridization of a cis-complementary regulatory nucleic acid (attenuator) controls the ability of the aptamer bind to its target molecule. The central portion of the TRAP, between the aptamer and the attenuator, is complementary to a target nucleic acid, such as an mRNA, which is referred to as a regulatory nucleic acid (regDNA) because it regulates activity of the aptamer in the TRAP by hybridization with the central (intervening) sequence. The studies reported here of the ATP-DNA TRAP suggest that, as well as inhibiting the aptamer, the attenuator also acts as a structural guide, much like a chaperone, to promote proper folding of the TRAP such that it can be fully activated by the regDNA. We also show that activation of the aptamer in the TRAP by the complementary nucleic acid at physiological temperatures is sensitive to single base mismatches. Aptamers that can be regulated by a specific nucleic sequence such as a in an mRNA have potential for many *in vivo* applications including to regulate a particular enzyme or signal transduction pathway or to imaging gene expression *in vivo*.

ABBREVIATIONS:

regDNA, regulatory DNA; TRAP: Targeted Reversibly Attenuated Probe

INTRODUCTION

Transcriptional changes are some of the earliest events that signal the presence of disease or change in the differentiated state of a cell. Consequently there is great interest in developing probes that can be used to identify altered gene expression or that can be triggered by a specific mRNA to initiate a cellular activity. Here we describe a novel nucleic acid probe design that contains an aptamer linked to a complementary attenuator via an intervening sequence. The aptamer is activated by hybridization of the intervening sequence with a complementary nucleic acid sequence that disrupts the aptamer:attenuator stem (Fig. 1A). We refer to these probes as TRAPs (Targeted Reversibly Attenuated Probes). The design of the TRAP relies on the ability of single-stranded nucleic acids to adopt alternative structures. In its primary structure the TRAP includes the sequence of an aptamer that can interact with its target molecule with high specificity and affinity. In the absence of complementary nucleic acid sequence the TRAP folds to hinder aptamer activity by virtue of hybridization between a portion of the aptamer and its complementary sequence, the attenuator. The presence of a nucleic acid that is complementary to the intervening antisense sequence results in hybridization and the formation of a rigid double-stranded DNA structure. The resulting structural constraint on the intervening sequence forces apart the shorter terminal stem, releases the aptamer from its attenuation constraint and allows it to fold into its active configuration.

Ribozymes that are regulated by molecular interactions at an allosteric site have been reported on several occasions. Various extensions to the hammerhead ribozyme have rendered it regulated by oligonucleotides (*1-3*) , ATP (*4*), theophylline (*5*), FMN (*6*) and cyclic nucleotides (*7*). Similarly RNA and DNA ligases have been produced that are regulated by ATP and theophylline (*8, 9*). Aptamers have been used to form riboswitches that regulate translation or transcription in bacteria or yeast (*10-12*). They

have also been applied as part of the allosteric mechanism for regulating ribozyme activity (*5, 13*). At least two examples of allosteric aptamers have been described. The one, a hemin-regulated aptamer, binds cytochrome c more tightly when hemin binds to a region of the aptamer that does not interact with cytochrome c (*14*). The likely mechanism for this allosteric regulation proposed by the authors on the basis of their studies is that the aptamer adopts an alternative structure when hemin binds to a G-quartet that is adjacent in the aptamer sequence to the cytrochrome c-binding region. A second allosteric aptamer involves regulation by the aminoglycoside, neomycin, which inhibits binding of an aptamer to *E. coli* formamidopyrimidine glycosylase (*15*). As for the hemin-binding aptamer, binding of neomycin alters the activity of the ligand-regulated aptamer (LIRA). In both cases cited, the allosteric regulators of aptamer activity were small molecules, either hemin or neomycin.

Regulation of an aptamer activity by an allosteric mechanism involving a nucleic acid regulator has not yet been reported. Here we describe a general approach to developing an aptamer that is regulated by a specific nucleic acid sequence. In this report, as an example, we have used the DNA ATP aptamer (*16*). We show that, in a TRAP configuration, activity of the ATP aptamer is specifically and quantitatively regulated by its target nucleic acid.

Previous studies of the TRAP concept were done with the hammerhead ribozyme in place of the aptamer in figure 1A. In these studies also, a simple polyAC intervening sequence was used. Studies of the ribozyme in this configuration showed that we could regulate the activity of the ribozyme by an attenuator (*2, 3*). But, they did not evaluate the use of natural sequences in the intervening sequence. The critical distinction is that natural sequences are likely to fold into a variety of structures that might coexist and could involve interactions of the intervening sequence with the aptamer or ribozyme or with the attenuator to create three-dimensional structures that differ from that proposed in figure 1A. To understand the structural considerations that guide formation of regulated nucleic acids such as the TRAPs, it is important to evaluate the distribution of folded structures in the population fold. These questions

cannot be evaluated with a ribozyme as the functional nucleic acid in the TRAP because, in assays for ribozymes, the substrate is the only radiolabeled component, the ribozyme is in excess (often10-fold or more) of the substrate, and the assay follows the cleavage of the substrate RNA. Thus, the only ribozyme TRAPs that have folded "properly" and hybridized to the substrate are detected. Ribozyme TRAPs that adopt alternate three-dimensional structures that do not bind the substrate are not detected by the assay even if they constitute 90% of the molecules in the population. With an aptamer as the functional nucleic acid, the assay involves radiolabeling the TRAP and all molecules in the population are detected. Thus, with an aptamer, aspects of uniformity of folding can be addressed with the TRAP design. The results of this study of aptamer TRAPs show that the attenuator inhibits aptamer activity and also suggest that the attenuator serves as a structural guide for forming the correct TRAP structure and to prevent unproductive folding of the oligonucleotide. We also show that the TRAP design allows discrimination at a physiological temperature between nucleic acids that differ by only a single nucleotide in sequence.

MATERIALS AND METHODS

Materials and Equipment

ATP-Agarose affinity resins and ATP were purchased from Sigma (St. Louis, MO). [γ-^{32}P]ATP was purchased from ICN (Costa Mesa, CA). Biotinylated ATP (Adenosine 5'-triphosphate [γ] Biotinyl-3,6,9,-trioxaundecanediamine) was from Affinity Labeling Technologies, Inc. (Lexington, KY). Streptavidin Agarose CL-4B was from Sigma (St. Louis, MO). HT-450 Tuffryn® membrane filters (0.45 µm pore size) were from Pall (Ann Arbor, MI). ITC experiments were performed using a VP-ITC isothermal titration calorimeter (Microcal, Inc., Northhampton, MA). Imagequant software (Amersham-Pharmacia) was used to analyze radioactive bands in gel scans obtained using a Typhoon scanner (Amersham-Pharmacia).

Oligonucleotides

The oligonucleotides used in this study are represented in figure 1B. The sequences of the three TRAPs most frequently used in the work are given here. All other sequences can be found in the Supporting Information.

8att-polyTG20 TRAP:

CCTGGGGGAGTATTGCGGAGGAAGG**TTTTTTGTTTTTGTTTTGTT**CCGCAATA

8att-cmRas20TRAP:

CCTGGGGGAGTATTGCGGAGGAAGG**GTACTCCTCAGGGCCGGCGG**CCGCAATA

9att-cmRas15TRAP:

CCTGGGGGAGTATTGCGGAGGAAGG**GTACTCCTCAGGGCC**CCGCAATAC.

Oligonucleotides were purchased as PAGE purified preparations.(Integrated DNA technologies, Coralville, IA).

ATP Binding Assays

Single-stranded ATP DNA TRAPs or that ATP DNA aptamer (2 - 20 pmoL, 5' labeled with ^{32}P) were incubated in the presence or absence of other ssDNAs, as defined in each experiment, at 75°C for 5 min in binding buffer (20 mM Tris·HCl, 300 mM NaCl, 5 mM $MgCl_2$, pH7.6) then cooled to room temperature slowly for 40-60 min. These samples were either loaded onto an ATP affinity column for the column assay or mixed with 40 μM biotinylated ATP and 10 μM streptavidin-agarose for the filter assay. For the column assay, each sample was incubated for 10 min on the column then washed with 20 ml of binding buffer and the retained DNA was eluted with 15-16 ml of 5 mM ATP in binding buffer. For the filter assay, each sample was equilibrated at room temperature for 10 min then filtered through an HT-450 filter and washed with 5 ml of binding buffer. For both assays, fractions were analyzed by scintillation counting or measuring Cerenkov radiation. The radioactive cpm bound to ATP was

divided by the total cpm in the sample to give the fraction bound. Reported error values are the standard deviations of the averages.

Isothermal Titration Calorimetry

Titrations of 50mM regDNA-cmRas20 into a cell containing 5mM 20mer 0att-cmRas20 TRAP or 8att-cmRas20 TRAP, respectively, were carried out at 37 °C in titration buffer (300 mM NaCl, 5 mM $MgCl_2$ and 20 mM HEPES (pH 7.6 at 23°C). For each titration, 5 µl (250 nmoL) of regDNA-cmRas20 was injected from a computer-controlled syringe at intervals of 300 or 600 s into the reaction cell that contained an initial volume of 1.43 ml of the appropriate oligonucleotide in the same buffer as the regDNA. Reverse titrations (oligonucleotide tritrated into regDNA) were also run. The syringe was rotated at 310 rpm. Data points were collected every 4 s. Each titration involved a total of 25 injections. Control experiments to determine the heats of dilution were performed using the same injection protocol of regDNA into a cell containing buffer but no oligonucleotide. The heat of dilution for each titrating oligonucleotide into buffere was determined experimentally. These values were subtracted from the corresponding experimentally obtained values for the appropriate oligonucleotide pairs to obtain the heats of interaction of each pair. The subtraction of the heats of dilution did not significantly change the values for heats of interaction for the oligonucleotides. All titrations were carried out at least three times to ensure consistency of the data. Before each titration the oligonucleotide was heated to 85°C and incubated for 5 min in the titration buffer. The oligonucleotide was then cooled to room temperature slowly for 40 min. The data were analyzed using Origin 7.0 (Microcal, Inc.) with ΔH (enthalpy change in kcal/mol), Ka (association constant in M^{-1}) and N (number of binding sites per molecule in the sample cell) as adjustable parameters. Thermodynamic parameters were calculated from the equation $\Delta G = \Delta H - T\Delta S$, where ΔG, ΔH and ΔS are the changes in free energy, enthalpy and entropy of binding, respectively. T is the absolute temperature.

Polyacrylamide Gel Electrophoresis

Nucleic acids and their hybrids were separated by electrophoresis through 12% non-denaturing polyacrylamide gels under a constant current of 35 mAmp at room temperature. The gel buffer and electrode buffers consisted of 89 mM Tris·HCl, 89 mM boric acid and 2 mM EDTA. The relative amounts of radiolabeled DNA in each band were quantified using Imagequant software after scanning the gel using a Typhoon scanner. Reported errors are the standard deviations of the averages.

RESULTS

Allosteric Regulation of the ATP Aptamer by a Regulatory Nucleic Acid

To determine if an aptamer activity could be controlled in the TRAP design by an oligonucleotide complementary to the intervening antisense loop, we tested an allosteric DNA TRAP (8att-cmRas20 TRAP) containing an ATP aptamer at the 5' end, followed by a 20 nt antisense that is complementary to a portion of a mutant Ras oncogene mRNA then an 8-nt attenuator sequence at the 3' end. As predicted, incubation with a 20nt regulatory DNA oligonucleotide (regDNA-cmRas20) resulted in increased aptamer (ATP-binding) activity of the TRAP (Fig. 2). Oligonucleotide sequences that were not complementary to the attenuator or to other portions of the TRAP were not effective in increasing TRAP activity (Fig. 2). These results show that the TRAP functions as designed. Regulation of aptamer activity is achieved by the presence of an oligonucleotide with a sequence complementary to the intervening antisense portion of the TRAP. The TRAP aptamer was also activated by regDNAs without prior melting and cooling (Fig. 2), suggesting that this form of regulation could occur *in vivo*.

Proportionality and Reversibility of TRAP Activation

To be useful as a sensor for a complementary nucleic acid such as a cellular mRNA, allosteric regulation by the antisense sequence in the TRAP should be proportional to the concentration of the complementary regulatory nucleic acid and

reversible. This was shown for the 8att-cmRas20 TRAP that was activated in a linear fashion by an increasing concentration of complementary regDNA-cmRas20 (Fig. 3A). Control experiments showed that the regDNA itself did not display aptamer-like activity and that sequences that were not complementary to the TRAP did not increase aptamer activity (Fig. 2 and data not shown). The increase in TRAP activity is stable for at least 24h (data not shown) but can be readily reversed if an equilibrium is established with a third single stranded nucleic acid that has a higher association constant for the regDNA than the regDNA has for the antisense segment of the TRAP. *In vivo*, reversal would be achieved by expressing an RNA that included additional sequence of the targeted regulatory mRNA that surrounds the sequence complementary to the intervening sequence of the TRAP. Here, we have demonstrated this property by using a regDNAext containing a central sequence that is complementary to the TRAP intervening sequence and 15 As on either end. Reversal of TRAP activation occurred at 23°C within 20 min of adding the complement of the regDNAext (crDNAext) to the TRAP that had been activated by a 10 min incubation with regDNAext (Fig. 3B). The observed proportional increase in TRAP aptamer activity with increasing regDNA/TRAP molar ratio and the ability to reverse this activation shows that the TRAP could be used to report the presence of an mRNA sequence or to mediate a signal from a particular mRNA sequence and that the activity of the TRAP can be reversed.

Attenuator Regulation of Aptamer Activity in the TRAP

The TRAP design dictates that allosteric regulation by the regDNA involves a balance of the strength of hybridization of the attenuator:aptamer stem and the antisense:regDNA hybrid. The impact of this balance of stability between two alternative structures was tested by varying the length of the attenuator (Fig. 4). As predicted, the ability of the regDNA to activate the aptamer in the TRAP decreased with increasing length of the attenuator (Fig. 4, gray bars). In this set of experiments a polyTG20 TRAP was used in place of the cmRas20 TRAP. Whereas, an internal structure is predicted for the cmRas intervening sequence by the Mfold software (*17*),

no structure is predicted for polyTG. By using the polyTG20 TRAP, we were able to test the effect of varying the length of attenuator in the absence of complications that could be introduced by the inclusion of structure in the intervening sequence. A practical advantage of the polyTG20 TRAP was also that, under the conditions tested, the basal activity was high enough to observe the incremental decrease in aptamer activity as a result of increasing the attenuator length (black bars).

If, as these data suggest, the TRAP is activated by disrupting hybridization between aptamer and its complementary attenuator, then a sequence complementary to the attenuator (cAtt) should also activate the aptamer in the TRAP by competing for the attenuator sequence as shown (Fig.4, white bars). Activity of the TRAPs with 12 and 14nt attenuators increased more with cAtt than did the activity of the TRAPs with shorter attenuators. The likely explanation for this observation is that the base compositions of the cAtts for these TRAPs were higher in %GC and therefore the TRAP:cAtt hybrids were more stable than for TRAPs with shorter attenuators. Another factor is that the ratio of cAtt:TRAP for these two TRAPs with the longest attenuators was 10:1 compared with 5:1 for the remaining TRAPs. However, this change in ratio is unlikely to be responsible for the much higher activity of these latter two TRAPs in the presence of cAtt because the ATP binding activity of the 8attpolyTG TRAP was identical at a ratio of cAtt:TRAP equal to 10:1 and 5:1 (data not shown).

Effect of the Intervening Sequence on TRAP Activity

Previous studies of the hammerhead ribozyme TRAP were exclusively done with intervening antisense sequences designed not to interact with the ribozyme or the attenuator (*2, 3, 18*). We have also examined the activity of the polyTG20 TRAP with a similar noninteracting intervening sequence for which there are no predicted hydrogen bonded pairs between bases in the aptamer and in the intervening sequence. However, the use of the TRAP to detect or respond to mRNA sequences will require that the mechanism function with a variety of base sequences in the intervening loop. Some of these intervening loop sequences will provide options for hydrogen bonding

between the aptamer and the intervening sequence in addition to the hybridization between aptamer and attenuator.

To examine the effect of the intervening antisense sequence on the ability of the TRAP to detect the presence of the a variety of regDNAs, we compared three TRAPs: 1) the 8att-polyTG20 TRAP with an intervening sequence of a polyT sequence interspersed with 3 Gs for maintaining register with the regDNA (structure 1, Fig. 5A), 2), the 8att-cmRas20 TRAP with an intervening sequence containing all four nucleotide bases and with options for base pairing within the sequence (structures 2a, b, c, Fig. 5A) and 3) the 0att-cmRas20 TRAP (structure 3, Fig. 5A) with the same sequence as the 8att-cmRas20 TRAP except lacking the 8nt attenuator. The polyTG intervening sequence is similar to that which was used with the hammerhead ribozyme TRAP and does not correspond to a known RNA sequence (*2*). The cmRas intervening sequence corresponds to a portion of a mutant Ras mRNA and is predicted by the Mfold software (*17*) to have internal structure.

Compared with the 8att-polyTG20 TRAP the activity of the 8att-cmRas20 TRAP was lower in the absence of the complementary regDNA (Fig. 5B). However, both TRAPs were activated to about the same maximum activity by excess complementary regDNA. These results suggest that action of the attenuator to inhibit aptamer activity might be aided by interactions within the intervening sequence that stabilize the closed (aptamer inactive) form of the TRAP but that these latter interactions do not prevent the regDNA from hybridizing with the intervening antisense sequence and fully activating the aptamer.

Role of the Attenuator as a Structural Guide for regDNA Hybridization with the TRAP

In the course of these studies we discovered that in some instances, the 0att-cmRas20 TRAP being an example, the antisense sequence can interact with the aptamer and strongly suppress its activity in the absence of an attenuator (Fig. 5B). However, unlike the TRAP that includes an attenuator, the aptamer linked to the

antisense in the absence of an attenuator (0att-cmRas20 TRAP) was not fully activated by regDNA. Even by a 100-fold excess of regDNA only increased the 0att-cmRas20 TRAP aptamer activity to 50% of the aptamer binding activity achieved by the 8att-cmRas20TRAP or of the ATP aptamer alone (Fig. 5B). This same inability of the 0att-cmRas20 TRAP to be fully activated was observed at 23°C and 37°C.

Analysis by the Mfold program of the 2-dimensional structure of the 0att-cmRas20 TRAP predicted that the folded structure of this oligonucleotide (ΔG, -4.2) was less stable than for the 8att-cmRas20 TRAP, which has the same sequence with the addition of the 8nt attenuator (ΔGs, -5.5 to -5.8). If correct, this analysis suggested that the thermodynamic basis for the resistance of the 0att-cmRas20 TRAP to activation by the regDNA-cmRas20 could not be accounted for by a much more stable secondary structure of the former. We also tested the possibility that the observed difference in maximal activation of the 0att- and 8att-cmRas20 TRAPs was due to a kinetic difference in the rate of hybridization with the complementary regDNA. However, even after a 24h incubation of the TRAPs with the regDNA-cmRas20, the same relative activations of the 0att- and 8att-cmRas20 TRAPs were observed.

To examine further the basis for the inability of the 0att-cmRas20 TRAP to be fully activated, we used isothermal titration calorimetry (ITC) to compare the thermodynamic parameters of the interaction of the regDNA with three oligonucleotides: 1) a complementary oligonucleotide corresponding to the intervening antisense sequence of the TRAP, 2) the 8att-cmRas20 TRAP and the 3) 0att-cmRas20 TRAP. The results (Table 1) showed that the calculated stabilities (ΔGs) of the complex between the regDNA-cmRas20 and either the 0att- and 8att- cmRas20 TRAPs were similar. However, whereas the thermodynamic parameters for the 8att-cmRas20 TRAP:regDNA-cmRas20 interaction could be fit assuming a single hybrid molecular species, the 0att-cmRas20 TRAP:regDNA-cmRas20 data could only be fit if it was assumed that there were two types of interaction, each representing about 50% of the DNA molecules. Representative data from which the values for this table were obtained are shown in Fig. 6. From this analysis it seems that the 0att-cmRas20 TRAP

can adopt at least two tertiary conformations that interact differently with the regDNA for hybridization. Such structures were not predicted by the Mfold program and may involve more complex structural elements than are entertained by this algorithm for 2-dimensional structural predictions .

Alone, the ITC analysis does not explain why only 50% of the aptamer activity is activated on hybridization with the regDNA. Although there are at least two predicted interactions that might involve two or more folded structures of the 0att-cmRas20 TRAP, neither interaction shows a very different stability from the other or from the 8att-cmRas20 TRAP. The most likely explanation for these results is that one or more of the hybridized 0att-cmRas20 TRAP structures involves interaction between the regDNA-cmRas20 and the aptamer that inhibits aptamer activity. Thus, the presence of the attenuator in the 8att-cmRas20 TRAP may act as a structural guide to appropriately align the antisense sequence in the "closed" TRAP making it available for invasion by the regDNA to form the correct structural intermediate for the subsequent separation of the attenuator and aptamer.

To test the hypothesis that the 8att-cmRas20 TRAP forms predominantly one structure and the 0att-cmRas20 TRAP forms more than one structure when hybridized with the regDNA-cmRas20 , hybridized and radiolabeled oligonucleotides were separated by non-denaturing acrylamide gel electrophoresis. The results demonstrate that the vast majority of the 8att-cmRas20 TRAP runs as a single band, in the presence and absence of regDNA-cmRas20, suggesting the presence of a predominant structure (Fig. 7). By contrast, the 0att-cmRas20 TRAP, with or without regDNA-cmRas20, separates into one major band with the remainder distributed amongst four to nine bands and sometimes in a smear of unresolved bands near the major band. The results suggest that the 0att-cmRas20 TRAP exists as multiple structural species. These experiments were performed with variations in incubation temperature (10 min incubation at 23°C vs. 37°C), times of incubation (10 min and 24 h incubation at 23°C) and temperatures at which electrophoresis was performed (electrophoresis at 4°C and 23°C with samples that had been incubated at either 23°C and 37°C). In all trials the

same observation was made that the 0att-cmRas20 TRAP separated into many bands on the gel whereas the 8att-cmRas20 TRAP remained mainly as a single band. An average of 86 ±7.8% (N=8) and 89 ±5.6% (N=12) of the total 8att-cmRas20 TRAP DNA resolved as a single band in the absence or presence of a 1 to 100-fold excess of regDNA respectively. By contrast, 46 ± 15% (N=10) and 57 ± 8.5% (N=30) of the 0att-cmRas20 TRAP was found in the most intense band in the absence and presence of a 1 to 100-fold excess of regDNA respectively. Thus, these results, along with the ITC data and the measurements of TRAP aptamer activity after hybridization with regDNA suggest that only about 50% of the 0att cmRas20 TRAP molecules adopt a structure that is able to interact with the regDNA in a productive way to activate the aptamer.

The TRAP's Ability to Distinguish Single Base Mismatches

Although not practical with oligonucleotides, single base mismatches can be detected by molecular beacons, nucleic acids with a similar stem-loop structure to the TRAP (*19-21*). However, optimal conditions for distinguishing single base mismatches by molecular beacons are at temperatures well above 37°C and also generally include high concentrations of Mg^{++}. Whereas the molecular beacon is generally regulated by a stem of 5 to 6 bases, the TRAP has a longer stem by which it is regulated. We reasoned that the apparent higher stability of the TRAP structure would make its activation more likely to be influenced at physiological temperatures by single base mismatches between the regDNA and the antisense intervening sequence of the TRAP. Therefore, regDNAm-cmRas15 with one or two base-pair mismatches were tested for their ability to activate a 9att-cmRas15 TRAP at 37°C and in the presence of only 5 mM $MgCl_2$. The results showed that the 9att-cmRas15 TRAP was capable of distinguishing single nucleotide mismatches between the regDNAm-cmRas15 and the intervening antisense sequence over at least a 10-fold range (Fig. 8).

DISCUSSION

We have described an oligonucleotide design in which a complementary nucleic acid can regulate an aptamer activity by an allosteric mechanism. The aptamer activity

in the TRAP is increased by the presence of complementary regDNA. In the absence of regDNA, the aptamer is inhibited by the attenuator (Fig. 4). Activation of the TRAP is sequence specific and is proportional to the amount of regDNA present (Figs 2,3).

Activation of the TRAP aptamer is determined by the balance in stability of the attenuator:aptamer stem and intervening sequence compared with the stability of the aptamer-target complex and regDNA: intervening sequence hybrid. This equilibrium resembles that established by the molecular beacon with its complementary DNA target. A systematic thermodynamic study demonstrated that the molecular beacon can discriminate between a complete match and a single mismatch in the target DNA sequence over a broader temperature range than can a linear nucleic acid probe (*20*). As the stem length was increased from 4 to 6 bases, the window of discrimination moved from a mid-value of about 65°C to about 50°C. Very little discrimination was observed at 37°C. By contrast, we found good discrimination between single base mismatches at 37°C using a 9att-cmRas15 TRAP (Fig 8). For optimizing the discriminatory capability of the TRAP, it was important to find the correct thermodynamic balance between the attenuator:aptamer heteroduplex and the antisense:regDNA hetroduplex. For example, 9nt in the attenuator and 15nt in the intervening sequence showed good discrimination single base-pair mismatches. Whereas the 8att-cmRas20 TRAP showed some discrimination between a complete match and a two position mismatch, there was no significant difference for the 8att-cmRas20 TRAP between a complete match and a single basepair mismatch (data not shown).

Although increasing the length of stem of the molecular beacons moved the window of sequence discrimination towards physiological temperatures, it also increased the response time such that a molecular beacon with a 6-stem base was only a little over 60% opened after 200 seconds compared with 4-stem beacon, which was completely opened by less than 10 seconds (*20*). By extension, an 8-stem molecular beacon would be expected to take many minutes to completely open. Our results suggest that the TRAP is not as sluggish in its response to the regDNA as the

molecular beacon is to its target DNA. Incubating the TRAP with its target molecule and the regDNA for 5 minutes results in the same amount of activity as obtained with the aptamer alone. The difference between TRAP and molecular beacon probably lies in the stability of the aptamer structure when bound to its target molecule. Whereas the beacon has only the ΔG of hybridization between antisense and target DNA to balance the ΔG of the stem helix, the TRAP equilibrium balances the ΔG of stem helix and against the combined ΔGs of aptamer interaction with its target molecule and regDNA hybridized with the intervening sequence. The additional stability of the released aptamer bound to its target molecule is expected to make the reverse reaction less favorable.

Our results show that maximally activated TRAP has the same activity as the aptamer alone when the TRAP is tested at 37°C (Supporting Information). Consequently, maximizing the range of change in aptamer activity due to regDNA will be achieved by decreasing the background activity of the TRAP in the absence of regDNA. Here we show that the intervening sequence can play a role in optimizing TRAP activity (Fig 5). Identical except for the 20 nt intervening sequence, the 8att-polyTG20 TRAP showed a much higher background activity than the 8att-cmRas20 TRAP. Whereas there is no predicted internal structure of polyTG, the cmRas intervening sequence was predicted to have internal structure. The internal structure introduced by the cmRas intervening sequence may lower the background activity of the TRAP by stabilizing the attenuator:aptamer stem.

Depending on its sequence, the intervening sequence can also interact with and inhibit the aptamer. In the 8att-cmRas20 TRAP example, the absence of an attenuator sequence in the TRAP resulted in an aptamer that was inhibited in the absence of regDNA. But the 0att-cmRas20 TRAP could not be fully activated by hybridization with regDNA even if the regDNA and TRAP were incubated together over a 24 h period. Analysis by ITC suggested that the 0att-cmRas20 TRAP interacts with the regDNA to form more than one structure (Table 1, Fig. 6). By contrast, the 8att-cmRas20 TRAP showed evidence of only a single hybridized structure as did the two oligonucleotides

with sequences of the regDNA and the intervening antisense of the TRAPs. Further structural analysis by gel electrophoresis of the regDNA hybrids with these two TRAPs supported the hypothesis that the 0att-cmRas20 TRAP forms several structures both in the presence and absence of the regDNA, whereas the 8att-cmRas20 TRAP forms only one major structure in both instances (Fig. 7). We believe it is likely that one or more of the hybridized forms of the 0att-cmRas20 TRAP includes structural features that prevent the aptamer from properly folding and from recognizing its target ATP. These results suggest that the attenuator plays three important roles in the TRAP. The first role is to inhibit aptamer activity in the absence of the regulatory nucleic acid as demonstrated for the polyTG TRAP in Fig.4. The second role of the attenuator is to act as a structural guide, much like a chaperone, to promote the folding of the remainder of the molecule into a three-dimensional structure that can be effectively invaded by the regulatory nucleic in a single and productive mode to fully activate the aptamer. In acting as a structural guide, the attenuator also performs its third role, which is to prevent unproductive folding of the TRAP oligonucleotide. These latter two roles, which are interdependent, are proposed as an explanation of the results of the ATP binding, ITC and gel electrophoresis analyses of the 8att-cmRas20 TRAP and the 0att-cmRas20 TRAP (Figs 5-7 and table 1).

The TRAP has many potential applications. One example is in imaging gene expression *in vivo*. Activation of the aptamer in the TRAP by a particular mRNA would provide a means of imaging cells *in vivo* that express the complementary mRNA. For imaging gene expression, molecular beacons make particularly good use of fluorescence options for signaling the presence of a specific sequence by coupling a fluorophore and a quenching agent, located at opposite ends of a nucleic acid probe, with a stem-loop structure. Although they can function *in vivo*, the molecular beacon's usefulness for *in vivo* applications is limited by the penetration of light through tissue and by the stability of the beacon inside cells (*22-24*). Not limited by the need for a fluorescent signal, the TRAP can be designed to bind a target molecule labeled with a radioisotope such as Tc^{99m} or F^{18}. The radiolabeled targets would be concentrated by the TRAP in cells in which the mRNA is expressed that is complementary to its

intervening sequence. Unlike for the molecular beacon, degradation of the TRAP *in vivo* will not create a background signal. Also, because of its sensitivity to a single base mismatch at temperature and salt concentrations close to those of the living cell, we anticipate that the TRAP might also be able to distinguish point mutations in mRNAs of living cells.

Although they both rely on a similar stem-loop structural concept, there are some fundamental differences between the TRAP and the molecular beacon. Both the TRAP and molecular beacon can be taken in by cells as synthetic oligonucleotides. However, unlike the molecular beacon, a TRAP containing an RNA aptamer can be synthesized by a living cell to create a steady state intracellular concentration of TRAP. TRAPs could also be used to modify cellular processes in response to specific nucleic acid sequences. Aptamers have been selected to regulate enzyme activity, signal transduction cascades and protein structural transitions (*25-29*). The TRAP design described here would provide a means of regulating these aptamers by changes in gene expression. A normal gene expression pattern could be harnessed to regulate the activity of an enzyme or an intermolecular interaction by way of a TRAP containing the appropriate aptamer.

ACKNOWLEDGMENTS

The authors thank Jon Applequist, Donald Burke, Gloria Culver, Richard Hamilton, Becky Stodola and Tianjiao Wang for valuable comments on the manuscript and helpful discussions.

REFERENCES

1. Porta, H., and Lizardi, P. M. (1995) An allosteric hammerhead ribozyme, *Biotechnology (N Y) 13*, 161-4.

2. Burke, D. H., Ozerova, N. D. S., and Nilsen-Hamilton, M. (2002) Allosteric hammerhead ribozyme TRAPs, *Biochemistry 41*, 6588-6594.

3. Saksmerprome, V., and Burke, D. H. (2003) Structural Flexibility and the Thermodynamics of Helix Exchange Constrain Attenuation and Allosteric Activation of Hammerhead Ribozyme TRAPs, *Biochemistry 42*, 13879-86.

4. Tang, J., and Breaker, R. R. (1997) Examination of the catalytic fitness of the hammerhead ribozyme by in vitro selection, *RNA 3*, 914-25.

5. Soukup, G. A., and Breaker, R. R. (1999) Engineering precision RNA molecular switches, *Proc Natl Acad Sci U S A 96*, 3584-9.

6. Araki, M., Okuno, Y., Hara, Y., and Sugiura, Y. (1998) Allosteric regulation of a ribozyme activity through ligand-induced conformational change, *Nucleic Acids Res 26*, 3379-84.

7. Koizumi, M., Soukup, G. A., Kerr, J. N., and Breaker, R. R. (1999) Allosteric selection of ribozymes that respond to the second messengers cGMP and cAMP, *Nat Struct Biol 6*, 1062-71.

8. Levy, M., and Ellington, A. D. (2002) ATP-dependent allosteric DNA enzymes, *Chem Biol 9*, 417-26.

9. Robertson, M. P., and Ellington, A. D. (2000) Design and optimization of effector-activated ribozyme ligases, *Nucleic Acids Res 28*, 1751-9.

10. Winkler, W. C., Cohen-Chalamish, S., and Breaker, R. R. (2002) An mRNA structure that controls gene expression by binding FMN, *Proc Natl Acad Sci U S A 99*, 15908-13.

11. Grate, D., and Wilson, C. (2001) Inducible regulation of the S. cerevisiae cell cycle mediated by an RNA aptamer-ligand complex, *Bioorg Med Chem 9*, 2565-70.

12. Suess, B., Hanson, S., Berens, C., Fink, B., Schroeder, R., and Hillen, W. (2003) Conditional gene expression by controlling translation with tetracycline-binding aptamers, *Nucleic Acids Res 31*, 1853-8.

13. Soukup, G. A., and Breaker, R. R. (2000) Allosteric nucleic acid catalysts, *Curr Opin Struct Biol 10*, 318-25.

14. Chinnapen, D. J., and Sen, D. (2002) Hemin-stimulated docking of cytochrome c to a hemin-DNA aptamer complex, *Biochemistry 41*, 5202-12.

15. Vuyisich, M., and Beal, P. A. (2002) Controlling Protein Activity with Ligand-Regulated RNA Aptamers, *Chemistry & Biology 9*, 907-913.

16. Huizenga, D. E., and Szostak, J. W. (1995) A DNA aptamer that binds adenosine and ATP, *Biochemistry 34*, 656-65.

17. Zuker, M. (2003) Mfold web server for nucleic acid folding and hybridization prediction, *Nucleic Acids Res 31*, 3406-15.

18. Saksmerprome, V., and Burke, D. H. (2004) Deprotonation Stimulates Productive Folding in Allosteric TRAP Hammerhead Ribozymes, *J Mol Biol 341*, 685-94.

19. Ramachandran, A., Zhang, M., Goad, D., Olah, G., Malayer, J. R., and El-Rassi, Z. (2003) Capillary electrophoresis and fluorescence studies on molecular beacon-based variable length oligonucleotide target discrimination, *Electrophoresis 24*, 70-7.

20. Tsourkas, A., Behlke, M. A., Rose, S. D., and Bao, G. (2003) Hybridization kinetics and thermodynamics of molecular beacons, *Nucleic Acids Res 31*, 1319-30.

21. Bonnet, G., Tyagi, S., Libchaber, A., and Kramer, F. R. (1999) Thermodynamic basis of the enhanced specificity of structured DNA probes, *Proc Natl Acad Sci U S A 96*, 6171-6.

22. Matsuo, T. (1998) In situ visualization of messenger RNA for basic fibroblast growth factor in living cells, *Biochim Biophys Acta 1379*, 178-84.

23. Sokol, D. L., Zhang, X., Lu, P., and Gewirtz, A. M. (1998) Real time detection of DNA.RNA hybridization in living cells, *Proc Natl Acad Sci U S A 95*, 11538-43.

24. Tyagi, S., and Kramer, F. R. (1996) Molecular beacons: probes that fluoresce upon hybridization, *Nat Biotechnol 14*, 303-8.

25. Chen, C. H., Chernis, G. A., Hoang, V. Q., and Landgraf, R. (2003) Inhibition of heregulin signaling by an aptamer that preferentially binds to the oligomeric form of human epidermal growth factor receptor-3, *Proc Natl Acad Sci U S A 100*, 9226-31.

26. Toulme, J. J., Darfeuille, F., Kolb, G., Chabas, S., and Staedel, C. (2003) Modulating viral gene expression by aptamers to RNA structures, *Biol Cell 95*, 229-38.

27. Rhie, A., Kirby, L., Sayer, N., Wellesley, R., Disterer, P., Sylvester, I., Gill, A., Hope, J., James, W., and Tahiri-Alaoui, A. (2003) Characterization of 2'-fluoro-RNA aptamers that bind preferentially to disease-associated conformations of prion protein and inhibit conversion, *J Biol Chem 278*, 39697-705.

28. Buerger, C., Nagel-Wolfrum, K., Kunz, C., Wittig, I., Butz, K., Hoppe-Seyler, F., and Groner, B. (2003) Sequence-specific peptide aptamers, interacting with the intracellular domain of the epidermal growth factor receptor, interfere with Stat3 activation and inhibit the growth of tumor cells, *J Biol Chem 278*, 37610-21.

29. Nishikawa, F., Kakiuchi, N., Funaji, K., Fukuda, K., Sekiya, S., and Nishikawa, S. (2003) Inhibition of HCV NS3 protease by RNA aptamers in cells, *Nucleic Acids Res 31*, 1935-43.

FIGURE LEGENDS

Figure 1. Design and Function of the TRAP and Oligonucleotide Designs for this Study.

A. Design of the TRAP: The TRAP consists of three segments: aptamer, intervening antisense and attenuator. Binding of the complementary sense regulatory nucleic acid to the antisense sequence in the TRAP forces the aptamer and attenuator apart providing the aptamer sequence with an opportunity to fold and interact with its target molecule.

B. Oligonucleotide designs: The oligonucleotides used in this study are shown graphically. Parallel lines indicate complementarities between sequences. Lines of the same color have the same nucleotide sequence. Sequences of the TRAPs are found in Materials and Methods and all other sequences are found in the Table 2.

Figure 2. Sequence specificity of activation of the TRAP Activity by regDNA.

The 8att-cmRas20 TRAP was tested for its ability to bind ATP in the presence and absence of complementary regDNA-cmRas20 (5x, 10x) or noncomplementary NC20 (NC) compared with its activity in the absence of any other nucleic acid (-). For some samples the TRAP and regDNA were not heated and cooled together prior to measuring aptamer activity (not preheated). The background binding activity was determined using a shuffled TRAP sequence alone (BK). The binding activity of aptamer alone was evaluated on the same column and on a N6-linked ATP sepharose (N6). Averages and standard deviations are shown. All but two values are averages from 4 or more independent experiments. For NC and N6, the results are the average of two independent experiments. Hatched bars, background; black bars, 8att-cmRas20 TRAP that was melted and annealed slowly with the regDNA-cmRas20 or noncomplementary DNA before measuring aptamer activity; gray bars, 8att-cmRas20 TRAP that was not melted and annealed before measuring aptamer activity. White bars, ATP aptamer.

Figure 3. Relation between TRAP activity and regDNA concentration and reversibility of TRAP activation.

A. Relation between TRAP activity and regDNA concentration. The molar ratio of the regDNA-cmRas20 to the 8att-cmRas20 TRAP was varied to determine the effect of the regDNA on aptamer activity. The results are compiled from a series of experiments in which the TRAP concentration was a value between 0.075 μM and 0.15 μM, depending on the experiment. In each experiment a similar linear relationship was observed between ATP binding activity to regDNA concentration. The filter assay employing ATP-biotin and streptavidin-sepharose was used to assess the ATP binding activity. The R^2 obtained by linear regression for this line was 0.98. The molar ratio of regDNA-cmRas20 to 8att-cmRas20 TRAP (regDNA/TRAP), is plotted (■).

B. Reversal of TRAP activation. The property of reversal (shown in the bars the far right) was tested by first incubating the 8att-cmRas20 TRAP for 10 min at 23°C regDNAext (same sequence as regDNA-cmRas20, but with 15 As on either end) then adding crDNAext (complementary to regDNAext) and waiting another 30 min. All conditions shown in this figure contained 0.067 μM 8at-cmRas20 TRAP. Control conditions were the TRAP without regDNA added (cont), with regDNA-cmRas20, or with regDNA-cmRas20 for 10 min followed by NCext (noncomplementary sequence with 15 Ts on either end) for 30 min. The purpose of the latter two controls was to test that, under the conditions of the assay shown in figures 2 and 3A (regDNA and TRAP interactions), the use of an oligonucleotide with polyT extensions had no effect on the interaction between TRAP and regDNA. The molar ratios of TRAP:regDNAext:crDNAext was 1:5:25. These results are from a single experiment in which duplicate independent measurements were averaged to obtain each value. Similar results were obtained in three independent experiments.

For both figures, a background value of 4% subtracted from each datapoint was determined from the average retention of oligonucleotides containing either random sequences or a shuffled 8att-cmRas20 TRAP sequence. Noncomplementary DNA was

unable to activate the aptamer in the TRAP. Background values were determined using random and shuffled oligonucleotides.

Figure 4. Effect of blocking the attenuator sequence on TRAP aptamer activity.

The polyTG20 TRAPs with 0, 5, 8, 10, 12 and 14 base-long attenuators were incubated in the absence of other oligonucleotides or in the presence of either 1) a 20 nt oligomer complementary to the entire attenuator region and a variable length of the adjacent intervening sequence (cAtt) or 2) the regDNA-polyAC20 complementary to the 20 nt intervening antisense sequence. The ratio of cAtt or regDNA to TRAP was 5 to 1 for TRAPs with attenuators of 0,5,8, and 10 and 10 to 1 for TRAPs with 12 and 14nt attenuators. Black bars: activity in the absence of other oligonucleotides; White bars: TRAP in the presence of cAtt; Gray bars: TRAP in the presence of regDNA.

Figure 5. Impact of the intervening sequence and attenuator on TRAP function.

A. Two-dimensional structures predicted by the Mfold program (http://www.bioinfo.rpi.edu/applications/Mfold/) for oligonucleotides containing the ATP aptamer and a cmRas antisense sequence with or without an 8nt attenuator. 1) The poly TG 20 TRAP has a single predicted structure with a ΔG of -10.6. 2a-c) The three predicted structures for the 8att-cmRas20 TRAP with an 8nt attenuator have ΔGs of -6.2 (a) or -6.1 (b,c). 3) The single predicted structure for the 0att-cmRas20 TRAP with no attenuator has a ΔG of -4.2.

B. The activities of four TRAP constructs are compared: 8att-polyTG20 TRAP with an 8-nt attenuator (gray bars), 0att-polyTG20 TRAP (hatched gray bars), 8att-cmRas20 TRAP with an 8-nt attenuator (black bars; middle section) or 0att-cmRas20 TRAP with no attenuator (right and left slashed white bars; left section). The TRAPs were incubated alone (0), in the presence of 5, 10 or 100-fold molar excess of the complementary regDNA (either regDNA-polyAC20 or regDNA-cmRas20) or a 10-fold excess of noncomplementary NC20 (NC). The ability of the regDNA-cmRas20 to control activity 0att-cmRas20 TRAP activity was tested at 23°C and 37°C (Right-hand section). All other incubations were at 23°C.

Figure 6. ITC data for hybridization of regDNA-cmRas20 with 8att-cmRas20 TRAP or 0att-cmRas20TRAP.

Representative plots and the fitted ITC data are shown in this figure. The 0att-cmRas20 TRAP (A), 8att-cmRas20 TRAP (B) and the 20nt intervening sequence of the cmRas20 TRAPs (C) were titrated with regDNA-cmRas20 and the heats of reaction were measured by isothermal titration calorimetry. For these examples the first oligonucleotide was initially at 5 μM in 1.4 ml and the final concentration of regDNA-cmRas20 was 7.6 μM in 1.65 ml with a resulting final molar ratio of 1.8 for regDNA-cmRas20/first oligonucleotide. For all three of these examples regDNA-cmRas20 was titrated into the cell with 600 s between injections. The upper set of three graphs shows the time courses for the three titrations. The lower set of graphs shows the heat absorbed as a function of the molar ratio of the interacting species. The compiled data from these and other analyses are shown in Table 1.

Figure 7. Effect of the attenuator on structural forms of cmRas20 TRAP: regDNA hybrids.

End labeled 0att- and 8att-cmRas20 ^{32}P-TRAPs (0.8 μM), were hybridized with the regDNA-cmRas20 in the absence of ATP by incubating the oligonucleotide pair together for 10 min at 23°C. The hybridized pairs were then resolved by non-denaturing polyacrylamide gel electrophoresis and the distribution of ^{32}P-DNA was determined. The 0att cmRas20 TRAP or the 8att-cmRas20 TRAPs were incubated alone (-) or with a 10-fold excess of noncomplementary NC20 (NC) or complementary regDNA-cmRas20. The dashed line shows the position of ^{32}P-ATP in the gel after electrophoresis. The numbers show the % of the total ^{32}P-TRAP in the corresponding band in this experiment. Average numbers for all experiments are given in the main text.

Figure 8. Discrimination of single base mismatches by a 9att-cmRas15 TRAP.

A 9att-cmRas15 TRAP with a 15 nt antisense intervening sequence and a 9 nt attenuator was tested for its ability to be activated at 37°C by four regDNA-cmRas15: a perfect match (black squares), a single base-pair mismatch at position 7 on the 15nt regDNAm-cmRas15 in which the perfect match (G) was changed to A for a C::A mismatch (gray squares, regDNAm7A-cmRas15) or to C for a C::C mismatch (white triangles, regDNAm7C-cmRas15), or in which the perfect match (TG) at positions 6 and 7 were changed to CA for a CA::AC mismatch (black circles, regDNAm6C7A-cmRas15). The regDNA to TRAP ratio was varied over a 20-fold range. The incubations were performed at 37°C and the results are expressed as percent of 9att-cmRas15 TRAP DNA bound to ATP with a background of 13% (nonspecific binding) subtracted. The background binding was determined using two oligonucleotides with randomized sequences, one of the TRAP and the other of the aptamer. The same average % bound was found for both randomized sequences. Each datapoint is an average of the results from between 2 and 8 experiments in which each experimental value was the average of two independent estimates.

TABLES AND FIGURES

Table 1: Attenuator effect on the thermodynamics of the interaction of regDNA-cmRas20 and 8att-cmRas20 TRAP

Oligonucleotide	Assumption of the Fitting model	N	ΔH (kcal/moL)	ΔS (cal/moL)	ΔG (kcal/moL)
20mer	1n	1.0	-110	-313	-12.1
0att-cmRas20 TRAP	2n	0.5	-81	-217	-14.0
		0.7	-67	-178	-12.1
8att-cmRas20 TRAP	1n	0.9	-82	-225	-11.5

Thermodynamic parameters were obtained from fitting ITC data for the interaction of the regDNA-cmRas20 with either the 0att-cmRas20 TRAP or the 8att-cmRas20 TRAP (Materials and Methods). In each case the first oligonucleotide was placed in the cell at 2.5 or 5 μM initial concentration. The second oligonucleotide was titrated into the cell with 25 injections and to a final ratio of about 1.8 over the first oligonucleotide. Each oligonucleotide pair was tested in two protocols, each protocol using a different member of the pair titrated into the cell. The plots were fit mathematically using algorithms that assume a single (1n) or two (2n) alternate binding complexes between the interacting oligonucleotides. The results from both protocols were averaged for the results shown in this table.

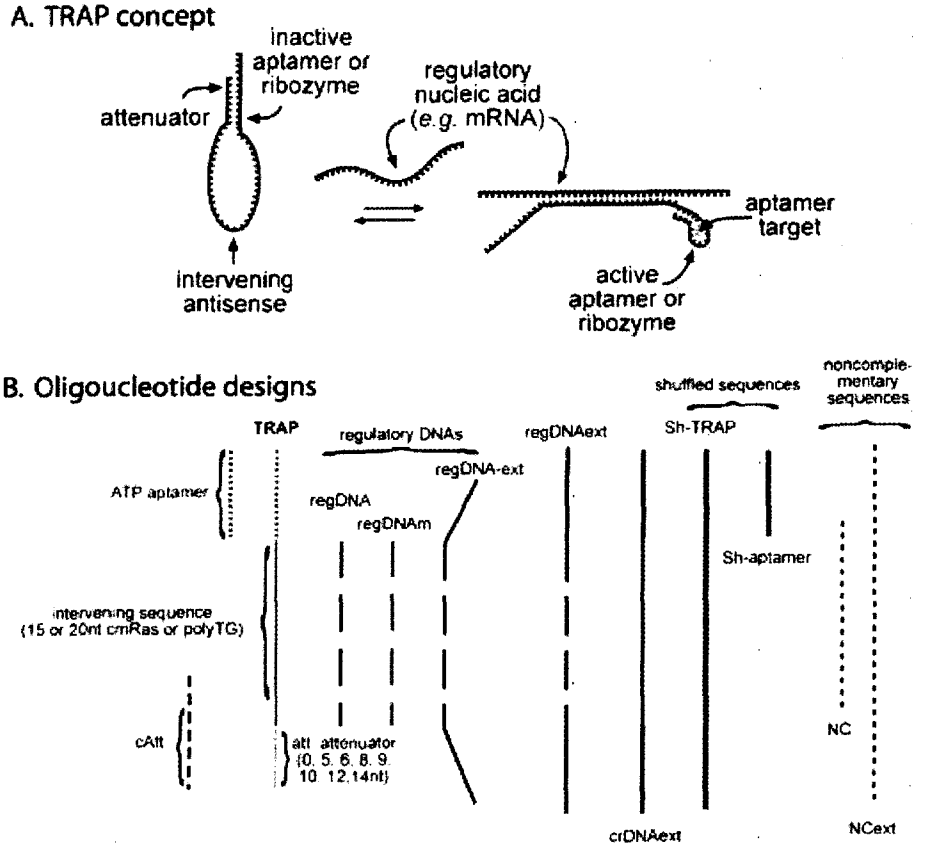
A. TRAP concept
inactive aptamer or ribozyme
attenuator
regulatory nucleic acid (e.g. mRNA)
aptamer target
intervening antisense
active aptamer or ribozyme
B. Oligoucleotide designs
TRAP
regulatory DNAs
regDNAext
shuffled sequences
Sh-TRAP
noncomple-mentary sequences
ATP aptamer
regDNA-ext
regDNA
regDNAm
Sh-aptamer
intervening sequence (15 or 20nt cmRas or polyTG)
cAtt
att attenuator (0, 5, 6, 8, 9, 10, 12,14nt)
NC
crDNAext
NCext

Figure 1

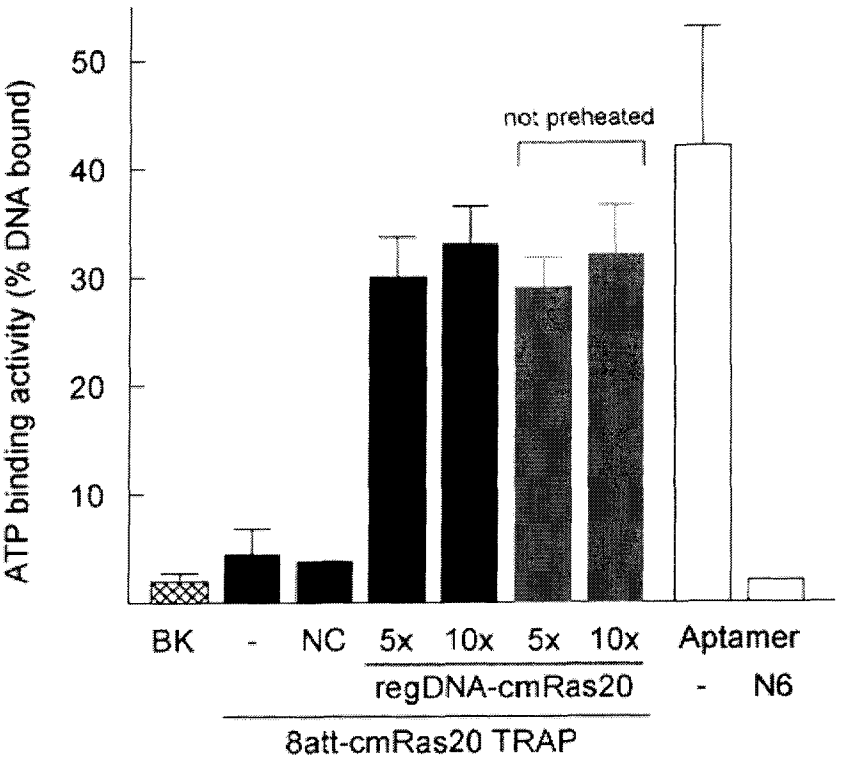
ATP binding activity (% DNA bound)
50
40
30
20
10
not preheated
BK
-
NC
5x
10x
5x
10x
Aptamer
regDNA-cmRas20
-
N6
8att-cmRas20 TRAP

Figure 2

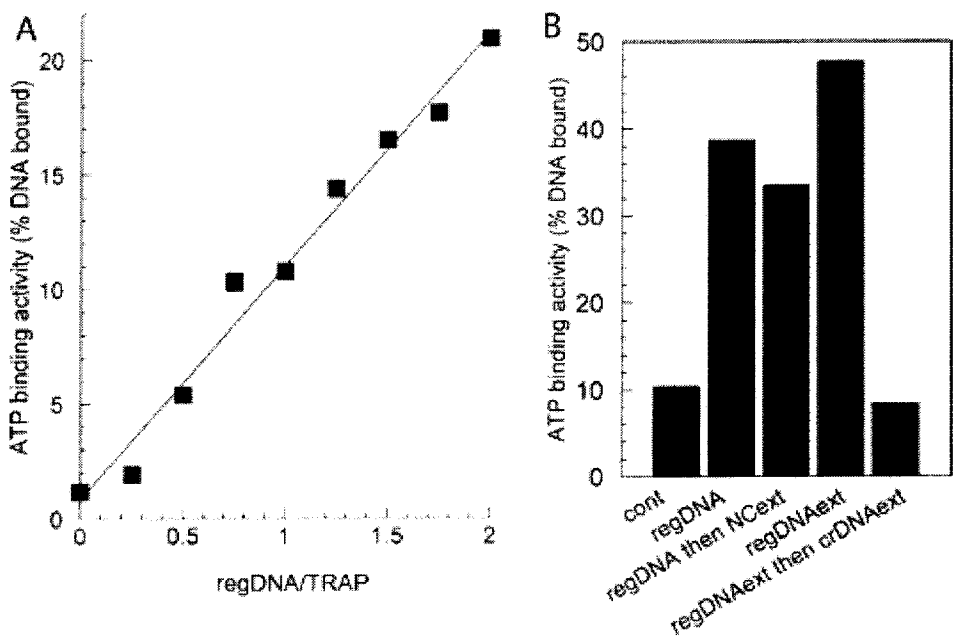
A
ATP binding activity (% DNA bound)
0
5
10
15
20
0
0.5
1
1.5
2
regDNA/TRAP
B
ATP binding activity (% DNA bound)
0
10
20
30
40
50
cont
regDNA
regDNA then NCext
regDNAext
regDNAext then crDNAext

Figure 3

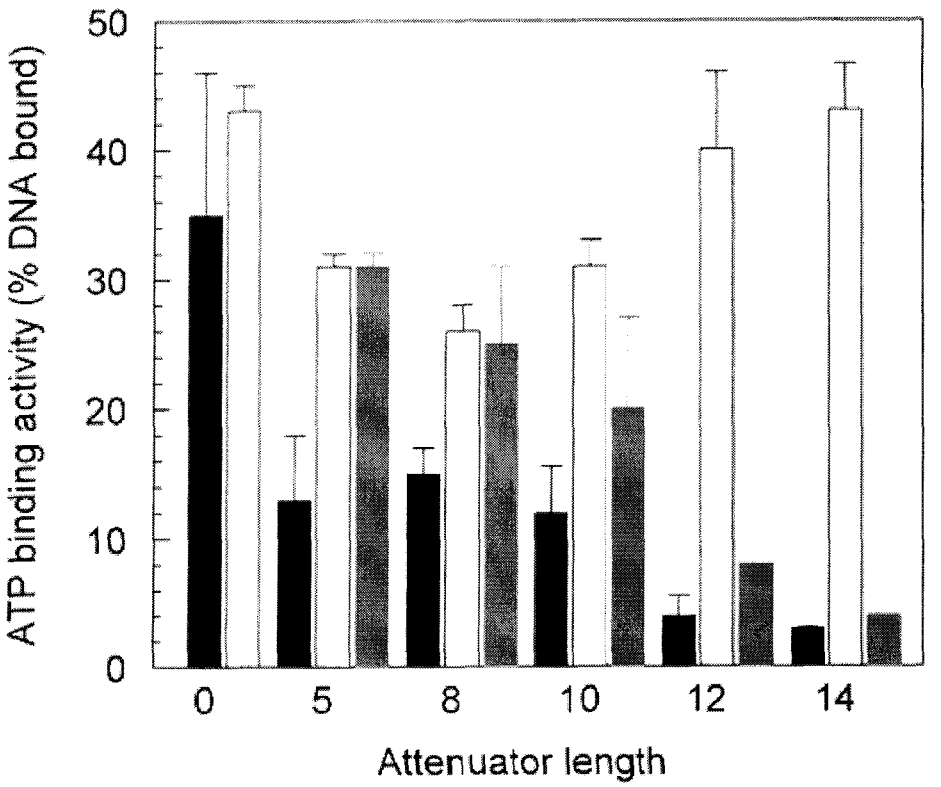
ATP binding activity (% DNA bound)
50
40
30
20
10
0
0
5
8
10
12
14
Attenuator length

Figure 4

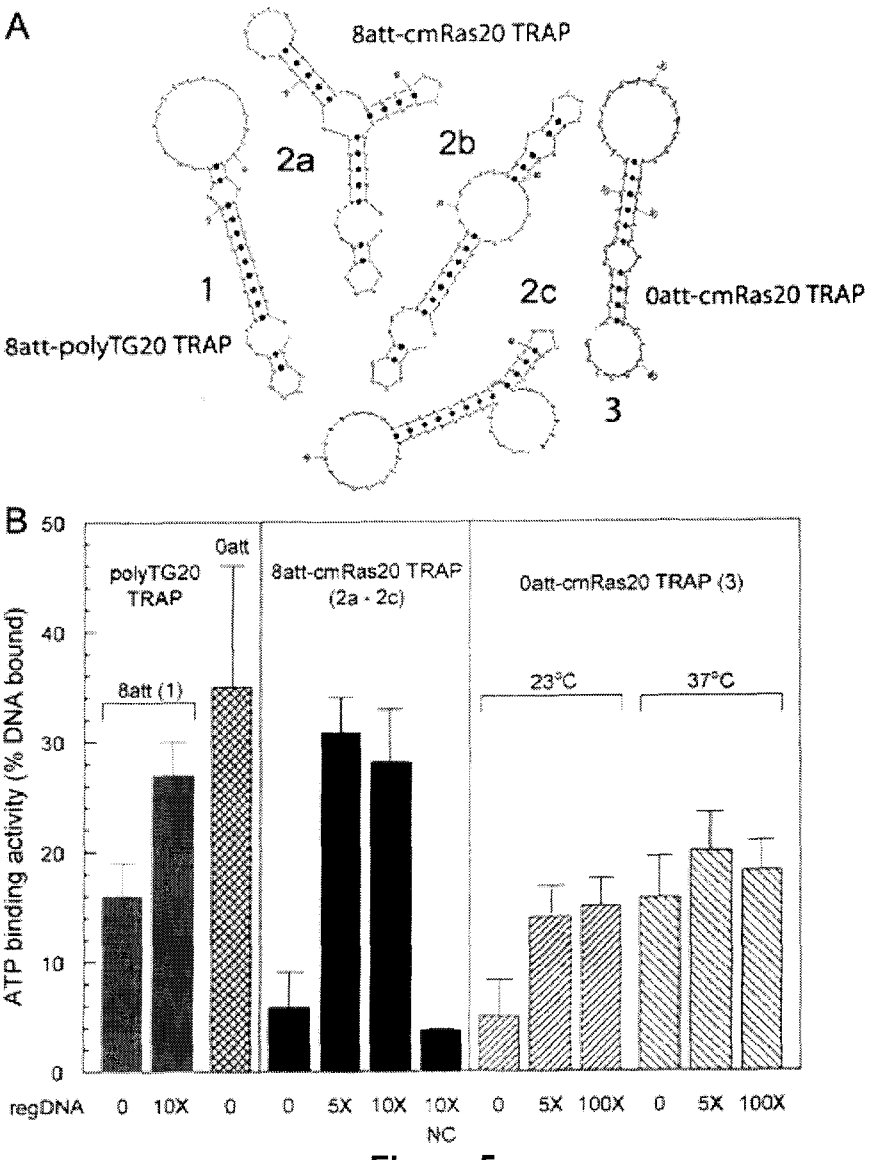
A
8att-cmRas20 TRAP
2a
2b
1
2c
0att-cmRas20 TRAP
8att-polyTG20 TRAP
3
B
ATP binding activity (% DNA bound)
50
40
30
20
10
0
polyTG20 TRAP
0att
8att-cmRas20 TRAP (2a - 2c)
0att-cmRas20 TRAP (3)
8att (1)
23°C
37°C
regDNA 0 10X 0 0 5X 10X 10X 0 5X 100X 0 5X 100X
NC

Figure 5

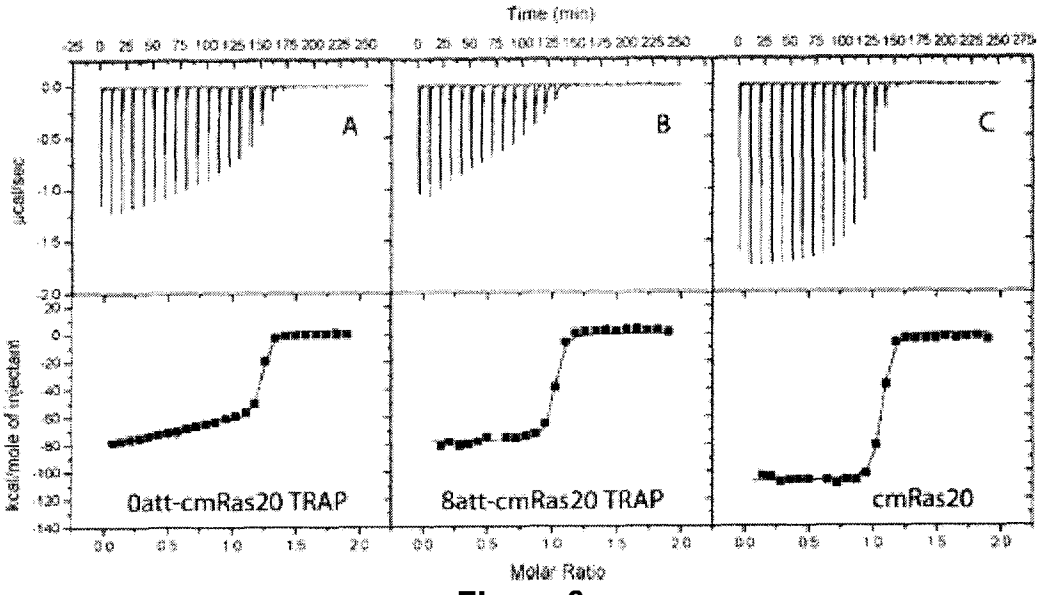
Time (min)
A
B
C
µcal/sec
kcal/mole of injectant
0att-cmRas20 TRAP
8att-cmRas20 TRAP
cmRas20
Molar Ratio

Figure 6

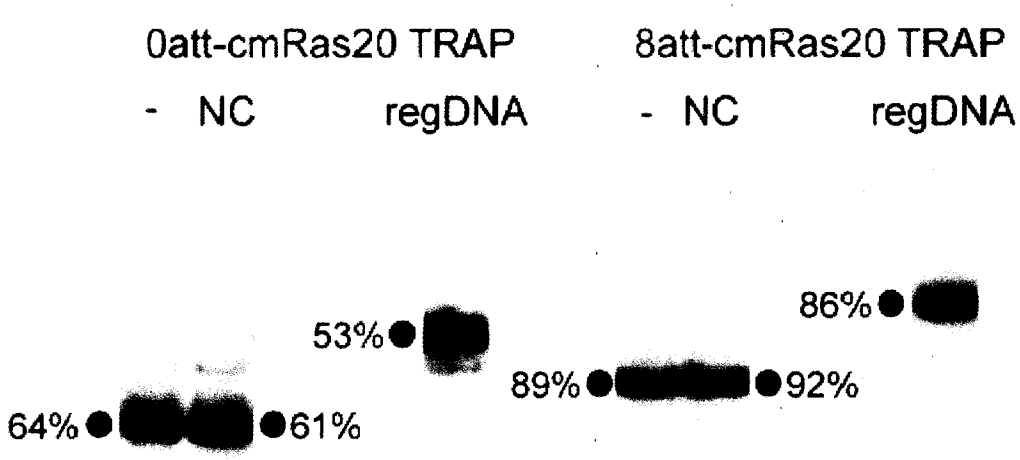
0att-cmRas20 TRAP
- NC
regDNA
8att-cmRas20 TRAP
- NC
regDNA
53%
64%
61%
86%
89%
92%

Figure 7

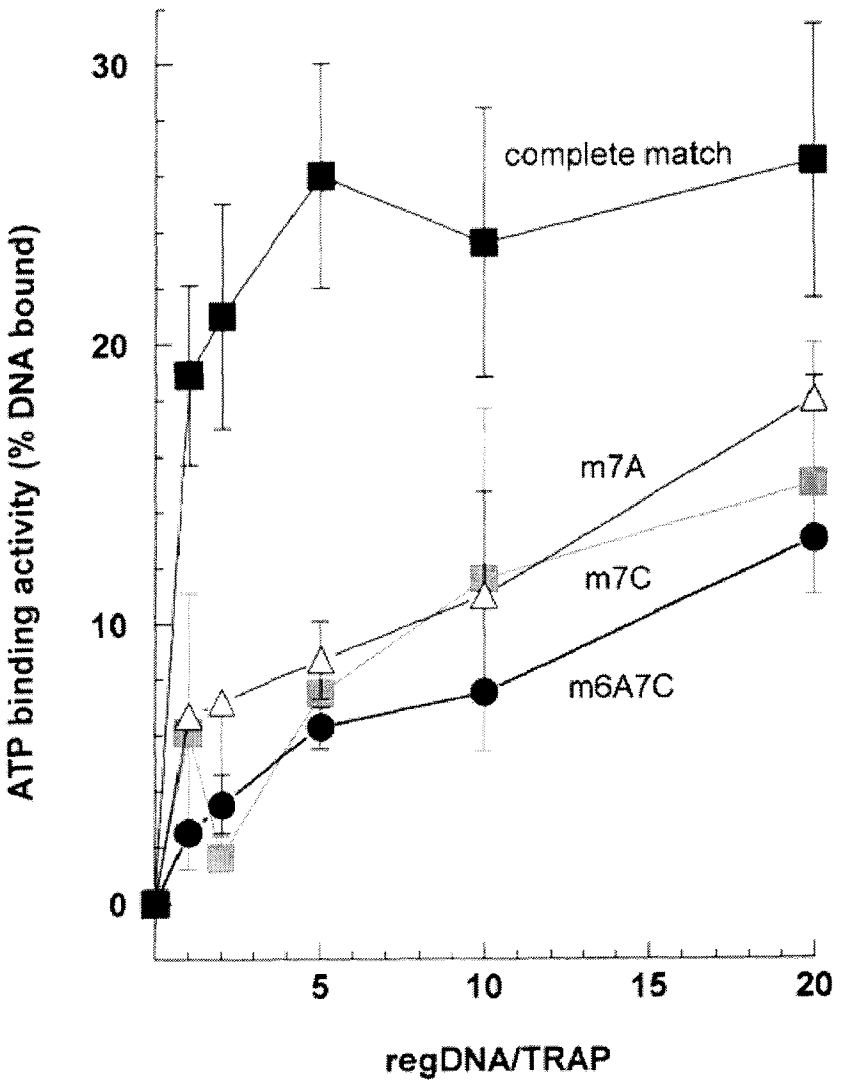
30
20
10
0
ATP binding activity (% DNA bound)
complete match
m7A
m7C
m6A7C
5
10
15
20
regDNA/TRAP

Figure 8

SUPPORTING INFORMATION

A. Oligonucleotides Used in This Study

The following tables list the sequences of the oligonucleotides used in this study and discuss the nomenclature for each.

ATP DNA Aptamer:	CCTGGGGGAGTATTGCGGAGGAAGG

ATP DNA TRAPs
The TRAPs cited in the manuscript differ by the length and sequences of their intervening sequences and the length of their attenuators. In the list below the intervening sequence is bolded and the attenuator is underlined.
polyTG-TRAPs: All polyTG TRAPs used in this manuscript had 20 nt intervening sequences. Their attenuator sequences varied in length as decribed below: 0att-polyTG TRAP: CCTGGGGGAGTATTGCGGAGGAAGG**TTTTTTGTTTTTGTTTTGTT** 5att-polyTG TRAP: CCTGGGGGAGTATTGCGGAGGAAGG**TTTTTTGTTTTTGTTTTGTT**CCGCA 8att-polyTG TRAP: CCTGGGGGAGTATTGCGGAGGAAGG**TTTTTTGTTTTTGTTTTGTT**CCGCAATA 10att-polyTG TRAP: CCTGGGGGAGTATTGCGGAGGAAGG**TTTTTTGTTTTTGTTTTGTT**CCGCAATACT 12att-polyTG TRAP: CCTGGGGGAGTATTGCGGAGGAAGG**TTTTTTGTTTTTGTTTTGTT**CCGCAATACTCC 14att-polyTG TRAP: CCTGGGGGAGTATTGCGGAGGAAGG**TTTTTTGTTTTTGTTTTGTT**CTCCGCAATACTCC
cmRas TRAPs: Two different lengths of intervening sequences were used for these TRAPs. Therefore they are identified by the length of the attenuator (#att) and the length of the intervening sequence (cmRas20 or cmRas15): 0att-cmRas20 TRAP: CCTGGGGGAGTATTGCGGAGGAAGG**GTACTCCTCAGGGCCGGCGG** 6att-cmRas20 TRAP: CCTGGGGGAGTATTGCGGAGGAAGG**GTACTCCTCAGGGCCGGCGG**CCGCAA 8att-cmRas20 TRAP: CCTGGGGGAGTATTGCGGAGGAAGG**GTACTCCTCAGGGCCGGCGG**CCGCAATA 10att-cmRas20 TRAP: CCTGGGGGAGTATTGCGGAGGAAGG**GTACTCCTCAGGGCCGGCGG**CCGCAATACT
9att-cmRas15 TRAP: CCTGGGGGAGTATTGCGGAGGAAGG**GTACTCCTCAGGGCC**CCGCAATAC

Regulatory DNAs:

A) ssDNAs that are completely complementarity to the TRAP intervening sequence, where # is the nt length of the DNA:

1) regDNA-polyAC20: *AACAAAACAAAAACAAAAAA*
2) regDNA-cmRas20: *CCGCCGGCCCTGAGGAGTAC*
3) regDNA-cmRas15: *GGCCCTGAGGAGTAC*

B) ssDNAs that are complementarity to the TRAP intervening sequence but contain some noncomplementary bases: regDNA15m##, where the ## represents the positions(s) of mismatch(es) within the intervening sequence. Mismatches are also identified in the sequences by lower case letters.

1) regDNA-cmRas15m7a: *GGCCCT a AGGAGTAC*
2) regDNA-cmRas15m6a,7a: *GGCCCc a AGGAGTAC*
3) regDNA-cmRas15m7c: *GGCCCT c AGGAGTAC*

C) ssDNAs that contain a central region of 20 bases complementary to the 8att-cmRas20 TRAP intervening sequence and that is surrounded by a terminal sequences of 15 As on each side

1) regDNA-cmRas20-ext
AAAAAAAAAAAAAAA*CCGCCGGCCCTGAGGAGT*ACAAAAAAAAAAAAAAA

cmRas sequences

ssDNAs that contain the 20 base sequence of cmRas that is also in the cmRas20TRAPs. This sequence is complementary to the regDNA-cmRas20

1) cmRas20: **GTACTCCTCAGGGCCGGCGG**
1) crDNA-cmRas20-ext:
TTTTTTTTTTTTTTT**GTACTCCTCAGGGCCGGCGG**TTTTTTTTTTTTTTT

cAtts:
ssDNAs containing a sequence that is complementary to the attenuator, where the first number is the number of bases in the complementary attenuator and the second number is the length of the oligonucleotide. The region complementary to the attenuator is underlined and italicized.

0cAtt20: AACAAAACAAAAACAAAAAA
5cAtt20: *TGCGG*AACAAAACAAAAACA
8cAtt20 : *TATTGCGG*AACAAAACAAAA
10cAtt20: *AGTATTGCGG*AACAAAACAA
12cAtt20: *GGGAGTATTGCG*AACAAAAC
14cAtt20: *GGAGTATTGCGGAG*AACAAA

Noncomplementary sequences

Sequences that are not complementary to any of the other sequences listed above. These sequences were created by picking random sequences or by shuffling sequences listed above. Shuffled sequences are referred to with the prefix Sh followed by the name of the sequence that was shuffled.

Random:
1) NC30: TCGCCACTAAATCATCGACGGATGTGCGGT
2) NC20: CTACAATGTCACCTCCATCC
2) NC20ext15: TTTTTTTTTTTTTTTTGGATGGAGGTGACATTGTAGTTTTTTTTTTTTTTT

Shuffled:
Sh8attcmRas20TRAP:
GGGCCGGGACCATATAGCGGTTACGAGGGGGCGGAGACGGACCCGCGTATTTC
ShATP DNA Aptamer: GGGGGTAAAGTATTCCGGGGCGGGA
Sh8att-polyTG20 TRAP:
GACTGTATTGGGTGCTGTCTTTTATAGGTCTGAGTAAAGTGGGCTTTGTGCTT

B. Comparison of the Activity of a Fully Activated TRAP with the Unmodified Aptamer.

The activity (% total 32P-DNA bound) of the aptamer was compared with that of the 8att-cmRas20TRAP and the 9att-cmRas15 TRAP in the presence of a range of concentrations of regDNA-cmRas20 or regDNAcmRas15 respectively are shown in Figure S1. The concentration of the TRAP ranged from 0.067-0.67 μM for different experiments. These experiments were performed at 37°C. In each experiment, independent duplicates were used to determine the percent of aptamer of TRAP bound to ATP. For the data shown, the results for the 8att-cmRas20TRAP are the averages of 2-6 experiments and the results for the 9att-cmRas15 TRAP are averages of 10-14 experiments. In each experiment, the average result for activated TRAP was divided by the average result for aptamer to give a value for the activity of the TRAP as a percentage of the aptamer activity. The number of experiments contributing to each value are shown above each bar. White bars, 8att-cmRas20TRAP and regDNA-cmRas20; Black bars, 9att-cmRas15 TRAP and regDNA-cmRas15. The results show that a fully activated TRAP has the same activity as the unmodified aptamer.

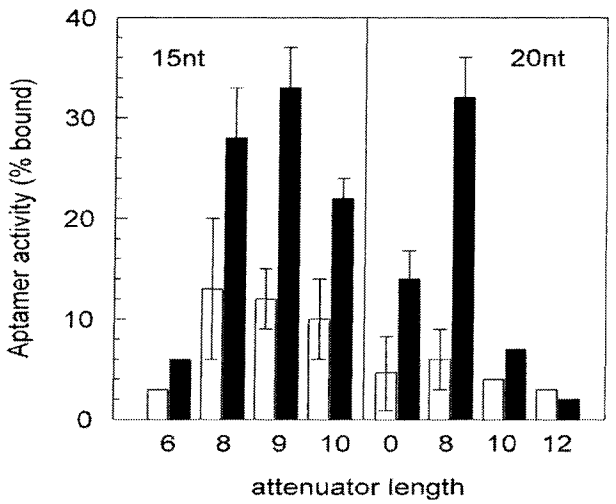

Figure S1. Activities of Activated TRAPs as a fraction of the activity of the unmodified ATP DNA aptamer

C. Effect of attenuator length on the ATP Binding Activity of cmRas TRAPs

cmRas20 and cmRas19 TRAPs were prepared with a range of attenuator lengths and tested for the ability of the complementary regDNA-cmRas to activate ATP binding activity. The cmRas15 TRAPs were tested at 37°C with and without regDNA-cmRas15 and the cmRas20 TRAPs were tested at 23°C with and without regDNAcmRas20. For both TRAPs, the ratio of regDNA to TRAP was 2 to 1. The results demonstrate that, as for the polyTG20 TRAP, there is an optimal length of attenuator for aptamer regulation. For the TRAPs tested, the optimal attenuator length was 8 to 9nt.

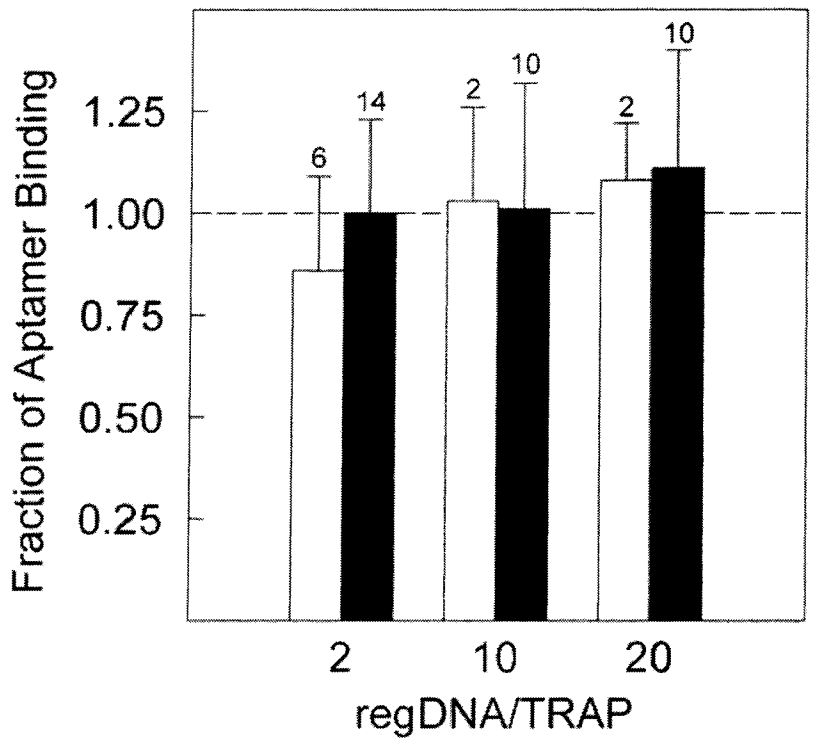

Figure S2. Effect of attenuator length on the ability to activate the TRAP aptamer activity

CHAPTER 4. THE USE OF TILED MICROARRAYS AND COMPUTATIONAL ANALYSIS TO SELECT ANTISENSE SEQUENCES FOR TESTING *IN VIVO*[*]

A paper to be submitted to *Nucleic Acid Research*

ABSTRACT

The efficient identification of sequences in mRNAs that are effective targets for antisense oligodeoxynucleotides (ODNs) *in vivo* is an important goal. *In vivo* tests of antisense ODNs are time consuming and expensive. Therefore, we investigated computational and *in vitro* experimental methods to identify antisense sequences that are effective *in vivo*. The Lcn2 mRNA sequence was used for this analysis. Two computational programs with different RNA secondary prediction algorithms were tested and found to predict a range of potential antisense sequences. As an *in vitro* test of antisense activity, I determined the ability of the Lcn2 mRNA to hybridize with a tiled microarray of 20mers complementary to overlapping sequential sequences in the mRNA. Hybridization was performed under nondenaturing conditions and at salt concentrations that resemble those in the cell. From these preliminary computational and *in vitro* studies seven oligodeoxynucleotides (ODNs) were chosen to be tested further *in vivo* as antisense ODNs to target the Lcn2 mRNA.

* The study done here is included in a manuscript which will be submitted to Nucleic Acid Research. The data in the manuscript done by other authors is not included here. In the manuscript, the worked done by other authors: Ahmed Awad and Xiaoling Song tested seven selected oligodeoxynucleotide as antisense ODNs to target the Lcn2 mRNA in mouse HC11 cells. Ahmed selected Bcl2 mRNA and with my help did similar tiled microarray experiments as I did here. Long Qu is finishing a more comprehensive statistical analysis for both Lcn2 mRNA and Bcl2 mRNA microarray data. Their results are briefly discussed with no data shown.

INTRODUCTION

The sequence-specific silencing of gene expression by antisense oligodeoxynucleotides has attracted great interest in the development of effective gene therapies for a wide variety of diseases (*1, 2*). There are a number of requirements for successful oligodeoxynucleotide-mediated inhibition of protein biosynthesis through the antisense mechanism. These include high affinity and faithful base pairing specificity of the antisense-mRNA pair, intracellular delivery capability and stability of the antisense molecule to nucleases in the biological environment (*3*). All these requirements presuppose that the target site of the mRNA is accessible to the antisense oligodeoxynucleotides. During their synthesis RNA molecules quickly fold and arrange themselves into tertiary structures that can include a large variety of secondary structural motifs (*4, 5*) and are complicated by RNA-associated proteins (*6*). These secondary and tertiary structures of RNAs leave only a small fraction of RNA sequences available for efficient antisense oligodeoxynucleotide hybridization (*7*). Thus, the biological efficacy of each antisense oligodeoxynucleotide is strongly affected by its target site accessibility. Because of its fundamental importance to antisense technology, many approaches, experimental and computational, have been developed to identify optimum antisense accessible sites in mRNAs.

In the direct test of *in vivo* efficacy oligodeoxynucleotides targeted to various regions of a mRNA are randomly chosen, synthesized individually and their antisense activities are measured (*8, 9*). However, this approach of empirically testing multiple oligodeoxynucleotides *in vivo* is expensive and very time consuming. The demands of time and expense limit coverage of the mRNA primary sequence investigated by this method and therefore a complete picture of the accessibility of all possible sites on a target mRNA is not obtained.

Computer algorithms based on minimum free calculations (*10-13*) or partition function calculations followed by statistical sampling (*14, 15*) can predict secondary structures of RNA sequences to be used to identify target accessibility and the rational

design of antisense and nucleic acid probes (*16-18*). However, these computer programs do not predict tertiary structures that may also influence target accessibility. Moreover, long RNAs such as mRNAs, fold into many different structures with similar free energies that can each fold into one or more tertiary structures. The combined uncertainty of the *in vivo* distribution of secondary structures and their associated tertiary structures makes it very difficult to identify probable antisense sequences from a primary structure.

Several *in vitro* approaches have been developed for identifying optimal target antisense sequences in mRNAs. One approach is to map the antisense-accessible sites on mRNAs by hybridization with random oligodeoxynucleotide libraries followed by either RNase H cleavage, or extension with reverse transcriptase (*19-21*). Hybridization of antisense oligodeoxynucleotides has also be analyzed by MALDI-TOF to identifying the accessible regions on an mRNA (*22*).

Oligodeoxynucleotide arrays provide a simple tool for quantitative measurement of the binding of a set of complementary oligodeoxynucleotide sequences to a target RNA. In this method, an array of oligodeoxynucleotides covalently linked to a glass surface is used to measure heteroduplex formation with the corresponding target mRNA, which is radio- or fluorescently labeled. The results obtained with this approach show a good correlation between binding strengths and antisense activity *in vivo* (*23, 24*). Since these studies were published computational methods for folding nucleic acids and identifying hybridization targets have been improved.

As an *in vitro* test of antisense activity, I determined the ability of the Lcn2 mRNA to hybridize with a tiled microarray of 20mers complementary to overlapping sequential sequences in the mRNA. Hybridization was performed under nondenaturing conditions and at salt concentrations that resemble those in the cell. From these preliminary computational and *in vitro* studies seven oligodeoxynucleotides (ODNs) were chosen to be tested further *in vivo* as antisense ODNs to target the Lcn2 mRNA. The efficacies of oligodeoxynucleotides, identified by each method, were further tested as antisense oligodeoxynucleotides *in vivo*.

MATERIALS AND METHODS

Oligodeoxynucleotides

All oligodeoxynucleotides used in this study were purchased from Integrated DNA Technologies (Coralville, IA). The oligodeoxynucleotides used for the tiled microarray were 20mer oligodeoxynucleotides and were obtained in a 96-well plate at a total amount of 15 nmoles each. Eighty four oligodeoxynucleotides were designed as 20mers that are complementary to the Lcn2 mRNA target from 5' to 3' in 10 nt overlapping intervals. 9 oligodeoxynucleotides with random sequences were also synthesized. Diethylpyrocarbonate (DEPC) treated-water was added to each well to give a final concentration of 100 mM per oligodeoxynucleotide. The plate was then stored at -20°C.

Sequence and Materials Information

Mus musculus lipocalin 2 (Lcn2) mRNA sequence is 853nt and the sequence can be obtained from NCBI.(NM_008491). The plasmid pcDNA3-Lcn2 has full length Lcn2 cDNA sequence and T7 promoter upstream of Lcn2 cDNA. The sequence information of 84 antisense oligodeoxynucleotides can be derived from Lcn2 mRNA sequence easily. The antisense oligonucleotides were named by the position of the first 5' end nucleotide of the corresponding 20nt target sequences on Lcn2 mRNA. For example, oligodeoxynucleotide 1 targets 1-20 nt of Lcn2 mRNA, oligodeoxynucleotide 11 targets 11-30 nt of Lcn2 mRNA, etc. The full name list of the 84 antisense oligodeoxynucleotides is in table 1. The sequences of the 9 random oligodeoxynucleotides are also listed in table 1. Corning Epoxide coated slides and Epoxide Coated Slide Starter Kit with 5ml Epoxide Spotting Solution are from Corning (Corning, NY). ChromsTide Alexa Fluor 546-14-UTP 1mM in TE Buffer and SYBR GREEN II are from Molecular Probes (Carlsbad, CA). The AmpliScribe T7 High Yield Transcription Kits is from Epicentre (Madison, WI). The Micro Bio-Spin P30 Chromatography Columns are from BioRad (Hercules, CA). The hybridization Cassette is from ArrayIt Microarray Technology (Sunnyvale, CA). The cartesian PixSys 5500

Arrayer and General Scanning ScanArray 5000 is at Microarray Facility http://www.plantgenomics.iastate.edu/microarray/equipment/.

Preparation of Fluorescently Labeled Lcn2 Transcripts

Fluorescently labeled RNA transcripts for hybridization to the oligodeoxynucleotide arrays were synthesized by *in vitro* transcription. Lcn2 mRNA was prepared from the plasmid pcDNA3-Lcn2 that contains a T7 promoter sequence. The plasmid was linearized with EcoRI. Transcriptions of Lcn2 mRNA sequences were carried out in 20 µl volume at 37°C for 2 hr in the presence of 2.5 mM each ATP, CTP, and GTP, 2.1 mM UTP and 0.4 mM ChromaTide Alexa Fluor 546-14-UTP using AmpliScribe T7-Flash Transcription Kit . After DNase I treatment, the RNA products were purified by Micro Bio-Spin P30 Chromatography Columns as described in the product protocol. The absorbances of RNA preparations (A260) and Alexa Fluor (A555) were measured and the base-to-dye ratio and concentration of the fluorophore-labeled RNA was determined according to the manufacturer's recommendations.

Printing of The Oligodeoxynucleotides Arrays

Antisense oligodeoxynucleotides were designed as 20mers that are complementary to the mRNA target from 5' to 3' in 10 nt overlapping intervals. The oligodeoxynucleotide solutions were transferred to a Corning 96-well microplate, dried by vacuum centrifugation and re-dissolved in two different printing solutions, Buffer A and Buffer B, to reach the desired concentrations. Printing solution A: Epoxide Spotting Solution from the Epoxide Coated Slide Starter Kit. Printing solution B: 150mM Dibasic Sodium Phosphate, DEPC treated H_2O, pH 8.5 at 23°C. Ninety three 20nt oligodeoxynucleotides were printed onto Corning epoxide coated slides according to the manufacturer's protocol (55% relative humidity during printing, followed by incubation at 70% relative humidity for 12-17 h). Some spots on the slides were printed with spotting solutions contain no oligodeoxynucleotides (as negative controls).

Pre-Hybridization

Pre-hybridization was done immediately preceding the application of the oligodeoxynucleotides onto the arrays. This step has the purpose of blocking the unused surface of the slide and removing loosely bound oligodeoxynucleotides. The preparation of the hybridization solutions can be completed while the arrays are being pre-hybridized. Pre-hybridization solution consisted of 5 x SSC,0.1%SDS, and 0.1 mg/mL acetylated bovine serum albumin (BSA). The 5 X SSC was diluted from 20 X SSC buffer. The 20 X SSC buffer contains 3M sodium chloride and 0.3M sodium citrate, pH 7.0 at 23 °C. The pre-hybridization solution was pre-warmed to 42 °C. Arrays were immersed in pre-hybridization solution and incubated at 42 °C for 45 to 60 minutes. Pre-hybridized arrays were transferred into 0.1 x SSC diluted from 20 X SSC buffer and incubated at ambient temperature (22 to 25 °C) for 5 minutes to wash. The same wash was repeated twice for a total of three washes. The arrays were transferred to water and incubated at ambient temperature for 30 seconds then dried by centrifugation at 1,600 x *g* for 2 minutes. While completing preparation of the hybridization solution the arrays were maintained in a dust-free environment.

Check The Printing Quality By SYBR GREEN II Staining

To check whether the oligodeoxynucleotides had been successfully printed onto the glass slides, the procedure described by Simpson *et al.* (*25*) was used. Summarized briefly, the procedure uses SYBR GREEN II to stain the single stranded oligodeoxynucleotides on the array. After washing, the arrays were dried by centrifugation at 1,600 x g for 2 minutes. The arrays were scanned using the Scan Array 5000 scanner at the Microarray facility. SYBR GREEN II dye has a fluorescence excitation maximum at 494 nm and a fluorescence emission maximum at 512nm. After the slide was scanned, the SYBR Green II was removed according the procedure described in Simpson *et al.* (*25*) and used for hybridization.

Array Hybridization And Image Analysis

Arrays were hybridized under physiological conditions using the hybridization buffer

(25 nM Alexa Fluor 546-14-UTP labeled Lcn2 mRNA, 0.2ug/ul of yeast tRNA, 0.2ug/ul of polyadenylic acid, 1U/ul RNase Inhibitor, 13.5 mM NaCl, 150 mM KCl, 0.22 mM Na_2HPO_4, 0.44 mM KH_2PO_4, 100 μM $MgSO_4$, 120 nM $CaCl_2$, 120 μM $MgCl_2$, 6 mM glutathione, 20 mM HEPES, pH 7.25). The array was covered with a cover glass and 100 μl hybridization buffer was pipetted onto the arrayed surface. The slide was then transferred to a hybridization chamber and left for hybridization at 37°C for 16 h. After washing twice in 1 X SSC buffer, 2 min each followed by washing twice in 0.1 X SSC, 1 min each, the slide was dried by centrifugation at 1,600g for 2 min and scanned using a Scan Array 5000 scanner. Alexa Fluor 546-14-UTP dye has a fluorescence excitation maximum at 550nm and a fluorescence emission maximum at 570nm. The image was analyzed using the microarray analysis software (GridGrinder, a free microarray analysis software released by Corning. Free download : http://gridgrinder.sourceforge.net/).

Lcn2 MRNA Secondary Structure Prediction

The secondary structures of Lcn2 mRNAs were estimated using the Mfold and Sfold web servers for nucleic acid secondary structure prediction. The Mfold web server for RNA secondary structure prediction is located at http://www.bioinfo.rpi.edu/applications/mfold/old/rna/ (*12*) and the Sfold web server is located at http://sfold.wadsworth.org/index.pl (*17*). For both programs, the default setting were used to predict Lcn2 mRNA secondary structures.

Prediction of Effective Antisense Oligodeoxynucleotide For Lcn2 MRNA

In this study, I chose two programs to predict the effective antisense oligodeoxynucleotides for the Lcn2 mRNA. Both programs are freely available from internet. OligoWalk is part of a software package, called RNA structure, based on the Mfold algorithms to predict antisense affinity to mRNA (*16*). The free software package can be downloaded at http://128.151.176.70/RNAstructure.html. Sfold is a software package developed by Ding *et al.*(*17*). It is free to use at http://sfold.wadsworth.org/index.pl . The algorithm for the Sfold is based on the

equilibrium partition function of RNA secondary structures and a statical sampling algorithm. Soligo is the program in Sfold developed for antisense target accessibility prediction and rational design of antisense oligodeoxynucleotides.

The Lcn2 mRNA sequence was analyzed using OligoWalk and Soligo, respectively. For OligoWalk, the first RNAFold program in RNAstructure (version 4.2) was used to fold the Lcn2mRNA. When RNAFold was used, the default parameters for the suboptimal structures are: Max% energy difference: 10%. Max Number of structures: 20. Window size: 15. The temperature was set to 37 °C. After the mRNA was folded, the OligoWalk program was used to predict the effective antisense oligonucleotides using default settings. The default selection for the mode is: Break local structure. Other parameters also need to be defined. As part of the default set up, the target (Lcn2 mRNA) suboptimal structures were not included in the free energy calculation. The antisense oligo was set to DNA. (RNA is another choice). The length of antisense oligo is 20nt and the concentration was set to 1μM (Default).

The RNAstructure software package was a free download and installed on a PC. The Sfold software had to be used through the internet. The length of antisense oligodeoxynucleotides was also set to 20nt in Soligo. The temperature used in Soligo was also 37 °C.

RESULTS

Design of Antisense Oligodeoxynucleotide Microarray Targeting Lcn2 MRNA

As shown in Fig.1C, there are 96 spots on each subgrid. It included 84 antisense oligodeoxynucleotides, 9 random sequences and 3 spots that contain only buffer. Two different printing solutions: Buffer A and Buffer B were used to print the same set of oligodeoxynucleotides. For Buffer A, three oligodeoxynucleotides concentration were used: 200 μM, 150 μM and 80 μM. For Buffer B, only 80 μM oligodeoxynucleotide concentration was used. The arrangement of four subgrids: A200, A150, A80 and B80 within one MegaGrid is shown in Fig.1B. The MegaGrid was repeated 12 times on a

single slide as shown in Fig. 1C. In this design, each oligodeoxynucleotide was repeated 12 times each time with a different combinations of buffer and oligodeoxynucleotide concentrations.

SYBR Green II Staining To Check Printing Quality

The SYBR Green II staining results are shown in Fig.2. A picture of the slide is shown in Fig.2E. Examples of the staining results of subgrids A200, A80, A150 and B80 are shown in Figs.2 A, B, C, and D respectively.

Hybridization Results of Alexa Fluor 546-14-UTP Labeled Lcn2 MRNA With Oligodeoxynucleotide Microarray

After hybridization, the slide was scanned (Fig. 3 E). Examples of hybridization results of subgrids A200, A80, A150 and B80 are shown in Fig.3 A, B, C, and D respectively. The subgrids shown here are the same as shown in Fig.2. The fluorescence intensity value of 4608 (96 X 12 X 4 = 4608) spots from 48 subgrids on one slide was read using GridGrinder. For each spot, the local background value was subtracted from the spot fluorescence intensity value. The local background value is the fluorescence intensity value just outside the defined spot area and was identified by the Gridgrinder program. This step was done for all the spots including the spots containing only buffer. After local background subtraction, the spots of A80 and B80 were chosen to be analyzed further. For 1152 (96 X12) spots from 12 subgrids of A80, the average readings from the spots that containing only buffer were subtracted from the readings of spots containing oligodeoxynucleotides. The negative values obtained after the subtraction were set to zero. The 8 random sequences (R2 to 9) were treated as one oligodeoxynucleotide and named as Random Oligo. The R1 was not included because from the printing results, R1 was printed on the row 1, column 5 of each subgrid and it was not well printed. Each oligodeoxynucleotide in A80 has 12 repeats on one slide. The 12 values of each antisense oligodeoxynucleotide were averaged and a normalized value was calculated for each oligodeoxynucleotide by dividing its averaged value by the average value of the Random Oligo defined above. The

normalized value for each of the 84 antisense oligodeoxynucleotides was plotted in Fig.4. For 1152 (96 X12) spots from 12 subgrids of B80, the same procedure was followed. The corresponding normalized values for B80 subgrids are plotted in Fig.5.

Antisense Oligodeoxynucleotide Prediction By OligoWalk and Soligo

853 nt Lcn2 mRNA was analyzed by Oligowalk and Soligo for antisense oligodeoxynucleotides prediction, respectively. There are total 834 20nt antisense oligodeoxynucleotides for Lcn2 mRNA because the last 19nt sequences on the 3' end of Lcn2 mRNA is not long enough for 20nt antisense oligonucleotide. For each antisense oligodeoxynucleotide, its predicted effectiveness for targeting Lcn2 mRNA was given in the form of the Gibbs free energy ($\triangle G$). The lower the $\triangle G$ value, the more effective the antisense oligodeoxynucleotide. From the predictions of Oligowalk, the 25 antisense oligodeoxynucleotides with the lowest $\triangle G$ values of the 834 antisense oligodeoxynucleotides are shown in Fig. 7A. From the predictions of Soligo, the 25 antisense oligodeoxynucleotides with the lowest $\triangle G$ value of the 834 antisense oligodeoxynucleotides are shown in Fig. 7B.

DISCUSSION

In this study, I used tiled oligodeoxynucleotide microarrays combined with computational analyses to select antisense oligodeoxynucleotide candidates for further *in vivo* testing. The high throughput ability of oligodeoxynucleotide microarray experiments allows the screening of large number of oligodeoxynucleotides simultaneously. As shown in Fig. 1, I was able to test 96 spots with 12 repeats for each spot in each of four different combinations of printing solution and oligodeoxynucelotide concentration on one slide. Because I only needed to test 83 antisense oligodeoxynucleotides for Lcn2 mRNA I could also test different printing solutions and vary the concentration of oligodeoxynucleotides. With the printing conditions optimized, further experiments can test many more oligodeoxynucleotides per slide. The hybridization was done at the physiological buffer condition and 37 C°. This maximizes the possibility of selected antisense oligodeoxynucleotides that work *in vivo.*

From the results shown in Fig.2, the printing was successful. For A200, the smearing of some of the spots indicates that the concentration of oligodeoxynucleotides was too high. For A150 and A80, even though there was some variation among spots, the overall printing quality was acceptable. For B80, the spots were small but appeared to be printed more evenly than B80 and B150. Notice that on the first row of all subgrid's there were several spots that were printed significantly less intensely than the majority. This was especially true for the B80 subgrids. As shown on Fig. 2D, on the B80 subgrid, the missing spots from row 1, column 5 to 12 corresponded to oligodeoxynucleotides: R1, 721, 601, 481, 361, 241 , 121 and 1, respectively. For the A200, A150 and A80 subgrids, the corresponding oligodeoxynucleotides were in the same positions. On the grids printed using buffer A, these same 8 oligodeoxynucleotides were printed less intensely compared to others. On the grids printed using buffer B these 8 oligodeoxynucleotide can not be seen by the naked eye. This is because the amount of oligodeoxynucleotide printed by buffer B was less than it by buffer A. The possible reasons for the poor printing of these 8 oligodeoxynucleotides could be errors in sample preparation or poor performance of certain printing pins of the Arrayer used to print the oligodeoxynucleotides. Because of the poor printing of these 8 oligodeoxynucleotides, the results got from these experiments may not reflect the true effectiveness of these 7 antisense oligodeoxynucleotides. Further experiments need to be carried out to address this issue. After examining the staining results using the color scale provided in Fig. 2F, except for the 8 oligonucleotides mentioned above, all the other oligodeoxynucleotides were found to be printed evenly with small variations between different spots. Buffers A and B both gave usable printing results at the 80 μM oligodeoxynucleotides concentration. Further optimization for buffer A should reduce the number of the donuts spot. For buffer B, even though the oligodeoxynucleotides were more evenly distributed in the spots, the spot morphology and the amount of oligodeoxynucleotide printed needs to be improved.

The hybridization results shown in Fig. 3 showed large differences between antisense oligodeoxynucleotides in terms of fluorescence intensity after hybridization.

With the naked eye and based on the color scale in Fig. 3F, one can see that the intensity of several spots are close to saturation (white). These big differences can not be explained by the variations in oligodeoxynucleotides printed. For example, in Fig. 2, the spot on row 5, column 8 of each subgrid has stronger signal compared to the other two spots on row 6, 7 of column 8. After hybridization, the two spots with less printing signal had much stronger hybridization signals than other spots with strong printing signals. Another example is the spot on row 2, column 2 that has very strong hybridization signal whereas its printing signal is not much different from the spots around it. Combining the results of visual examination on Fig. 2 and Fig. 3, the primary conclusion was that there were big differences in hybridization with Lcn2 mRNA among the tested antisense oligodeoxynucleotides on the microarray slides.

Further quantitative analysis of the hybridization results supported the judgement based on the visual examination. The results shown in Figures 4 and 5 indicated antisense oligodeoxynucleotide 741 had the strongest interaction with Lcn2 mRNA. Its hybridization signal was the strongest in both sets of results. The top 10 antisense oligodeoxynucleotides from this analysis are listed in table 2. There were two differences in the predictions of optimal antisense oligodeoxynucleotides in the top10 list of the two printings (A80 and B80) of the microarray. Oligodeoxynucleotide 431 is in A80 top10 list but not in B80 top10 list. Oligodeoxynucleotide 491 is in B80 top10 list but not in A80 top10 list. The other 9 antisense oligodeoxynucleotides were common between these two analysis. The random oligodeoxynucleotides showed very low hybridization signals. The average fluorescence intensity of Random Oligo is 187 in A80 and 128 in B80 whereas the average fluorescence intensity of oligodeoxynucleotide 741 is 55956 in A80 and 51820 in B80. This indicated that the assay was reproducible. All the top10 antisense oligodeoxynucleotides in both A80 and B80 analysis had much larger hybridization signal than the others. This indicated that the assay had a sufficient range to allow identification of the best binders. For the purpose of this work, which was to select the antisense oligodeoxynucleotides candidates for further *in vivo* testing, the existence of several antisense oligodeoxynucleotides with very strong hybridization signals shown in Fig.4 and 5 made

the selection much easier. In support of the analysis shown here, Long Qu used the same original data from GridGrinder and independently did a similar data analysis. His results are consistent with the ones I describe here.

In Fig. 6, the top 25 antisense oligodeoxynucelotides in the results of A80 and B80 are shown in Fig. 6A and Fig. 6B, respectively. The overall normalized value of fluorescence intensity in A80 (Fig. 6A) is less than it in B80 (Fig. 6B). The average fluorescence intensity of Random Oligo is 187 in A80 and 128 in B80. It is about 1.5 times difference in the average fluorescence intensity of Random Oligo between A80 and B80. The overall lower normalized value of fluorescence intensity of A80 shown in Fig. 6A is most likely due to the higher fluorescence intensity of the Random Oligo used to normalize this dataset. Olgonucleotides 1, 361 and 601 are in Fig. 6A but not in Fig. 6B. Olgonucleotides 231, 391 and 611 are in Fig. 6B but not in Fig. 6A. The small number of differences in the lists of top 25 oligodeoxynucleotides between A80 and B80 indicates the results from A80 and B80 are very similar. This is consistent with the results shown in table 2.

Neither I nor Long included the quantitative value of the printing results in the analysis. Normalization of hybridization results to hybridization results of random sequences, based on the assumption that the printing efficiency is consistent throughout the microarray, is generally a good practice to improve the data quality. Given the large difference of the values for the top 10 antisense oligodeoxynucleotides shown in Fig.4, 5 and the considering the generally evenly printing results shown in Fig. 2, normalization of hybridization results to printing results probably will not significantly change the results from these microarrays although it may reduce the errors.

By contrast with the results from the microarray in which several antisense oligodeoxynucleotides stood out, the computational analyses did not produce similar results. In Fig. 7A, the top 25 antisense oligodeoxynucleotides in the results of Oligowalk prediction are shown. In Fig.7 B, the top 25 antisense oligodeoxynucleotides in the results of Soligo prediction are shown. In both results, the ΔG values of the 25 antisense oligodeoxynucleotides are in a small range. All 834 antisense

oligodeoxynucleotides were tested computationally. The minimum difference between each antisense oligodeoxynucleotide was 1nt for the computational analyses, whereas in the difference between antisense oligodeoxynucleotides in the microarray it was 10nt. The 1nt minimum difference may result the top 25 antisense oligodeoxynucleotides concentrating in several regions as shown in Fig. 7 for both programs. But even considering this difference between the two analyses, the two computational analysis did not clearly distinguish a small number of optimal antisense oligodeoxynucleotides such as the predictions of oligodeoxynucleotide 741 and 501 that came from the microarray experiments.

In table 2, the top 10 antisense oligodeoxynucleotides from the Oligowalk prediction did not match with the Soligo prediction. The different computational approaches taken by these two methods may result in their different predictions. Oligowalk is an Mfold based method (*16*). The secondary structure of the target mRNA is predicted using a free energy minimization algorithm. Based on the predicted secondary structure, the final overall $\triangle G$ ($\triangle G_{overall}$) value as shown in Fig. 7A was calculated for each antisense oligodeoxynucleotide based on the $\triangle G$ of several interactions. These interactions include the free energy needed to break the target's local folding ($\triangle G_B$), the free energy of antisense oligodeoxynucleotide self folding ($\triangle G_s$), the free energy of interaction between antisense oligodeoxynucleotides ($\triangle G_i$) and the free energy of duplex forming between antisense and its target sequences ($\triangle G_{duplex}$) . The $\triangle G_{overall}$ is calculated by subtracting the $\triangle G_B$, $\triangle G_s$ and $\triangle G_i$ from $\triangle G_{duplex.}$ (*16*). Different from OligoWalk method, the Soligo method is based on the algorithms developed by Ding *et al.*(*14, 15, 17*). In Soligo, the single stranded probability profile of the target mRNA sequences was estimated by a statistical sampling algorithm according to the Boltzmann equilibrium distribution which uses the calculated partition function of the target RNA secondary structure (*18*). The single stranded probability profile of the target mRNA sequence was incorporated into the prediction of the effective antisense sites. The $\triangle G_B$, $\triangle G_i$, $\triangle G_s$, and $\triangle G_{duplex}$ are still taken into account. Sfold algorithms also utilizes free energy parameters obtained from experiments to calculate the partition function. The statistical sampling algorithm in Soligo provides a representative single stranded probability

profile based on all possibilities of secondary structures of target mRNAs, whereas the Oligowalk algorithm only uses the secondary structures with minimum free energy (MFE) or the structures with free energy within certain range of MFE. This difference may result in the different prediction results for Lcn2 mRNA seen in Fig. 7 and table 2.

Based on the results from three different methods, microarray, Oligowalk and Soligo, and the predicted Lcn2 mRNA secondary structure by Mfold and Sfold, 7 antisense oligodeoxynucleotides were selected for further *in vivo* testing. In table 3 and Fig.8 the detailed information and the predicted folding of the related target sequences on Lcn2 mRNA are summarized for these 7 oligodeoxynucleotides. The most stable secondary structure of Lcn2 mRNA is almost identical when predicted by Mfold and Sfold . So in Fig.8, the secondary structure of Lcn2 mRNA predicted by Mfold is shown.

Loop structures in RNAs can promote antisense activity (*26*) and RNA/RNA interaction (*27*). In Fig. 8, the region A was a hairpin loop structure. In table 3, oligodeoxynucleotide 252 received a low ΔG from both Oligowalk and Soligo prediction. Oligodeoxynucleotide 251 showed up in both in the A80 and B80 top10 list but received a higher ΔG from both Oligowalk and Soligo prediction compared to oligodeoxynucleotide 252. Combining the information above, oligodeoxynucleotide 252 was chosen as one of the seven antisense oligodeoxynucleotides. Oligodeoxynucleotide 735 was chosen for similar reasons. The target sequences of oligodeoxynucleotide 735 overlapped with the best antisense oligodeoxynucleotide 741 based on the results of microarray experiments. The target region of oligodeoxynucleotide 735 has two loop structures as shown in region D of Fig.8. It received low ΔG values from both the Oligowalk and Sfold predictions. Based on the same reasons listed above oligodeoxynucleotide 735 was also selected for *in vivo* testing. As shown in Fig. 4 and 5, oligodeoxynucleotides 501 and 561 had very high hybridization signals, second only to the highest signal of oligodeoxynucleotide 741. Oligodeoxynucleotide 561 received poor ratings from both the Oligowalk and Soligo predictions, as indicated by the high ΔG value shown in table 3. Oligodeoxynucleotide

501received a good rating from the Oligowalk prediction and a poor rating from the Soligo prediction as indicated by corresponding $_{\Delta}G$ values shown in table 3. The results of these two antisense oligodeoxynucleotides from *in vivo* testing can provide useful information for the evaluating the three methods. So they were both selected.

The target region of oligodeoxynucleotides 581and 591 are shown in region C of Fig. 8. It is a region rich in loop structures. Oligodeoxynucleotides 561 and 571 both had good hybridization signals whereas oligodeoxynucleotide 581 and 591both had low hybridization signals as shown in Fig 4 and 5. Oligodeoxynucleotide 581 and 591 received good ratings from both the Oligowalk and Soligo predictions as indicated by the low $_{\Delta}G$ values shown in table 3. The target sequences of oligodeoxynucleotide 561 is also located in region C of Fig.8. The structures of the target sequences of oligodeoxynucleotides 581 and 591 are similar to the structure of the target sequence of oligodeoxynucleotide 561 (Fig. 8C), yet, the results of the analyses of the efficacy of oligodeoxynucleotides 581 and 591 for hybridizing with the full-length mRNA from the microarray experiment and computational analysis are quite different from the results for oligodeoxynucleotide 561. Whereas the microarray showed that the oligodeoxynucleotide 561 was a much better antisense ODN than oligodeoxynucleotides 581 and 591, the computational analysis indicated that the oligodeoxynucleotide 581 and 591 were much better antisense ODNs than oligodeoxynucleotides 561. Therefore comparison of these oligonucleotides by *in vivo* testing should provide a basis for the evaluating the three methods. So oligodeoxynucleotides 581, 591 and 561 were selected for *in vivo* testing. The oligodeoxynucleotide 741 was also selected for its high hybridization signal in the microarray as shown in Figures 4 and 5.

From these preliminary computational and *in vitro* studies, seven oligodeoxynucleotides (ODNs) shown in table 3 were chosen to be tested *in vivo* as antisense ODNs to target the Lcn2 mRNA of the mouse HC11 cell line. Each of the top three microarray-chosen ODNs (Oligodeoxynucelotides 501, 561 and 741) decreased the Lcn2 protein level as demonstrated by Western blot analysis. Also, they caused

a reduction in the Lcn2 mRNA level as determined by real-time RT-PCR. The other four selected Oligodeoxynucelotides 252, 581, 591 and 735 failed to decrease the level of Lcn2 protein or mRNA.

In a study done by Devireddy et al. (*28*), two phosphorothioate oligonucleotides were used as antisense ODNs to inhibit Lcn2 expression. Antisense ODNs 1 targeting 11 - 27 nt of Lcn2 mRNA and antisense ODNs 2 targeting 607 - 615 nt of Lcn2 mRNA. FI5.12 cell were transfected with 2 μM of each antisense ODNs. Both antisense ODNs were found out to reduce the Lcn2 expression level and antisense ODN 1 was shown to be particularly effective (*28*). Antisense ODN 2 (targeting 607-615 nt of Lcn2 mRNA) was only 8 nt long. The 20 nt oligodeoxynucleotide 601 was listed as one of the top 25 antisense ODNs in the A80 microarray results (Fig. 6A) and the 20 nt oligodeoxynucleotide 611 was listed as one of the top 25 antisense ODNs in B80 microarray results (Fig. 6B). Even though the length of antisense ODNs is different, the results from microarray experiments show some agreement with the experiment results of antisense ODN 2. The similar agreement about antisense ODN 2 was not found in the results of computational analysis (Fig. 7). Antisense ODN 1, is not listed as one of the top 25 antisense ODNs identified by our microarray experiments and computational analyses. This indicates the strength and accuracy of the tiled microarray experiments may need to be further tested. However, we have also not tested the efficacy of ODN 1 as an antisense oligonucleotide.

As a second example of testing the effectiveness of microarrays for predicting functional antisense oligonucleotides, the Bcl-2 mRNA coding sequence was examined for antisense ODNs hybridization using microarray. The microarray results were found to be consistent with previous reports of RNA sequence accessible to antisense ODN hybridization *in vivo*. Together, these results show that the *in vitro* microarray analysis predicted appropriate sequences for effective antisense ODNs *in vivo* with better accuracy compared to the prediction from computational analyses.

ACKNOWLEDGMENTS

I thank Hailing Jin from microarray facility for her support and suggestions. I thank Long Qu for his help and suggestions in the microarray data analysis. I thank Ahmed Awad and Xiaoling Song for their work and results that I referenced in this chapter.

REFERENCES

1. Opalinska, J. B., and Gewirtz, A. M. (2002) Nucleic-acid therapeutics: basic principles and recent applications, *Nat Rev Drug Discov 1*, 503-14.

2. Biroccio, A., Leonetti, C., and Zupi, G. (2003) The future of antisense therapy: combination with anticancer treatments, *Oncogene 22*, 6579-88.

3. Fiset, P. O., and Soussi-Gounni, A. (2001) Antisense oligonucleotides: problems with use and solutions, *Rev. Biol. Biotech. 1*, 27-33.

4. Rivas, E., and Eddy, S. R. (1999) A dynamic programming algorithm for RNA structure prediction including pseudoknots, *J Mol Biol 285*, 2053-68.

5. Uhlenbeck, O. C., Pardi, A., and Feigon, J. (1997) RNA structure comes of age, *Cell 90*, 833-40.

6. Carr-Schmid, A., Jiao, X., and Kiledjian, M. (2006) Identification of mRNA bound to RNA binding proteins by differential display, *Methods Mol Biol 317*, 299-314.

7. Vickers, T. A., Koo, S., Bennett, C. F., Crooke, S. T., Dean, N. M., and Baker, B. F. (2003) Efficient reduction of target RNAs by small interfering RNA and RNase H-dependent antisense agents. A comparative analysis, *J Biol Chem 278*, 7108-18.

8. Wang, A., Cheung, P. K., Zhang, H., Carthy, C. M., Bohunek, L., Wilson, J. E., McManus, B. M., and Yang, D. (2001) Specific inhibition of coxsackievirus B3 translation and replication by phosphorothioate antisense oligodeoxynucleotides,

Antimicrob Agents Chemother 45, 1043-52.

9. Ziegler, A., Luedke, G. H., Fabbro, D., Altmann, K. H., Stahel, R. A., and Zangemeister-Wittke, U. (1997) Induction of apoptosis in small-cell lung cancer cells by an antisense oligodeoxynucleotide targeting the Bcl-2 coding sequence, *J Natl Cancer Inst 89*, 1027-36.

10. Zuker, M., and Stiegler, P. (1981) Optimal computer folding of large RNA sequences using thermodynamics and auxiliary information, *Nucleic Acids Res 9*, 133-48.

11. Zuker, M. (1989) On finding all suboptimal foldings of an RNA molecule, *Science 244*, 48-52.

12. Zuker, M. (2003) Mfold web server for nucleic acid folding and hybridization prediction, *Nucleic Acids Res 31*, 3406-15.

13. Zuker, M. (2000) Calculating nucleic acid secondary structure, *Curr Opin Struct Biol 10*, 303-10.

14. Ding, Y., and Lawrence, C. E. (2003) A statistical sampling algorithm for RNA secondary structure prediction, *Nucleic Acids Res 31*, 7280-301.

15. Ding, Y., Chan, C. Y., and Lawrence, C. E. (2005) RNA secondary structure prediction by centroids in a Boltzmann weighted ensemble, *Rna 11*, 1157-66.

16. Mathews, D. H., Burkard, M. E., Freier, S. M., Wyatt, J. R., and Turner, D. H. (1999) Predicting oligonucleotide affinity to nucleic acid targets, *Rna 5*, 1458-69.

17. Ding, Y., Chan, C. Y., and Lawrence, C. E. (2004) Sfold web server for statistical folding and rational design of nucleic acids, *Nucleic Acids Res 32*, W135-41.

18. Ding, Y., and Lawrence, C. E. (2001) Statistical prediction of single-stranded regions in RNA secondary structure and application to predicting effective antisense target sites and beyond, *Nucleic Acids Res 29*, 1034-46.

19. Ho, S. P., Bao, Y., Lesher, T., Malhotra, R., Ma, L. Y., Fluharty, S. J., and Sakai, R. R. (1998) Mapping of RNA accessible sites for antisense experiments with oligonucleotide libraries, *Nat Biotechnol 16*, 59-63.

20. Allawi, H. T., Dong, F., Ip, H. S., Neri, B. P., and Lyamichev, V. I. (2001) Mapping of RNA accessible sites by extension of random oligonucleotide libraries with reverse transcriptase, *Rna 7*, 314-27.

21. Lloyd, B. H., Giles, R. V., Spiller, D. G., Grzybowski, J., Tidd, D. M., and Sibson, D. R. (2001) Determination of optimal sites of antisense oligonucleotide cleavage within TNFalpha mRNA, *Nucleic Acids Res 29*, 3664-73.

22. Bleczinski, C. F., and Richert, C. (1998) Monitoring the hybridization of the components of oligonucleotide mixtures to immobilized DNA via matrix-assisted laser desorption/ionization time-of-flight mass spectrometry, *Rapid Commun Mass Spectrom 12*, 1737-43.

23. Milner, N., Mir, K. U., and Southern, E. M. (1997) Selecting effective antisense reagents on combinatorial oligonucleotide arrays, *Nat Biotechnol 15*, 537-41.

24. Sohail, M., Hochegger, H., Klotzbucher, A., Guellec, R. L., Hunt, T., and Southern, E. M. (2001) Antisense oligonucleotides selected by hybridisation to scanning arrays are effective reagents in vivo, *Nucleic Acids Res 29*, 2041-51.

25. Simpson, D. A., Feeney, S., Boyle, C., and Stitt, A. W. (2000) Retinal VEGF mRNA measured by SYBR green I fluorescence: A versatile approach to quantitative PCR, *Mol Vis 6*, 178-83.

26. Franch, T., Petersen, M., Wagner, E. G., Jacobsen, J. P., and Gerdes, K. (1999) Antisense RNA regulation in prokaryotes: rapid RNA/RNA interaction facilitated by a general U-turn loop structure, *J Mol Biol 294*, 1115-25.

27. Asano, K., Niimi, T., Yokoyama, S., and Mizobuchi, K. (1998) Structural basis for binding of the plasmid ColIb-P9 antisense Inc RNA to its target RNA with the

5'-rUUGGCG-3' motif in the loop sequence, *J Biol Chem 273*, 11826-38.

28. Devireddy, L. R., Teodoro, J. G., Richard, F. A., and Green, M. R. (2001) Induction of apoptosis by a secreted lipocalin that is transcriptionally regulated by il-3 deprivation, *Science 293*, 829-834.

FIGURE LEGENDS

Figure 1. Design of the Oligodeoxynucleotide Microarray

(A) The schematic representative of the design fo a single microarray slide. Each slide contained 12 MegaGrids. Each MegaGrid contains 4 subgrids. All 12 MegaGrids were the same except the position on the slide.

(B) The schematic representative of the design of a single MegaGrid. Each MegaGrid contains 4 subgrids. The composition of oligodeoxynucleotides on the 4 subgrids are the same. But either the printing solution used or the concentration of the oligodeoxynucleotides are different. Buffer A was printing solution A. Buffer B was printing solution B. The concentration of oligodeoxynucleotides used to print each subgrid is shown. For the subgrids where the buffer A and 200 μM oligodeoxynucleotides were used, the subgrids were named A80. For the subgrids where the buffer A and 150 μM oligodeoxynucleotides were used, the subgrids were named A150. For the subgrids where the buffer A and 80 μM oligodeoxynucleotides were used, the subgrids were named A80. For the subgrids where the buffer B and 80 μM oligodeoxynucleotides were used, the subgrids were named B80. Each MegaGrid contains four subgrids: A200, A150, A80 and B80. MegaGrid was repeated 12 times on each slide. So on one slide there are 12 subgrids of A200, A150, A80 and B80, respectively.

(C) The schematic representative of the design of a single subgrid. Each subgrid has 96 spots printed on it. The spots in red identify the positions in which the buffer without oligo was printed. The spots in green identify the positions in which each of nine oligodeoxynucleotides with random sequences (R1 to 9 in table 1) were printed. The spots in black are the 84 antisense oligodeoxynucleotides targeting Lcn2 mRNA.

Figure 2. The SYBR Green II Staining Results

The microarray slide was stained by SYBR Green II after pre-hybridization. The results of whole slides (E) as well as examples of four different subgrids were shown here. A

rainbow color scale (F) from blue to red plus white for maximum intensities was used by the Scanner used to represent the relative fluorescence intensities.

(A) An example of a subgrid using buffer A and 200 μM oligodeoxynucleotides (A200). The subgrid was taken from MegaRow 3, MegaColumn 1 of the slide as shown in E.

(B) An example of a subgrid using buffer A and 80 μM oligodeoxynucleotides (A80). The subgrid was taken from MegaRow 3, MegaColumn 2 of the slide as shown in E.

(C) An example of a subgrid using buffer A and 150 μM oligodeoxynucleotides (A150). The subgrid was taken from MegaRow 4, MegaColumn 1 of the slide as shown in E.

(D) An example of subgrid using buffer B and 80 μM oligodeoxynucleotides (B80). The subgrid was taken from MegaRow 4, MegColumn 2 of the slide as shown in E.

Figure 3. The Hybridization Results

The hybridization results of whole slides (E) as well as examples of four different subgrids are shown. The four subgrids shown here are the same as shown in Fig. 2. The same rainbow color scale (F) as in Fig. 2 was used by the Scanner to represent the relative fluorescence intensities.

(A) Subgrid A200 taken from MegaRow 3, MegaColumn 1 of the slide as shown in E.

(B) Subgrid A80 taken from MegaRow 3, MegaColumn 2 of the slide as shown in E.

(C) Subgrid A150 taken from MegaRow 4, MegaColumn 1 of the slide as shown in E.

(D) Subgrid B80 taken from MegaRow 4, MegColumn 2 of the slide as shown in E.

Figure 4. Summary of the Subgrids A80 Hybridization Results

The Y axis is the normalized value of fluorescence intensity. The X axis is the oligodeoxynucleotides' names listed in the ascending order. Because of the space limitation, only each third of the 84 antisense oligodeoxynucleotides are labeled on the

X-axis. The total listed of antisense oligodeoxynucleotide's named and in ascending order can be found in table 1. The bar for each antisense oligodeoxynucleotide represents the normalized value of fluorescence intensity of each oligodeoxynucleotide in A80 subgrids on one microarray slide. The normalized value of each oligodeoxynucleotide is its average fluorescence intensity divided by the average fluorescence intensity of Random Oligo as defined in previous results section.

Figure 5. Summary of The Subgrids B80 Hybridization Results

The Y axis is the normalized value of fluorescence intensity. The X axis is the oligodeoxynucleotides' names listed in the ascending order. Because of the space limitation, only each third antisense oligodeoxynucleotide is labeled on the X-axis. The total list of antisense oligodeoxynucleotides named in ascending order can be found in table 1. The bar for each antisense oligodeoxynucleotide represents the normalized value of fluorescence intensity of each oligodeoxynucleotide in B80 subgrids on one microarray slide. The normalized value of each oligodeoxynucleotide is its average fluorescence intensity divided by the average fluorescence intensity of Random Oligo as defined in previous results section.

Figure 6. The Top 25 Antisense Oligodeoxynucleotides in A80 and B80 Results

From A80 and B80 results, the normalized values of fluorescence intensity and names of the 25 antisense oligodeoxynucleotides with the highest normalized values among the 84 20 nt antisense oligodeoxynucleotides targeting Lcn2 mRNA are listed. The Y axis is the normalized value of fluorescence intensity. The X -axis is the name of antisense oligodeoxynucleotide indicating the position of 5' end of its targeting sequence on Lcn2 mRNA. For example, antisense oligodeoxynucleotide named 81 indicates that its targeting region on Lcn2 mRNA was from 81 to 100 nt.

(A) The top 25 antisense oligodeoxynucleotides from A80.

(B) The top 25 antsiense oligodeoxynucleotides from B80.

Figure 7. The Top 25 Antisense Oligodeoxynucleotides Predicted by Oligowalk

and Soligo

The $-_{\Delta}G$ values and names of the 25 antisense oligodeoxynucleotides with the lowest $_{\Delta}G$ values among the 834 20 nt antisense oligodeoxynucleotides targeting Lcn2 mRNA are listed. The Y axis is the $-_{\Delta}G$ value in Kcal/mol. The X -axis is the name of antisense oligodeoxynucleotide indicating the position of 5' end of its targeting sequence on Lcn2 mRNA. For example, antisense oligodeoxynucleotide named 355 indicates that its targeting region on Lcn2 mRNA was from 355 to 374nt.

(A) The top 25 antisense oligodeoxynucleotides predicted by OligoWalk.

(B) The top 25 antsiense oligodeoxynucleotides predicted by Soligo.

Figure 8. The Folding by Mfold of Target Sequences of Seven Antisense Oloigodeoxynucleotides Selected for *In vivo* Testing

The 853nt Lcn2 mRNA folded by Mfold is shown in the middle of figure. The four regions on Lcn2 mRNA from which the target sequences of the seven antisense oligodeoxynucleotides selected for *in vivo* testing are circled. The target sequence of the antisense oligonucleotide 252 is shown in region A. The target sequence of the antisense oligodeoxynucleotide 501 is shown in region B. The target sequences of the antisense oligodeoxynucleotides 561, 581 and 591 are shown in region C. The target sequences of the antisense oligodeoxynucleotides 735 and 741 are shown in region D. All the target sequences are shaded in a light pink color. The overlapping sequences are shown in deeper pink color compared to the sequences that have no overlap.

Tables and Figures

Table 1. The sequence information of oligodeoxynucleotides used

84 Antisense Oligodeoxynucleotides targeting Lcn2 mRNA with 10nt overlapping from 5' to 3' end. Each oligodeoxynucleotide is 20nt long. The number shown below which indicates the position of 5' end of its target sequences on Lcn2 mRNA was used as the name of corresponding antisense oligodeoxynucelotide.											
1	11	21	31	41	51	61	71	81	91	101	111
121	131	141	151	161	171	181	191	201	211	221	231
241	251	261	271	281	291	301	311	321	331	341	351
361	371	381	391	401	411	421	431	441	451	461	471
481	491	501	511	521	531	541	551	561	571	581	591
601	611	621	631	641	651	661	671	681	691	701	711
721	731	741	751	761	771	781	791	801	811	821	831

9 Random Sequences		
Name	Sequence	Length
Random Sequence 1 (R1)	TCTTTCGGTAAGCCGCATGG	20 nt
Random Sequence 2 (R2)	CCTGGGGGGCTAAGGACGTG	20nt
Random Sequence 3 (R3)	CGTCCGTTTGGAAACGCCTT	20nt
Random Sequence 4 (R4)	TCGTCACAATACAGGGAGGG	20nt
Random Sequence 5 (R5)	CCGGATTTTGCCTCGTATAA	20nt
Random Sequence 6 (R6)	GGAGTGATCGAAATTGGACT	20nt
Random Sequence 7 (R7)	AAAAGCACTAATTGGAGTCG	20nt
Random Sequence 8 (R8)	GGACGCATCGATTGAACTGC	20nt
Random Sequence 9 (R9)	GTTCGCGGCCATGTAGTGGT	20nt

Table 2. Summary of top 10 oligodeoxynucleotides from three methods.

Oligodeoxynucleotides	Microarray		OligoWalk	Soligo
	A80	B80		
251	√	√		
252				√
253				√
254				√
255				√
256				√
257				√
421	√	√		
431	√			
461	√	√		
478				√
491		√		
494			√	
499			√	
500			√	
501	√	√	√	
502			√	
503			√	
504			√	
505			√	
521	√	√		
561	√	√		
571	√	√		
734				√
735				√
741	√	√		
749			√	
750			√	
751	√	√		
798				√

Table 3. Oligodeoxynucleotides (ODNs) selected for *in vivo* testing as the antisense ODNs

Name	Antisense Oligonucleotides (5' to 3')	Target sequences on Lcn2 mRNA	GC content	ΔG (Kcal/mol)	
				Sfold	OligoWalk
252	GCTATTGTTCTCTTGTAGCT	252-271	40.00%	-11.4	-15.8
501	CAGCTCCTTGGTTCTTCCAT	501-520	50.00%	-0.2	-23.9
561	GTCGTCCTTGAGGCCCAGAG	561-580	65.00%	-2.3	-1
581	GGGACAGAGAAGATGATGTT	581-600	45.00%	-9.9	-17.7
591	TTGGTCGGTGGGGACAGAGA	591-610	60.00%	-9.9	-18.5
735	CTTGGTATGGTGGCTGGTGG	735-754	60.00%	-11.6	-16
741	ATGCTCCTTGGTATGGTGGC	741-760	55.00%	-7.4	-14.6

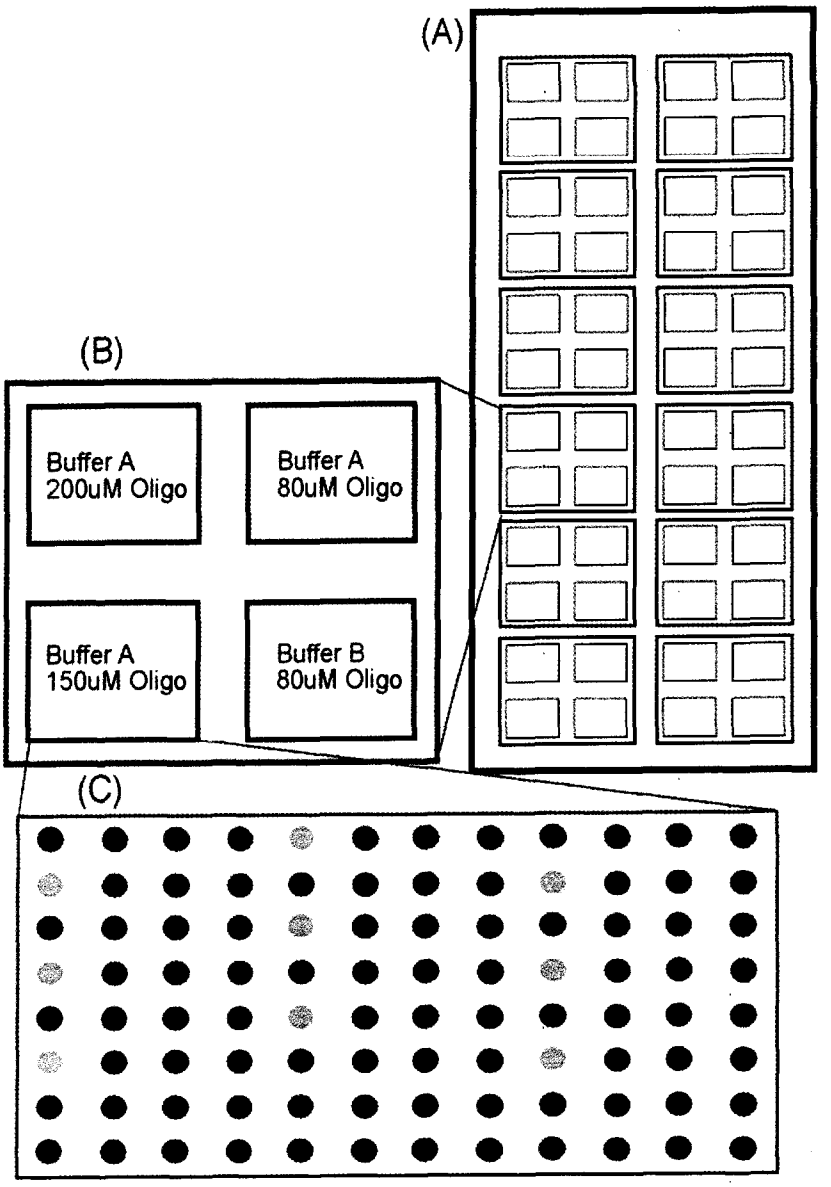
(A)
(B)
Buffer A
200uM Oligo
Buffer A
80uM Oligo
Buffer A
150uM Oligo
Buffer B
80uM Oligo
(C)

Figure 1

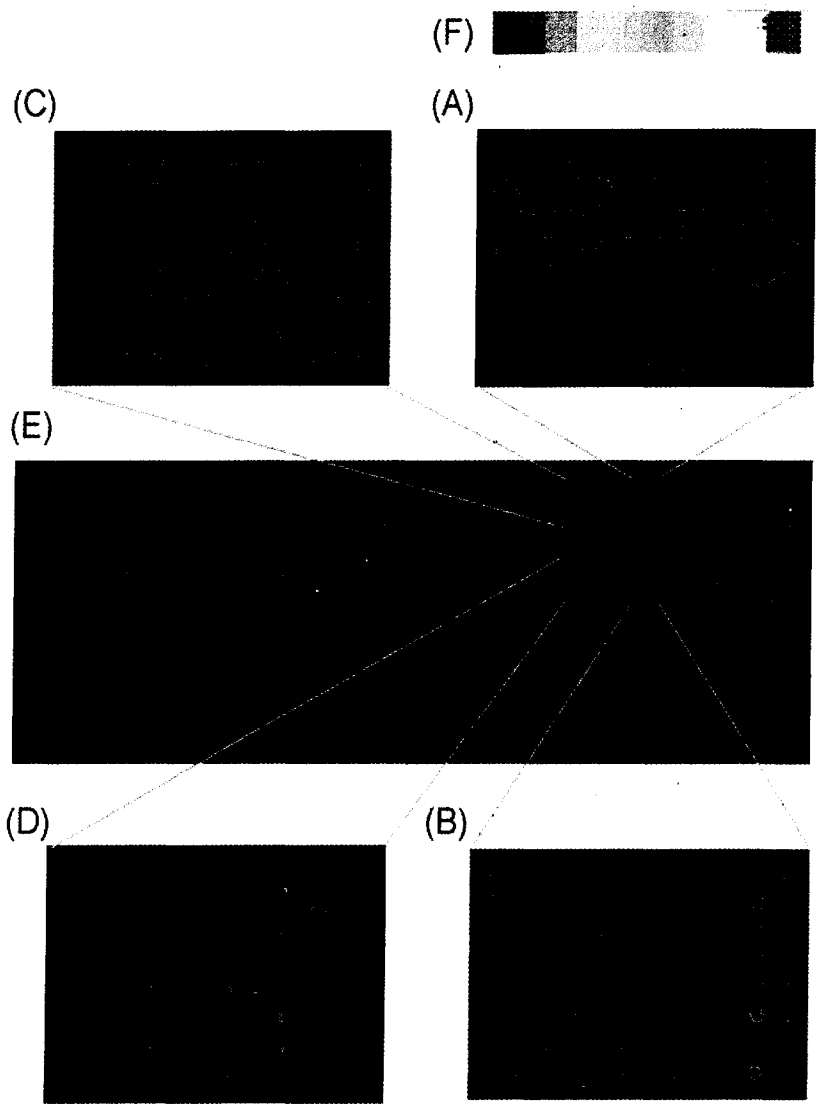

Figure 2

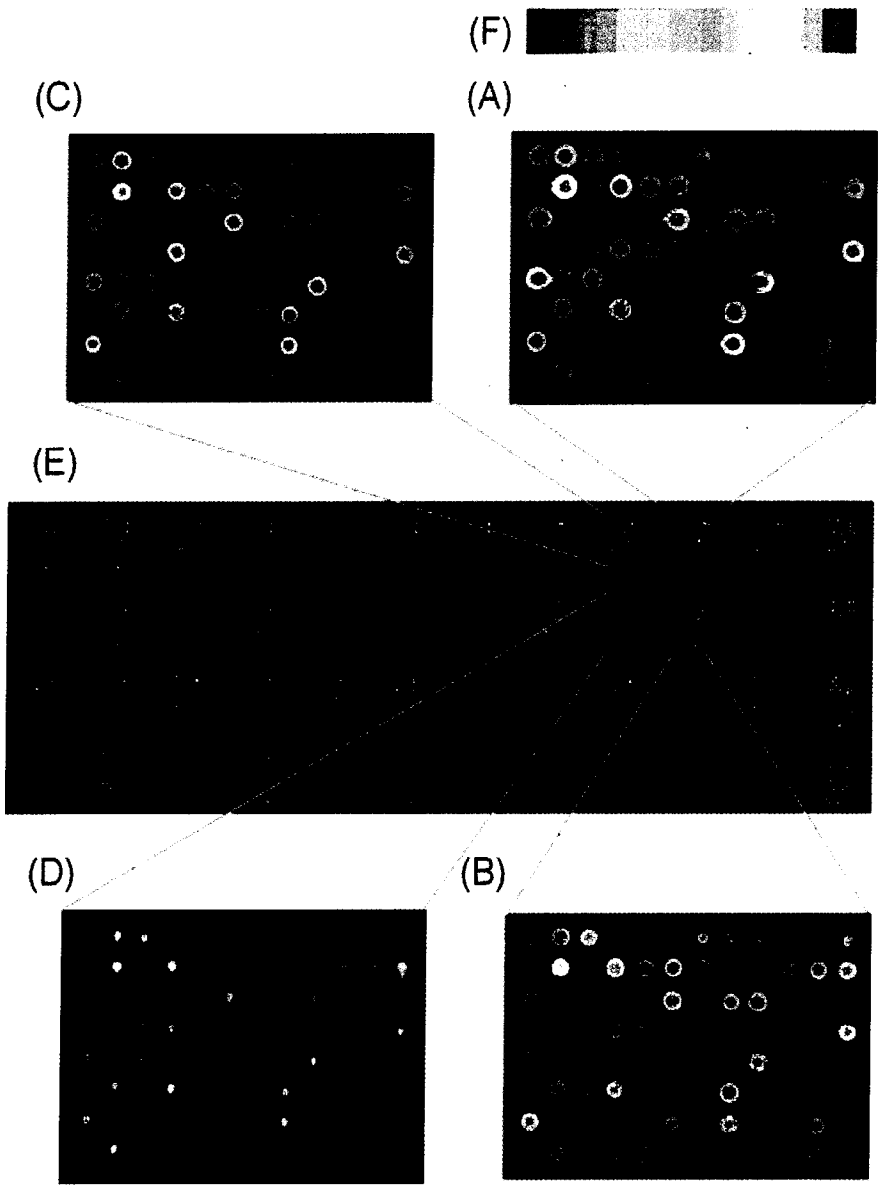

Figure 3

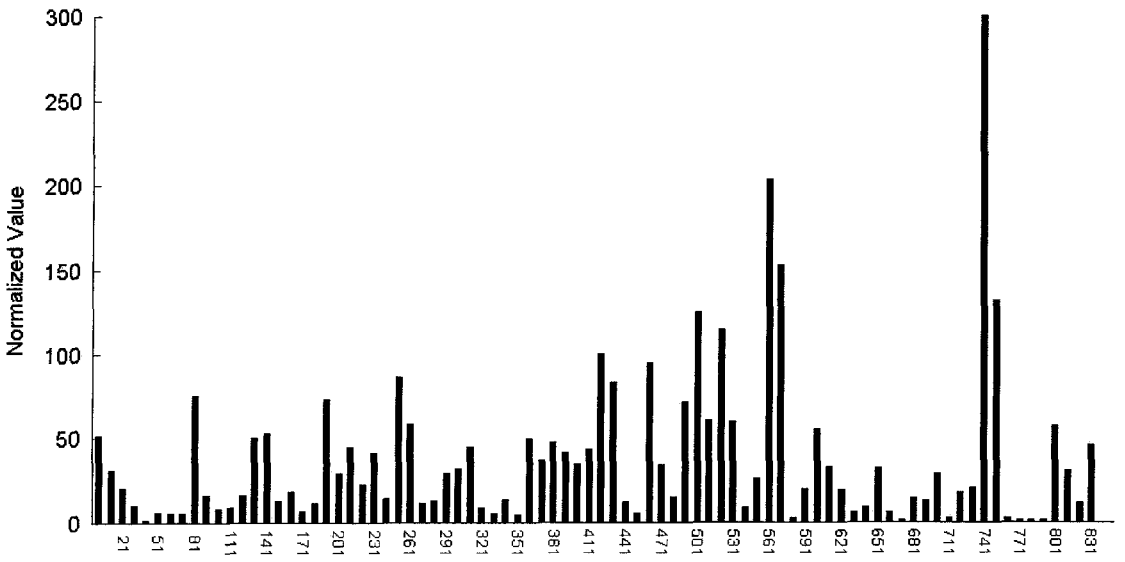
Normalized Value
300
250
200
150
100
50
0
21
51
81
111
141
171
201
231
261
291
321
351
381
411
441
471
501
531
561
591
621
651
681
711
741
771
801
831

Figure 4

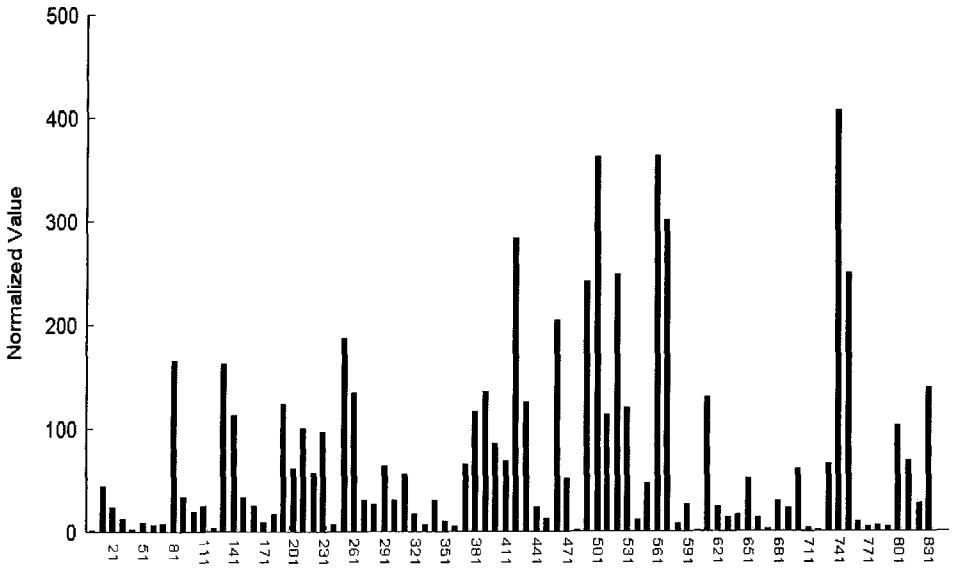
Normalized Value
500
400
300
200
100
0
21
51
81
111
141
171
201
231
261
291
321
351
381
411
441
471
501
531
561
591
621
651
681
711
741
771
801
831

Figure 5

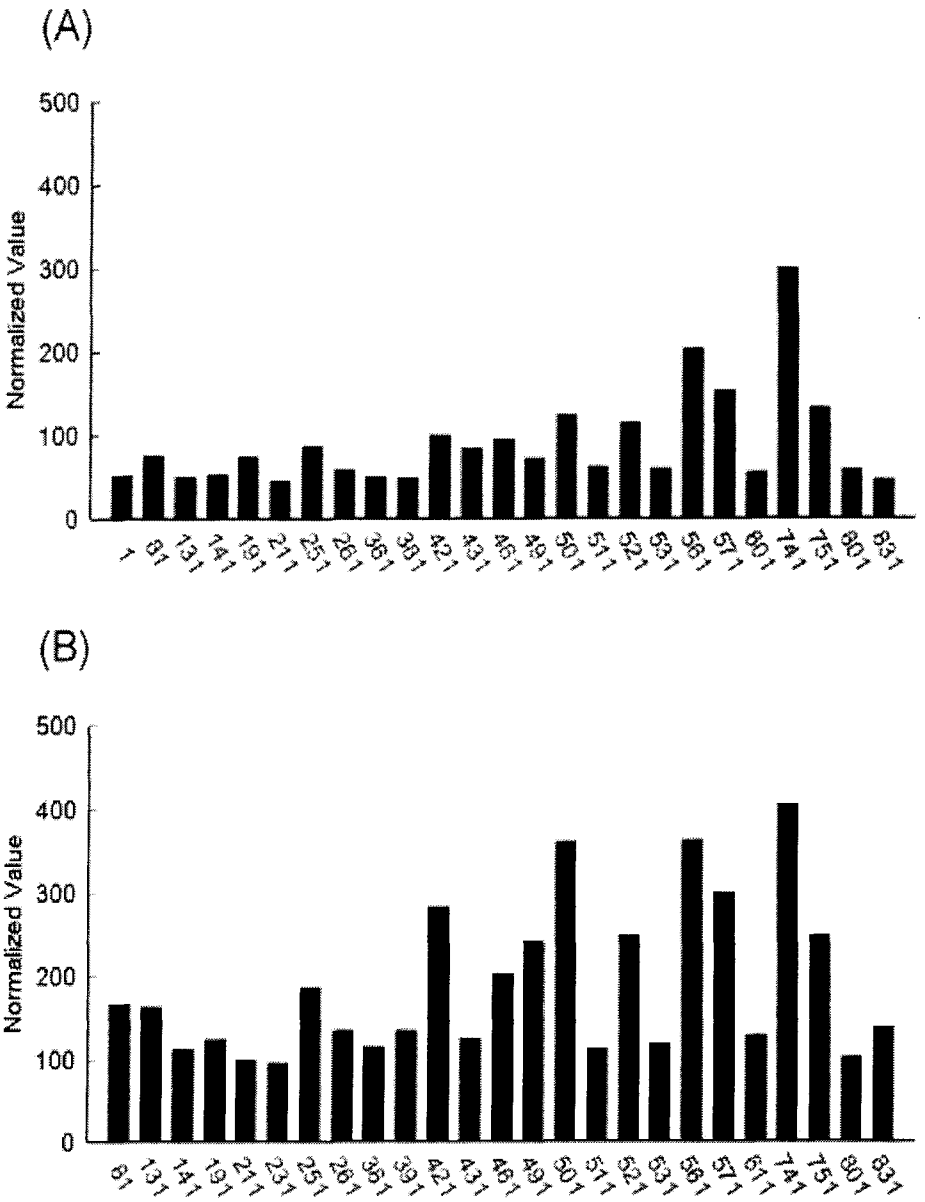
(A)
Normalized Value
500
400
300
200
100
0
1
81
131
141
191
211
251
261
361
381
421
431
461
491
501
511
521
531
561
571
601
741
751
801
831
(B)
Normalized Value
500
400
300
200
100
0
61
131
141
191
211
231
251
261
361
391
421
431
461
491
501
511
521
531
561
571
611
741
751
801
831

Figure 6

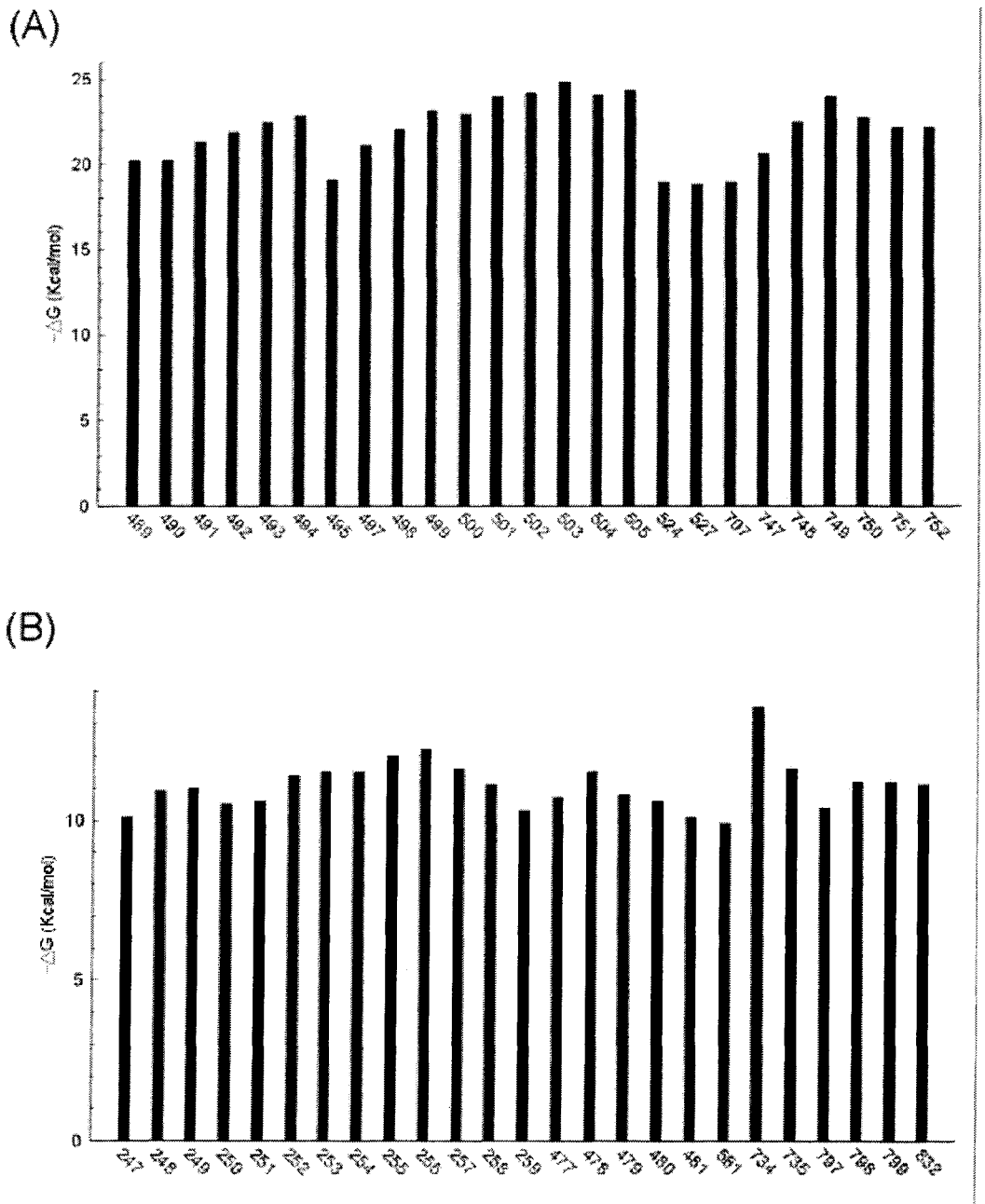
(A)
-ΔG (Kcal/mol)
25
20
15
10
5
0
489 490 491 492 493 494 496 497 498 499 500 501 502 503 504 505 524 527 707 747 748 749 750 751 752
(B)
-ΔG (Kcal/mol)
10
5
0
247 248 249 250 251 252 253 254 255 256 257 258 259 477 478 479 480 481 561 734 735 797 798 799 832

Figure 7

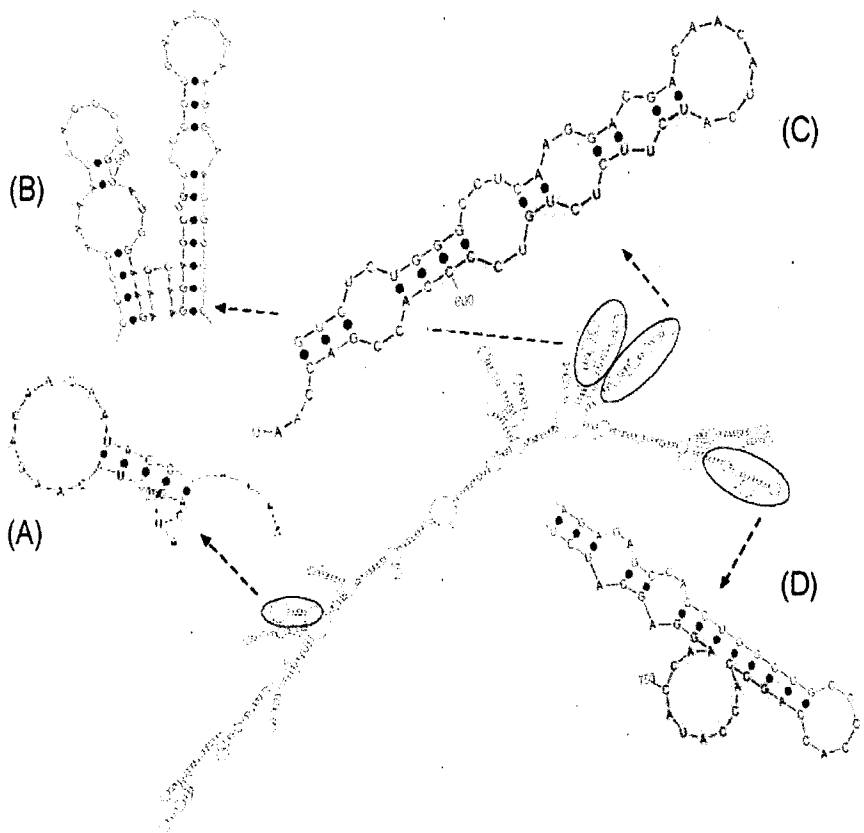

Figure 8

CHAPTER 5. DEVELOPMENT OF A MALACHITE GREEN RNA TRAP FOR Lcn2 mRNA

A paper to be submitted to *RNA*

Abstract

In vivo detection and imaging of RNA molecules in living cells will provide critical temporal and spatial information about the specific RNA molecule for biological and biomedical research and applications. It is well known that changes in the expression level of certain genes correlate with the occurrence of certain diseases or with cell differentiation. Non-invasive probes that can image the expression of such genes in real time would help the early diagnosis of disease and provide an accurate evaluation of cell status.

Here we utilized an *in vitro* selected malachite green (MG) RNA aptamer to develop a MG RNA TRAP probe for the purpose of imaging mRNA *in vivo*. Thirty two nt , 30nt and 28nt MG aptamers were created from the existing 38nt MG RNA aptamer initially selected by SELEX. These truncated aptamers were also modified to destabilize the stable secondary structure. The Kds of these truncated and modified MG RNA aptamers for MG were estimated and the results showed the 32nt , 30nt and 28nt MG RNA aptamers still affinities for MG within 1-fold of the parent aptamer. Selected from a previous study (Chapter 4), the 20nt antisense oligonucleotide that targets 741-760 nt of Lcn2 mRNA was chosen to be used in the MG RNA TRAP. Through rational design, a TRAP that has a 32nt modified MG RNA aptamer and a 9nt attenuator was found to have up to 20-fold activation upon interaction with 20nt regDNA.

To facilitate transfer of the TRAP concept to *in vivo* conditions a yeast selection system was created to test the function of selected TRAPs *in vivo* in which inhibition of URA3 expression by an active MG aptamer inserted in its 5'UTR is reflected by slow growth in a yeast spot assay. A hammerhead (HH) ribozyme - MG - hepatitis delta virus (HDV) - ribozyme expression cassette was also built to produce RNA molecules with defined and homogenous 5' ends and 3' ends. To determine if an optimal TRAP

could be derived by combinatorial selection, SELEX was carried out using 3 different ssDNA pools. The primary results indicated that the key for a successful selection of a MG RNA TRAP using SELEX could be an effective negative selection to get rid of the sequences that bind MG in the absence of regDNA. In comparison with SELEX, rational design was found to be a more effective means of developing a well-regulated MG TRAP for detecting the presence of Lcn2 mRNA.

INTRODUCTION

In the last ten years, the discovery of small non-coding RNAs (ncRNAs), such as small interfering RNAs (siRNAs), microRNAs (miRNAs) and riboswitches, have broadened our understanding of the scope of biological activities of RNA molecules (*1*). Another big surprise came in 1982 when Cech *et al.* (*2, 3*) reported the first catalytic RNA or ribozyme: the self-splicing intron of the Tetrahymena pre-rRNA. Accumulating evidence through many years of research began to fully reveal the kingdom of RNAs hiding from the central land. Now we know RNAs not only play the role of messenger to convey and interpret the genetic information stored in DNA, but also have essential catalytic activity and contribute to the structure of molecular complexes that regulate gene expression. The expression levels and stabilities as well as the temporal and spatial distributions of specific RNAs in a cell are directly related to their functions. It is very important to understand the dynamics and localization of RNA molecules in the living cell. It will help us to understand how the RNA molecules fulfill their diversified functions.

Changes in the expression levels of certain genes are correlated with the occurrence of certain diseases or with the differentiation states of a cell. For example, mammaglobin antigen transcripts were detected in 100% of human breast adenocarcinoma cell lines (BrCa) and were absent from normal lymph nodes (*4*). Through microarray analysis, many transcripts were revealed to undergo dramatic changes during cancer development and inflammation (*5, 6*). The rapidly developing knowledge of the genome enables a view of gene regulation in the genomic level rather

than a single gene at one time. In many cases, the increase or decrease of certain mRNAs is the earliest event of certain biological processes, such as apoptosis, tumor occurrence and cell differentiation. Real time and non-invasive detection of such changes in mRNA levels may provide critical information for the early diagnosis of diseases or determination of cell differentiation state or could be used for monitoring certain biological events.

There are many *in vitro* methods developed to detect and quantify RNA molecules using purified DNA or RNA samples obtained from cell lysates. These methods include Northern blotting (*7*), *in situ* hybridization (*8*), RT-PCR (*9*), Nucleic Acid Sequence Based Application (NASBA) (*10*), expressed sequence tags (ESTs) (*11*), real time RT-PCR (*12*), Serial Analysis of Gene Expression (SAGE) (*13*), differential display (*14*), and DNA microarray (*15*). Along with the rapidly advancing knowledge of genomic sequences for many organisms, the *in vitro* methods mentioned above enable the fast, accurate and systematic detection and identification of RNA targets in the cell. But these *in vitro* methods can not provide temporal and spatial information about the RNA target in the living cell.

Many efforts have been given to detect and imaging RNA, especially mRNA molecule in living cells. For example, MS2-GFP fusion protein containing a nuclear-localization signal was used to capture the co-expressed Ash1 mRNA carrying an insertion of six tandem copies of the stem-loop binding site for bacteriophage MS2 coat protein (*16*). The Ash1 mRNA was visualized through fluorescence of re-localized GFP. Using GFP as a reporter, other studies had been done in which the selected RNA targets were visualized in individual living cells (*17, 18*).

For the system using MS2-GFP fusion protein, even though the mRNA detected was produced inside the cell, it is modified from native mRNA. With fluorescence *in vivo* hybridization (FIVH), fluorescence labeled unstructured linear nucleic acid probes were used to detect and image the specific RNA in the living cells (*19-21*). But the linear unstructured probes suffer drawbacks such as a high background signal and lack of conformational change upon binding to the target. It is also difficult to use linear

unstructured probes to detect single base difference compared with using stem-loop structured probes such as molecular beacons (*22*). Peptide linked molecular beacons have been used to detect native mRNA in living cells (*23, 24*).

Integrating ribozymes/aptamers into the design of molecular beacons, we developed the ribozymes/aptamer-based structured nucleic acid probe - targeted reversibly attenuated probes (TRAPS) (*25, 26*). In the aptamer -based TRAPs, an aptamer is used as the module to signal the interaction between TRAP and its nucleic acid target through the binding of aptamer to its ligand. The study done in the ATP-DNA TRAP shown that it can be fully activated by the regDNA. Also, the activation of the ATP DNA aptamer in the ATP DNA TRAP by a complementary nucleic acid at physiological temperatures is sensitive to single-base mismatches (*26*). Aptamer-based TRAPs that can be regulated by a specific nucleic sequence such as in an mRNA have the potential for being used to image RNA molecules *in vivo*. Even though aptamers are selected *in vitro* through SELEX (*27, 28*), many have been applied to both extracellular (*29-36*) and intracellular (*37-42*) *in vivo* applications. In most *in vivo* applications, aptamers have been used as antagonists of their target ligand molecules. But they could be used in a broad range of other *in vivo* applications as well. Several studies have been done to utilize aptamers to image cells using extracellular targets. For example, an [^{123}I or ^{125} I] labeled thrombin aptamer was used to imaging thrombus in blood (*29*) and a [^{99m}Tc] labeled neutrophil elastase aptamer was used to imaging inflammation in a rat reverse passive arthitus reaction model (*43*). Aptamers can be used to regulate transcription or translation processes. For example, by inserting the MG RNA aptamer before the AUG of a cyclin transcript in *S. cerevisiae*, the translation of modified cyclin transcript was regulated by tetramethylrosamine (TMR), a structural analog of MG (*44*). Another example of the MG RNA aptamer and TMR that works *in vivo* was the development of a TMR-dependent transcription activator through in vivo selection in *S. cerevisiae* (*45*). The transcription rate of an engineered RNA molecule containing the MG aptamer increased 10-fold in the presence of TMR.

Lcn2 is a member of lipocalin protein family (*46*). Many members of lipocalin family have the function of binding and transporting small hydrophobic molecules (*47*). Lcn2 was first identified as a secreted protein regulated by growth factors and later shown to be an acute phase protein and involved in the inflammatory response (*48, 49*). Although the *in vivo* function of Lcn2 is not fully understood, it has been verified that Lcn2 has very high expression during tissue involution in uterus and mammary gland (*50*). Lcn2 mRNA was observed to have over ~100 fold increase over the average level on day 5 of gestation in the mouse mammary gland (*50*). This dramatic expression change in the uterus and mammary gland makes it an ideal target transcript for developing an RNA TRAP utilizing the MG RNA aptamer.

Here we report the development of a MG RNA TRAP targeting Lcn2 mRNA. The efficacy of rational design and SELEX are tested in the process. Through rational design, a TRAP containing a 32nt mutant MG RNA aptamer and 9nt attenuator was shown to be activated up to 20-fold upon interaction with a 20nt regDNA. A yeast negative and positive selection system was created to further verify the function of produced RNA TRAP molecule *in vivo*. Our results show the advantages and disadvantages of rational design and SELEX, respectively. It provides general guidance for the future development of TRAPs that may utilize RNA aptamers other than the MG aptamer.

Materials and Methods

Materials and Equipments

Malachite green was from Sigma (St. Louis, MO). Malachite green isothiocyanate was from Invitrogen (Carlsbad, CA). EZ-link Biotin-LC-PEO Amine was from Pierce (Rockford, IL). [α-^{32}P]CTP was purchased from ICN (Costa Mesa, CA). Streptavidin-agarose CL-4B was from Sigma and Pierce. HT-450 Tuffryn membrane filters (0.45 m pore size) were from Pall (Ann Arbor, MI). Imagequant software (Amersham-Pharmacia) was used to analyze radioactive bands in gel scans obtained using a Typhoon scanner (Amersham-Pharmacia). The concentration of nucleic acid

molecules was determined by a NanoDrop ND-100 UV spectrophotometer (NanoDrop Technologies, Inc.) Fluorescent spectra were taken on a Cary Eclipse (Varian, Australia) fluorescence spectrophotometer with a Xenon pulse lamp. Yeast YPD media was purchased from Sigma. The FastStart Taq DNA polymerase was purchased from Roche (Indianapolis, IN). SuperScript III reverse transcriptase was from Invitrogen. Micro Bio-Spin P30 Tris columns were from Bio-Rad (Hercules, CA). Yeast extract, yeast nitrogen base without amino acids, tryptone peptone and yeast agar were purchased from Becton Dickinson and Company (Franklin Lakes, NJ). Uracil dropout media supplement was from Qbiogene (Morgan Irvine, CA). TLC plates(Silica gel, Polyester, 250uM thickness) was from VWR (West Chester, PA).

RNA and DNA molecules

The names, descriptions and sequence information for DNA and RNA molecules in this study are listed in Table 1, 2, 3 4 , 5, 6 and 7. The oligonucleotide with an unique oligo number indicates it was purchased from Integrated DNA Technology (IDT) (Coralville, IA) or Iowa State University DNA Facility (Ames, IA). The oligonucleotide without oligo number was produced by experiments or listed for information. Oligonucleotides are listed from 5' end to 3' ends if not particularly annotated. Oligonucleotides described as PAGE-purified preparations were purified by polyacrylamide gel electrophoresis (PAGE). All other purchased oligonucleotides were prepared as standard desalted preparations. All MG RNA TRAPs were synthesized by *in vitro* transcription using the AmpliScribe™ T7-FlashT Transcription Kit from EPICENTRE (Madison, WI) and purified by denaturing (7M Urea) 8% PAGE. The gel-purified MG RNA TRAPs were quantified by using a NanoDrop ND-100 UV spectrophotometer. The double strand (ds) DNA template for *in vitro* transcription were obtained by PCR. The PCR strategy to make ds DNA templates for different TRAPs is shown in Fig. 4A. The PCR reactions contained 1 nM template, 1 μM forward primer, 1 μM reverse primer, 2 mM Mg^{++} and 200 μM dNTP. The PCR conditions were: 95°C 4 min pre-denaturation, 95°C 2 min denaturation, 55°C 2 min annealing, 72°C 1 min elongation and 15 cycles. Each PCR reaction ended with a 10min incubation at 72°C.

The PCR products were purified using Micro Bio-Spin P30 Tris columns (Bio-Rad, Hercules, CA) and used in the *in vitro* transcription reaction.

Fluorescence Spectra Measurement

Fluorescent spectra were taken on a Cary Eclipse fluorescence spectrophotometer using a single quartz cuvette or 96 well microplate. Experiments were performed at the excitation wavelength of 630nm with 5nm slit and emission scan of 640-800nm with 5nm slit. PMT voltage was set to high. The fluorescence emission value of each spectrum was reported and exported to Microsoft Excel files and drawn appropriately. The maximum emission peak of each spectra was selected to use in the data analysis.

Estimation of Kd's of MG RNA aptamers

For each MG RNA aptamer, from 0.05 μM to 20 μM, 18 different concentrations of RNA samples were tested with MG concentration at 0.2 μM for all samples. All tests were done in binding buffer (10mM HEPES, 0.1M KCl, 5mM $MgCl_2$, pH 7.4 at 23°C). The maximum peak value for each spectrum was reported and exported to Microsoft Excel files and drawn appropriately. Based on the equation: $F=[L]*F_{max} / (Kd +[L])$, the non-linear least-square regression was used to fit the data and to estimate Kd. For each regression, R^2 value was also given. The regression analysis was done using CoStat (Cohort, Monterey, CA).

Yeast Strain and Plasmids

The yeast strain 200897 was from the American Type Culture Collection(ATCC). Organism: *Saccharomyces cerevisiae*. ATCC number: 200897. Genotype: MATalpha ade2delta::hisG his3delta200 leu2delta0 met15delta0 trpdelta63 ura3delta0. The pYX vectors are a comprehensive set of yeast/E.coli shuttle vectors for expression in *S. cerevisiae* (pYX021 and pYX043 plasmids are the gifts of Dr. Alan Myers). pYX021 and pYX043 both are yeast integrative plasmids. A pYES2 plasmid is a yeast 2μ

plasmid carrying a URA3 marker and a Gal-1 promoter for galactose-inducible gene expression in S. cerevisiae (the pYes2 plasmid was a gift from Dr. Daniel Voytas).

Construction of Yeast Integrative Plasmid

To obtain a yeast vector by which the MG aptamer is expressed as part of the URA3 mRNA, oligonucleotides corresponding to the 40MG0 aptamer sequence were chemical synthesized and ligated into pYX043, previously digested with Xho I and SacII. The resulting recombinant plasmid (pYX043MG) was digested with Xho I and SacII to cut off part of pYX043MG including the polyA tail after the MCS, f1 origin and the existing Leu2 promoter. The sequence including the polyA tail after the MCS and the f1 origin from pYX043 was amplified by PCR (PCR1). The resulting PCR1 product included XhoI and XbaI cutting sites. A second PCR (PCR2) was carried out to obtain a fragment that included the 786 promoter from pYX021. The PCR2 product included XbaI and SacII cutting sites. The PCR1 product was digested with XhoI and XbaI. The PCR2 product was digested with XbaI and SacII. Then the enzyme digested PCR1 and PCR2 products were ligated into PYX043MG, previously digested with Xho I and SacII. The resulting recombinant plasmid was called pYX043786.

To obtain a yeast expression plasmid for a URA3 mRNA containing a 5' MG aptamer, PCR was carried out to obtain a fragment including the URA3 coding sequence from pYes2. The PCR product was digested with SacII and BsrGI and cloned into the plasmid pYX043786 which had been digested with SacII and BsrGI. The resulting recombinant plasmid (P3) was digested with Eco47III and SacII. Oligonucleotides corresponding to the 40MG0 aptamer sequence were chemical synthesized and ligated into P3, previously digested with Eco47III and SacII. The resulting recombinant plasmid (P6) has one copy of MG aptamer coding sequence inserted into URA3 5'UTR sequence.

Yeast Transformation and Media

To obtain yeast with plasmids expressing URA3 with or without the MG aptamer in the 5'UTR integrated into the yeast genome, the recombinant plasmids (P3 and P6)

was linearized using Eco47III and transformed into 200897 using the Lazy Bones yeast transformation method (*51*). Transformants resulting from homologous recombination were isolated by selection on SD-Uracil plates. SD-Uracil liquid media (per liter): 6.7 g yeast nitrogen base W/o amino acids, 1.92g Uracil dropout media supplement, 2% glucose. YPD liquid media (Per liter) :10 g yeast extract, 20 g tryptone peptone, add dH20, bring volume to 900ml. After autoclaving at 121 °C for 15 min, add 100ml 20% Glucose. SD-Uracil plates : 2% yeast agar in SD-Uracil liquid media.

Yeast Cell Growth and Spot Assay

Yeast cells were cultured in SD-Uracil liquid media at 30 °C shaker overnight. The OD of the overnight culture was determined by absorbency at 600 nm using UV/Visible spectrophotometer. Yeast cultures with OD600 nm absorbing around 0.5 were used for spot assays. If overgrown, the cells were diluted with water; 4 to 6 serial dilutions were made of each yeast culture and 3-5 µl of each dilution was spotted onto an assigned grid on the appropriate plates. The spots were allowed to dry before incubating at 30° C for 2 to 3 days. Pictures were taken at the desired time points.

Construction of 5'HH-MG-3'HDV Ribozyme Constructs

Oligonucleotides corresponding to 31- 85nt of the modified 85nt wild-type genomic hepatitis delta virus (HDV) sequences (HDV0) (*52*) were chemically synthesized and ligated into pcDNA3.1(-), previously digested with Xho I and EcoRI. The resulting plasmid was pR1. Oligonucleotides corresponding to a modified 50nt hammerhead ribozyme (HH) sequence (HH0) (*52*), the 40nt MG aptamer (40MG0) and 30nt (1-30)nt of the modified 85nt wild-type genomic HDV sequences (HDV0) were ligated into the pR1 vector, previously digested with Nhe I and EcoR I. The 30nt (1-30nt) of HDV0 sequence and 55nt (31-85nt) of HDV0 sequence mentioned above were joined together to form the full length HDV0 sequence. The resulting plasmid was pR2. Oligonucleotides corresponding to HH ribozyme sequences with low Mg^{2+} requirement for maximum activity (HH1, *53*) were ligated into the pR2 vector, previously digested with Nhe I and SacII. The resulting plasmid was pR3. Oligonucleotides corresponding

to a randomized HH ribozyme sequence (HH2) were ligated into pR2 vector, previously digested with Nhe I and SacII. The resulting plasmid was pR4. Oligonucleotides corresponding to a mutant (inactive) HDV ribozyme sequence (HDV1) were ligated into the pR3 vector, previously digested with AgeI I and Kpn I. The resulting plasmid was pR5. Oligonucleotides corresponding to the mutant (inactive) HDV ribozyme sequence (HDV1) were ligated into the pR4 vector, previously digested with AgeI and KpnI. The resulting plasmid was pR6.

RNA Transcription Reaction

Plasmids were digested with the Hind III restriction enzyme to linearize the DNA and provide templates for run-off transcription reaction. After complete enzyme digestion, the mixtures were phenol-chloroform extracted, ethanol precipitated and the cut plasmids re-suspended in water.

Transcription from linearized dsDNA templates were performed in 20 µl reaction volumes containing 40mM Tris-HCl buffer, 10mM NaCl, 1mM spermine, 0.05% Tween 20, 6mM $MgCl_2$, pH7.9 at 23 °C, 40mM dithiothreitol (DTT), 0.08ug/ul templates, 1.25mM ATP, GTP, UTP and CTP, 1U/µl Ribonuclease, 1U/µl T7 RNA polymerase and trace amount of [α-^{32}P] CTP (25 µCi/20ul). The transcription reactions were kept at 37 °C for 3 h. 0.05U/µl DNase I was added to mixture at the end of the transcription reaction and the mixture incubated at 37 °C for 15 min to digest dsDNA template. Following DNase I digestion, half of each reaction was removed, the $MgCl_2$ concentration was adjusted to 40mM and the sample was subjected to three rounds of thermal cycling (1 min at 72 °C, 5 min at 65 °C and 10 min at 37 °C) to facilitate the ribozyme folding into its active structure. The product of each transcription reaction was resolved by 8% denaturing polyacrylamide gel electrophoresis. The incorporation of [α-^{32}P] CTP in the transcription reaction allowed visualization of the bands with a phosphor-imager.

Synthesis of Biotinylated MG

3 mM EZ-link Biotin-LC-PEO Amine and 0.6 mM MG-isothiocyanate were mixed in 10ml 100% CH_2Cl_2. The mixture was put in a dark room and incubated on a rotating shaker for 1 h at room temperature. After the incubation was completed, the mixture was applied to a thin layer chromatography (TLC) plates (Silica gel, Polyester, 250uM thickness). After being air dried, the TLC plate was developed for 1 h using a mobile phase containing 90% CH_2Cl_2, 10% Methanol. The band containing the biotinylated MG was cut out and the MG extracted using N ,N-Dimethylformamide (DMF). The silica gel was removed by centrifuge at 16,000 g for 5 min. The biotinylated MG in DMF was concentrated under vacuum. The absorbency at 619 nm of purified Biotinylated MG was checked using a UV/Vis spectrophotometer and the concentration of biotinylated MG was calculated using a standard curve of MG absorbency at 619 nm.

Coupling of Biotinylated MG with Streptavidin Agarose Beads

30uM biotinylated MG and 7.5uM streptavidin (25 µM/ml packed agarose) were mixed in buffer containing 10 mM HEPES, 0.1M KCl, 5 mM $MgCl_2$, pH 7.4 at 23 °C and incubated 4 h in the dark room at room temperature. After incubation, the reaction mixture was transferred into an empty Poly-Prep chromatography column and washed with buffer containing 0.1M sodium acetate, 0.1M acetic acid, 0.1M KCl, 5mM $MgCl_2$, pH 4.5 at 23 °C. The flow-through and wash, which contained un-coupled biotinylated MG, were collected and their absorption at 619 nm was determined. The concentration of biotinylated MG that passed through the column was determined based on the MG standard curve. From this data the coupling efficiency and amount of MG coupled to the agarose were calculated.

Filter Assay

Single-stranded MG RNA TRAPs (^{32}P labeled during *in vitro* transcription) or MG RNA aptamers (2 - 20 pmoL, 5' labeled with ^{32}P) were incubated in the presence or absence of other ssDNAs, as defined in each experiment, at 75°C for 5 min then cooled to room temperature for 10 min. These samples were mixed with 20 µM Biotinylated

MG : streptavidin-agarose or other concentration noted in each experiment. Each sample was equilibrated at room temperature for 10 min then filtered through an HT-450 filter and washed with 5 ml of binding buffer. Fractions were analyzed for ^{32}P by measuring Cerenkov radiation. The radioactive cpm bound to biotinylated MG was divided by the total cpm in the original sample to give the fraction bound.

In Vitro SELEX

Three different ssDNA pools were used in three independent TRAP SELEX (S10, S15 and S20 as shown in Table 7) . All MG TRAPs' RNA pools were synthesized by *in vitro* transcription using the AmpliScribeTM T7-FlashT Transcription Kit from EPICENTRE and purified by denaturing (7M Urea) 8% PAGE. The three RNA pools were named as the N10, N15 and N20 pools with their names corresponding to the length of randomization region in the TRAP RNA. Concentrations of the gel purified MG TRAPs'RNA pools were quantified by NanoDrop ND-100 UV spectrophotometer. The double strand (ds) DNA templates for *in vitro* transcription were obtained by PCR using purchased ssDNA pools. The PCR reaction contained a 5 nM template, 2 μM forward primer, 2 μM reverse primer, 2 mM Mg2+and 200 μM dNTP. The PCR conditions were: 95°C 4 min pre-denaturation, 95°C 2 min denaturation, 55°C 2 min annealing, 72°C 3 min elongation and 15 cycles. Each PCR reaction ended with 10min incubation at 72°C. The PCR products were purified using Micro Bio-Spin P30 Tris. columns and used in the *in vitro* transcription reactions.

TRAP SELEX was done using filter capture. In each round, 1 or 3 consecutive negative selections were done first followed by 1 positive selection. Each round began with 5-10 μg TRAP RNA pool. In the negative selections the TRAP RNA pools were first incubated for 10 min at room temperature with or without 5 X non-regDNA and 5 X E.coli tRNA, as defined in each experiment. At the end of incubation, each mixture was transferred into a tube that contained biotinylated MG coupled with streptavidin-agarose. After 10 min incubation, the mixture was filtered through an HT-450 filter and washed with 5 ml of binding buffer. The flow-through was collected and ethanol precipitated. The precipitated nucleic acids were dissolved in water and applied to the

next negative or positive selection. In the positive selections, 5 X regDNA was incubated with the TRAP RNA pools. The flow-through from the filter was discarded. The filter was washed using water and the bound TRAPs were eluted with water and ethanol precipitated. RT-PCR was carried out using the re-dissolved ethanol precipitated nucleic acid from the positive selections.

The reverse transcription (RT) reactions used 10 μM reverse primer (SR1 in Table 7) and SuperScript™ III reverse transcriptase. The reaction mix was incubated at 55 °C for 1 hour. 2ul of RT product was used in the subsequent PCR reaction to regenerate dsDNA pool. The PCR conditions were the same as those used to amplify the original ssDNA pool. After each round a new RNA pool was generated and the pool was tested for MG binding using fluorescence spectral measurements.

RESULTS

Destabilization of the MG RNA Aptamer and Kd Determinations

The 38nt MG RNA aptamer has strong stem loop structure (Fig. 1a ,c). Two stems flanking the binding pocket provide strong support for its overall stability. It is easy to understand that if an aptamer has a very stable structure, it will be difficult to regulate its binding activity by an attenuator. A short attenuator will not interrupt the binding and by the time the attenuator is long enough to destroy the binding activity it is difficult to dislodge and release the inhibition on the aptamer. In order to make the MG RNA aptamer less stable and more easily regulated, we synthesized several truncated MG RNA aptamers with the length 34nt, 32nt, 30nt and 28nt, respectively. We also introduced the modifications into the 32nt MG RNA aptamer. We gave each sequence a simple and unique name (Table 1). Every sequence of the MG RNA aptamer variations listed in Table 1 was analyzed by Mfold (*54*) which provided a predicted folding and corresponding ΔG of each sequence. Four examples of secondary structure given by Mfold are shown in Fig. 2A.

From Table 1, we can see that by shortening the length of the stem formed by the 5' and 3' ends, the resulting overall stability (ΔG) of the MG RNA aptamers was reduced. One concern about this destabilizing effort is that although the truncation and modifications will make the aptamer less stable, the binding affinity for MG may also be reduced or lost. If the affinity of a truncated or modified aptamer for its ligand was reduced significantly compared with the wild type (38MG0), it could not be used in the TRAPs. Therefore, the dissociation constants (Kds) of selected aptamers were estimated using a non-linear least-square regression analysis of the results from fluorescence spectral measurements. The fitting curve and experiment data are drawn together on Fig. 2B for the two aptamers. The estimated Kd and R^2 values of the regression analyses for three selected aptamers are listed in Table 2.

Determine the Target Region of Attenuator on MG RNA aptamer

Modular rational design is the most widely used method to obtain allosteric nucleic acids such as allosteric ribozymes (*55-57*) and allosteric aptamers (*58*). The crystal structure of the 38nt malachite green aptamer has been solved to a resolution of 2.8 Å (*59*). In Fig. 1a (*59*), the nucleotide bases that are involved in the critical interaction with the ligand were labeled in the color other than black. The bulge loop between the two stems in the MG aptamer is the binding pocket. The broad side of the bulge loop between G24 and U32 of 40MG0 sequence is the obvious target for an attenuator in a MG TRAP. To test this possibility, seven 10nt ssDNA oligonucleotides targeting different regions of the 40MG0 aptamer were synthesized as shown in Fig.3 B. The sequences of all 10nt oligonucleotides were listed in Table 3. Upon binding to the MG RNA aptamer, the fluorescence of MG increased more than ~2,000 fold (*60*). Three representative fluorescent spectra are shown in Fig. 3A to illustrate the use of fluorescence to monitor the binding between MG and MG RNA aptamer. The results in Fig. 3C show that oligonucleotide E inhibited about 75% of MG aptamer binding. The ratio of the 10nt oligonucleotides to the MG aptamer was 1000:1. Oligonucleotide E which targets the bulge loop of the binding pocket had the highest inhibitory effect among the seven oligonucleotides tested.

Screening for the MG TRAPs allosteric regulated by regDNA

After determining that the most effective region for targeting the 40MG0 aptamer in order to inactivate it was the broad side of the bulge loop where the binding pocket is located, 15 MG TRAPs were designed based on different combinations of MG aptamer sequences (32MG1, 32MG2, 32MG4, 32MG6, 30MG1 and 28MG0) with attenuator lengths of 9nt, 10nt and 11nt (Table 4). PCR reactions were carried out to amplify the dsDNA needed to produce the MG TRAPs RNA through *in vitro* transcription. The PCR strategy is shown in Fig. 4A. The forward primer was used to produce the desired MG RNA aptamer sequence. The reverse primer was used to generate an attenuator segment with a defined sequence and length. The MG TRAP RNAs were purified by gel purification as described above. In the presence of 2uM MG, each MG TRAP RNA alone or with 5X regDNA or 5X non-regDNA were subjected to fluorescence spectral measurement. The 32MG0 aptamer was used as the positive control and the spectrum of binding buffer (10mM HEPES, 0.1M KCl, 5mM $MgCl_2$, pH 7.4 at 23 °C) was subtracted from each sample's spectrum. TRAP 32MG1-9 showed the best fold increase in fluorescence in the presence of 5X regDNA compared with 5X non-regDNA (Fig. 4B).

Design of the Yeast *In Vivo* Selection System

The MG RNA TRAP was developed *in vitro*. In order to verify that the MG-TRAP functions *in vivo*, a yeast *in vivo* selection system was designed. The MG RNA aptamer has previously been shown to work in *vivo* (*44, 45*). In the *in vivo* studies done so far, TMR was used as the ligand of MG RNA aptamer. As shown in Fig. 1b, TMR is a structural analog of MG. It contains an oxygen bridging two of the three benzol rings. The affinity of the MG RNA aptamer for TMR is more than ten times higher than its affinity for MG (~ 40nM compared to 800nM) (*61*). Used in yeast study, TMR was shown to go into the yeast cell quickly and has little effect on yeast growth at the 1μM concentration used in the cell media (*44, 45*). So TMR was chosen to be the ligand of choice for the MG RNA aptamer in the yeast study done for this work. The strategy, as shown in Fig. 5A, involves the MG RNA aptamer inserted into the 5'UTR

of a selected marker gene. A functional TRAP and its target gene are also expressed in the yeast cell. In the presence of MG the inserted aptamer prevents translation from the mRNA, which is recognized by an appropriate test (for example growth in the select marker is required for growth). In the condition of high expression of MG TRAP RNA and its target mRNA, the functional TRAP can recognize its target gene and bind to TMR. Then the MG RNA aptamer inserted into the 5'UTR of selected marker gene will have little chance to bind to TMR and the marker gene will be translated with little inhibition or even normally. As shown in Fig. 5B, in the absence of its target RNA, a functional TRAP will form a structure that inhibits the MG RNA aptamer portion of the TRAP from binding to TMR. Without the competition of the TRAP for binding of TMR, the MG RNA aptamer inserted into the 5' UTR of the marker gene will bind to TMR and form a structure that is stable enough to inhibit translation of the marker protein by up to more than 90% as shown in previous study (*44*). Through the expression status of the marker gene, the function of desired MG TRAP RNA could be tested. To test this idea, a series of yeast constructs were made. In Fig. 5C, plasmid P6 which originated from pYX043 had URA3 replace Leu2 as the reported gene. One copy of the 40MG0 aptamer sequence was inserted into 5' UTR of URA3. The 786 promoter from pYX021 was cloned into pYX043 to drive expression of URA3 gene. 786 promoter is a constitutive promoter for the yeast heat shock transcription factor 1(HSF1) gene (Saccharomyces Genome database: http://www.yeastgenome.org/). According to the pYX vectors manual, the gene under 786 promoter has about 15 copies of transcripts per cell if the plasmids are integrated into the genome. Plasmid P3 was also prepared with the same sequences as P6 but without the MG aptamer sequence inserted into 5' UTR of URA3.

Inhibition of Yeast Growth Assayed by the Spot Assay

In the previous study where one copy of MG RNA aptamer was inserted into the 5'UTR of cyclin transcripts in *S. cerevisiae*, Grate etal. (*44*) used 40MG0 sequence instead of 38MG0 sequence. Compared to the 38MG0, 40MG0 has one more Watson-Crick base pair inserted into the stem that flanks the aptamer's binding pocket and

lacks the a potential AUG start codon in the original 38MG0 aptamer sequence. One more base pair also provides more stability needed to inhibit translation. The 40MG0 sequence was also used in this study and inserted into the 5'UTR of URA3 transcripts. Results from the spot assay showed that the growth of yeast cells expressing URA3 transcripts bearing the 40MG0 sequence in 5'UTR (P6/200897 in Fig. 6) was greatly inhibited by the presence of 10 μM (Fig. 6A) and 20 μM TMR (Fig. 6B) in the SD-Uracil plates. Yeast cells transformed by plasmid bearing URA3 coding sequence without 40MG0 coding sequence inserted into 5'UTR (P3/200897 in Fig. 6) did not shown growth inhibition.

5'HH-MG-3'HDV Ribozyme Vector to Generate RNA with Homogenous Ends

Through rational design, a functional 32MG1-9 TRAP has been shown in this work to be regulated by regDNA *in vitro*. Inhibition of URA3 mRNA translation by a 40MG0 inserted in the 5'UTR of URA3 gene was also observed using the spot assay in the yeast. In the future, we need to put a TRAP developed *in vitro* inside the cell and test its function *in vivo*. The MG TRAP is a short RNA molecule and its function will be sensitive to sequence variations if present in a larger RNA molecule. Therefore it will be desirable to cut the aptamer sequence out of the RNA in which it is first synthesized. The strategy used here to generate the desired TRAP RNA molecules is promoter independent. The fully processed product from HH-MG-HDV expression cassette as shown in Fig. 7A will have defined 5' and 3' ends that does not depend on the transcriptional start and termination sites. This will be achieved because the ribozyme in the transcripts will cleave the RNA and produce homogenous ends as shown in Fig. 7B.

In Fig. 8, the RNA produced from 5 different constructs was analyzed by 8% denaturing PAGE. R2 and R3 both had fully functional HH and HDV ribozyme sequences. In R3, the 46 nt HH1, which was selected *in vitro* by others (*53*) to have a very high cleavage rate at low Mg^{++} concentrations, replaced the 50 nt HH0 in R2. In R4, a shuffled sequence of HH1 (HH2) replaced HH0 in R2 and the HDV0 sequence was unchanged. In R5, the HDV1 sequence replaced HDV0 sequence in R3 and the

HH1 sequence was unchanged. In R6, the HDV1 sequence replaced the HDV0 sequence in R4 and both HH ribozyme and HDV ribozyme were designed to be inactivities in R6. On the left side of the gel, RNA was loaded directly from the *in vitro* transcription reaction. The modification introduced in the HDV ribozyme sequence diminished the HDV cleavage activity shown as the absence of HDV sequence from MG aptamer sequence. The shuffled HH0 sequence that replaced HH1 resulted in loss of the HH cleavage activity. The MG sequence was not separated from the HH sequence. On the right side of gel, all samples went through 3 rounds of denaturation and re-naturation in the presence of 40mM Mg^{++}, which resulted in increased cleavage.

In Vitro SELEX to Select MG RNA TRAPs

Rational design is a fast and simple way to achieve functional allosteric nucleotide acid molecules. As shown above, after truncation and modification of the 38MG0, the 32MG1 sequence was found to be well regulated by a 9nt attenuator. The sequence space that rational design explores is very small compared to the SELEX process. In order to achieve a better MG RNA TRAP in terms of fold of activation by regDNA , *in vitro* SELEX was carried out using filter capture. Biotinylated MG was synthesized and purified by thin layer chromatography (TLC) (Fig. 9). The primary results for the SELEX assay are summarized in Fig. 10. For the N10 pool, the first round included 1 negative selection followed by 1 positive selection. The second to fourth rounds included 3 consecutive negative selections followed by 1 positive selection per round. For N15 and N20 pools, each round included 3 consecutive negative selections followed by 1 positive selection. In the first and second rounds of the N10 pool selection and first round of N15 pool selection, 5 X Non-regDNA and 5 X *E. coli* tRNA were present during the first negative selection. All other negative selections in the 3 pools did not include non-regDNA and *E. coli* tRNA.

Before selection the N10 R0 RNA pool was found to be regulated by regDNA, but it also had high binding activity in the absence of regDNA (Fig. 10A). After the first round with 1 negative selection, the resulting N10 R1 RNA pool had higher MG binding activity than the N10 R0 pool itself. The next round included 3 consecutive negative

selections. The fold activation by regDNA was increased from the N10 R1 to the N10 R2 pool. Compared with the N10R2 pool, the N10R3 pool showed increased activation by regDNA. From the N10 R3 pool to the N10R4 pool, there was no improvement in the activation. The overall performance of N10 pool showed no significant improvement over 4 rounds of SELEX.

The N15 pool had a longer randomized attenuator region (Fig. 10B). Each round of N15 pool selection included 3 consecutive negative selections. In the first round, 5X non-regDNA and 5X *E. coli* tRNA were present during the first negative selection. There was no obvious change in the fold of activation from the pool. The second round of N15 pool included neither non-regDNA nor *E. coli* tRNA. The activation was reduced a little from the first round.

The N20 pool went through one round in the absence of non-regDNA and *E. coli* tRNA (Fig. 10B). The activity of pool in the presence of regDNA was increased after one round but the resulting pool showed less activation by the regDNA compared to the original pool.

The TRAP SELEX experiments here were not taken through many rounds of selection compared with the number of rounds needed to select for an aptamer. However, considering the short length of the randomized region, the pool should show significant improvement in many fewer rounds than are usually required for selecting an aptamer, which is usually 8 to 14 rounds. The lack of improvement observed in these preliminary results of *in vitro* SELEX for selection of an MG TRAP suggested that the selection pressure in the negative selection may not have been sufficient.

DISCUSSION

The TRAP design integrates the binding property of the aptamer and the stem-loop structure of molecular beacons. It is an unique nucleic acid based probe which has great potential for *in vivo* imaging applications. The binding by an active aptamer module on a TRAP can transfer the presence of the target nucleic acid molecule into

the binding event between the aptamer and its ligand. The ligand molecule can be labeled with fluorescence, a quantum dot (*62*) or positron emitting isotopes (*63*). By contrast the signal output of the molecular beacon is limited to the fluorescence molecule because its mechanism of action requires a paired quencher and fluorophore. Fluorescence is not strong enough to penetrate most tissues and bone. This limits the *in vivo* use of molecular beacons for use in a broader range of imaging applications than the cultured cell. The ability of TRAP to utilize quantum dots and positron emitting isotopes for the signal output makes it a superior candidate to be developed for biological and biomedical applications, especially for *in vivo* non-invasive molecular imaging. For example, the TRAP could be use to enrich the intracellular concentration of an ^{18}F-labeled ligand upon interaction with a target mRNA in the body. The 3D real time image can be visualized through positron emission tomography (PET), which detects ^{18}F.

Similar to other allosteric nucleic acid molecules utilizing aptamers, such as the allosteric chimeric ribozyme-aptamer molecules with ribozyme activities regulated by aptamer ligands, successful regulation of the TRAP activity by its effector molecule (target nucleic acid molecule) is closely related to the structural stability and binding property of aptamer chosen. So far, many effector regulated ribozymes have been developed using the ATP aptamer (*57, 64-66*), theophylline aptamer (*65-68*) and FMN aptamer (*55, 66, 67, 69*). All three aptamers demonstrate global ligand-induced conformational changes. At the same time, efforts to utilize the arginine aptamer (*65*) and chloramphenicol aptamer (*66*) to develop allosteric ribozymes regulated by the aptamer ligands were not successful. The reason was suspected to be that the arginine and chloramphenicol aptamers did not possess global or relevant ligand-induced conformational changes found in ATP, theophylline and FMN aptamers (*70*). The MG aptamer does not demonstrate global, ligand-induced conformational changes. The two stems flanking the binding pocket provide stability as well as rigidity (Fig. 1). In the studies in which the MG aptamer was used to develop allosteric nucleic acid molecules, the MG aptamer was destabilized by truncation (*58*) or modification of stems

(*71*). This may be the way to make the MG aptamer more flexible so that it can be regulated in the case that it does not have ligand-induced conformational changes.

In the 2.8 Å crystal structure of the malachite green aptamer bound to tetramethylrosamine (TMR) , the binding pocket was located in the bulge loop flanking by two stems (Fig.1a, from *59*). One stem is longer and formed by the 5' and 3' ends. The other stem is shorter and is located between the hairpin loop and bulge loop. The colored residues are involved in binding the ligand. The G8:C28 (orange) base-pair, the G24·A31·G29:C7 base quadruple (blue) and the perpendicularly stacking A9 and A30 adenosines (magenta) are involved in direct base stacking with the ligand. The A27·C10:G23 base triplet (cyan) and the A26·U11:A22 base triplet (cyan) provide additional stability to the pocket by base stacking and base paring. The U25 (silver in Figure 1a) is involved in the U-turn which makes the base triplets and quadruplet feasible. The structural information provided by the 3D crystal structure was critical for TRAP rational design in determining which modifications and truncations to make.

As shown in Fig. 2A, the three base pairs shaded in blue in the 38MG0 aptamer were truncated to make the 34MG0 and 32MG0 aptamers. Our initial efforts of using the 34MG0 and 32MG0 aptamers to design functional TRAPs were not successful. The attenuator was either too long so that the TRAP could not be activated by regDNA or the attenuator was too short so that the TRAP had high aptamer binding activity in the absence of regDNA. We decided to introduce modifications in the base pairs shaded in red in Fig. 2A to further destabilize MG aptamer after truncating the stems. After the MG aptamer was truncated and modified, the affinity to its ligand could be decreased. However, although the overall stability of the MG aptamer was reduced after being truncated and modified, the affinity of MG aptamer was not significantly decreased compared to the 38MG0 (Tables 1 and 2). The 32nt MG aptamer had a similar affinity to MG with the 38MG0 aptamer. The results also showed the adaptability of the structure of 38MG0 aptamer. The two stems can be extensively manipulated as long as the binding pocket is untouched.

To start the MG TRAP design, an experiment was carried out to find the region on the MG aptamer with which the attenuator could interact easily. The MG RNA aptamer had been selected by *in vitro* SELEX to be used in the process of chromophore-assisted laser inactivation (CALI) (*72*). Babendure etal. (*60*) discovered that the fluorescence of MG increased more than ~2,000 fold after being bound by the MG RNA aptamer. The fluorescence can be used to measure the binding of the MG aptamer to MG. As shown in Fig. 3A, 400 nM MG alone without any RNA (sample 1) and 4 μM yeast tRNA plus 400 nM MG (sample 2) did not show any fluorescence peak whereas 1μM 40MG0 plus 400 nM MG (sample 3) showed fluorescence with excitation at 630 nm where the emission spectra collected from 640-800 nm. The maximum emission was found at about 650 nm (*60*). Seven 10nt ssDNA oligonucleotides were used to find out which region on the 40MG0 aptamer sequence was a good target for an attenuator (Fig. 3B). Oligonucleotide E which targeted 21-30 nt of the 40MG0 aptamer was the best inhibitor of the MG aptamer. The region targeted by oligonucleotide E included the 3 nt in the stem that is closed by the hairpin and bulge loops and 7 nt into the bulge loop. Eight out of 10 nt complementary to oligonucleotide E are involved in the interaction with MG (the 40MG0 has one more base GC base pair at the stem form by 5' and 3' end compared to the 38MG0 shown in Fig.1) . Seven of 10 nt of oligonucleotide F also target residues in the bulge loop that are involved in MG binding. The small inhibition effect of oligonucleotide F may be because its interaction with MG aptamer involves bases in the longer and more stable stem formed by 5' and 3' ends compared to the shorter, less stable stem targeted by oligonucleotide E. Also, the residues involved in the direct interaction with MG form strong base stack interactions with MG. Therefore it may be difficult for oligonucleotides F to intervene. These residues are close to the long stable stem. By contrast, the residues participating in forming and stabilizing the binding pocket that are targeted by oligonucleotide E do not directly interact with the ligand and may therefore more easily to be intervened. So, the oligonucleotide E seems to attack from the weaker side of the binding pocket and therefore effectively inhibits aptamer activity. The 1000:1 ratio of oligonucleotides to aptamer needed in these studies to demonstrate inhibition of the aptamer in trans by

oligonucleotide E and others was in part because the intermolecular interaction was far weaker than intramolecular interaction. Another reason is that DNA complement was used here, which forms a less stable hybrid than an RNA complement. The oligonucleotides that targeted regions out of binding pocket did not show good inhibition indicating that the design of attenuator should concentrate on targeting the broad side of bulge loop where the binding pocket is located.

After the broad side of the bulge loop was verified to be the optimal target of the attenuator, a series PCR reactions were carried out to produce dsDNA templates for 15 different MG TRAPs. The template contained the MG aptamer sequence and a 20nt antisense sequence targeting 741-760 nt of Uterocalin mRNA (Fig. 4A). The target region on uterocalin mRNA was selected in a previous study where a tiled microarray of 20nt oligonucleotides and antisense experiments was done to find out the accessible region on uterocalin mRNA (Chapter 4). The forward primer for producing the templates for the 15 TRAPs contained the T7 promoter and the desired MG aptamer sequence. The modifications on MG RNA aptamer were introduced through PCR reactions using the appropriate primer. The reverse primers with different lengths and sequences were used to form the desired attenuator sequences. The templates and primers for the PCR reactions are listed in Table 4. The regDNA and non-regDNA used in this study are also listed in Table 4. The 15 different MG TRAPs are listed in Table 5. The naming scheme, sequence, description and ΔG values predicted by Mfold are also listed in Table 5. The screening experiment of 15 TRAPs was done in 96 well format. From these studies, two TRAPs, 32MG1-9 and 30MG1-9, had better regDNA-dependent activation compared to the other tested TRAPs. The 32MG1aptamer had two G:U base pairs compared to two G:C base pair in the 32MG0 aptamer (red shaded region in Fig. 2A). The 30MG0 aptamer had one G:U base pairs compared to one G:C base pairs in 32MG0 aptamer. The results indicated that the G:U wobble base pair was a good choice to put into the MG aptamer to replace the G:C base pair in order to provide structural flexibility without losing much stability.

The 32MG2 (one G:U, one G:C) TRAPs with 9 , 10 or 11 nt attenuator, 32MG4 (one A:U, one G:U) TRAPs with 9 , 10 or 11 nt attenuator and the 32MG5 (one G:U, one A:U) TRAPs with 9 , 10 or 11 nt attenuator did not have good regDNA-dependent activation. For these TRAPs, increasing the strength of attenuator may reduce the aptamer activity of the TRAP in the absence of regDNA, but it will probably also reduce the extent of activation by regDNA as well. Shortening the attenuator may increase the extent of activation by regDNA but it will also probably increase the regDNA-independent activation. The results indicated that the MG aptamer sequences in these TRAPs may still be too stable to be well regulated.

The 28MG0-9 TRAP had a good fold increase in aptamer activity when the activity in the presence of the regDNA was compared with TRAP alone, but it had much less fold increase in aptamer activity when activation by regDNA was compared with activation by non-regDNA. The lose of specificity indicates that the 28MG0 aptamer was not sufficiently stable.

In both the 32MG1 TRAPs and 30MG1 TRAPs, increasing the attenuator length from 9 nt to 10 nt reduced the fold activation significantly. This indicated that the introduced G:U base pair brought the MG aptamer to the edge of being flexible enough to be regulated and stable enough to keep the specificity. The two TRAPs, 32MG1-9 and 30MG1-9, were subjected to the further testing and characterization.

Even though the TRAP can be designed to be functional *in vitro*, successful functioning *in vivo* is not guaranteed. To test the TRAPs function *in vivo*, a yeast selection system was developed. As shown in Fig. 5A and 5B, the function of the TRAP was reflected by expression of the reporter gene. The success of selection mainly relied on two things: first, the MG aptamer inserted into the 5' UTR was functional and it only efficiently inhibited the expression of the reporter gene in the presence of TMR as shown in Fig. 5B. Second, the active MG aptamer module in the TRAP showed to be able to efficiently compete with the inserted MG aptamer for binding to TMR and release the inhibition as shown in Fig. 5A. If these two elements

were found to work well, this system could be used to test the properties of individual TRAPs.

Two plasmids, P6 and P3, were constructed to test whether the MG aptamer was functional when inserted into the 5' UTR and whether it inhibited expression of a reporter gene in the presence of TMR. The feature map of plasmid P6 is shown in Fig. 5C. The plasmid P3, identical to P6 except that it lacked the 40MG0 aptamer sequence inserted into 5' UTR of URA3, was used as a negative control. In the yeast strain 200897, the URA3 gene was deleted from genome so that it can not grow on SD-U media. After transformed by P6 or P3, the resulting yeast cell P6/200897 and P3/200897 can grow on SD-U media. When 10 μM TMR was presented in the SD-U media, the growth of P6/200897 was greatly inhibited compared to the growth on SD-U media without TMR (Fig. 6A). The growth of P3/200897 was very similar on both media (Fig. 6A). In Fig. 6B, the TMR concentration was increase to 20 μM and a similar inhibition of growth of P6/200897 by TMR was observed. Growth of the control P3/200897 cells was not inhibited on TMR containing SD-U media compared to the SD-U media without TMR. This results showed the MG aptamer inserted into 5' UTR of URA3 gene was functional and it inhibited translation of URA3 mRNA only in the presence of its ligand-TMR. In the previous study done by Grate etal. (*44*), the MG aptamer was inserted immediately before (6 nt upstream) the start codon of CLB2 and the expression of CLB2 was inhibited more than 90% based on the data got from western blot. The quantitative measurement of inhibition of URA3 was not done. The TMR concentration used in the CLB2 study was 1 μM. In these studies we observed full inhibition of yeast growth at 10 μM TMR. In these studies, the MG aptamer was also inserted 6 nt upstream of the start codon of URA3. The higher concentration of TMR required to observe the full inhibition of yeast cell proliferation may be due to leaky expression of URA3 at the lower TMR concentrations providing enough orotidine 5'-monophosphate decarboxylase (encoded by URA3) to support yeast growth at a high enough level to escape detection by the spot assay.

The 786 promoter of the yeast heat shock transcription factor 1 (HSF1) is a house keeping gene with a low level of expression. Further comparisons of the effects of different promoters on inhibition by TMR may reveal a relationship between the strength of promoter and the effectiveness of inhibition of yeast growth. If needed, several MG aptamer sequences can be inserted into the 5' UTR of URA3 gene, which may provide stronger inhibition at similar TMR concentrations.

One advantage of selecting the URA3 gene as reporter was the ability to carry out counter-selection when 5-fluoro-orotic acid (5-FOA) was added into SD media. Yeast cells with wild-type URA3 genes convert 5-FOA into the toxic substance 5' fluorouridine monophosphate, severely limiting growth of the cells (*73*). The ability to carry out positive and negative selection with one marker suggested that the yeast system could be developed into an *in vivo* TRAP SELEX system. In the negative selections the yeast cells expressing TRAPs that have weaker attenuators and inhibit URA3 in the absence of target mRNA will be eliminated on SD-U media. In the positive selections, the target mRNA was expressed inside the yeast cell and the yeast cell expressing the TRAPs that can not inhibit URA3 in the presence of the target mRNA will be eliminated on SD media containing 5-FOA. The *in vivo* TRAP SELEX system is needed to clone TRAP RNA pool into yeast cells and the assay needs to be sensitive enough to establish sufficient selection pressure. The knowledge gained from testing individual TRAPs can facilitate the development of appropriate designs for the *in vivo* TRAP SELEX system.

By using P3/200897 as the controls, the growth of yeast cell was not inhibited on the SD-U media with 10 μM and 20 μM TMR. So the current experimental set up of the spot assay is well suited for the testing the TRAPs and aptamer's activity inside the yeast cell. Future experiments will entail expressing the MG RNA aptamer inside the yeast to see whether it will release the inhibition by TMR in the P6/200897 yeast cells. Also, we need to use PCR to verify the integration sites in the genome. We need to verify that the URA3 mRNA is carrying the MG sequence at its 5' UTR as we think they were. This could be done using RNase protection assay (*74*) or with 5' RACE (Rapid Amplification of cDNA Ends) (*75*). All these studies will be part of *in vivo* testing and

development of the MG RNA TRAP. It is likely to be done along with the further *in vitro* optimization of MG RNA TRAP.

TRAPs as well as aptamers are short nucleic acid molecules and their functions are sensitive to sequence variations in the RNAs that contain them. In order to express the TRAPs and aptamers inside the yeast cell, one challenge was to generate RNA molecules with defined 5' and 3' end. In other studies, the aptamer targeting the HIV-1 reverse transcriptase (RT) was cloned into an expression vector flanked by two self-cutting ribozyme. The resulting aptamer had minimum flanking sequence derive from cleavage at both ends by the self-cleaving ribozymes. In other studies, the 5' ribozyme-aptamer-3' ribozyme expression cassette was expressed in mammalian cells driven by a U6 promoter from an expression vector (*38, 76*). Successful inhibition of HIV-1 replication was observed and 50%-80% of the U6-expressed aptamer was shown to be located in the cytoplasm. This 5' ribozyme-aptamer-3' ribozyme expression cassette can be used to generate aptamer and TRAP in yeast. The 5' and 3' ribozyme used in the cited study required base pairing with the cleavage substrate. In TRAP the 5' end is defined by the aptamer sequence, which is constant. Therefore we can modify the 5' ribozyme sequence to base pair with the 5' end of TRAP. But the 3' end of TRAP is attenuator sequence that will be varied from TRAP to TRAP during selection. Therefore the HDV ribozyme was used as the 3' ribozyme. HDV ribozyme does not need to pair with the substrate, which is released after being cut, and can accommodate any desired 3' end without sequence adjustment. The HH-target RNA -HDV expression cassette was successfully cloned into a plasmid and an RNA with homogeneous ends was produced from *in vitro* transcripts (*52*).

The designed HH-aptamer/TRAP-HDV is shown in Fig. 7. The sequences of HH and HDV ribozyme used in this study are shown in Table 6. As shown in Fig.8, R2 and R3 both had fully functional HH and HDV ribozyme and the 40nt MG aptamer sequence was produced by both constructs. In R3, the 46 nt HH1, which was selected *in vitro* by others to have very high cleavage rates at low Mg^{++} concentrations replaced the 50 nt HH0 in R2. In R4, a shuffled sequence of HH1 (HH2) replaced HH1 in R3. In the R4

reaction lane, the MG, HH and MG-HDV bands are missing, indicating the loss of the HH ribozyme activity with replacement of the shuffled HH2 sequence for HH0. In R5, the HDV1 replaced HDV0 in R3. In the R5 reaction lane, the MG, HDV and HH-MG bands are missing reflecting the loss of HDV ribozyme activity. In R6, the HH2 and HDV1, mutants of HH1 and HDV0, respectively were used to replace the respective active ribozymes. In the R6 reaction lane, the only band seen was the full length HH-MG-HDV RNA. The results demonstrated the production of a 40nt MG aptamer fragment in the R2 and R3 reaction lanes was due to cleavage by the ribozymes. With 3 rounds of thermal cycles and increasing the $[Mg^{++}]$ from 6 to 40 mM to help the RNA to fold correctly, 100% cleavage by the functional ribozymes was seen with R2, R3, R4 and R5. Inside the cell, the free Mg^{++} concentration is about 0.2 to 1 mM (*77*). This concentration is much lower than the 40mM in which full ribozyme activity was observed. But the successful use of ribozymes inside the cell in previous studies and the fact that the ribozyme was naturally fully functional inside the cell made the HH-aptamer/TRAP -HDV expression cassette a practical method to express aptamer and TRAP inside yeast cells.

Short RNA molecules, such as ribozymes, aptamers, small hairpin RNAs (shRNAs) and antisense oligonucleotides, have been expressed inside cells to explore their biological or biomedical functions. Inside eukaryote cells, RNA polymerase II transcribes protein-encoding genes. RNA polymerase I synthesizes rRNAs and RNA polymerase III synthesizes 5s rRNA, tRNA, 7SL RNA, U6 snRNA and many other small nuclear RNAs (snRNAs). mRNA made by RNA polymerase II goes through post-transcriptional modification such as 5' and 3' end modification and has a 5' cap and polyA tail. The transcripts of RNA polymerase I and III do not have 5' caps and 3' end polyA tails. It has been shown that in yeast *Saccharomyces cerevisiae*, the transcripts of RNA polymerase I and III can be polyadenylated if the 3' end of the transcript has been generated independently by a hammerhead ribozyme (*78*). In another study in yeast *Saccharomyces cerevisiae*, transcripts synthesized *in vivo* by the bacteriophage T7 RNA polymerase were found not to be capped. However, the 3' end polyadenylation that occurred was sufficient for such non-capped transcripts to be

exported from the nucleus (*79*). This group replaced the mRNA cleavage and polyadenylation signals with a self-cleaving hammerhead ribozyme element. The resulting RNA was unadenylated. Even though a significant fraction of this RNA reached the cytoplasm, the unadenylated transcripts were accumulated near their site of synthesis in nucleus. Insertion of a stretch of DNA-encoded adenosine residues immediately upstream of the ribozyme element (a synthetic A tail) relieved the nuclear accumulation (*80*).

If the HH-Aptamer/TRAP-HDV expression cassette (Fig. 7) were used in yeast *Saccharomyces cerevisiae* driven by highly expressed pol II promoter such as the Gal 1 promoter, the resulting aptamer and TRAP will have no 5' cap and 3' poly A tail after cleavage by ribozyme at the both ends. In view of the evidence about the polyadenylation and nuclear export of transcripts in yeast *Saccharomyces cerevisiae* mentioned above, it is expected that inserting a stretch of DNA-encoded adenosine residues is inserted immediately upstream of the HDV ribozyme element (a synthetic A tail) will allow the HH-aptamer/TRAP-HDV transcripts to be efficiently be exported to the cytoplasm after self-cleavage to form the aptamer/TRAP. Cytoplasmic localization of the TRAP is desired because this is where the target mRNA is located.

Even though rational design can produce a TRAP that is specifically allosteric regulated by regDNA as shown in Fig. 4B, the number of sequences screened by this approach was limited to a small fraction of all possible sequence combinations. The *in vitro* SELEX process has been used to generate allosteric ribozymes, such as the allosteric ribozyme ligase (*64*) and the hammerhead ribozyme (*81*). In order to produce a MG TRAP with better sensitivity and specificity, TRAP selex was carried out using three TRAP RNA pools as shown in Table 7. Filter capture was selected to be the partition method used in TRAP selex. Biotinylated MG was coupled to streptavidin agarose beads to capture the bound RNA. The chemical reaction to make biotinylated MG is shown in Fig. 9C. The initial effort in which MG-isothiocyanate (Fig. 9A) was mixed with biotin-amine (Fig.9B) in aqueous solution was not successful. After the

coupling reaction was moved to a non-polar organic solvent (100% CH_2Cl_2), it produced the desired compound: biotinylated MG (Fig. 9D).

From the results in Fig. 10A, after 4 rounds of SELEX, the performance of the N10 RNA pool in terms of regDNA-dependent activation was not increased significantly. Similar results were seen in the N15 and N20 pools (Fig. 10B). One major difference in TRAP SELEX compared with SELEX for aptamers is that every sequence in the RNA pool used in the TRAP SELEX contains a full aptamer module. The key of SELEX for aptamers is to preserve and amplify the sequences with binding ability. The key of SELEX for the TRAP is to get rid of the sequences with unwanted binding ability. Because every TRAP possesses an aptamer module, it will exhibit its binding activity if the attenuator is weak. In other words, the key for success of TRAP SELEX will be to only keep the TRAPs that exhibit their aptamer activities when they are wanted, for example, in the presence of regDNA or target mRNA. So, the conditions for negative selection need to be well set up so that the TRAPs with aptamer activity in the absence of regDNA are removed efficiently. If the negative selection is not powerful enough to remove the unwanted TRAPs, such as TRAPs with weak attenuators, they will exhibit very good aptamer activity in the presence of regDNA in positive selection and be amplified and enriched in the subsequent RT-PCR step. Due to the heterogeneous folding of RNA molecules, it was very difficult to efficiently remove the TRAPs with weak attenuators in the negative selections. Based on this consideration, three consecutive negative selections were carried out in each round. The results showed that the repeat of a low pressure negative selection did not provide enough selection pressure needed to promote the effective evolution of a TRAP RNA pool.

The need for high pressure negative selection is a common requirement for the selection of allosteric nucleic acids. For example, in the selection of an ATP-dependent DNA enzyme, in the first three rounds, the negative selection was first set up to proceed for 21 hour and followed by 1 hour positive selection (*82*). These investigators ran into the same problem that the effector-independent activity began to accumulate. The solution was to proceed with the negative selection for 19 days! This increase in

stringency in round 4 resulted in a more-than-30-fold increase in effector-dependent activation.

In the selection of effector-dependent ribozymes or deoxyribozymes, the longer incubation time in the negative selection will allow more molecules with effector-independent enzyme activity to exhibit its enzyme activity resulting in cutting itself or ligated to a substrate. The shorter or longer molecule can then be efficiently remove from the pool by PAGE. But aptamer binding activity will not result in physically changing of the TRAP molecules. So simply increasing the incubation time in the negative selection will not work for TRAP SELEX.

The design of N20 pool was an effort to get around the problem of inadequate negative selection in SELEX. By randomizing the 10nt sequence of 32MG0 aptamer on TRAP, it reduced the regDNA-independent aptamer activity of N20 pool to a low level (Fig 10 B). The 10nt sequence was 9 to 18 nt of aptamer and it included the hairpin loop and part of following stem. None of the 10 nt involved in the binding with ligand as shown in Fig. 1. The designed N20 pool had two 10nt randomized regions on each TRAP and it had the best regDNA-dependent activation among the three pools before selection. After one round, the increase in activity regulated by regDNA decreased showing that the negative selection may have caused a similar problem for selection from the N20 pool as for selection from the previous N10 and N15 pools.

Another solution for selecting a well-regulated MG TRAP by SELEX could be to utilize the ability of a 630 nm laser to activate MG catalyzed cleavage of MG aptamer (*72*). After MG is bound by MG aptamer, it will release an active OH· radical with very short half-life if a 630 nm laser was given. The released OH· radical cleaves the 38MG0 aptamer between the U25 and A26. Negative selections of TRAP SELEX could include a laser treatment to cleave the TRAPs with regDNA-independent aptamer activity and to remove them from the pool by PAGE. By applying repeated treatments by laser in the presence of MG and increasing the incubation time with each repeated laser treatment, an efficient negative selection in TRAP SELEX may be achieved.

Including the aptamer module on the TRAP brings the ligand-capture and enrichment abilities to the TRAP which is the basis for signal output. At the same time, integrating the aptamer into the stem-loop structured probes adds another functional module than the stem structure itself, which is in molecular beacon. The interaction between aptamer and attenuator on the TRAP not only holds the antisense sequence to prevent non-specific interactions similar to the function of stem structure in molecular beacons, but also prevents the binding of aptamer to its ligand. Upon release of this interaction, the formation of aptamer : ligand complex will provide the extra driving force, which is absent in the molecular beacons, to promote the TRAP to fully open and recognize its target nucleic acid molecule. At the same time, the ability of the aptamer to form a stable complex with its ligand upon dissociation from the attenuator indicates that inhibition of aptamer needs to be strong enough to prevent the TRAP from being activated in the absence of target molecule.

As shown in Fig 11 A, the (ΔG_1° + ΔG_2°) represents the free energy given by aptamer folding and binding for its ligand. This indicates the stability of aptamer as well as the affinity of aptamer to its ligand. ΔG_3° indicates how stable the TRAP was in the absence of target mRNA. In the presence of target mRNA, the initial interaction between closed TRAP and mRNA will mostly likely involve a small number of base pairing interactions followed by the extension of base pairing from the initial core to 20 bp like a closed zipper. Once the TRAP is fully interacting with target mRNA, it is very stable as illustrated in Fig.4B and 4C (ΔG_4°). If the difference between ΔG_3° and (ΔG_1° + ΔG_2°) is too small, the TRAP could be opened by non-target molecules and lose its specificity. If the difference is to big, then it could not be efficiently opened by target mRNA and could lose its sensitivity. So the difference between ΔG_3° and (ΔG_1° +ΔG_2°) are thermodynamic parameters related to a successful TRAP design. Using 32MG1-9 as an example, if Kd of 32MG1 is set to 500 nM, then the approximate ΔG_2° value can be calculated (ΔG_2° = - RTln(1/Kd)) which is about - 8.9 Kcal/mol. The ΔG_1° predicted by Mfold was about -7.3 kcal/mol (Table 1). The ΔG_3° of 32MG1-9 was about -28.5 kcal/mol predicted by Mfold (Table 5). The difference between ΔG_3° and (ΔG_1°+ΔG_2°) was about -12 kcal/mol. But examining the 32 MG aptamer's ΔG_1° value in Table 1

and 32 MG TRAP's ΔG°_{3} value in Table 5, assuming that the Kd for different 32MG aptamers do not vary much as shown in Table 2, the difference between ΔG°_{3} and $(\Delta G^{\circ}_{1} + \Delta G^{\circ}_{2})$ for different 32MG TRAPs are very similar. So this value alone may not be enough to explain the difference between the TRAPs.

Unlike the cartoon representative shown in Fig. 10B, in reality the 20nt antisense sequence was not un-paired in the TRAP structure. Folding of the 32MG1-9 predicted by Mfold showed that, among the 20nt in the antisense sequences, 13nt participated in 8 base pairs, 6 Walson-Crick base pairs and 2 G:U wobble pairs. There were three G:C base pairings between antisense sequence and aptamer sequence and 5 base pairs within antisense sequence itself. The strong interaction between antisense and aptamer clearly helped to establish the low regDNA-independent activation of the 32MG1-9 TRAP. How the antisense sequence participates in the overall folding of TRAP is directly related to the overall stability of TRAP and interaction of the TRAP with target molecules. This may also be an important factor in determining the TRAP's sensitivity and specificity.

So far, there is not enough data from functional TRAPs to be summarized into a simple sequence of steps and thermodynamic parameters for general TRAP design. In the future, the further characterization and optimization of MG TRAPs selected from rational design and SELEX may provide useful information for this purpose. Computational design of oligonucleotide-sensing allosteric ribozyme utilized several sequence and thermodynamic parameters to filter off the unqualified sequences (*83*). The parameters derived from the MG TRAP development could be used in the future to realize the systematic computational design of TRAP for any selected aptamer and antisense sequences.

ACKNOWLEDGMENTS

I thank Jayeeta Banerjee for working with me on yeast selection system. She did the yeast spots assay (Fig.6). I wish to thank Drs. Alan Myers and Daniel Voytas for their generosity of providing us yeast strain and plasmids. I thank Dr. Gloria Culver

and her lab members for their support and help in the techniques of working with RNA and polyacrylamide gel electrophoresis.

REFERENCES

1. Kawasaki, H., Wadhwa, R., and Taira, K. (2004) World of small RNAs: from ribozymes to siRNA and miRNA, *Differentiation 72*, 58-64.

2. Kruger, K., Grabowski, P. J., Zaug, A. J., Sands, J., Gottschling, D. E., and Cech, T. R. (1982) Self-splicing RNA: autoexcision and autocyclization of the ribosomal RNA intervening sequence of Tetrahymena, *Cell 31*, 147-57.

3. Zaug, A. J., and Cech, T. R. (1982) The intervening sequence excised from the ribosomal RNA precursor of Tetrahymena contains a 5-terminal guanosine residue not encoded by the DNA, *Nucleic Acids Res 10*, 2823-38.

4. Min, C. J., Tafra, L., and Verbanac, K. M. (1998) Identification of superior markers for polymerase chain reaction detection of breast cancer metastases in sentinel lymph nodes, *Cancer Res 58*, 4581-4.

5. Rhodes, D. R., and Chinnaiyan, A. M. (2005) Integrative analysis of the cancer transcriptome, *Nat Genet 37 Suppl*, S31-7.

6. Calvano, S. E., Xiao, W., Richards, D. R., Felciano, R. M., Baker, H. V., Cho, R. J., Chen, R. O., Brownstein, B. H., Cobb, J. P., Tschoeke, S. K., Miller-Graziano, C., Moldawer, L. L., Mindrinos, M. N., Davis, R. W., Tompkins, R. G., and Lowry, S. F. (2005) A network-based analysis of systemic inflammation in humans, *Nature 437*, 1032-7.

7. Alwine, J. C., Kemp, D. J., Parker, B. A., Reiser, J., Renart, J., Stark, G. R., and Wahl, G. M. (1979) Detection of specific RNAs or specific fragments of DNA by fractionation in gels and transfer to diazobenzyloxymethyl paper, *Methods Enzymol 68*, 220-42.

8. Bassell, G. J., Powers, C. M., Taneja, K. L., and Singer, R. H. (1994) Single mRNAs visualized by ultrastructural in situ hybridization are principally localized at actin filament intersections in fibroblasts, *J Cell Biol 126*, 863-76.

9. Lee, M. S., LeMaistre, A., Kantarjian, H. M., Talpaz, M., Freireich, E. J., Trujillo, J. M., and Stass, S. A. (1989) Detection of two alternative bcr/abl mRNA junctions and minimal residual disease in Philadelphia chromosome positive chronic myelogenous leukemia by polymerase chain reaction, *Blood 73*, 2165-70.

10. Guatelli, J. C., Whitfield, K. M., Kwoh, D. Y., Barringer, K. J., Richman, D. D., and Gingeras, T. R. (1990) Isothermal, in vitro amplification of nucleic acids by a multienzyme reaction modeled after retroviral replication, *Proc Natl Acad Sci U S A 87*, 1874-8.

11. Adams, M. D., Kelley, J. M., Gocayne, J. D., Dubnick, M., Polymeropoulos, M. H., Xiao, H., Merril, C. R., Wu, A., Olde, B., Moreno, R. F., and et al. (1991) Complementary DNA sequencing: expressed sequence tags and human genome project, *Science 252*, 1651-6.

12. Gibson, U. E., Heid, C. A., and Williams, P. M. (1996) A novel method for real time quantitative RT-PCR, *Genome Res 6*, 995-1001.

13. Adams, M. D., Dubnick, M., Kerlavage, A. R., Moreno, R., Kelley, J. M., Utterback, T. R., Nagle, J. W., Fields, C., and Venter, J. C. (1992) Sequence identification of 2,375 human brain genes, *Nature 355*, 632-4.

14. Liang, P., and Pardee, A. B. (1992) Differential display of eukaryotic messenger RNA by means of the polymerase chain reaction, *Science 257*, 967-71.

15. Schena, M., Shalon, D., Davis, R. W., and Brown, P. O. (1995) Quantitative monitoring of gene expression patterns with a complementary DNA microarray, *Science 270*, 467-70.

16. Bertrand, E., Chartrand, P., Schaefer, M., Shenoy, S. M., Singer, R. H., and Long, R. M. (1998) Localization of ASH1 mRNA particles in living yeast, *Mol Cell 2*, 437-45.

17. Forrest, K. M., and Gavis, E. R. (2003) Live Imaging of Endogenous RNA Reveals a Diffusion and Entrapment Mechanism for nanos mRNA Localization in Drosophila, *Curr Biol 13*, 1159-68.

18. Fusco, D., Accornero, N., Lavoie, B., Shenoy, S. M., Blanchard, J. M., Singer, R. H., and Bertrand, E. (2003) Single mRNA molecules demonstrate probabilistic movement in living mammalian cells, *Curr Biol 13*, 161-7.

19. Tsuji, A., Koshimoto, H., Sato, Y., Hirano, M., Sei-Iida, Y., Kondo, S., and Ishibashi, K. (2000) Direct observation of specific messenger RNA in a single living cell under a fluorescence microscope, *Biophys J 78*, 3260-74.

20. Molenaar, C., Abdulle, A., Gena, A., Tanke, H. J., and Dirks, R. W. (2004) Poly(A)+ RNAs roam the cell nucleus and pass through speckle domains in transcriptionally active and inactive cells, *J Cell Biol 165*, 191-202.

21. Molenaar, C., Marras, S. A., Slats, J. C., Truffert, J. C., Lemaitre, M., Raap, A. K., Dirks, R. W., and Tanke, H. J. (2001) Linear 2' O-Methyl RNA probes for the visualization of RNA in living cells, *Nucleic Acids Res 29*, E89-9.

22. Tyagi, S., and Kramer, F. R. (1996) Molecular beacons: probes that fluoresce upon hybridization, *Nat Biotechnol 14*, 303-8.

23. Nitin, N., Santangelo, P. J., Kim, G., Nie, S., and Bao, G. (2004) Peptide-linked molecular beacons for efficient delivery and rapid mRNA detection in living cells, *Nucleic Acids Res 32*, e58.

24. Tyagi, S., and Alsmadi, O. (2004) Imaging native beta-actin mRNA in motile fibroblasts, *Biophys J 87*, 4153-62.

25. Burke, D. H., Ozerova, N. D., and Nilsen-Hamilton, M. (2002) Allosteric hammerhead ribozyme TRAPs, *Biochemistry 41*, 6588-94.

26. Cong, X., and Nilsen-Hamilton, M. (2005) Allosteric aptamers: targeted reversibly attenuated probes, *Biochemistry 44*, 7945-54.

27. Tuerk, C., and Gold, L. (1990) Systematic evolution of ligands by exponential enrichment: RNA ligands to bacteriophage T4 DNA polymerase, *Science 249*, 505-10.

28. Ellington, A. D., and Szostak, J. W. (1990) In vitro selection of RNA molecules that bind specific ligands, *Nature 346*, 818-22.

29. Dougan, H., Lyster, D. M., Vo, C. V., Stafford, A., Weitz, J. I., and Hobbs, J. B. (2000) Extending the lifetime of anticoagulant oligodeoxynucleotide aptamers in blood, *Nucl Med Biol 27*, 289-97.

30. Rusconi, C. P., Scardino, E., Layzer, J., Pitoc, G. A., Ortel, T. L., Monroe, D., and Sullenger, B. A. (2002) RNA aptamers as reversible antagonists of coagulation factor IXa, *Nature 419*, 90-4.

31. Rusconi, C. P., Roberts, J. D., Pitoc, G. A., Nimjee, S. M., White, R. R., Quick, G., Jr., Scardino, E., Fay, W. P., and Sullenger, B. A. (2004) Antidote-mediated control of an anticoagulant aptamer in vivo, *Nat Biotechnol 22*, 1423-8.

32. Carrasquillo, K. G., Ricker, J. A., Rigas, I. K., Miller, J. W., Gragoudas, E. S., and Adamis, A. P. (2003) Controlled delivery of the anti-VEGF aptamer EYE001 with poly(lactic-co-glycolic)acid microspheres, *Invest Ophthalmol Vis Sci 44*, 290-9.

33. Hwang, B., Han, K., and Lee, S. W. (2003) Prevention of passively transferred experimental autoimmune myasthenia gravis by an in vitro selected RNA aptamer, *FEBS Lett 548*, 85-9.

34. Jeon, S. H., Kayhan, B., Ben-Yedidia, T., and Arnon, R. (2004) A DNA aptamer prevents influenza infection by blocking the receptor binding region of the viral hemagglutinin, *J Biol Chem 279*, 48410-9.

35. Hicke, B. J., Marion, C., Chang, Y. F., Gould, T., Lynott, C. K., Parma, D., Schmidt, P. G., and Warren, S. (2001) Tenascin-C aptamers are generated using tumor cells and purified protein, *J Biol Chem 276*, 48644-54.

36. Schmidt, K. S., Borkowski, S., Kurreck, J., Stephens, A. W., Bald, R., Hecht, M., Friebe, M., Dinkelborg, L., and Erdmann, V. A. (2004) Application of locked nucleic acids to improve aptamer in vivo stability and targeting function, *Nucleic Acids Res 32*, 5757-65.

37. Chaloin, L., Lehmann, M. J., Sczakiel, G., and Restle, T. (2002) Endogenous expression of a high-affinity pseudoknot RNA aptamer suppresses replication of HIV-1, *Nucleic Acids Res 30*, 4001-8.

38. Joshi, P. J., North, T. W., and Prasad, V. R. (2005) Aptamers directed to HIV-1 reverse transcriptase display greater efficacy over small hairpin RNAs targeted to viral RNA in blocking HIV-1 replication, *Mol Ther 11*, 677-86.

39. Yang, C., Yan, N., Parrish, J., Wang, X., Shi, Y., and Xue, D. (2006) RNA aptamers targeting the cell death inhibitor CED-9 induce cell kiling in C. elegans, *J Biol Chem*.

40. Hu, K., Beck, J., and Nassal, M. (2004) SELEX-derived aptamers of the duck hepatitis B virus RNA encapsidation signal distinguish critical and non-critical residues for productive initiation of reverse transcription, *Nucleic Acids Res 32*, 4377-89.

41. Jain, C., and Belasco, J. G. (2000) Rapid genetic analysis of RNA-protein interactions by translational repression in Escherichia coli, *Methods Enzymol 318*, 309-32.

42. Werstuck, G., and Green, M. R. (1998) Controlling gene expression in living cells through small molecule-RNA interactions, *Science 282*, 296-8.

43. Charlton, J., Sennello, J., and Smith, D. (1997) In vivo imaging of inflammation using an aptamer inhibitor of human neutrophil elastase, *Chem Biol 4*, 809-16.

44. Grate, D., and Wilson, C. (2001) Inducible regulation of the S. cerevisiae cell cycle mediated by an RNA aptamer-ligand complex, *Bioorg Med Chem 9*, 2565-70.

45. Buskirk, A. R., Landrigan, A., and Liu, D. R. (2004) Engineering a ligand-dependent RNA transcriptional activator, *Chem Biol 11*, 1157-63.

46. Liu, Q., Ryon, J., and Nilsen-Hamilton, M. (1997) Uterocalin: a mouse acute phase protein expressed in the uterus around birth, *Mol Reprod Dev 46*, 507-14.

47. Flower, D. R. (1996) The lipocalin protein family: structure and function, *Biochem J 318 (Pt 1)*, 1-14.

48. Nilsen-Hamilton, M., Hamilton, R., Adams, G. (1982) Rapid selective stimulation by growth factors of the inocorporation by BALB/C 3T3 cells of(35S)methionine into a glycoprotein and five superinducible proteins, *Biochemical and Biophysical Res Commun 108*, 158-166.

49. Liu, Q., and Nilsen-Hamilton, M. (1995) Identification of a new acute phase protein, *J Biol Chem 270*, 22565-70.

50. Ryon, J., Bendickson, L., and Nilsen-Hamilton, M. (2002) High expression in involuting reproductive tissues of uterocalin/24p3, a lipocalin and acute phase protein, *Biochem J 367*, 271-7.

51. Amberg, D. C., Burke, D. J., and Strathern, J. N. (2005) *Methods In Yeast Genetics*, 2005 Edition ed., Cold Spring Harbor Laboratory Press.

52. Walker, S. C., Avis, J. M., and Conn, G. L. (2003) General plasmids for producing RNA in vitro transcripts with homogeneous ends, *Nucleic Acids Res 31*, e82.

53. Persson, T., Hartmann, R. K., and Eckstein, F. (2002) Selection of hammerhead ribozyme variants with low Mg2+ requirement: importance of stem-loop II, *Chembiochem 3*, 1066-71.

54. Zuker, M. (2003) Mfold web server for nucleic acid folding and hybridization prediction, *Nucleic Acids Res 31*, 3406-15.

55. Araki, M., Okuno, Y., Hara, Y., and Sugiura, Y. (1998) Allosteric regulation of a ribozyme activity through ligand-induced conformational change, *Nucleic Acids Res 26*, 3379-84.

56. Jose, A. M., Soukup, G. A., and Breaker, R. R. (2001) Cooperative binding of effectors by an allosteric ribozyme, *Nucleic Acids Res 29*, 1631-7.

57. Tang, J., and Breaker, R. R. (1997) Rational design of allosteric ribozymes, *Chem Biol 4*, 453-9.

58. Stojanovic, M. N., and Kolpashchikov, D. M. (2004) Modular aptameric sensors, *J Am Chem Soc 126*, 9266-70.

59. Baugh, C., Grate, D., and Wilson, C. (2000) 2.8 A crystal structure of the malachite green aptamer, *J Mol Biol 301*, 117-28.

60. Babendure, J. R., Adams, S. R., and Tsien, R. Y. (2003) Aptamers switch on fluorescence of triphenylmethane dyes, *J Am Chem Soc 125*, 14716-7.

61. Grate, D. (2000) in *Biology* pp 177, UNIVERSITY OF CALIFORNIA, SANTA CRUZ, SANTA CRUZ.

62. Medintz, I. L., Uyeda, H. T., Goldman, E. R., and Mattoussi, H. (2005) Quantum dot bioconjugates for imaging, labelling and sensing, *Nat Mater 4*, 435-46.

63. Tavitian, B. (2003) In vivo imaging with oligonucleotides for diagnosis and drug development, *Gut 52 Suppl 4*, iv40-7.

64. Robertson, M. P., and Ellington, A. D. (1999) In vitro selection of an allosteric ribozyme that transduces analytes to amplicons, *Nat Biotechnol 17*, 62-6.

65. Soukup, G. A., and Breaker, R. R. (1999) Engineering precision RNA molecular switches, *Proc Natl Acad Sci U S A 96*, 3584-9.

66. Robertson, M. P., and Ellington, A. D. (2000) Design and optimization of effector-activated ribozyme ligases, *Nucleic Acids Res 28*, 1751-9.

67. Soukup, G. A., Emilsson, G. A., and Breaker, R. R. (2000) Altering molecular recognition of RNA aptamers by allosteric selection, *J Mol Biol 298*, 623-32.

68. Kertsburg, A., and Soukup, G. A. (2002) A versatile communication module for controlling RNA folding and catalysis, *Nucleic Acids Res 30*, 4599-606.

69. Wang, D. Y., Lai, B. H., and Sen, D. (2002) A general strategy for effector-mediated control of RNA-cleaving ribozymes and DNA enzymes, *J Mol Biol 318*, 33-43.

70. Patel, D. J., Suri, A. K., Jiang, F., Jiang, L., Fan, P., Kumar, R. A., and Nonin, S. (1997) Structure, recognition and adaptive binding in RNA aptamer complexes, *J Mol Biol 272*, 645-64.

71. Buskirk, A. R., Kehayova, P. D., Landrigan, A., and Liu, D. R. (2003) In vivo evolution of an RNA-based transcriptional activator, *Chem Biol 10*, 533-40.

72. Grate, D., and Wilson, C. (1999) Laser-mediated, site-specific inactivation of RNA transcripts, *Proc Natl Acad Sci U S A 96*, 6131-6.

73. Boeke, J. D., Trueheart, J., Natsoulis, G., and Fink, G. R. (1987) 5-Fluoroorotic acid as a selective agent in yeast molecular genetics, *Methods Enzymol 154*, 164-75.

74. Rottman, J. B. (2002) The ribonuclease protection assay: a powerful tool for the veterinary pathologist, *Vet Pathol 39*, 2-9.

75. Schaefer, B. C. (1995) Revolutions in rapid amplification of cDNA ends: new strategies for polymerase chain reaction cloning of full-length cDNA ends, *Anal Biochem 227*, 255-73.

76. Joshi, P., and Prasad, V. R. (2002) Potent inhibition of human immunodeficiency virus type 1 replication by template analog reverse transcriptase inhibitors derived by SELEX (systematic evolution of ligands by exponential enrichment), *J Virol 76*, 6545-57.

77. Flatman, P. W. (1991) Mechanisms of magnesium transport, *Annu Rev Physiol 53*, 259-71.

78. Duvel, K., Pries, R., and Braus, G. H. (2003) Polyadenylation of rRNA- and tRNA-based yeast transcripts cleaved by internal ribozyme activity, *Curr Genet 43*, 255-62.

79. Dower, K., and Rosbash, M. (2002) T7 RNA polymerase-directed transcripts are processed in yeast and link 3' end formation to mRNA nuclear export, *Rna 8*, 686-97.

80. Dower, K., Kuperwasser, N., Merrikh, H., and Rosbash, M. (2004) A synthetic A tail rescues yeast nuclear accumulation of a ribozyme-terminated transcript, *Rna 10*, 1888-99.

81. Koizumi, M., Kerr, J. N., Soukup, G. A., and Breaker, R. R. (1999) Allosteric ribozymes sensitive to the second messengers cAMP and cGMP, *Nucleic Acids Symp Ser*, 275-6.

82. Levy, M., and Ellington, A. D. (2002) ATP-dependent allosteric DNA enzymes, *Chem Biol 9*, 417-26.

83. Penchovsky, R., and Breaker, R. R. (2005) Computational design and experimental validation of oligonucleotide-sensing allosteric ribozymes, *Nat Biotechnol*.

FIGURE LEGENDS

Figure 1. The structure information of the MG aptamer and its ligand (*59*).

(a) Secondary structure schematic of the aptamer. (b) Chemical structure of malachite green (MG) and tetramethylrosamine (TMR). The aptamer was selected to bind MG and the structure was solved with TMR as the ligand. (c) Front and back schematic views of the tertiary structure. Color coding for both the secondary and tertiary structure schematics is as follows: TMR, red; the canonical G8:C28 base-pair, orange; U25, the uridine involved in the U-turn, silver; the A26·U11:A22 and A27·C10:G23 base triples, cyan; the G24·A31·G29:C7 base quadruple, blue; the perpendicularly stacking A9 and A30 adenosines, magenta; bound strontium ions, green. (Reprinted from Journal of Molecular Biology , 301, Christopher Baugh, Dilara Grate and Charles Wilson, 2.8 Å crystal structure of the malachite green aptamer, 117-128, Copyright (2000), with permission from Elsevier).

Figure 2. Folding of selected MG RNA aptamers and Kd estimation.

A. The folding of four selected MG RNA aptamers predicted by Mfold. In the folding of the 38MG0 aptamer, the three base pairs shaded in blue were the ones that were deleted to get different aptamer sequences. The two base pairs shaded in red were the ones that were both modified and deleted to get different aptamer sequences.

B. The Kd estimation results of the 38MG0 and 32 MG0 aptamers. The MG concentration was set at 0.2 uM in all experiments. The RNA concentration is shown on the X-axis. The Y-axis is the fluorescence intensity measured using a single quartz cuvette. The filled red triangle is the experimental data of 38MG0 aptamer binding to MG. The red line is the curve fit of the experimental data from the 38MG0 aptamer binding to MG using non-linear least square regression analysis. The filled green rectangle was the experimental data of 32MG0 aptamer. The green line was the curve fit of the experimental data from the 32MG0 aptamer binding to MG using non-linear

least square regression. The Kd and R^2 values shown in red and green are the values for the 38MG0 and 32MG0 aptamers, respectively.

Figure 3. Interaction of 10nt oligonucleotides with 40MG0 aptamer.

A. Representative fluorescence spectra of three samples. For all samples, the buffer used was binding buffer (10 mM HEPES, 0.1 M KCl, 5 mM $MgCl_2$, pH 7.4 at 23 °C) and the MG concentration was 400 nM. For sample (1), there was no RNA added. For sample (2), 4 μM Yeast tRNA was added. For sample (3), 1 μM 40MG0 aptamer was added. In the spectrum of sample (3), the maximum peak was labeled.

B. A cartoon representation of seven 10nt oligonucleotides targeting different regions of the 40MG0 aptamer. The seven oligonucleotides were named as A, B, C, D, E, F and G. The neighboring 10nt oligonucleotides have a 5nt overlap in the target sequence.

C. Inhibition of the 40MG0 aptamer binding to MG by 10nt oligonucleotides. For all samples, the buffer used was binding buffer (10 mM HEPES, pH 7.4, 0.1 M KCl, 5 mM $MgCl_2$) and the MG concentration was 400 nM. Annotations on the figure: No RNA: no RNA included; Yeast tRNA: 4uM Yeast tRNA include; (A/B/C/D/E/F/G) + Aptamer: 1mM oligonucleotides (A/B/C/D/E/F/G) and 1uM 40MG0 aptamer included. The fluorescence peak value of each sample was normalized using the fluorescence peak value of 1uM 40MG0 aptamer binding with 400nM MG in binding buffer. The Y axis represented the percentage of aptamer activity.

Figure 4. Screening of 15 different MG TRAPs.

A. A cartoon representative of the PCR strategy used to generate dsDNA templates for MF TRAPs. The blue line represents the forward primer, which includes the T7 promoter sequence. The red line represents the reverse primer, which includes different lengths of attenuators to produce different TRAPs. The red dot on one of forward primer indicates that a modification was introduced through PCR. The green

line represents the aptamer sequence on the template. The black line represents the 20nt antisense sequence targeting 741-760 nt of uterocalin mRNA.

B. The screen of 15 different TRAPs through fluorescence measurements. For all samples, the buffer used was binding buffer (10 mM HEPES,, 0.1 M KCl, 5 mM $MgCl_2$, pH 7.4 at 23 °C) and the MG concentration was 2 μM. The RNA concentration in each sample was 0.5 μM.The fluorescence peak value of each sample was normalized using the fluorescence peak value of 0.5 μM 32MG0 aptamer binding with 2 μM MG in binding buffer. The Y axis represents the percentage of aptamer activity. The binding buffer was used as the background control and its spectrum was subtracted from the spectrum of all samples. The concentration of regDNA and non-regDNA was 2.5 μM each. Each TRAP had three samples: TRAP alone, TRAP plus 5 X regDNA and TRAP plus 5 X non-regDNA. The two numbers shown above each set of three samples is the fold increase in fluorescence intensity of TRAP plus 5X regDNA compared to TRAP alone and TRAP plus 5 X non-regDNA respectively.

Figure 5. Design of Yeast Selection and P6 plasmid.

A. A cartoon representative of how a functional MG TRAP should work inside a yeast cell. The big circle represented a yeast cell. Inside it, the black line with polyA represented the mRNA of the reporter gene in which the sequence encoding the MG aptamer was inserted in the 5' UTR before the translation start site. The thick black line represents the open reading frame on the mRNA.The blue line represents the inserted 40MG0 aptamer sequence. The two overlapping ellipses filled with black represents the ribosome. The ellipse with 40S represented the 40S subunit of ribosome. The targeted reversibly attenuated probe (TRAP) is represented by blue, green and red line linked together. The blue line represents the MG RNA aptamer sequence. The green line represents the 20nt antisense sequence in the TRAP. The red line represents the attenuator sequence. The pink line represents the target mRNA. The polygon filled with red represents TMR.

B. The annotation of this figure is same as for **A**.

C. The plasmid map of P6. 786 and Gal1 were the promoter sequences. URA3 and Amp were the coding sequences. 40 nt MG aptamer represents the sequence encoding the 40MG0 aptamer. Eco 47III was used to linearize P6 for transformation and integration.

Figure 6. Spot Assay.

A. The yeast strain 200897 was transformed by Eco 47III linearized P3 and P6, respectively. The resultant yeast cells were P3/200897 and P6/200897. Beginning with a yeast suspension absorbing 0.5 OD at 600 nm, serial 10 X dilutions were put on the two kinds of media: SD-U and SD-U containing 10 uM TMR. Every dilution was repeated once on each plate. Every yeast suspension was spotted on two different plates in each media. The picture were taken approximately 3 days after spotting.

B. The yeast cells used were same as in A, P3/200897 and P6/200897. Beginning with a suspension absorbing 0.5 OD at 600 nm, the series 10 X dilution was put on the two kinds of media: SD-U and SD-U containing 20 uM TMR. Every dilution was repeated three times on one plate. Every yeast cell was spotted twice on one plate in each media. The picture were taken approximately 3 days after spotting.

Figure 7. Design of HH-MG-HDV expression cassette.

A. The linear structure of the HH-MG-HDV expression cassette. The HH ribozyme was placed at the 5' end. The target sequence, MG aptamer or TRAP sequence was placed in the middle. The HDV ribozyme was placed in the 3' end.

B. The detailed structure and product information from the HH-MG-HDV expression cassette (*52*). R2 contained HH0, 40MG0 and HDV0 sequences. R3 contained HH1, 40MG0 and HDV0 sequences. R4 contained HH2, 40MG0 and HDV0 sequences. R5 contained HH1, 40MG0 and HDV1 sequences. R6 contained HH2, 40MG0 and HDV1 sequences (Ribozyme sequences are listed in Table 6). The rectangular areas indicate the included sequences in corresponding constructs. The arrow indicates a ribozyme cleavage site. Six fully and partially cleaved products are listed. The shaded

P1 stem in the HDV ribozyme are the positions in which restriction enzyme cutting sites can be introduced to facilitate cloning.

Figure 8. The cleavage of HH-MG-HDV RNA.

Half of the products from *in vitro* transcription reactions (6 mM $MgCl_2$) of five different constructs (R2, R3, R4, R5 and R6) were run on a 8% 8 M Urea polyacrylamide gel. The other halves of the products were subjected to the three rounds of thermal cycling (1 min at 72 °C, 5 min at 65 °C and 10 min at 37 °C) in the presence of 40 mM $MgCl_2$ followed by PAGE on the same gel. The bands were labeled with corresponding sequence elements included.

Figure 9. Biotinylated MG Synthesis.

A. The structure of malachite green isothiocyanate.

B. The structure of EZ-link biotin-LC-PEO amine (Biotin-amine).

C. The reaction scheme represented the coupling reaction between malachite green isothiocyanate and EZ-link biotin-LC-PEO amine.

D. The TLC results of malachite green (MG) isothiocyanate and biotinylated MG (MG-biotin).

Figure 10. Summary of the Results of Fluorescence Measurements from TRAP SELEX.

A. The fluorescence measurements of the N10 RNA pool during the process of 4 rounds of SELEX. For all samples, the buffer used was binding buffer (10 mM HEPES, 0.1 M KCl, 5 mM $MgCl_2$, pH 7.4 at 23 °C). The RNA concentration and MG concentration in each sample were 0.5 μM and 2 μM or 1 μM and 4 μM, respectively. The fluorescence peak value of each sample was normalized using the fluorescence peak value of the same concentration of the 32MG0 aptamer and MG in binding buffer. The Y axis represents the percentage of aptamer activity. The concentration of

regDNA and non-regDNA was five times that of the RNA pool concentration. Each pool had three samples: pool alone, pool plus 5 X regDNA and pool plus 5 X non-regDNA. The two numbers shown above each set of three samples was the fold increase in fluorescence intensity of the pool plus 5X regDNA compared to the pool alone and the pool plus 5 X non-regDNA respectively. R0 represents the pool before any selection. R1 represents the pool that went through 1 round with defined negative and positive selections. The same naming scheme was used for R2 , R3, R4, etc.

B. Fluorescence measurements of the N15 RNA pool during the process of 2 rounds of SELEX and N20 pool during the process of 1 round of SELEX. The annotation was same as with A.

Figure 11. Thermodynamics Related to TRAP Design.

A. The curve line represents denatured MG aptamer in the random coil. ΔG_3° and ΔG_1° is the change of free energy upon folding. ΔG_2° is the change of free energy when the folded aptamer binds to its ligand, which was represented by the red-filled polygon.

B. The targeted reversibly attenuated probe (TRAP) is represented by blue, green and red lines linked together. The blue line represents the MG RNA aptamer sequence. The green line represents the 20nt antisense sequence in the TRAP. The red line represents the attenuator sequence. The pink line represents the target mRNA. The polygon filled with red represents TMR. The curved line represents the denatured TRAP in a random coil. ΔG_3° is the change of free energy upon folding. ΔG_4° is the change of free energy when the folded TRAP binds to ligand and the effector (regDNA or target mRNA). The circle with a dashed line represents the folded aptamer binding to the ligand with the (ΔG_1° +ΔG_2°) as a contribution to the overall free energy ΔG_4°.

C. The thermodynamics related to TRAP design. The line with two arrows represents the energy gap between the closed TRAP and aptamer : ligand complex.

Tables and Figures

Table 1: Sequences of MG RNA Aptamers used.

Name[1]	Description	Length	$_{\Delta}G°$ (Kcal/ mol)	Synthetic Oligo[2]
40MG0	The MG RNA aptamer inserted into 5'UTR in Yeast study. (*44*)	40nt	-21.41	None
	GGAUCCGCGA CUGGGGAGAC CCAGGUAACG AAUCGGAUCC			
38MG0	The MG RNA aptamer comes out of SELEX, structure with TMR determined. (*59, 72*)	38nt	-17.9	Oligo258
	GGAUCCCGAC UGGCGAGAGC CAGGUAACGA AUGGAUCC			
34MG0	Truncated from 38MG0: U_4C_5 and $G_{34}A_{35}$	34nt	-13.3	Oligo1374
	GGACCGAC UGGCGAGAGC CAGGUAACGA AUGUCC			
32MG0	Truncated from 34MG0: A_3 and U_{32}	32nt	-12.8; -12.2	Oligo1375
	GGCCGACUGG CGAGAGCCAG GUAACGAAUG CC			
32MG1	From 32MG0: $C_{17}C_{18}$ to $U_{17}U_{18}$. G_9C_{18} to G_9U_{18}, $G_{10}C_{17}$ to $G_{10}U_{17}$	32nt	-7.3	Oligo1410
	GGCCGACUGG CGAGAGUUAG GUAACGAAUG CC			
32MG2	From 32MG0: C_{18} to U_{18}. G_9C_{18} to G_9U_{18}	32nt	-9.8	None
	GGCCGACUGG CGAGAGCUAG GUAACGAAUG CC			
32MG3	From 32MG0: G_9 to A_9, C_{18} to U_{18}. G_9C_{18} to A_9U_{18}	32nt	-10.1	None
	GGCCGACUAG CGAGAGCUAG GUAACGAAUG CC			
32MG4	From 32MG0: G_9 to A_9, C_{17} to U_{17},C_{18} to U_{18}. G_9C_{18} to A_9U_{18},$G_{10}C_{17}$ to $G_{10}U_{17}$	32nt	-7.7	None
	GGCCGACUAG CGAGAGUUAG GUAACGAAUG CC			
32MG5	From 32MG0: G_{10} to A_{10}, C_{17} to U_{17},C_{18} to U_{18}. G_9C_{18} to G_9U_{18},$G_{10}C_{17}$ to $A_{10}U_{17}$	32nt	-7.8	None
	GGCCGACUGA CGAGAGUUAG GUAACGAAUG CC			
32MG6	From 32MG0: G_9 to A_9, G_{10} to A_{10}, C_{17} to U_{17},C_{18} to U_{18}. G_9C_{18} to A_9U_{18},$G_{10}C_{17}$ to $A_{10}U_{17}$	32nt	-7.7	None
	GGCCGACUAA CGAGAGUUAG GUAACGAAUG CC			
30MG0	Truncated from 32MG0: G_9 and C_{18}	30nt	-8.8	None
	GGCCGACUGC GAGAGCAGGU AACGAAUGCC			
30MG1	From 30MG0: C_{16} to U_{16}. G_9C_{16} to G_9U_{16}	30nt	-6.8	Oligo1421
	GGCCGACUGC GAGAGUAGGU AACGAAUGCC			
28MG0	Truncated from 30MG0: G_9 and C_{16}	28nt	-5.7	Oligo1422
	GGCCGACUCG AGAGAGGUAA CGAAUGCC			

[1] Zero (0) after MG in the name indicates there is no mutation. It is either the original sequences from other studies or the truncated ones.

[2] None indicates there was no corresponding RNA oligonucleotides purchased from IDT. The Oligonucleotide number was the name given when it was purchased from IDT.

Table 2: Kd estimation of three synthetic MG RNA aptamers

Name	Sequence	Kd	R^2
38MG0	GGAUCCCGACUGGCGAGAGCCAGGUAACGAAUGGAUCC	563 nM	0.955
34MG0	GGACCGACUGGCGAGAGCCAGGUAACGAAUGUCC	991 nM	0.958
32MG0	GGCCGACUGGCGAGAGCCAGGUAACGAAUGCC	725 nM	0.951

Table 3: Sequences of 10nt ssDNA oligonucleotides

Name	Description	Length	Oligo Number[1]
A	Complementary from 1 to 10 nt of 40MG0	10nt	Oligo993
	TCGCGGATCC		
B	Complementary from 6 to 15 nt of 40MG0	10nt	Oligo994
	CCCAGTCGCG		
C	Complementary from 11 to 20 nt of 40MG0	10nt	Oligo995
	GTCTCCCCAG		
D	Complementary from 16 to 25 nt of 40MG0	10nt	Oligo996
	CCTGGGTCTC		
E	Complementary from 21 to 30 nt of 40MG0	10nt	Oligo997
	CGTTACCTGG		
F	Complementary from 26 to 35 nt of 40MG0	10nt	Oligo998
	CGATTCGTTA		
G	Complementary from 30 to 40 nt of 40MG0	10nt	Oligo999
	GGATCCGATT		

[1] The Oligo number was the name given when it was purchased.

Table 4: Sequences of ssDNA oligonucleotides used in the TRAP rational Design.

Name	Description	Length	Oligo Number[1]
regDNA	Sequence of Uterocalin cDNA 741-760nt	20nt	Oligo1399
	GCCACCATACCAAGGAGCAT		
non-regDNA	Mixture of four 19nt Random ssDNA pools (25% each pool)	20nt	Oligo1401/2/3/4
	NNNNNNNNNNNNNNNNNN (A/T/G/C)		
T1	PCR template for 32MG TRAPs (PAGE[3])	47nt	Oligo1411
	ACTGGCGAGAGTTAGGTAACGAATGCCATGCTCCTTGGTATGGTGGC		
T2	PCR template for 30MG TRAPs	45nt	Oligo1423
	ACTGCGAGAGTAGGTAACGAATGCCATGCTCCTTGGTATGGTGGC		
T3	PCR template for 28MG TRAPs	43nt	Oligo1425
	ACTCGAGAGAGGTAACGAATGCCATGCTCCTTGGTATGGTGGC		
F1	Forward Primer for 32MG1 TRAPs	45nt	Oligo1412
	TTCTAATACGACTCACTATAGGCCGACTGGCGAGAGTTAGGTAAC		
F2	Forward Primer for 32MG2 TRAPs	45nt	Oligo1414
	TTCTAATACGACTCACTATAGGCCGACTGGCGAGAGCTAGGTAAC		
F3	Forward Primer for 32MG3 TRAPs	45nt	Oligo1415
	TTCTAATACGACTCACTATAGGCCGACTAGCGAGAGCTAGGTAAC		
F4	Forward Primer for 32MG4 TRAPs	45nt	Oligo1416
	TTCTAATACGACTCACTATAGGCCGACTAGCGAGAGTTAGGTAAC		
F5	Forward Primer for 32MG5 TRAPs	45nt	Oligo1417
	TTCTAATACGACTCACTATAGGCCGACTGACGAGAGTTAGGTAAC		
F6	Forward Primer for 32MG6 TRAPs	45nt	Oligo1418
	TTCTAATACGACTCACTATAGGCCGACTAACGAGAGTTAGGTAAC		
F7	Forward Primer for 30MG1 TRAPs	43nt	Oligo1424
	TTCTAATACGACTCACTATAGGCCGACTGCGAGAGTAGGTAAC		
F8	Forward Primer for 28MG0 TRAPs	41nt	Oligo1426
	TTCTAATACGACTCACTATAGGCCGACTCGAGAGAGGTAAC		
R1	Reverse Primer Provides 9nt attenuator sequence	33nt	Oligo1413
	TTTTGTAACGAATGCCACCATACCAAGGAGCAT		
R2	Reverse Primer Provides 10nt attenuator sequence	34nt	Oligo1419
	TTTTGGTAACGAATGCCACCATACCAAGGAGCAT		
R3	Reverse Primer Provides 11nt attenuator sequence	35nt	Oligo1420
	TTTTAGGTAACGAATGCCACCATACCAAGGAGCAT		

[1] The Oligo number was the name given when it was purchased.

Table 5: Sequences of Designed MG TRAPs[1] and Predicted ΔG value.

Name[2]	Description	Length	ΔG (Kacl/mol)
32MG1-9	MG TRAP bearing 32MG1 aptamer and 9nt attenuator sequence GGCCGACUGG CGAGAGUUAG **GUAACGAAU**G CC AUGCUCCUUGGUAUGGUGGC *AUUCGUUAC* AAAA	65nt	-28.5
32MG1-10	MG TRAP bearing 32MG1 aptamer and 10nt attenuator sequence GGCCGACUGG CGAGAGUUA**G GUAACGAAU**G CC AUGCUCCUUGGUAUGGUGGC *AUUCGUUACC* AAAA	66nt	-29.6
32MG1-11	MG TRAP bearing 32MG1 aptamer and 11nt attenuator sequence GGCCGACUGG CGAGAGUU**AG GUAACGAAU**G CC AUGCUCCUUGGUAUGGUGGC *AUUCGUUACCU* AAAA	67nt	-32.5
32MG2-10	MG TRAP bearing 32MG2 aptamer and 10nt attenuator sequence GGCCGACUGG CGAGAGCUA**G GUAACGAAU**G CC AUGCUCCUUGGUAUGGUGGC *AUUCGUUACC* AAAA	66nt	-30.5
32MG2-11	MG TRAP bearing 32MG2 aptamer and 11nt attenuator sequence GGCCGACUGG CGAGAGCU**AG GUAACGAAU**G CC AUGCUCCUUGGUAUGGUGGC *AUUCGUUACCU* AAAA	67nt	-31.5
32MG3-10	MG TRAP bearing 32MG3 aptamer and 10nt attenuator sequence GGCCGACUAG CGAGAGCUA**G GUAACGAAU**G CC AUGCUCCUUGGUAUGGUGGC *AUUCGUUACC* AAAA	66nt	-30.8
32MG3-11	MG TRAP bearing 32MG3 aptamer and 11nt attenuator sequence GGCCGACUAG CGAGAGCU**AG GUAACGAAU**G CC AUGCUCCUUGGUAUGGUGGC *AUUCGUUACCU* AAAA	67nt	-30.8
32MG4-10	MG TRAP bearing 32MG4 aptamer and 10nt attenuator sequence GGCCGACUAG CGAGAGUUA**G GUAACGAAU**G CC AUGCUCCUUGGUAUGGUGGC *AUUCGUUACC* AAAA	66nt	-28.4
32MG4-11	MG TRAP bearing 32MG4 aptamer and 11nt attenuator sequence GGCCGACUAG CGAGAGUU**AG GUAACGAAU**G CC AUGCUCCUUGGUAUGGUGGC *AUUCGUUACCU* AAAA	67nt	-29.3
32MG5-10	MG TRAP bearing 32MG5 aptamer and 10nt attenuator sequence GGCCGACUGA CGAGAGUUA**G GUAACGAAU**G CC AUGCUCCUUGGUAUGGUGGC *AUUCGUUACC* AAAA	66nt	-28.5
32MG5-11	MG TRAP bearing 32MG5 aptamer and 11nt attenuator sequence GGCCGACUGA CGAGAGUU**AG GUAACGAAU**G CC AUGCUCCUUGGUAUGGUGGC *AUUCGUUACCU* AAAA	67nt	-28.6
32MG6-10	MG TRAP bearing 32MG6 aptamer and 10nt attenuator sequence GGCCGACUAA CGAGAGUUA**G GUAACGAAU**G CC AUGCUCCUUGGUAUGGUGGC *AUUCGUUACC* AAAA	66nt	-28.4

32MG6-11	MG TRAP bearing 32MG6 aptamer and 11nt attenuator sequence GGCCGACUAA CGAGAGUU**AG GUAACGAAU**G CC AUGCUCCUUGGUAUGGUGGC *AUUCGUUACCU* AAAA	67nt	-28.6
30MG1-9	MG TRAP bearing 30MG1 aptamer and 9nt attenuator sequence GGCCGACUGC GAGAGUAG**GU AACGAAU**GCC AUGCUCCUUGGUAUGGUGGC *AUUCGUUAC* AAAA	63nt	-28
30MG1-10	MG TRAP bearing 30MG1 aptamer and 10nt attenuator sequence GGCCGACUGC GAGAGUA**GGU AACGAAU**GCC AUGCUCCUUGGUAUGGUGGC *AUUCGUUACC* AAAA	64nt	-27.5
30MG1-11	MG TRAP bearing 30MG1 aptamer and 11nt attenuator sequence GGCCGACUGC GAGAGU**AGGU AACGAAU**GCC AUGCUCCUUGGUAUGGUGGC *AUUCGUUACCU* AAAA	65nt	-28
28MG0-9	MG TRAP bearing 28MG0 aptamer and 9nt attenuator sequence GGCCGACUCG AGAGAG**GUAA CGAAU**GCC AUGCUCCUUGGUAUGGUGGC *AUUCGUUAC* AAAA	61nt	-26.9
28MG1-10	MG TRAP bearing 28MG0 aptamer and 10nt attenuator sequence GGCCGACUCG AGAGA**GGUAA CGAAU**GCC AUGCUCCUUGGUAUGGUGGC *AUUCGUUACC* AAAA	62nt	-26.4
28MG1-11	MG TRAP bearing 28MG0 aptamer and 11nt attenuator sequence GGCCGACUCG AGAG**AGGUAA CGAAU**GCC AUGCUCCUUGGUAUGGUGGC *AUUCGUUACCU* AAAA	63nt	-26.5

[1] The underlined sequence indicates the attenuator sequence. The sequence in bold is the regions with which the attenuators designed to interact.

[2] The name of MG TRAP was made of two parts. The first part was the aptamer sequence used in TRAP. The number after the dashed line indicated the length of attenuator of that TRAP.

Table 6: Sequences of HH ribozyme and HDV ribozyme

Name	Description	Length
HH0	Hammerhead ribozyme sequence (*52*)	50nt
	UCGCGGAUCCCUGAUGAGUCCGUGAGGACGAAACGGUACCCGGUACCGUC	
HH1	Hammerhead ribozyme sequence with low Mg^{2+} requirement From HH0: ($U_{19}C_{20}CGUGAGG_{27}A_{28}$) to HH1($C_{19}U_{20}UUU_{23}G_{24}$) (*53*)	46nt
	UCGCGGAUCCCUGAUGAGCUUUUGCGAAACGGUCCGCGGGACCGUC	
HH2	Shuffled Hammerhead ribozyme (HH1) sequence	46nt
	UCUAUGGAGUCCUCACUCCGAUGCGGGGGAAUUCCGCGGGACCGUC	
HDV0	HDV Ribozyme sequence (*52*)	85nt
	GGCCGGCAUGGUCCCAGCCUCCUCGCUGGCGCCGGCUGGGCAACACCGGU AGGGGACCGUCCCCUACCUGGUGGCGAAUGGGACC	
HDV1	Mutated HDV Ribozyme sequence (mutation introduced :75C to A, 78A to G)	85nt
	GGCCGGCAUGGUCCCAGCCUCCUCGCUGGCGCCGGCUGGGCAACACCGGU AGGGGACCGUCCCCUACCUGGUGGAGAGUGGGACC	

Table 7: Sequences of ssDNA Oligonucleotides AND MG RNA TRAP pools used in the TRAP SELEX[1]

Name	Description	Length	Oligo Number[2]
S10	ssDNA pool with 10nt randomized attenuator sequence (PAGE[3])	96nt	Oligo1398
	ACTATAGGCCGACTGGCGAGAGCCAGGTAACGAATGCC ATGCTCCTTGGTATGGTGGCNNNNNNNNNNAACAAAAAAAAAAAAAAAACAAAAA AAA		
N10 RNA pool	TRAP RNA pool with 10nt attenuator sequence randomized	90nt	None
	GGCCGACUGGCGAGAGCCAGGUAACGAAUGCCAUGCUCCUUGGUAUGGUGGC NNNNNNNNNNAACAAAAAAAAAAAAAAAACAAAAAAA		
S15	ssDNA pool with 15nt randomized attenuator sequence (PAGE[3])	101nt	Oligo1405
	ACTATAGGCCGACTGGCGAGAGCCAGGTAACGAATGCC ATGCTCCTTGGTATGGTGGCNNNNNNNNNNNNNNAACAAAAAAAAAAAAAAAC AAAAAAAA		
N15 RNA pool	TRAP RNA pool with 15nt attenuator sequence randomized	95nt	None
	GGCCGACUGGCGAGAGCCAGGUAACGAAUGCCAUGCUCCUUGGUAUGGUGGC NNNNNNNNNNNNNNAACAAAAAAAAAAAAAAAACAAAAAAA		
S20	ssDNA pool with 10nt randomized attenuator and 10nt randomized 32MG0 aptamer sequenc (PAGE[3])	102nt	Oligo1408
	GGAAAAAAAAAAGGCCGACTNNNNNNNNNNAGGTAACGAATGCC ATGCTCCTTGGTATGGTGGCNNNNNNNNNNAACAAAAAAAAAAAAAAAACAAAAA AAA		
N20 RNA pool	TRAP RNA pool with 10nt MG aptamer sequence and 10nt attenuator sequence randomized	102nt	None
	GGAAAAAAAAAAGGCCGACUNNNNNNNNNNAGGUAACGAAUGCC AUGCUCCUUGGUAUGGUGGCNNNNNNNNNNAACAAAAAAAAAAAAAAAACAAAA AAAA		
SF1	Forward Primer for the S10 and S15 ssDNA pool	35nt	Oligo1396
	TTCTAATACGACTCACTATAGGCCGACTGGCGAGA		
SF2	Forward Primer for the S20 ssDNA pool	40nt	Oligo1409
	TTCTAATACGACTCACTATAGGAAAAAAAAAAGGCCGACT		
SR1	Reverse Primer for the S10, S15 and S20 ssDNA pools	28nt	Oligo1397
	TTTTTTTTGTTTTTTTTTTTTTTTGTT		

[1] RegDNA and non-regDNA used in TRAP Selex were listed in Table 4.

[2] The Oligo number was the name assigned when it was synthesized.

[3] PAGE indicates the oligo was purchased as the PAGE purified preparations.

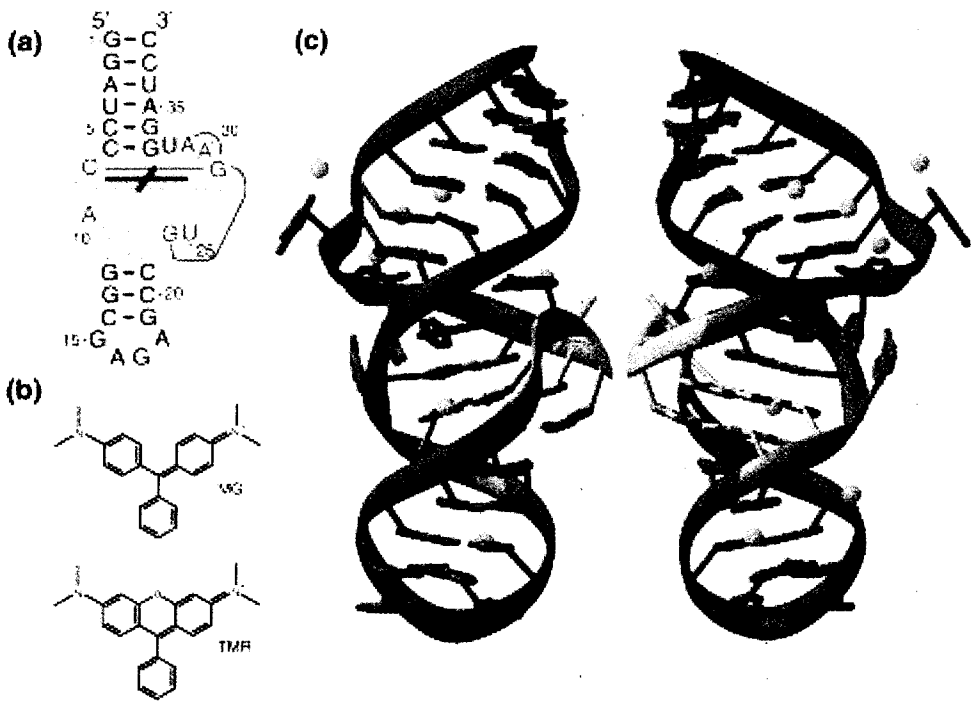

Figure 1

(A)

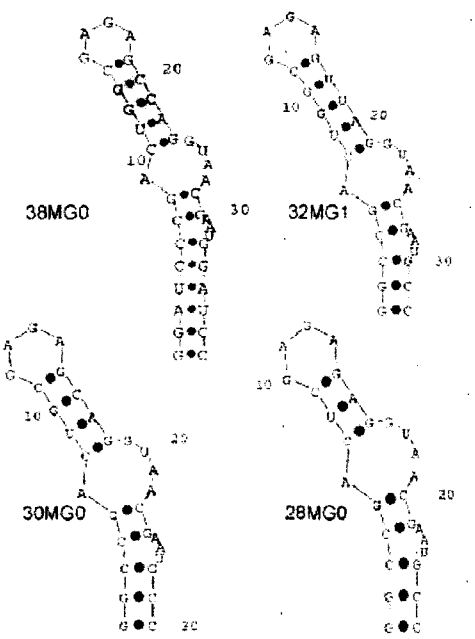
38MG0
32MG1
30MG0
28MG0

(B)

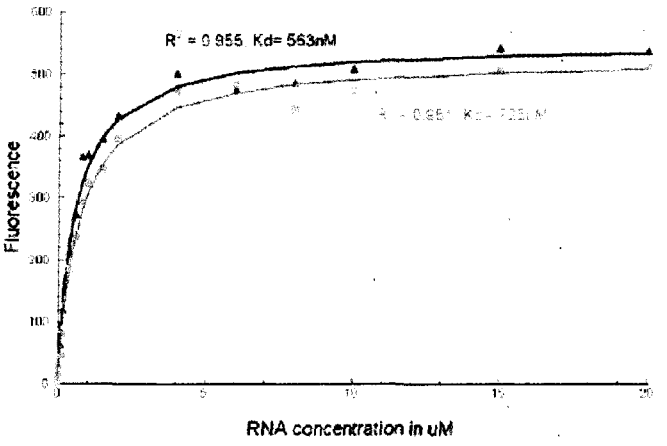
Kd dertermination of 38MG0 and 32MG0 RNA Aptamer
R² = 0.955 Kd= 563nM
Fluorescence
RNA concentration in uM

Figure 2

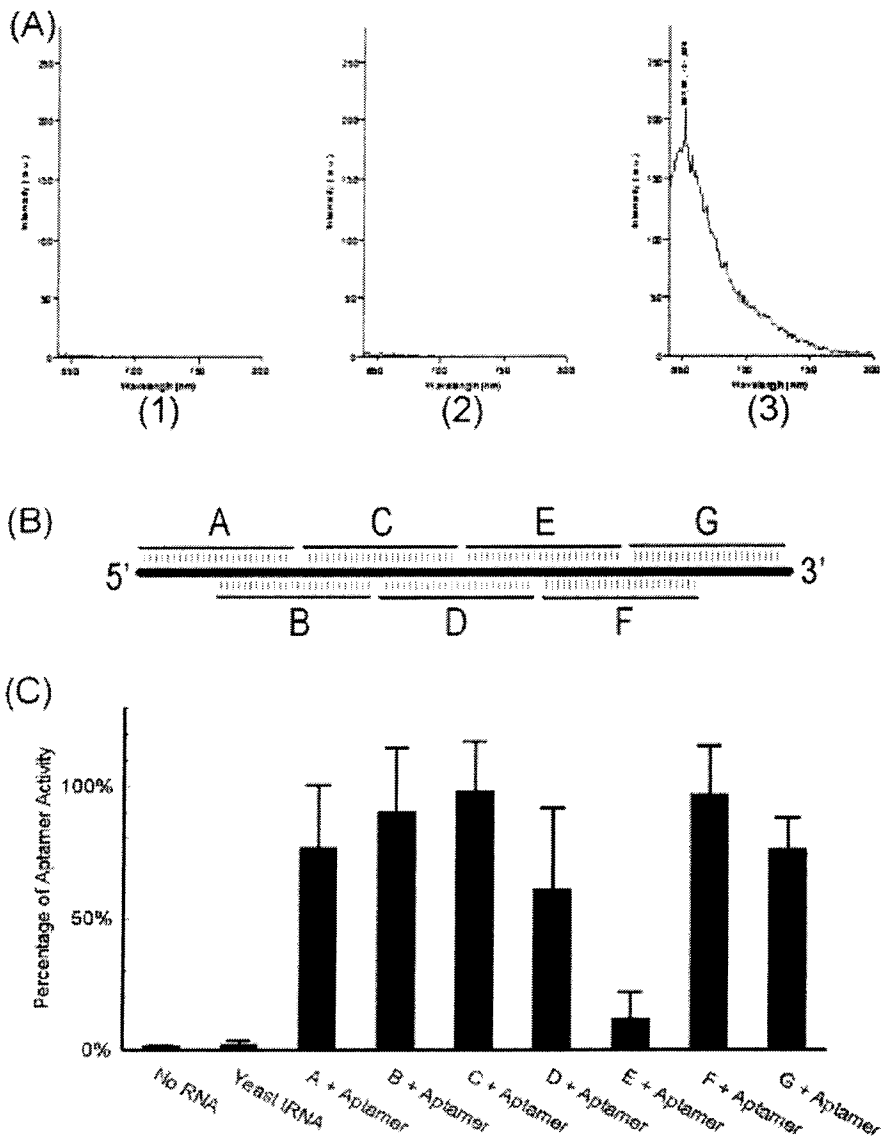
(A)
(1)
(2)
(3)
(B)
A
C
E
G
5'
3'
B
D
F
(C)
Percentage of Aptamer Activity
100%
50%
0%
No RNA
Yeast tRNA
A + Aptamer
B + Aptamer
C + Aptamer
D + Aptamer
E + Aptamer
F + Aptamer
G + Aptamer

Figure 3

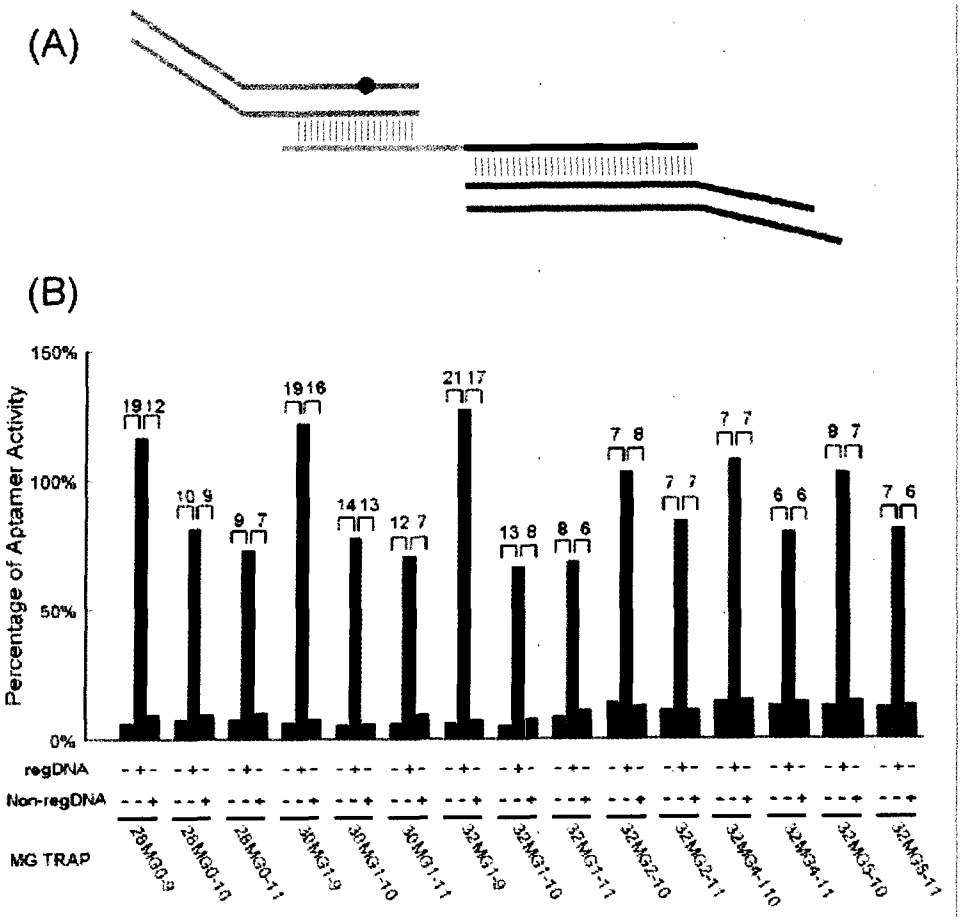
(A)
(B)
150%
100%
50%
0%
Percentage of Aptamer Activity
19 12
10 9
9 7
19 16
14 13
12 7
21 17
13 8
8 6
7 8
7 7
7 7
6 6
8 7
7 6
regDNA
Non-regDNA
MG TRAP
28MG30-9
28MG30-10
28MG30-11
30MG1-9
30MG1-10
30MG1-11
32MG1-9
32MG1-10
32MG1-11
32MG2-10
32MG2-11
32MG4-1-10
32MG4-11
32MG5-10
32MG5-11

Figure 4

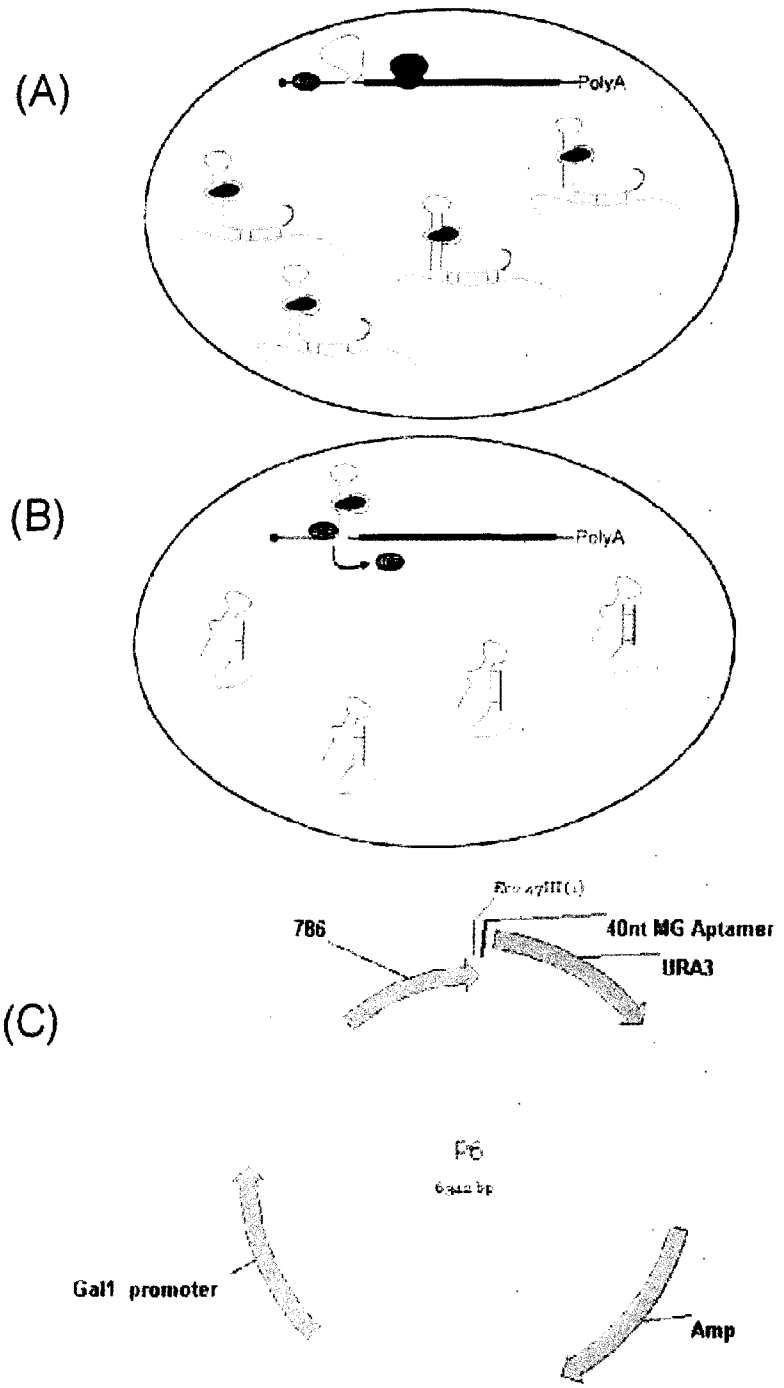

Figure 5

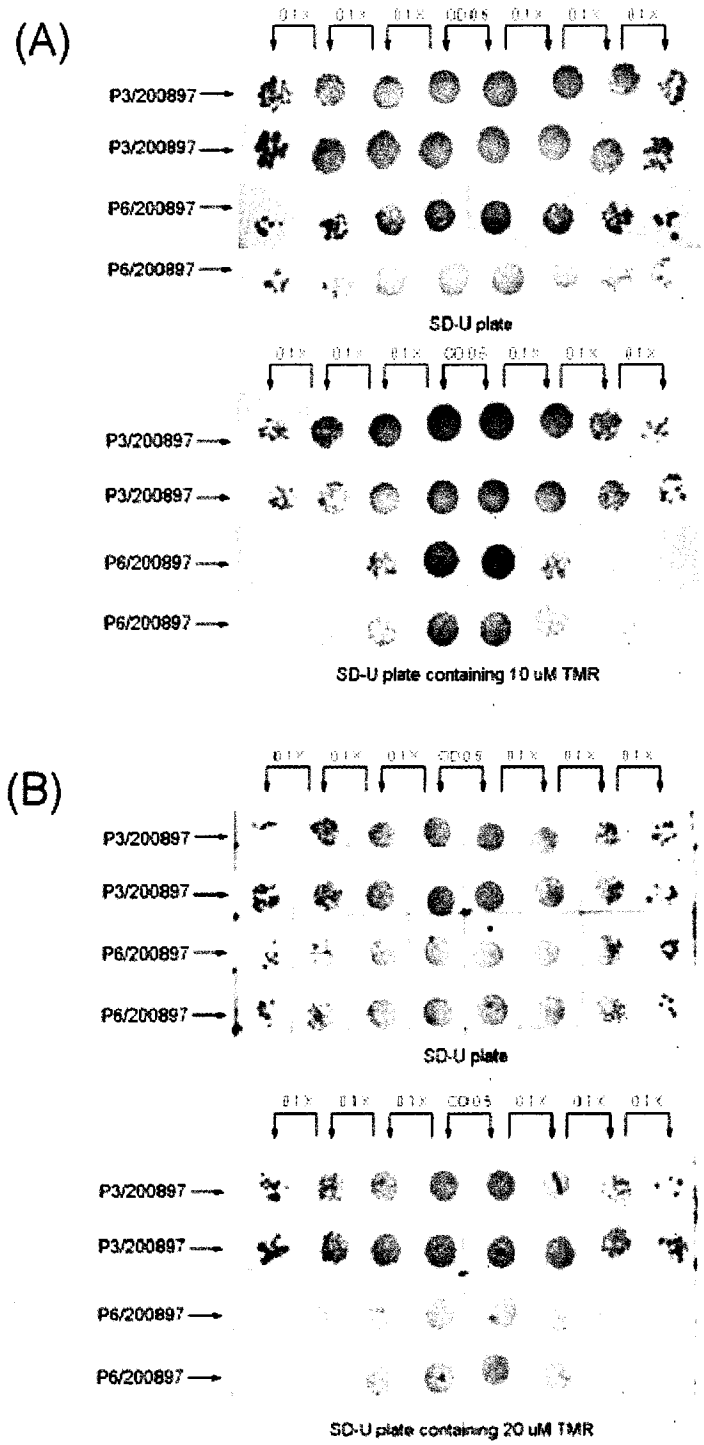
(A)
P3/200897
P3/200897
P6/200897
P6/200897
SD-U plate
P3/200897
P3/200897
P6/200897
P6/200897
SD-U plate containing 10 uM TMR
(B)
P3/200897
P3/200897
P6/200897
P6/200897
SD-U plate
P3/200897
P3/200897
P6/200897
P6/200897
SD-U plate containing 20 uM TMR

Figure 6

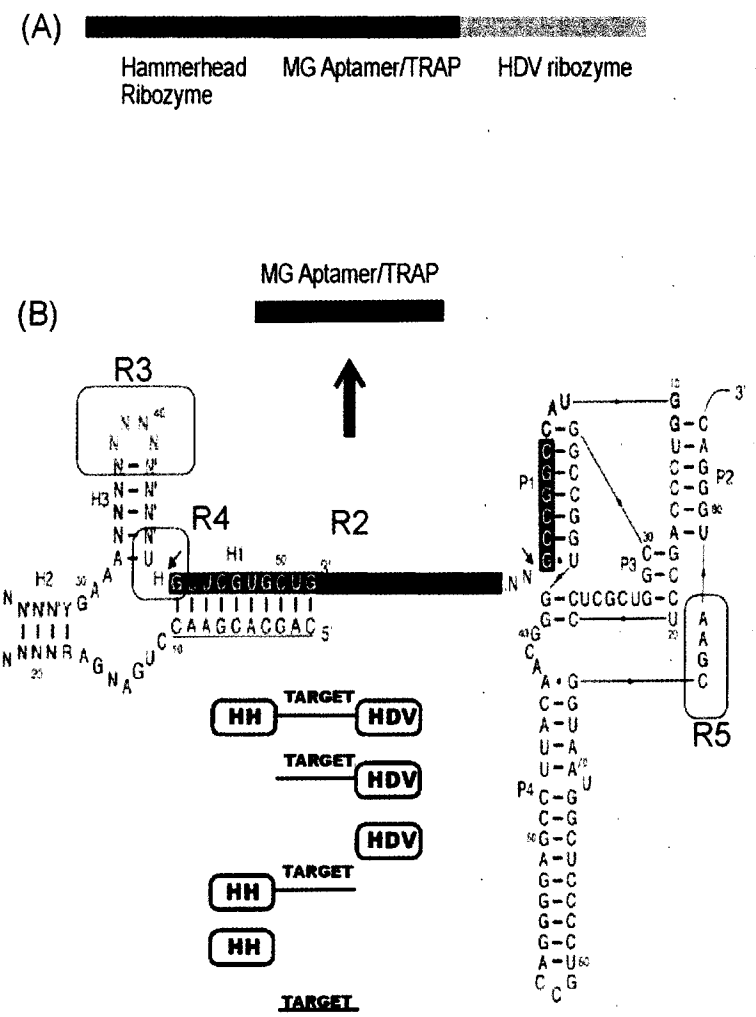
(A)
Hammerhead Ribozyme
MG Aptamer/TRAP
HDV ribozyme
(B)
MG Aptamer/TRAP
R3
R4
R2
R5
P1
P2
P3
P4
TARGET
HH
HDV

Figure 7

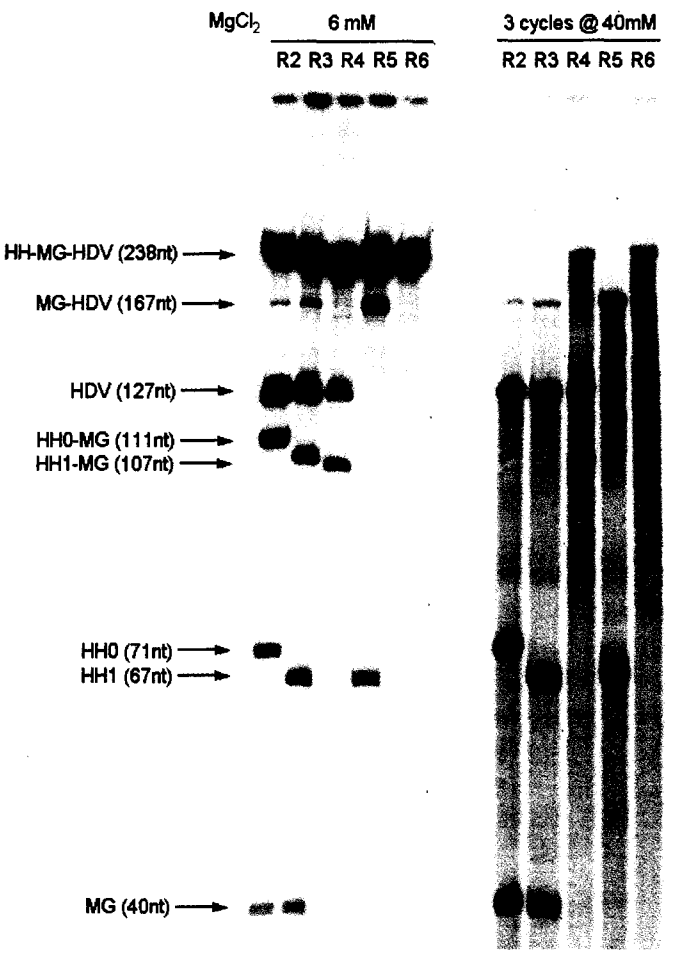
MgCl2
6 mM
3 cycles @ 40mM
R2 R3 R4 R5 R6
R2 R3 R4 R5 R6
HH-MG-HDV (238nt)
MG-HDV (167nt)
HDV (127nt)
HH0-MG (111nt)
HH1-MG (107nt)
HH0 (71nt)
HH1 (67nt)
MG (40nt)

Figure 8

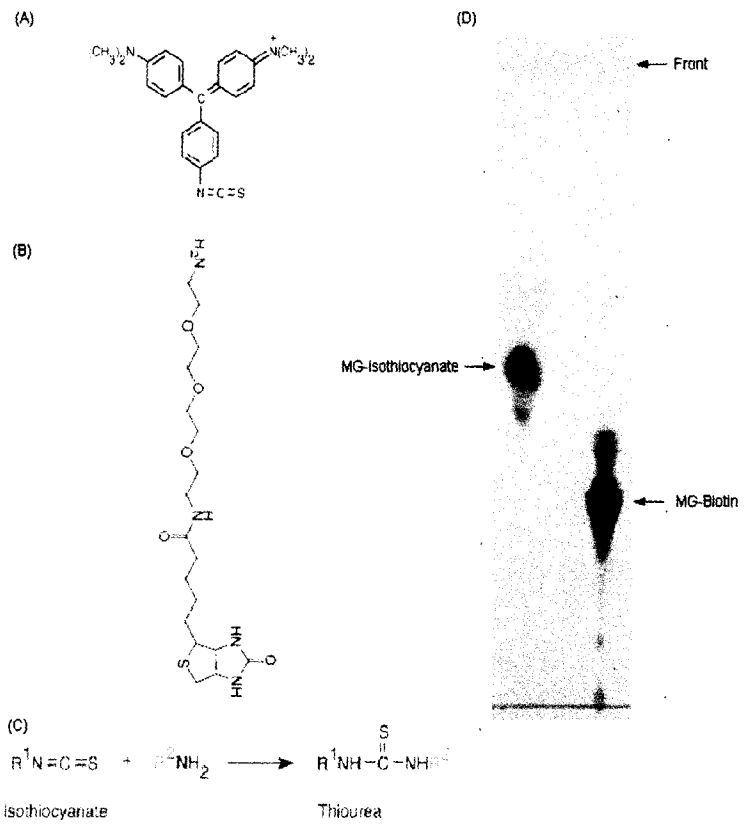
(A)
(B)
(C)
(D)
Front
MG-Isothiocyanate
MG-Biotin
Isothiocyanate
Thiourea

Figure 9

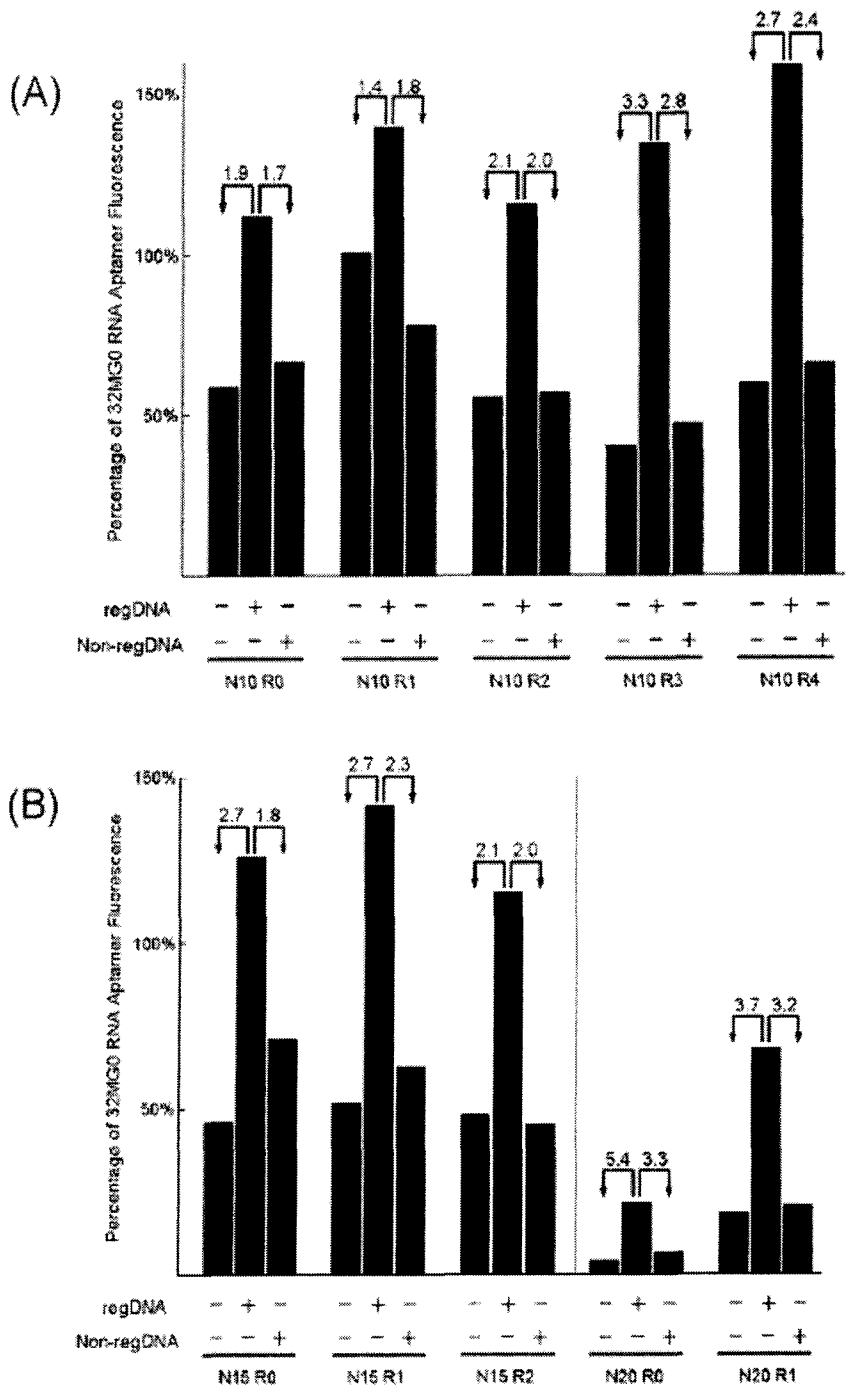
(A)
Percentage of 32MG0 RNA Aptamer Fluorescence
150%
100%
50%
1.9 1.7
1.4 1.8
2.1 2.0
3.3 2.8
2.7 2.4
regDNA
Non-regDNA
N10 R0
N10 R1
N10 R2
N10 R3
N10 R4
(B)
Percentage of 32MG0 RNA Aptamer Fluorescence
150%
100%
50%
2.7 1.8
2.7 2.3
2.1 2.0
5.4 3.3
3.7 3.2
regDNA
Non-regDNA
N15 R0
N15 R1
N15 R2
N20 R0
N20 R1

Figure 10

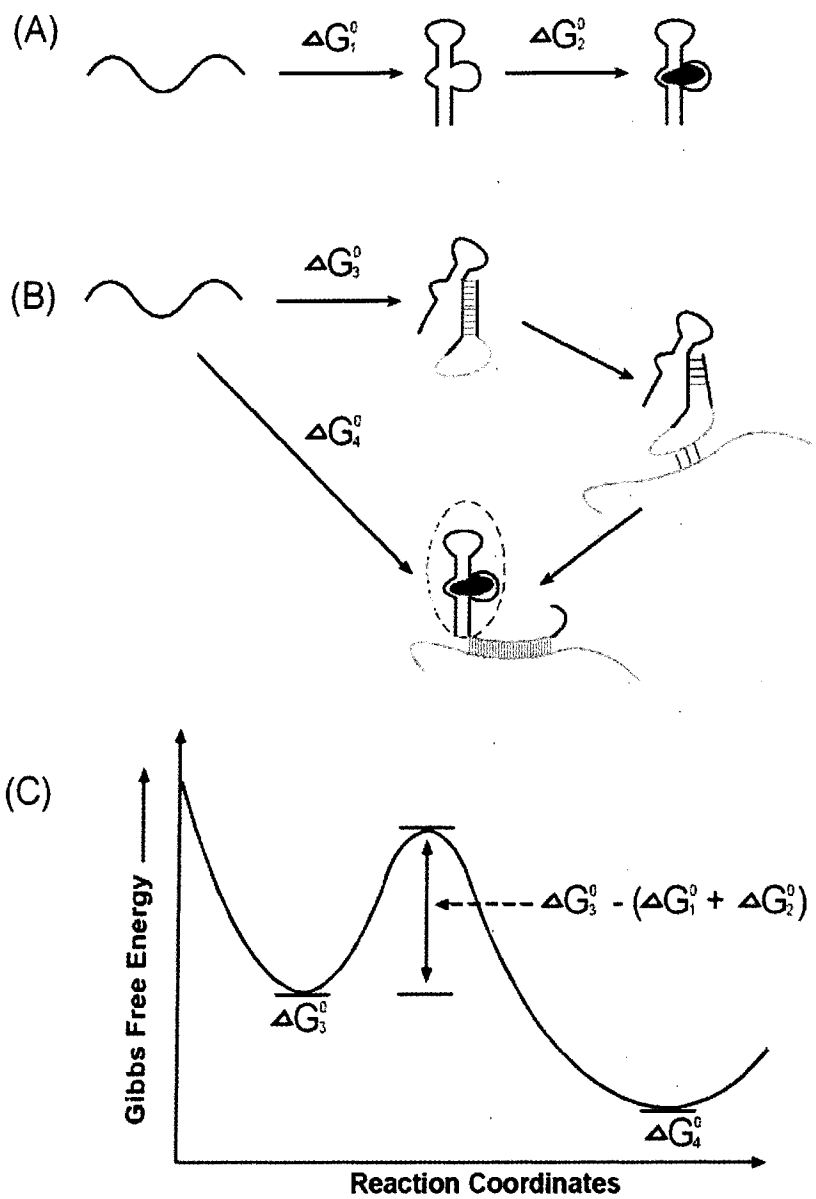
(A)
ΔG_1^0
ΔG_2^0
(B)
ΔG_3^0
ΔG_4^0
(C)
Gibbs Free Energy
$\Delta G_3^0 - (\Delta G_1^0 + \Delta G_2^0)$
ΔG_3^0
ΔG_4^0
Reaction Coordinates

Figure 11

CHAPTER 6. GENERAL CONCLUSION

THE TRAP DESIGN IS PRACTICAL

The development of functional ATP DNA TRAPs and MG RNA TRAPs showed that the idea of TRAP is workable. Both the ATP DNA TRAP and MG RNA TRAP were shown to have regDNA-dependent aptamer activity. The 9att-cmRas15-ATP DNA TRAP has the ability to distinguish single nucleotide mismatches. The 32MG1-9 MG RNA TRAP demonstrates a 20-fold increase in aptamer activity upon hybridizing with regDNA. In both cases, target mRNA-dependent activation has not yet been realized. But the data so far shows that the basic principles of TRAP design are practical. Further optimization and selection should result in the generation of a TRAP with target mRNA-dependent aptamer activity *in vitro* and *in vivo*.

COOPERATIVE INTERACTIONS AMONG THE THREE ELEMENTS OF THE TRAP DESIGN ARE CRITICAL FOR ITS FUNCTION

The three elements of the TRAP design are the aptamer, intervening sequence and attenuator sequence. Each element was introduced into the TRAP design to perform specific tasks. The aptamer has the ability to bind to its ligand. The intervening sequence was designed to interact with the target nucleic acid molecule. The attenuator is responsible for preventing the aptamer from binding to its ligand in the absence of the ligand. In the TRAP, the three elements interact extensively. Not only does the attenuator base pair with the aptamer by design, but also the intervening sequence has base pair interactions with aptamer and with itself due to elements of complementary sequence. Therefore the question of how to design the TRAP so that the interactions among three elements prompt the desired performance of each element was the key for success of TRAP design.

Base pairing within the intervening sequence is important and too low or too high a percentage of base pairing in the intervening sequence may damage the overall performance of TRAP. When the base pairing percentage is very low, the length of

attenuator needed to inhibit the aptamer may be too long such that effective activation of the TRAP by the regDNA is decreased. If the base pairing percentage is very high, it may inhibit the interaction between the intervening sequence and target nucleic acid molecule. Therefore optimal TRAP activity depends on the balance of the intensity of interaction between the three elements and within themselves. Quantitative values such as the percentage of base pairing of the intervening sequence, the ΔG difference between aptamer: ligand complex and TRAP will provide guidance for achieving the correct a balance so that the three elements will cooperate with each other.

THE INTERACTION BETWEEN TRAP AND ITS TARGET MRNA IS BOTH SEQUENTIAL AND STRUCTURALLY CONFINED

Using computational analysis and microarray experiments, the region of the Lcn2 mRNA to be targeted by the intervening sequence of the TRAP was selected. Our results showed that the 32MG1-9 TRAP had regDNA-dependent aptamer activity but it failed to recognize its target Lcn2 mRNA under the same conditions under which regDNA was recognized. In the computational analysis and microarray experiments, the 20nt long antisense oligonucleotide and was not part of folded stem-loop structure involving other sequences. This difference is likely to be critical and suggests that the failure of the 32MG12-9 TRAP to recognize Lcn2 mRNA may be because the intervening sequence has a strong interaction with the aptamer and in self base pairings. Similarly the target sequence in the mRNA may participate in intramolecular folding. The interaction between these two sequences may not be strong enough to provide the force for releasing the inhibition of aptamer by attenuator sequence.

THE TRAP HAS A UNIQUE POTENTIAL TO BE DEVELOPED INTO A PROBE FOR *IN VIVO* IMAGING OF NUCLEIC ACID MOLECULES

Aptamers have been used widely for *in vivo* applications (*12, 14-16, 18*). Riboswitches were recently discovered as natural aptamers that regulate transcription and translation in the bacteria and eukaryotes (*259, 290*). This evidence shows that aptamers can perform their functions inside the cell.

The TRAP utilizes an aptamer for signal output. There is a broad range of ligand options for the aptamer in the TRAP. The freedom in ligand selection and the power of SELEX to generate aptamers that recognize the desired ligand made the TRAP a good candidate as a nucleic acid probe for *in vivo* gene imaging. We showed that, *in vitro*, a functional MG RNA TRAP responded with a 20-fold increase in fluorescence in the present of regDNA. A similar principle can be applied for *in vivo* applications. If RNA TRAPs are expressed in cells or delivered into cells, the presence of the target mRNA could be visualized by the increase of fluorescence or radioactive signal.

Besides the binding ability of aptamer to its ligand, the signal output of the TRAP design can also utilize the catalytic activity of the ribozyme. For example, a ribozyme that will catalyze a chemical reaction upon binding to its ligand could be selected *in vitro* by SELEX. Allosteric ribozymes (aptazymes) with ribozyme activity regulated by small effector molecules have been developed (*160, 291*). The effector molecules for aptazymes included peptides (*291*), FMN, ATP and theophylline (*128*). In the aptazymes developed so far, the ribozyme either performed a phosphodiester cleavage reaction or had ligase activity. In both case, nucleic acids were the substrates for the ribozyme. Recently, a Diels-Alderase ribozyme catalyzing true intermolecular interaction was selected through SELEX by *in vitro* compartmentalization (*292*). The selected Diels-Alderase ribozyme catalyzed the cycloaddition reaction between dienes and dienophiles in solution. Such an enzyme-like ribozyme could be used to design a TRAP that reports the presence of target nucleic acid molecule by an enzyme catalyzed chemical reaction. If an appropriate enzyme catalyzed chemical reaction were applied, it could increase the signal output of the TRAP significantly.

DESIGNING A FUNCTIONAL TRAP CAN BE ACHIEVED EFFICIENTLY AND SYSTEMATICALLY

Because the way the TRAP recognizes its target nucleic acid molecule is through base pairing, the TRAP needs to be designed and optimized for each specific target sequence. Through rational design, we developed functional ATP DNA TRAPs and MG RNA TRAPs targeting regDNA designed from sequences of human 61L Ras gene

and the mouse Lcn2 gene, respectively. In each case, every TRAP was experimentally selected from a number of TRAPs with different sequences. Even though the rational design was simple and accomplished relatively rapidly, the process was low-throughput and still took significant time and effort. The SELEX procedure increased the number of sequences screened and therefore had greater potential to generate a functional TRAP compared to rational design. However, in this study the use of SELEX was not successful for improving the TRAP. Another approach to developing a functional TRAP with high efficiency would be the use of a high throughput assay such as microarray. For example, different TRAPs could be linked to a solid surface to form an oligonucleotide array. Functional TRAPs could be selected after the array was hybridized with target nucleic acids and fluorescence labeled ligands under defined conditions.

Computational design combined with experimental validation of the TRAP is another high-throughput method that might be used for efficiently and systematically developing a TRAP to recognize any desired target nucleic acid. By analyzing the experimentally selected functional TRAPs, the sequential and thermodynamic parameters needed for practical computational design could be deduced. We can expect that the development of computational and experimental high throughput methods will great improved the efficiency of TRAP design.

CHAPTER 7. LITERATURE CITED*

1. Baugh, C., Grate, D., and Wilson, C. (2000) 2.8 A crystal structure of the malachite green aptamer, *J Mol Biol 301*, 117-28.

2. Molenaar, C., Abdulle, A., Gena, A., Tanke, H. J., and Dirks, R. W. (2004) Poly(A)+ RNAs roam the cell nucleus and pass through speckle domains in transcriptionally active and inactive cells, *J Cell Biol 165*, 191-202.

3. Molenaar, C., Marras, S. A., Slats, J. C., Truffert, J. C., Lemaitre, M., Raap, A. K., Dirks, R. W., and Tanke, H. J. (2001) Linear 2' O-Methyl RNA probes for the visualization of RNA in living cells, *Nucleic Acids Res 29*, E89-9.

4. Tsuji, A., Koshimoto, H., Sato, Y., Hirano, M., Sei-Iida, Y., Kondo, S., and Ishibashi, K. (2000) Direct observation of specific messenger RNA in a single living cell under a fluorescence microscope, *Biophys J 78*, 3260-74.

5. Santangelo, P., Nitin, N., and Bao, G. (2006) Nanostructured Probes for RNA Detection in Living Cells, *Ann Biomed Eng*, 1-12.

6. Tyagi, S., and Kramer, F. R. (1996) Molecular beacons: probes that fluoresce upon hybridization, *Nat Biotechnol 14*, 303-8.

7. Tyagi, S., Bratu, D. P., and Kramer, F. R. (1998) Multicolor molecular beacons for allele discrimination, *Nat Biotechnol 16*, 49-53.

8. Cong, X., and Nilsen-Hamilton, M. (2005) Allosteric aptamers: targeted reversibly attenuated probes, *Biochemistry 44*, 7945-54.

9. Burke, D. H., Ozerova, N. D., and Nilsen-Hamilton, M. (2002) Allosteric hammerhead ribozyme TRAPs, *Biochemistry 41*, 6588-94.

* This Chapter includes references cited in chapters 1, 2 and 6. References cited in chapters 3, 4 and 5 are listed in respective chapters.

10. Tuerk, C., and Gold, L. (1990) Systematic evolution of ligands by exponential enrichment: RNA ligands to bacteriophage T4 DNA polymerase, *Science 249*, 505-10.

11. Ellington, A. D., and Szostak, J. W. (1990) In vitro selection of RNA molecules that bind specific ligands, *Nature 346*, 818-22.

12. Blank, M., and Blind, M. (2005) Aptamers as tools for target validation, *Curr Opin Chem Biol 9*, 336-42.

13. Tombelli, S., Minunni, M., and Mascini, M. (2005) Analytical applications of aptamers, *Biosens Bioelectron 20*, 2424-34.

14. Proske, D., Blank, M., Buhmann, R., and Resch, A. (2005) Aptamers-basic research, drug development, and clinical applications, *Appl Microbiol Biotechnol*, 1-8.

15. Nimjee, S. M., Rusconi, C. P., and Sullenger, B. A. (2005) Aptamers: an emerging class of therapeutics, *Annu Rev Med 56*, 555-83.

16. Nimjee, S. M., Rusconi, C. P., Harrington, R. A., and Sullenger, B. A. (2005) The potential of aptamers as anticoagulants, *Trends Cardiovasc Med 15*, 41-5.

17. Nutiu, R., and Li, Y. (2005) Aptamers with fluorescence-signaling properties, *Methods 37*, 16-25.

18. Zhang, Z., Blank, M., and Schluesener, H. J. (2004) Nucleic acid aptamers in human viral disease, *Arch Immunol Ther Exp (Warsz) 52*, 307-15.

19. Tavitian, B. (2003) In vivo imaging with oligonucleotides for diagnosis and drug development, *Gut 52 Suppl 4*, iv40-7.

20. Clark, S. L., and Remcho, V. T. (2002) Aptamers as analytical reagents, *Electrophoresis 23*, 1335-40.

21. Burgstaller, P., Girod, A., and Blind, M. (2002) Aptamers as tools for target prioritization and lead identification, *Drug Discov Today 7*, 1221-8.

22. Brody, E. N., and Gold, L. (2000) Aptamers as therapeutic and diagnostic agents, *J Biotechnol 74*, 5-13.

23. Medintz, I. L., Uyeda, H. T., Goldman, E. R., and Mattoussi, H. (2005) Quantum dot bioconjugates for imaging, labelling and sensing, *Nat Mater 4*, 435-46.

24. Lin, C. H., and Patel, D. J. (1997) Structural basis of DNA folding and recognition in an AMP-DNA aptamer complex: distinct architectures but common recognition motifs for DNA and RNA aptamers complexed to AMP, *Chem Biol 4*, 817-32.

25. Zuker, M. (2003) Mfold web server for nucleic acid folding and hybridization prediction, *Nucleic Acids Res 31*, 3406-15.

26. Ding, Y., Chan, C. Y., and Lawrence, C. E. (2004) Sfold web server for statistical folding and rational design of nucleic acids, *Nucleic Acids Res 32*, W135-41.

27. Mathews, D. H., Burkard, M. E., Freier, S. M., Wyatt, J. R., and Turner, D. H. (1999) Predicting oligonucleotide affinity to nucleic acid targets, *Rna 5*, 1458-69.

28. Penchovsky, R., and Breaker, R. R. (2005) Computational design and experimental validation of oligonucleotide-sensing allosteric ribozymes, *Nat Biotechnol.*

29. Jayasena, V. K., and Gold, L. (1997) In vitro selection of self-cleaving RNAs with a low pH optimum, *Proc Natl Acad Sci U S A 94*, 10612-7.

30. Wang, Y., and Rando, R. R. (1995) Specific binding of aminoglycoside antibiotics to RNA, *Chem Biol 2*, 281-90.

31. Huizenga, D. E., and Szostak, J. W. (1995) A DNA aptamer that binds adenosine and ATP, *Biochemistry 34*, 656-65.

32. Ye, X., Gorin, A., Ellington, A. D., and Patel, D. J. (1996) Deep penetration of an alpha-helix into a widened RNA major groove in the HIV-1 rev peptide-RNA aptamer complex, *Nat Struct Biol 3*, 1026-33.

33. Kelly, J. A., Feigon, J., and Yeates, T. O. (1996) Reconciliation of the X-ray and NMR structures of the thrombin-binding aptamer d(GGTTGGTGTGGTTGG), *J Mol Biol 256*, 417-22.

34. Jayasena, S. D. (1999) Aptamers: an emerging class of molecules that rival antibodies in diagnostics, *Clin Chem 45*, 1628-50.

35. Jenison, R. D., Gill, S. C., Pardi, A., and Polisky, B. (1994) High-resolution molecular discrimination by RNA, *Science 263*, 1425-9.

36. Jensen, K. B., Atkinson, B. L., Willis, M. C., Koch, T. H., and Gold, L. (1995) Using in vitro selection to direct the covalent attachment of human immunodeficiency virus type 1 Rev protein to high-affinity RNA ligands, *Proc Natl Acad Sci U S A 92*, 12220-4.

37. Gunther, S., Sommer, G., Von Breunig, F., Iwanska, A., Kalinina, T., Sterneck, M., and Will, H. (1998) Amplification of full-length hepatitis B virus genomes from samples from patients with low levels of viremia: frequency and functional consequences of PCR-introduced mutations, *J Clin Microbiol 36*, 531-8.

38. Golden, M. C., Collins, B. D., Willis, M. C., and Koch, T. H. (2000) Diagnostic potential of PhotoSELEX-evolved ssDNA aptamers, *J Biotechnol 81*, 167-78.

39. Smith, D., Kirschenheuter, G. P., Charlton, J., Guidot, D. M., and Repine, J. E. (1995) In vitro selection of RNA-based irreversible inhibitors of human neutrophil elastase, *Chem Biol 2*, 741-50.

40. Richardson, F. C., Zhang, C., Lehrman, S. R., Koc, H., Swenberg, J. A., Richardson, K. A., and Bendele, R. A. (2002) Quantification of 2'-fluoro-2'-deoxyuridine and 2'-fluoro-2'-deoxycytidine in DNA and RNA isolated from rats and woodchucks using LC/MS/MS, *Chem Res Toxicol 15*, 922-6.

41. Heidenreich, O., and Eckstein, F. (1992) Hammerhead ribozyme-mediated cleavage of the long terminal repeat RNA of human immunodeficiency virus type 1, *J Biol Chem 267*, 1904-9.

42. Pieken, W. A., Olsen, D. B., Benseler, F., Aurup, H., and Eckstein, F. (1991) Kinetic characterization of ribonuclease-resistant 2'-modified hammerhead ribozymes, *Science 253*, 314-7.

43. Pagratis, N. C., Bell, C., Chang, Y. F., Jennings, S., Fitzwater, T., Jellinek, D., and Dang, C. (1997) Potent 2'-amino-, and 2'-fluoro-2'-deoxyribonucleotide RNA inhibitors of keratinocyte growth factor, *Nat Biotechnol 15*, 68-73.

44. Lin, Y., and Jayasena, S. D. (1997) Inhibition of multiple thermostable DNA polymerases by a heterodimeric aptamer, *J Mol Biol 271*, 100-11.

45. Jellinek, D., Green, L. S., Bell, C., Lynott, C. K., Gill, N., Vargeese, C., Kirschenheuter, G., McGee, D. P., Abesinghe, P., Pieken, W. A., and et al. (1995) Potent 2'-amino-2'-deoxypyrimidine RNA inhibitors of basic fibroblast growth factor, *Biochemistry 34*, 11363-72.

46. Jellinek, D., Lynott, C. K., Rifkin, D. B., and Janjic, N. (1993) High-affinity RNA ligands to basic fibroblast growth factor inhibit receptor binding, *Proc Natl Acad Sci U S A 90*, 11227-31.

47. Lato, S. M., Ozerova, N. D., He, K., Sergueeva, Z., Shaw, B. R., and Burke, D. H. (2002) Boron-containing aptamers to ATP, *Nucleic Acids Res 30*, 1401-7.

48. Jhaveri, S., Olwin, B., and Ellington, A. D. (1998) In vitro selection of phosphorothiolated aptamers, *Bioorg Med Chem Lett 8*, 2285-90.

49. Kato, Y., Minakawa, N., Komatsu, Y., Kamiya, H., Ogawa, N., Harashima, H., and Matsuda, A. (2005) New NTP analogs: the synthesis of 4'-thioUTP and 4'-thioCTP and their utility for SELEX, *Nucleic Acids Res 33*, 2942-51.

50. Eulberg, D., and Klussmann, S. (2003) Spiegelmers: biostable aptamers, *Chembiochem 4*, 979-83.

51. Nolte, A., Klussmann, S., Bald, R., Erdmann, V. A., and Furste, J. P. (1996) Mirror-design of L-oligonucleotide ligands binding to L-arginine, *Nat Biotechnol 14*, 1116-9.

52. Klussmann, S., Nolte, A., Bald, R., Erdmann, V. A., and Furste, J. P. (1996) Mirror-image RNA that binds D-adenosine, *Nat Biotechnol 14*, 1112-5.

53. Williams, K. P., Liu, X. H., Schumacher, T. N., Lin, H. Y., Ausiello, D. A., Kim, P. S., and Bartel, D. P. (1997) Bioactive and nuclease-resistant L-DNA ligand of vasopressin, *Proc Natl Acad Sci U S A 94*, 11285-90.

54. Griffin, L. C., Tidmarsh, G. F., Bock, L. C., Toole, J. J., and Leung, L. L. (1993) In vivo anticoagulant properties of a novel nucleotide-based thrombin inhibitor and demonstration of regional anticoagulation in extracorporeal circuits, *Blood 81*, 3271-6.

55. Cox, J. C., and Ellington, A. D. (2001) Automated selection of anti-protein aptamers, *Bioorg Med Chem 9*, 2525-31.

56. Cox, J. C., Rudolph, P., and Ellington, A. D. (1998) Automated RNA selection, *Biotechnol Prog 14*, 845-50.

57. Cox, J. C., Rajendran, M., Riedel, T., Davidson, E. A., Sooter, L. J., Bayer, T. S., Schmitz-Brown, M., and Ellington, A. D. (2002) Automated acquisition of aptamer sequences, *Comb Chem High Throughput Screen 5*, 289-99.

58. Mendonsa, S. D., and Bowser, M. T. (2004) In vitro selection of high-affinity DNA ligands for human IgE using capillary electrophoresis, *Anal Chem 76*, 5387-92.

59. Mosing, R. K., Mendonsa, S. D., and Bowser, M. T. (2005) Capillary Electrophoresis-SELEX Selection of Aptamers with Affinity for HIV-1 Reverse Transcriptase, *Anal Chem 77*, 6107-12.

60. Shtatland, T., Gill, S. C., Javornik, B. E., Johansson, H. E., Singer, B. S., Uhlenbeck, O. C., Zichi, D. A., and Gold, L. (2000) Interactions of Escherichia coli RNA with bacteriophage MS2 coat protein: genomic SELEX, *Nucleic Acids Res 28*, E93.

61. Hermann, T., and Patel, D. J. (2000) Adaptive recognition by nucleic acid aptamers, *Science 287*, 820-5.

62. Kwon, M., Chun, S. M., Jeong, S., and Yu, J. (2001) In vitro selection of RNA against kanamycin B, *Mol Cells 11*, 303-11.

63. Hamasaki, K., Killian, J., Cho, J., and Rando, R. R. (1998) Minimal RNA constructs that specifically bind aminoglycoside antibiotics with high affinities, *Biochemistry 37*, 656-63.

64. Wang, Y., Killian, J., Hamasaki, K., and Rando, R. R. (1996) RNA molecules that specifically and stoichiometrically bind aminoglycoside antibiotics with high affinities, *Biochemistry 35*, 12338-46.

65. Yang, Y., Kochoyan, M., Burgstaller, P., Westhof, E., and Famulok, M. (1996) Structural basis of ligand discrimination by two related RNA aptamers resolved by NMR spectroscopy, *Science 272*, 1343-7.

66. Sassanfar, M., and Szostak, J. W. (1993) An RNA motif that binds ATP, *Nature 364*, 550-3.

67. Burgstaller, P., Kochoyan, M., and Famulok, M. (1995) Structural probing and damage selection of citrulline- and arginine-specific RNA aptamers identify base positions required for binding, *Nucleic Acids Res 23*, 4769-76.

68. Geiger, A., Burgstaller, P., von der Eltz, H., Roeder, A., and Famulok, M. (1996) RNA aptamers that bind L-arginine with sub-micromolar dissociation constants and high enantioselectivity, *Nucleic Acids Res 24*, 1029-36.

69. Lin, Y., Qiu, Q., Gill, S. C., and Jayasena, S. D. (1994) Modified RNA sequence pools for in vitro selection, *Nucleic Acids Res 22*, 5229-34.

70. Vianini, E., Palumbo, M., and Gatto, B. (2001) In vitro selection of DNA aptamers that bind L-tyrosinamide, *Bioorg Med Chem 9*, 2543-8.

71. Blum, J. H., Dove, S. L., Hochschild, A., and Mekalanos, J. J. (2000) Isolation of peptide aptamers that inhibit intracellular processes, *Proc Natl Acad Sci U S A 97*, 2241-6.

72. Butz, K., Denk, C., Fitscher, B., Crnkovic-Mertens, I., Ullmann, A., Schroder, C. H., and Hoppe-Seyler, F. (2001) Peptide aptamers targeting the hepatitis B virus core protein: a new class of molecules with antiviral activity, *Oncogene 20*, 6579-86.

73. Fabbrizio, E., Le Cam, L., Polanowska, J., Kaczorek, M., Lamb, N., Brent, R., and Sardet, C. (1999) Inhibition of mammalian cell proliferation by genetically selected peptide aptamers that functionally antagonize E2F activity, *Oncogene 18*, 4357-63.

74. Roychowdhury-Saha, M., Lato, S. M., Shank, E. D., and Burke, D. H. (2002) Flavin recognition by an RNA aptamer targeted toward FAD, *Biochemistry 41*, 2492-9.

75. Fan, P., Suri, A. K., Fiala, R., Live, D., and Patel, D. J. (1996) Molecular recognition in the FMN-RNA aptamer complex, *J Mol Biol 258*, 480-500.

76. Lorsch, J. R., and Szostak, J. W. (1994) In vitro selection of RNA aptamers specific for cyanocobalamin, *Biochemistry 33*, 973-82.

77. Jeong, S., Eom, T., Kim, S., Lee, S., and Yu, J. (2001) In vitro selection of the RNA aptamer against the Sialyl Lewis X and its inhibition of the cell adhesion, *Biochem Biophys Res Commun 281*, 237-43.

78. Darfeuille, F., Cazenave, C., Gryaznov, S., Duconge, F., Di Primo, C., and Toulme, J. J. (2001) RNA and N3'-->P5' kissing aptamers targeted to the trans-activation responsive (TAR) RNA of the human immunodeficiency virus-1, *Nucleosides Nucleotides Nucleic Acids 20*, 441-9.

79. Boiziau, C., Dausse, E., Yurchenko, L., and Toulme, J. J. (1999) DNA aptamers selected against the HIV-1 trans-activation-responsive RNA element form RNA-DNA kissing complexes, *J Biol Chem 274*, 12730-7.

80. Yamamoto, R., Katahira, M., Nishikawa, S., Baba, T., Taira, K., and Kumar, P. K. (2000) A novel RNA motif that binds efficiently and specifically to the Ttat protein of HIV and inhibits the trans-activation by Tat of transcription in vitro and in vivo, *Genes Cells 5*, 371-88.

81. Urvil, P. T., Kakiuchi, N., Zhou, D. M., Shimotohno, K., Kumar, P. K., and Nishikawa, S. (1997) Selection of RNA aptamers that bind specifically to the NS3 protease of hepatitis C virus, *Eur J Biochem 248*, 130-8.

82. Sekkai, D., Dausse, E., Di Primo, C., Darfeuille, F., Boiziau, C., and Toulme, J. J. (2002) In vitro selection of DNA aptamers against the HIV-1 TAR RNA hairpin, *Antisense Nucleic Acid Drug Dev 12*, 265-74.

83. Sayer, N., Ibrahim, J., Turner, K., Tahiri-Alaoui, A., and James, W. (2002) Structural characterization of a 2'F-RNA aptamer that binds a HIV-1 SU glycoprotein, gp120, *Biochem Biophys Res Commun 293*, 924-31.

84. Burke, D. H., Hoffman, D. C., Brown, A., Hansen, M., Pardi, A., and Gold, L. (1997) RNA aptamers to the peptidyl transferase inhibitor chloramphenicol, *Chem Biol 4*, 833-43.

85. Bock, L. C., Griffin, L. C., Latham, J. A., Vermaas, E. H., and Toole, J. J. (1992) Selection of single-stranded DNA molecules that bind and inhibit human thrombin, *Nature 355*, 564-6.

86. Fukuda, K., Vishinuvardhan, D., Sekiya, S., Kakiuchi, N., Shimotohno, K., Kumar, P. K., and Nishikawa, S. (1997) Specific RNA aptamers to NS3 protease domain of hepatitis C virus, *Nucleic Acids Symp Ser*, 237-8.

87. Fukuda, K., Vishnuvardhan, D., Sekiya, S., Hwang, J., Kakiuchi, N., Taira, K., Shimotohno, K., Kumar, P. K., and Nishikawa, S. (2000) Isolation and characterization of RNA aptamers specific for the hepatitis C virus nonstructural protein 3 protease, *Eur J Biochem 267*, 3685-94.

88. Gal, S. W., Amontov, S., Urvil, P. T., Vishnuvardhan, D., Nishikawa, F., Kumar, P. K., and Nishikawa, S. (1998) Selection of a RNA aptamer that binds to human activated protein C and inhibits its protease function, *Eur J Biochem 252*, 553-62.

89. Hwang, J., Fauzi, H., Fukuda, K., Sekiya, S., Kakiuchi, N., Shimotohno, K., Taira, K., Kusakabe, I., and Nishikawa, S. (2000) The RNA aptamer-binding site of hepatitis C virus NS3 protease, *Biochem Biophys Res Commun 279*, 557-62.

90. Kumar, P. K., Machida, K., Urvil, P. T., Kakiuchi, N., Vishnuvardhan, D., Shimotohno, K., Taira, K., and Nishikawa, S. (1997) Isolation of RNA aptamers specific to the NS3 protein of hepatitis C virus from a pool of completely random RNA, *Virology 237*, 270-82.

91. Latham, J. A., Johnson, R., and Toole, J. J. (1994) The application of a modified nucleotide in aptamer selection: novel thrombin aptamers containing 5-(1-pentynyl)-2'-deoxyuridine, *Nucleic Acids Res 22*, 2817-22.

92. Takeno, H., Yamamoto, S., Tanaka, T., Sakano, Y., and Kikuchi, Y. (1999) Selection of an RNA molecule that specifically inhibits the protease activity of subtilisin, *J Biochem (Tokyo) 125*, 1115-9.

93. Griffin, L. C., Toole, J. J., and Leung, L. L. (1993) The discovery and characterization of a novel nucleotide-based thrombin inhibitor, *Gene 137*, 25-31.

94. Jellinek, D., Green, L. S., Bell, C., and Janjic, N. (1994) Inhibition of receptor binding by high-affinity RNA ligands to vascular endothelial growth factor, *Biochemistry 33*, 10450-6.

95. Binkley, J., Allen, P., Brown, D. M., Green, L., Tuerk, C., and Gold, L. (1995) RNA ligands to human nerve growth factor, *Nucleic Acids Res 23*, 3198-205.

96. Bell, C., Lynam, E., Landfair, D. J., Janjic, N., and Wiles, M. E. (1999) Oligonucleotide NX1838 inhibits VEGF165-mediated cellular responses in vitro, *In Vitro Cell Dev Biol Anim 35*, 533-42.

97. Hartmann, G., Bidlingmaier, M., Eigler, A., Hacker, U., and Endres, S. (1997) Cytokines and therapeutic oligonucleotides, *Cytokines Cell Mol Ther 3*, 247-56.

98. Lebruska, L. L., and Maher, L. J., 3rd. (1999) Selection and characterization of an RNA decoy for transcription factor NF-kappa B, *Biochemistry 38*, 3168-74.

99. Zhai, G., Iskandar, M., Barilla, K., and Romaniuk, P. J. (2001) Characterization of RNA aptamer binding by the Wilms' tumor suppressor protein WT1, *Biochemistry 40*, 2032-40.

100. Ulrich, H., Magdesian, M. H., Alves, M. J., and Colli, W. (2002) In vitro selection of RNA aptamers that bind to cell adhesion receptors of Trypanosoma cruzi and inhibit cell invasion, *J Biol Chem 277*, 20756-62.

101. Hicke, B. J., Watson, S. R., Koenig, A., Lynott, C. K., Bargatze, R. F., Chang, Y. F., Ringquist, S., Moon-McDermott, L., Jennings, S., Fitzwater, T., Han, H. L., Varki, N., Albinana, I., Willis, M. C., Varki, A., and Parma, D. (1996) DNA aptamers block L-selectin function in vivo. Inhibition of human lymphocyte trafficking in SCID mice, *J Clin Invest 98*, 2688-92.

102. Jenison, R. D., Jennings, S. D., Walker, D. W., Bargatze, R. F., and Parma, D. (1998) Oligonucleotide inhibitors of P-selectin-dependent neutrophil-platelet adhesion, *Antisense Nucleic Acid Drug Dev 8*, 265-79.

103. Lee, J. F., Hesselberth, J. R., Meyers, L. A., and Ellington, A. D. (2004) Aptamer database, *Nucleic Acids Res 32*, D95-100.

104. Ponomarenko, J. V., Orlova, G. V., Frolov, A. S., Gelfand, M. S., and Ponomarenko, M. P. (2002) SELEX_DB: a database on in vitro selected oligomers adapted for recognizing natural sites and for analyzing both SNPs and site-directed mutagenesis data, *Nucleic Acids Res 30*, 195-9.

105. Jiang, F., Patel, D. J., Zhang, X., Zhao, H., and Jones, R. A. (1997) Specific labeling approaches to guanine and adenine imino and amino proton assignments in the AMP-RNA aptamer complex, *J Biomol NMR 9*, 55-62.

106. Jiang, L., and Patel, D. J. (1998) Solution structure of the tobramycin-RNA aptamer complex, *Nat Struct Biol 5*, 769-74.

107. Jiang, L., Majumdar, A., Hu, W., Jaishree, T. J., Xu, W., and Patel, D. J. (1999) Saccharide-RNA recognition in a complex formed between neomycin B and an RNA aptamer, *Structure Fold Des 7*, 817-27.

108. Dieckmann, T., Suzuki, E., Nakamura, G. K., and Feigon, J. (1996) Solution structure of an ATP-binding RNA aptamer reveals a novel fold, *Rna 2*, 628-40.

109. Jiang, F., Kumar, R. A., Jones, R. A., and Patel, D. J. (1996) Structural basis of RNA folding and recognition in an AMP-RNA aptamer complex [see comments], *Nature 382*, 183-6.

110. Battiste, J. L., Mao, H., Rao, N. S., Tan, R., Muhandiram, D. R., Kay, L. E., Frankel, A. D., and Williamson, J. R. (1996) Alpha helix-RNA major groove recognition in an HIV-1 rev peptide-RRE RNA complex, *Science 273*, 1547-51.

111. Wang, K. Y., McCurdy, S., Shea, R. G., Swaminathan, S., and Bolton, P. H. (1993) A DNA aptamer which binds to and inhibits thrombin exhibits a new structural motif for DNA, *Biochemistry 32*, 1899-904.

112. Wang, K. Y., Gerena, L., Swaminathan, S., and Bolton, P. H. (1995) Determination of the number and location of the manganese binding sites of DNA quadruplexes in solution by EPR and NMR, *Nucleic Acids Res 23*, 844-8.

113. Wallis, M. G., von Ahsen, U., Schroeder, R., and Famulok, M. (1995) A novel RNA motif for neomycin recognition, *Chem Biol 2*, 543-52.

114. Sokol, D. L., Zhang, X., Lu, P., and Gewirtz, A. M. (1998) Real time detection of DNA.RNA hybridization in living cells, *Proc Natl Acad Sci U S A 95*, 11538-43.

115. Akiyama, T., and Hogan, M. E. (1996) Microscopic DNA flexibility analysis. Probing the base composition and ion dependence of minor groove compression with an artificial dna bending agent, *J Biol Chem 271*, 29126-35.

116. Barkley, B. D. a. Z., B.H. (1979), *J.Chem.Phys. 70*, 2991-3007.

117. Smith, S. B., Cui, Y., and Bustamante, C. (1996) Overstretching B-DNA: the elastic response of individual double-stranded and single-stranded DNA molecules, *Science 271*, 795-9.

118. Riccelli, P. V., Hilario, J., Gallo, F. J., Young, A. P., and Benight, A. S. (1996) DNA and RNA oligomer sequences from the 3' noncoding region of the chicken glutamine synthetase gene from intramolecular hairpins, *Biochemistry 35*, 15364-72.

119. Bonnet, G., Tyagi, S., Libchaber, A., and Kramer, F. R. (1999) Thermodynamic basis of the enhanced specificity of structured DNA probes, *Proc Natl Acad Sci U S A 96*, 6171-6.

120. Gerstein, M., Lesk, A. M., and Chothia, C. (1994) Structural mechanisms for domain movements in proteins, *Biochemistry 33*, 6739-49.

121. Porta, H., and Lizardi, P. M. (1995) An allosteric hammerhead ribozyme, *Biotechnology (N Y) 13*, 161-4.

122. Tang, J., and Breaker, R. R. (1997) Rational design of allosteric ribozymes, *Chem Biol 4*, 453-9.

123. Tang, J., and Breaker, R. R. (1998) Mechanism for allosteric inhibition of an ATP-sensitive ribozyme, *Nucleic Acids Res 26*, 4214-21.

124. Patel, D. J., and Suri, A. K. (2000) Structure, recognition and discrimination in RNA aptamer complexes with cofactors, amino acids, drugs and aminoglycoside antibiotics, *J Biotechnol 74*, 39-60.

125. Patel, D. J., Suri, A. K., Jiang, F., Jiang, L., Fan, P., Kumar, R. A., and Nonin, S. (1997) Structure, recognition and adaptive binding in RNA aptamer complexes, *J Mol Biol 272*, 645-64.

126. Araki, M., Okuno, Y., Hara, Y., and Sugiura, Y. (1998) Allosteric regulation of a ribozyme activity through ligand-induced conformational change, *Nucleic Acids Res 26*, 3379-84.

127. Koizumi, M., Kerr, J. N., Soukup, G. A., and Breaker, R. R. (1999) Allosteric ribozymes sensitive to the second messengers cAMP and cGMP, *Nucleic Acids Symp Ser*, 275-6.

128. Robertson, M. P., and Ellington, A. D. (2000) Design and optimization of effector-activated ribozyme ligases, *Nucleic Acids Res 28*, 1751-9.

129. Levy, M., and Ellington, A. D. (2002) ATP-dependent allosteric DNA enzymes, *Chem Biol 9*, 417-26.

130. Vuyisich, M., and Beal, P. (2002) Controlling protein activity with ligand-regulated RNA aptamers, *Chem Biol 9*, 907.

131. Babendure, J. R., Adams, S. R., and Tsien, R. Y. (2003) Aptamers switch on fluorescence of triphenylmethane dyes, *J Am Chem Soc 125*, 14716-7.

132. Stojanovic, M. N., and Kolpashchikov, D. M. (2004) Modular aptameric sensors, *J Am Chem Soc 126*, 9266-70.

133. McCaskill, J. S. (1990) The equilibrium partition function and base pair binding probabilities for RNA secondary structure, *Biopolymers 29*, 1105-19.

134. Soukup, G. A., and Breaker, R. R. (2000) Allosteric nucleic acid catalysts, *Curr Opin Struct Biol 10*, 318-25.

135. Jose, A. M., Soukup, G. A., and Breaker, R. R. (2001) Cooperative binding of effectors by an allosteric ribozyme, *Nucleic Acids Res 29*, 1631-7.

136. Soukup, G. A., and Breaker, R. R. (1999) Nucleic acid molecular switches, *Trends Biotechnol 17*, 469-76.

137. Winkler, W., Nahvi, A., and Breaker, R. R. (2002) Thiamine derivatives bind messenger RNAs directly to regulate bacterial gene expression, *Nature 419*, 952-6.

138. Kubodera, T., Watanabe, M., Yoshiuchi, K., Yamashita, N., Nishimura, A., Nakai, S., Gomi, K., and Hanamoto, H. (2003) Thiamine-regulated gene expression of Aspergillus oryzae thiA requires splicing of the intron containing a riboswitch-like domain in the 5'-UTR, *FEBS Lett 555*, 516-20.

139. Sudarsan, N., Barrick, J. E., and Breaker, R. R. (2003) Metabolite-binding RNA domains are present in the genes of eukaryotes, *Rna 9*, 644-7.

140. Winkler, W. C., Nahvi, A., Roth, A., Collins, J. A., and Breaker, R. R. (2004) Control of gene expression by a natural metabolite-responsive ribozyme, *Nature 428*, 281-6.

141. Mandal, M., and Breaker, R. R. (2004) Adenine riboswitches and gene activation by disruption of a transcription terminator, *Nat Struct Mol Biol 11*, 29-35.

142. Mandal, M., Lee, M., Barrick, J. E., Weinberg, Z., Emilsson, G. M., Ruzzo, W. L., and Breaker, R. R. (2004) A glycine-dependent riboswitch that uses cooperative binding to control gene expression, *Science 306*, 275-9.

143. Sudarsan, N., Wickiser, J. K., Nakamura, S., Ebert, M. S., and Breaker, R. R. (2003) An mRNA structure in bacteria that controls gene expression by binding lysine, *Genes Dev 17*, 2688-97.

144. Luban, J., and Goff, S. P. (1995) The yeast two-hybrid system for studying protein-protein interactions, *Curr Opin Biotechnol 6*, 59-64.

145. Cassiday, L. A., and Maher, L. J., 3rd. (2003) Yeast genetic selections to optimize RNA decoys for transcription factor NF-kappa B, *Proc Natl Acad Sci U S A 100*, 3930-5.

146. Buskirk, A. R., Kehayova, P. D., Landrigan, A., and Liu, D. R. (2003) In vivo evolution of an RNA-based transcriptional activator, *Chem Biol 10*, 533-40.

147. Buskirk, A. R., Landrigan, A., and Liu, D. R. (2004) Engineering a ligand-dependent RNA transcriptional activator, *Chem Biol 11*, 1157-63.

148. SenGupta, D. J., Zhang, B., Kraemer, B., Pochart, P., Fields, S., and Wickens, M. (1996) A three-hybrid system to detect RNA-protein interactions in vivo, *Proc Natl Acad Sci U S A 93*, 8496-501.

149. Buratti, E., and Baralle, F. E. (2005) Another step forward for SELEXive splicing, *Trends Mol Med 11*, 5-9.

150. Coulter, L. R., Landree, M. A., and Cooper, T. A. (1997) Identification of a new class of exonic splicing enhancers by in vivo selection, *Mol Cell Biol 17*, 2143-50.

151. Yamamoto, R., Baba, T., and Kumar, P. K. (2000) Molecular beacon aptamer fluoresces in the presence of Tat protein of HIV-1, *Genes Cells 5*, 389-96.

152. Jhaveri, S., Kirby, R., Conrad, R., Maglott, E. J., Bowser, M., Kennedy, R. T., Glick, G., and Ellington, A. D. (2000) Designed Signaling Aptamers that Transduce Molecular Recognition to Changes in Fulorescence Intensity, *J Am Chem Soc 122*, 2469-73.

153. Blank, M., Weinschenk, T., Priemer, M., and Schluesener, H. (2001) Systematic evolution of a DNA aptamer binding to rat brain tumor microvessels. selective targeting of endothelial regulatory protein pigpen, *J Biol Chem 276*, 16464-8.

154. Frauendorf, C., and Jaschke, A. (2001) Detection of small organic analytes by fluorescing molecular switches, *Bioorg Med Chem 9*, 2521-4.

155. Stojanovic, M. N., and Landry, D. W. (2002) Aptamer-based colorimetric probe for cocaine, *J Am Chem Soc 124*, 9678-9.

156. Li, J. J., Fang, X., and Tan, W. (2002) Molecular aptamer beacons for real-time protein recognition, *Biochem Biophys Res Commun 292*, 31-40.

157. Lorger, M., Engstler, M., Homann, M., and Goringer, H. U. (2003) Targeting the variable surface of African trypanosomes with variant surface glycoprotein-specific, serum-stable RNA aptamers, *Eukaryot Cell 2*, 84-94.

158. Nutiu, R., Yu, J. M., and Li, Y. (2004) Signaling aptamers for monitoring enzymatic activity and for inhibitor screening, *Chembiochem 5*, 1139-44.

159. Elghanian, R., Storhoff, J. J., Mucic, R. C., Letsinger, R. L., and Mirkin, C. A. (1997) Selective colorimetric detection of polynucleotides based on the distance-dependent optical properties of gold nanoparticles, *Science 277*, 1078-81.

160. Liu, J., and Lu, Y. (2004) Adenosine-dependent assembly of aptazyme-functionalized gold nanoparticles and its application as a colorimetric biosensor, *Anal Chem 76*, 1627-32.

161. Macaya, R. F., Schultze, P., Smith, F. W., Roe, J. A., and Feigon, J. (1993) Thrombin-binding DNA aptamer forms a unimolecular quadruplex structure in solution, *Proc Natl Acad Sci U S A 90*, 3745-9.

162. Ho, H. A., Bera-Aberem, M., and Leclerc, M. (2005) Optical sensors based on hybrid DNA/conjugated polymer complexes, *Chemistry 11*, 1718-24.

163. Sparano, B. A., and Koide, K. (2005) A strategy for the development of small-molecule-based sensors that strongly fluoresce when bound to a specific RNA, *J Am Chem Soc 127*, 14954-5.

164. Liss, M., Petersen, B., Wolf, H., and Prohaska, E. (2002) An aptamer-based quartz crystal protein biosensor, *Anal Chem 74*, 4488-95.

165. Lee, M., and Walt, D. R. (2000) A fiber-optic microarray biosensor using aptamers as receptors, *Anal Biochem 282*, 142-6.

166. Kirby, R., Cho, E. J., Gehrke, B., Bayer, T., Park, Y. S., Neikirk, D. P., McDevitt, J. T., and Ellington, A. D. (2004) Aptamer-based sensor arrays for the detection and quantitation of proteins, *Anal Chem 76*, 4066-75.

167. McCauley, T. G., Hamaguchi, N., and Stanton, M. (2003) Aptamer-based biosensor arrays for detection and quantification of biological macromolecules, *Anal Biochem 319*, 244-50.

168. Savran, C. A., Knudsen, S. M., Ellington, A. D., and Manalis, S. R. (2004) Micromechanical detection of proteins using aptamer-based receptor molecules, *Anal Chem 76*, 3194-8.

169. Vicens, M. C., Sen, A., Vanderlaan, A., Drake, T. J., and Tan, W. (2005) Investigation of molecular beacon aptamer-based bioassay for platelet-derived growth factor detection, *Chembiochem 6*, 900-7.

170. Heyduk, E., and Heyduk, T. (2005) Nucleic acid-based fluorescence sensors for detecting proteins, *Anal Chem 77*, 1147-56.

171. Dick, L. W., Jr., and McGown, L. B. (2004) Aptamer-enhanced laser desorption/ionization for affinity mass spectrometry, *Anal Chem 76*, 3037-41.

172. Michaud, M., Jourdan, E., Ravelet, C., Villet, A., Ravel, A., Grosset, C., and Peyrin, E. (2004) Immobilized DNA aptamers as target-specific chiral stationary phases for resolution of nucleoside and amino acid derivative enantiomers, *Anal Chem 76*, 1015-20.

173. Deng, Q., Watson, C. J., and Kennedy, R. T. (2003) Aptamer affinity chromatography for rapid assay of adenosine in microdialysis samples collected in vivo, *J Chromatogr A 1005*, 123-30.

174. Murphy, M. B., Fuller, S. T., Richardson, P. M., and Doyle, S. A. (2003) An improved method for the in vitro evolution of aptamers and applications in protein detection and purification, *Nucleic Acids Res 31*, e110.

175. Pavski, V., and Le, X. C. (2001) Detection of human immunodeficiency virus type 1 reverse transcriptase using aptamers as probes in affinity capillary electrophoresis, *Anal Chem 73*, 6070-6.

176. Berezovski, M., Nutiu, R., Li, Y., and Krylov, S. N. (2003) Affinity analysis of a protein-aptamer complex using nonequilibrium capillary electrophoresis of equilibrium mixtures, *Anal Chem 75*, 1382-6.

177. Fredriksson, S., Gullberg, M., Jarvius, J., Olsson, C., Pietras, K., Gustafsdottir, S. M., Ostman, A., and Landegren, U. (2002) Protein detection using proximity-dependent DNA ligation assays, *Nat Biotechnol 20*, 473-7.

178. White, R. R., Sullenger, B. A., and Rusconi, C. P. (2000) Developing aptamers into therapeutics, *J Clin Invest 106*, 929-34.

179. White, R. R., Shan, S., Rusconi, C. P., Shetty, G., Dewhirst, M. W., Kontos, C. D., and Sullenger, B. A. (2003) Inhibition of rat corneal angiogenesis by a nuclease-resistant RNA aptamer specific for angiopoietin-2, *Proc Natl Acad Sci U S A 100*, 5028-33.

180. Pestourie, C., Tavitian, B., and Duconge, F. (2005) Aptamers against extracellular targets for in vivo applications, *Biochimie 87*, 921-30.

181. Ma, X., and He, F. (2003) Advances in the study of SR protein family, *Genomics Proteomics Bioinformatics 1*, 2-8.

182. Chaloin, L., Lehmann, M. J., Sczakiel, G., and Restle, T. (2002) Endogenous expression of a high-affinity pseudoknot RNA aptamer suppresses replication of HIV-1, *Nucleic Acids Res 30*, 4001-8.

183. Joshi, P. J., North, T. W., and Prasad, V. R. (2005) Aptamers directed to HIV-1 reverse transcriptase display greater efficacy over small hairpin RNAs targeted to viral RNA in blocking HIV-1 replication, *Mol Ther 11*, 677-86.

184. Yang, C., Yan, N., Parrish, J., Wang, X., Shi, Y., and Xue, D. (2006) RNA aptamers targeting the cell death inhibitor CED-9 induce cell kiling in C. elegans, *J Biol Chem*.

185. Hu, K., Beck, J., and Nassal, M. (2004) SELEX-derived aptamers of the duck hepatitis B virus RNA encapsidation signal distinguish critical and non-critical residues for productive initiation of reverse transcription, *Nucleic Acids Res 32*, 4377-89.

186. Burke, D. H., and Nickens, D. (2002) Expressing RNA aptamers inside cells to reveal proteome and ribonome function, *Briefings in Functional Genomics and proteomics 1*, 169-188.

187. Jain, C., and Belasco, J. G. (2000) Rapid genetic analysis of RNA-protein interactions by translational repression in Escherichia coli, *Methods Enzymol 318*, 309-32.

188. Werstuck, G., and Green, M. R. (1998) Controlling gene expression in living cells through small molecule-RNA interactions, *Science 282*, 296-8.

189. Grate, D., and Wilson, C. (1999) Laser-mediated, site-specific inactivation of RNA transcripts, *Proc Natl Acad Sci U S A 96*, 6131-6.

190. Grate, D., and Wilson, C. (2001) Inducible regulation of the S. cerevisiae cell cycle mediated by an RNA aptamer-ligand complex, *Bioorg Med Chem 9*, 2565-70.

191. Grate, D. (2000) in *Biology* pp 177, UNIVERSITY OF CALIFORNIA, SANTA CRUZ, SANTA CRUZ.

192. Pendergrast, P. S., Marsh, H. N., Grate, D., Healy, J. M., and Stanton, M. (2005) Nucleic acid aptamers for target validation and therapeutic applications, *J Biomol Tech 16*, 224-34.

193. Ng, E. W., and Adamis, A. P. (2005) Targeting angiogenesis, the underlying disorder in neovascular age-related macular degeneratio, *Can J Ophthalmol 40*, 352-68.

194. Ruckman, J., Green, L. S., Beeson, J., Waugh, S., Gillette, W. L., Henninger, D. D., Claesson-Welsh, L., and Janjic, N. (1998) 2'-Fluoropyrimidine RNA-based aptamers to the 165-amino acid form of vascular endothelial growth factor (VEGF165). Inhibition of receptor binding and VEGF-induced vascular permeability through interactions requiring the exon 7-encoded domain, *J Biol Chem 273*, 20556-67.

195. Kohn, D. B., Bauer, G., Rice, C. R., Rothschild, J. C., Carbonaro, D. A., Valdez, P., Hao, Q., Zhou, C., Bahner, I., Kearns, K., Brody, K., Fox, S., Haden, E., Wilson, K., Salata, C., Dolan, C., Wetter, C., Aguilar-Cordova, E., and Church, J. (1999) A clinical trial of retroviral-mediated transfer of a rev-responsive element decoy gene into CD34(+) cells from the bone marrow of human immunodeficiency virus-1-infected children, *Blood 94*, 368-71.

196. Kruger, K., Grabowski, P. J., Zaug, A. J., Sands, J., Gottschling, D. E., and Cech, T. R. (1982) Self-splicing RNA: autoexcision and autocyclization of the ribosomal RNA intervening sequence of Tetrahymena, *Cell 31*, 147-57.

197. Zaug, A. J., and Cech, T. R. (1982) The intervening sequence excised from the ribosomal RNA precursor of Tetrahymena contains a 5-terminal guanosine residue not encoded by the DNA, *Nucleic Acids Res 10*, 2823-38.

198. Alwine, J. C., Kemp, D. J., Parker, B. A., Reiser, J., Renart, J., Stark, G. R., and Wahl, G. M. (1979) Detection of specific RNAs or specific fragments of DNA by fractionation in gels and transfer to diazobenzyloxymethyl paper, *Methods Enzymol 68*, 220-42.

199. Bassell, G. J., Powers, C. M., Taneja, K. L., and Singer, R. H. (1994) Single mRNAs visualized by ultrastructural in situ hybridization are principally localized at actin filament intersections in fibroblasts, *J Cell Biol 126*, 863-76.

200. Mullis, K., Faloona, F., Scharf, S., Saiki, R., Horn, G., and Erlich, H. (1986) Specific enzymatic amplification of DNA in vitro: the polymerase chain reaction, *Cold Spring Harb Symp Quant Biol 51 Pt 1*, 263-73.

201. Saiki, R. K., Scharf, S., Faloona, F., Mullis, K. B., Horn, G. T., Erlich, H. A., and Arnheim, N. (1985) Enzymatic amplification of beta-globin genomic sequences and restriction site analysis for diagnosis of sickle cell anemia, *Science 230*, 1350-4.

202. Guatelli, J. C., Whitfield, K. M., Kwoh, D. Y., Barringer, K. J., Richman, D. D., and Gingeras, T. R. (1990) Isothermal, in vitro amplification of nucleic acids by a multienzyme reaction modeled after retroviral replication, *Proc Natl Acad Sci U S A 87*, 1874-8.

203. Bush, C. E., Donovan, R. M., Peterson, W. R., Jennings, M. B., Bolton, V., Sherman, D. G., Vanden Brink, K. M., Beninsig, L. A., and Godsey, J. H. (1992) Detection of human immunodeficiency virus type 1 RNA in plasma samples from high-risk pediatric patients by using the self-sustained sequence replication reaction, *J Clin Microbiol 30*, 281-6.

204. Adams, M. D., Dubnick, M., Kerlavage, A. R., Moreno, R., Kelley, J. M., Utterback, T. R., Nagle, J. W., Fields, C., and Venter, J. C. (1992) Sequence identification of 2,375 human brain genes, *Nature 355*, 632-4.

205. Liang, P., and Pardee, A. B. (1992) Differential display of eukaryotic messenger RNA by means of the polymerase chain reaction, *Science 257*, 967-71.

206. Schena, M., Shalon, D., Davis, R. W., and Brown, P. O. (1995) Quantitative monitoring of gene expression patterns with a complementary DNA microarray, *Science 270*, 467-70.

207. Wansink, D. G., Schul, W., van der Kraan, I., van Steensel, B., van Driel, R., and de Jong, L. (1993) Fluorescent labeling of nascent RNA reveals transcription by RNA polymerase II in domains scattered throughout the nucleus, *J Cell Biol 122*, 283-93.

208. Jackson, D. A., Hassan, A. B., Errington, R. J., and Cook, P. R. (1993) Visualization of focal sites of transcription within human nuclei, *Embo J 12*, 1059-65.

209. Jacobson, M. R., and Pederson, T. (1998) Localization of signal recognition particle RNA in the nucleolus of mammalian cells, *Proc Natl Acad Sci U S A 95*, 7981-6.

210. Huang, Q., and Pederson, T. (1999) A human U2 RNA mutant stalled in 3' end processing is impaired in nuclear import, *Nucleic Acids Res 27*, 1025-31.

211. Glotzer, J. B., Saffrich, R., Glotzer, M., and Ephrussi, A. (1997) Cytoplasmic flows localize injected oskar RNA in Drosophila oocytes, *Curr Biol 7*, 326-37.

212. Bertrand, E., Chartrand, P., Schaefer, M., Shenoy, S. M., Singer, R. H., and Long, R. M. (1998) Localization of ASH1 mRNA particles in living yeast, *Mol Cell 2*, 437-45.

213. Forrest, K. M., and Gavis, E. R. (2003) Live Imaging of Endogenous RNA Reveals a Diffusion and Entrapment Mechanism for nanos mRNA Localization in Drosophila, *Curr Biol 13*, 1159-68.

214. Fusco, D., Accornero, N., Lavoie, B., Shenoy, S. M., Blanchard, J. M., Singer, R. H., and Bertrand, E. (2003) Single mRNA molecules demonstrate probabilistic movement in living mammalian cells, *Curr Biol 13*, 161-7.

215. Leonetti, J. P., Mechti, N., Degols, G., Gagnor, C., and Lebleu, B. (1991) Intracellular distribution of microinjected antisense oligonucleotides, *Proc Natl Acad Sci U S A 88*, 2702-6.

216. Mechti, N., Leonetti, J. P., Clarenc, J. P., Degols, G., and Lebleu, B. (1991) Nuclear location of synthetic oligonucleotides microinjected somatic cells: its implication in an antisense strategy, *Nucleic Acids Symp Ser*, 147-50.

217. Nitin, N., Santangelo, P. J., Kim, G., Nie, S., and Bao, G. (2004) Peptide-linked molecular beacons for efficient delivery and rapid mRNA detection in living cells, *Nucleic Acids Res 32*, e58.

218. Tyagi, S., and Alsmadi, O. (2004) Imaging native beta-actin mRNA in motile fibroblasts, *Biophys J 87*, 4153-62.

219. Mhlanga, M. M., Vargas, D. Y., Fung, C. W., Kramer, F. R., and Tyagi, S. (2005) tRNA-linked molecular beacons for imaging mRNAs in the cytoplasm of living cells, *Nucleic Acids Res 33*, 1902-12.

220. Fresco, J. R., Alberts, B. M., and Doty, P. (1960) Some molecular details of the secondary structure of ribonucleic acid, *Nature 188*, 98-101.

221. Nussinov, R., Pieczenik, G., Griggs, J. R., and Kleitman, D. J. (1978) in *Siam Journal on Applied Mathematics* pp 68-82.

222. Eddy, S. R. (2004) How do RNA folding algorithms work?, *Nat Biotechnol 22*, 1457-8.

223. Eddy, S. R. (2004) What is dynamic programming?, *Nat Biotechnol 22*, 909-10.

224. Nussinov, R., and Pieczenik, G. (1984) Folding of two large nucleotide chains, *J Theor Biol 106*, 261-73.

225. Nussinov, R., and Pieczenik, G. (1984) Structural and combinatorial constraints on base pairing in large nucleotide sequences, *J Theor Biol 106*, 245-59.

226. Zuker, M., and Stiegler, P. (1981) Optimal computer folding of large RNA sequences using thermodynamics and auxiliary information, *Nucleic Acids Res 9*, 133-48.

227. Zuker, M. (2000) Calculating nucleic acid secondary structure, *Curr Opin Struct Biol 10*, 303-10.

228. Zuker, M. (1989) On finding all suboptimal foldings of an RNA molecule, *Science 244*, 48-52.

229. Hofacker, I. L., Fontana, W., Stadler, P. F., Bonhoeffer, L. S., Tacker, M., and Schuster, P. (1994) in *Monatshefte Fur Chemie* pp 167-188.

230. Hofacker, I. L. (2003) Vienna RNA secondary structure server, *Nucleic Acids Res 31*, 3429-31.

231. Ding, Y., and Lawrence, C. E. (2003) A statistical sampling algorithm for RNA secondary structure prediction, *Nucleic Acids Res 31*, 7280-301.

232. Soukup, G. A., and Breaker, R. R. (1999) Engineering precision RNA molecular switches, *Proc Natl Acad Sci U S A 96*, 3584-9.

233. Kuwabara, T., Warashina, M., Tanabe, T., Tani, K., Asano, S., and Taira, K. (1998) A novel allosterically trans-activated ribozyme, the maxizyme, with exceptional specificity in vitro and in vivo, *Mol Cell 2*, 617-27.

234. Robertson, M. P., and Ellington, A. D. (1999) In vitro selection of an allosteric ribozyme that transduces analytes to amplicons, *Nat Biotechnol 17*, 62-6.

235. Soukup, G. A., Emilsson, G. A., and Breaker, R. R. (2000) Altering molecular recognition of RNA aptamers by allosteric selection, *J Mol Biol 298*, 623-32.

236. Seetharaman, S., Zivarts, M., Sudarsan, N., and Breaker, R. R. (2001) Immobilized RNA switches for the analysis of complex chemical and biological mixtures, *Nat Biotechnol 19*, 336-41.

237. Kertsburg, A., and Soukup, G. A. (2002) A versatile communication module for controlling RNA folding and catalysis, *Nucleic Acids Res 30*, 4599-606.

238. Wang, D. Y., Lai, B. H., and Sen, D. (2002) A general strategy for effector-mediated control of RNA-cleaving ribozymes and DNA enzymes, *J Mol Biol 318*, 33-43.

239. Vaish, N. K., Dong, F., Andrews, L., Schweppe, R. E., Ahn, N. G., Blatt, L., and Seiwert, S. D. (2002) Monitoring post-translational modification of proteins with allosteric ribozymes, *Nat Biotechnol 20*, 810-5.

240. Piganeau, N., Jenne, A., Thuillier, V., and Famulok, M. (2001) An Allosteric Ribozyme Regulated by Doxycyline This work was supported by Aventis Gencell and by a grant from the Volkswagen Foundation (Priority program "conformational control") to M.F. We thank M. Blind, G. Mayer, D. Proske, and G. Sengle (Universitat Bonn) for helpful discussions as well as J. Crouzet, J. F. Mayaux, and M. Finer (Aventis Gencell) for support, *Angew Chem Int Ed Engl 40*, 3503.

241. Hartig, J. S., and Famulok, M. (2002) Reporter ribozymes for real-time analysis of domain-specific interactions in biomolecules: HIV-1 reverse transcriptase and the primer-template complex, *Angew Chem Int Ed Engl 41*, 4263-6.

242. Wu, L., and Curran, J. F. (1999) An allosteric synthetic DNA, *Nucleic Acids Res 27*, 1512-6.

243. Chinnapen, D. J., and Sen, D. (2002) Hemin-stimulated docking of cytochrome c to a hemin-DNA aptamer complex, *Biochemistry 41*, 5202-12.

244. Mironov, A. S., Gusarov, I., Rafikov, R., Lopez, L. E., Shatalin, K., Kreneva, R. A., Perumov, D. A., and Nudler, E. (2002) Sensing small molecules by nascent RNA: a mechanism to control transcription in bacteria, *Cell 111*, 747-56.

245. Miranda-Rios, J., Navarro, M., and Soberon, M. (2001) A conserved RNA structure (thi box) is involved in regulation of thiamin biosynthetic gene expression in bacteria, *Proc Natl Acad Sci U S A 98*, 9736-41.

246. Rodionov, D. A., Vitreschak, A. G., Mironov, A. A., and Gelfand, M. S. (2003) Regulation of lysine biosynthesis and transport genes in bacteria: yet another RNA riboswitch?, *Nucleic Acids Res 31*, 6748-57.

247. Stormo, G. D., and Ji, Y. (2001) Do mRNAs act as direct sensors of small molecules to control their expression?, *Proc Natl Acad Sci U S A 98*, 9465-7.

248. Winkler, W. C., Cohen-Chalamish, S., and Breaker, R. R. (2002) An mRNA structure that controls gene expression by binding FMN, *Proc Natl Acad Sci U S A.*

249. Vitreschak, A. G., Rodionov, D. A., Mironov, A. A., and Gelfand, M. S. (2002) Regulation of riboflavin biosynthesis and transport genes in bacteria by transcriptional and translational attenuation, *Nucleic Acids Res 30*, 3141-51.

250. Nou, X., and Kadner, R. J. (2000) Adenosylcobalamin inhibits ribosome binding to btuB RNA, *Proc Natl Acad Sci U S A 97*, 7190-5.

251. Nahvi, A., Barrick, J. E., and Breaker, R. R. (2004) Coenzyme B12 riboswitches are widespread genetic control elements in prokaryotes, *Nucleic Acids Res 32*, 143-50.

252. McDaniel, B. A., Grundy, F. J., Artsimovitch, I., and Henkin, T. M. (2003) Transcription termination control of the S box system: direct measurement of

S-adenosylmethionine by the leader RNA, *Proc Natl Acad Sci U S A 100*, 3083-8.

253. Epshtein, V., Mironov, A. S., and Nudler, E. (2003) The riboswitch-mediated control of sulfur metabolism in bacteria, *Proc Natl Acad Sci U S A 100*, 5052-6.

254. Winkler, W. C., Nahvi, A., Sudarsan, N., Barrick, J. E., and Breaker, R. R. (2003) An mRNA structure that controls gene expression by binding S-adenosylmethionine, *Nat Struct Biol 10*, 701-7.

255. Kochhar, S., and Paulus, H. (1996) Lysine-induced premature transcription termination in the lysC operon of Bacillus subtilis, *Microbiology 142 (Pt 7)*, 1635-9.

256. Patte, J. C., Akrim, M., and Mejean, V. (1998) The leader sequence of the Escherichia coli lysC gene is involved in the regulation of LysC synthesis, *FEMS Microbiol Lett 169*, 165-70.

257. Mandal, M., Boese, B., Barrick, J. E., Winkler, W. C., and Breaker, R. R. (2003) Riboswitches control fundamental biochemical pathways in Bacillus subtilis and other bacteria, *Cell 113*, 577-86.

258. Winkler, W. C. (2005) Riboswitches and the role of noncoding RNAs in bacterial metabolic control, *Curr Opin Chem Biol.*

259. Nudler, E., and Mironov, A. S. (2004) The riboswitch control of bacterial metabolism, *Trends Biochem Sci 29*, 11-7.

260. Floege, J., Ostendorf, T., Janssen, U., Burg, M., Radeke, H. H., Vargeese, C., Gill, S. C., Green, L. S., and Janjic, N. (1999) Novel approach to specific growth factor inhibition in vivo: antagonism of platelet-derived growth factor in glomerulonephritis by aptamers, *Am J Pathol 154*, 169-79.

261. Green, L. S., Jellinek, D., Bell, C., Beebe, L. A., Feistner, B. D., Gill, S. C., Jucker, F. M., and Janjic, N. (1995) Nuclease-resistant nucleic acid ligands to vascular permeability factor/vascular endothelial growth factor, *Chem Biol 2*, 683-95.

262. Watson, S. R., Chang, Y. F., O'Connell, D., Weigand, L., Ringquist, S., and Parma, D. H. (2000) Anti-L-selectin aptamers: binding characteristics, pharmacokinetic parameters, and activity against an intravascular target in vivo, *Antisense Nucleic Acid Drug Dev 10*, 63-75.

263. Hicke, B. J., Marion, C., Chang, Y. F., Gould, T., Lynott, C. K., Parma, D., Schmidt, P. G., and Warren, S. (2001) Tenascin-C aptamers are generated using tumor cells and purified protein, *J Biol Chem 276*, 48644-54.

264. Darfeuille, F., Hansen, J. B., Orum, H., Di Primo, C., and Toulme, J. J. (2004) LNA/DNA chimeric oligomers mimic RNA aptamers targeted to the TAR RNA element of HIV-1, *Nucleic Acids Res 32*, 3101-7.

265. Schmidt, K. S., Borkowski, S., Kurreck, J., Stephens, A. W., Bald, R., Hecht, M., Friebe, M., Dinkelborg, L., and Erdmann, V. A. (2004) Application of locked nucleic acids to improve aptamer in vivo stability and targeting function, *Nucleic Acids Res 32*, 5757-65.

266. Willis, M. C., Collins, B. D., Zhang, T., Green, L. S., Sebesta, D. P., Bell, C., Kellogg, E., Gill, S. C., Magallanez, A., Knauer, S., Bendele, R. A., Gill, P. S., Janjic, N., and Collins, B. (1998) Liposome-anchored vascular endothelial growth factor aptamers, *Bioconjug Chem 9*, 573-82.

267. Dougan, H., Lyster, D. M., Vo, C. V., Stafford, A., Weitz, J. I., and Hobbs, J. B. (2000) Extending the lifetime of anticoagulant oligodeoxynucleotide aptamers in blood, *Nucl Med Biol 27*, 289-97.

268. Rusconi, C. P., Roberts, J. D., Pitoc, G. A., Nimjee, S. M., White, R. R., Quick, G., Jr., Scardino, E., Fay, W. P., and Sullenger, B. A. (2004) Antidote-

mediated control of an anticoagulant aptamer in vivo, *Nat Biotechnol 22*, 1423-8.

269. Carrasquillo, K. G., Ricker, J. A., Rigas, I. K., Miller, J. W., Gragoudas, E. S., and Adamis, A. P. (2003) Controlled delivery of the anti-VEGF aptamer EYE001 with poly(lactic-co-glycolic)acid microspheres, *Invest Ophthalmol Vis Sci 44*, 290-9.

270. Charlton, J., Kirschenheuter, G. P., and Smith, D. (1997) Highly potent irreversible inhibitors of neutrophil elastase generated by selection from a randomized DNA-valine phosphonate library, *Biochemistry 36*, 3018-26.

271. Farokhzad, O. C., Jon, S., Khademhosseini, A., Tran, T. N., Lavan, D. A., and Langer, R. (2004) Nanoparticle-aptamer bioconjugates: a new approach for targeting prostate cancer cells, *Cancer Res 64*, 7668-72.

272. Tavitian, B., Terrazzino, S., Kuhnast, B., Marzabal, S., Stettler, O., Dolle, F., Deverre, J. R., Jobert, A., Hinnen, F., Bendriem, B., Crouzel, C., and Di Giamberardino, L. (1998) In vivo imaging of oligonucleotides with positron emission tomography, *Nat Med 4*, 467-71.

273. Charlton, J., Sennello, J., and Smith, D. (1997) In vivo imaging of inflammation using an aptamer inhibitor of human neutrophil elastase, *Chem Biol 4*, 809-16.

274. DeAnda, A., Jr., Coutre, S. E., Moon, M. R., Vial, C. M., Griffin, L. C., Law, V. S., Komeda, M., Leung, L. L., and Miller, D. C. (1994) Pilot study of the efficacy of a thrombin inhibitor for use during cardiopulmonary bypass, *Ann Thorac Surg 58*, 344-50.

275. Reyderman, L., and Stavchansky, S. (1998) Pharmacokinetics and biodistribution of a nucleotide-based thrombin inhibitor in rats, *Pharm Res 15*, 904-10.

276. Rusconi, C. P., Scardino, E., Layzer, J., Pitoc, G. A., Ortel, T. L., Monroe, D., and Sullenger, B. A. (2002) RNA aptamers as reversible antagonists of coagulation factor IXa, *Nature 419*, 90-4.

277. Ostendorf, T., Kunter, U., Eitner, F., Loos, A., Regele, H., Kerjaschki, D., Henninger, D. D., Janjic, N., and Floege, J. (1999) VEGF(165) mediates glomerular endothelial repair, *J Clin Invest 104*, 913-23.

278. Drolet, D. W., Nelson, J., Tucker, C. E., Zack, P. M., Nixon, K., Bolin, R., Judkins, M. B., Farmer, J. A., Wolf, J. L., Gill, S. C., and Bendele, R. A. (2000) Pharmacokinetics and safety of an anti-vascular endothelial growth factor aptamer (NX1838) following injection into the vitreous humor of rhesus monkeys, *Pharm Res 17*, 1503-10.

279. Tucker, C. E., Chen, L. S., Judkins, M. B., Farmer, J. A., Gill, S. C., and Drolet, D. W. (1999) Detection and plasma pharmacokinetics of an anti-vascular endothelial growth factor oligonucleotide-aptamer (NX1838) in rhesus monkeys, *J Chromatogr B Biomed Sci Appl 732*, 203-12.

280. Green, L. S., Jellinek, D., Jenison, R., Ostman, A., Heldin, C. H., and Janjic, N. (1996) Inhibitory DNA ligands to platelet-derived growth factor B-chain, *Biochemistry 35*, 14413-24.

281. Ostendorf, T., Kunter, U., Grone, H. J., Bahlmann, F., Kawachi, H., Shimizu, F., Koch, K. M., Janjic, N., and Floege, J. (2001) Specific antagonism of PDGF prevents renal scarring in experimental glomerulonephritis, *J Am Soc Nephrol 12*, 909-18.

282. Ostendorf, T., Kunter, U., van Roeyen, C., Dooley, S., Janjic, N., Ruckman, J., Eitner, F., and Floege, J. (2002) The effects of platelet-derived growth factor antagonism in experimental glomerulonephritis are independent of the transforming growth factor-beta system, *J Am Soc Nephrol 13*, 658-67.

283. Leppanen, O., Janjic, N., Carlsson, M. A., Pietras, K., Levin, M., Vargeese, C., Green, L. S., Bergqvist, D., Ostman, A., and Heldin, C. H. (2000) Intimal hyperplasia recurs after removal of PDGF-AB and -BB inhibition in the rat carotid artery injury model, *Arterioscler Thromb Vasc Biol 20*, E89-95.

284. Pietras, K., Ostman, A., Sjoquist, M., Buchdunger, E., Reed, R. K., Heldin, C. H., and Rubin, K. (2001) Inhibition of platelet-derived growth factor receptors reduces interstitial hypertension and increases transcapillary transport in tumors, *Cancer Res 61*, 2929-34.

285. Wlotzka, B., Leva, S., Eschgfaller, B., Burmeister, J., Kleinjung, F., Kaduk, C., Muhn, P., Hess-Stumpp, H., and Klussmann, S. (2002) In vivo properties of an anti-GnRH Spiegelmer: an example of an oligonucleotide-based therapeutic substance class, *Proc Natl Acad Sci U S A 99*, 8898-902.

286. Hwang, B., Han, K., and Lee, S. W. (2003) Prevention of passively transferred experimental autoimmune myasthenia gravis by an in vitro selected RNA aptamer, *FEBS Lett 548*, 85-9.

287. Bless, N. M., Smith, D., Charlton, J., Czermak, B. J., Schmal, H., Friedl, H. P., and Ward, P. A. (1997) Protective effects of an aptamer inhibitor of neutrophil elastase in lung inflammatory injury, *Curr Biol 7*, 877-80.

288. Santulli-Marotto, S., Nair, S. K., Rusconi, C., Sullenger, B., and Gilboa, E. (2003) Multivalent RNA aptamers that inhibit CTLA-4 and enhance tumor immunity, *Cancer Res 63*, 7483-9.

289. Jeon, S. H., Kayhan, B., Ben-Yedidia, T., and Arnon, R. (2004) A DNA aptamer prevents influenza infection by blocking the receptor binding region of the viral hemagglutinin, *J Biol Chem 279*, 48410-9.

290. Tucker, B. J., and Breaker, R. R. (2005) Riboswitches as versatile gene control elements, *Curr Opin Struct Biol 15*, 342-8.

291. Robertson, M. P., Knudsen, S. M., and Ellington, A. D. (2004) In vitro selection of ribozymes dependent on peptides for activity, *Rna 10*, 114-27.

292. Agresti, J. J., Kelly, B. T., Jaschke, A., and Griffiths, A. D. (2005) Selection of ribozymes that catalyse multiple-turnover Diels-Alder cycloadditions by using in vitro compartmentalization, *Proc Natl Acad Sci U S A 102*, 16170-5.

ACKNOWLEDGMENTS

I thank my major professor, Dr. Marit Nilsen-Hamilton, for her supervision, encouragement, discussions and support throughout. Without the extensive guidance offered by Dr. Marit Nilsen-Hamilton, would be impossible to make the progress presented in this study. Dr. Marit Nilsen-Hamilton was the inventor of TRAP idea presented in this study and gave invaluable advice during my work. I am deeply impressed by her dedication and love for the scientific research as a scientist. I am looking forward for the fruitful discussion and cooperation with her in the future.

I thank Drs. Gloria Culver, Ted Huiatt, Robert Jernigan and W. Allen Miller for serving on my POS committee. I thank them for their constructive suggestions for many experiments. I thank them for their critical reading and comments on my dissertation

I thank Lee Bendickson for his enormous support and help during all time in the lab. I thank Dr. Ahmed Awad who worked on the microarray and antisense experiments. I thank Xiaoling Song who worked on the antisense experiments. I thank Long Qu who worked on microarray data analysis. I thank Jayeeta Banerjee for working with me on the yeast selection system. I also thank past and current members working on the GRABIT project, including Dr. Richard Hamilton, Becky Stodola, Marjian Mokhtarian, Dr. Aimin Yan, Lisa Patrin and Tianjiao Wang for their help and discussion. I thank other past and present lab members for their kind help and suggestions.

I wish to thank Drs. Alan Myers and Daniel Voytas for their generosity of providing us with yeast strain and plasmids. I thank Dr. Gloria Culver and her lab members for their support and help in the techniques of working with RNA and polyacrylamide gel electrophoresis.

Finally, I thank my wife for her patience, understanding, love and support. I thank my parents and my sister for their constant caring and loving.